KRUGER, A

THE WET-PROCESS FOR PHOSPHORIC ACID PRODUCTION

PhD (Chemistry) UP 1998

The wet-process for phosphoric acid production

by

Annalize Kruger

Presented in partial fulfilment of the requirements for the degree

Philosophiae Doctor

Chemistry

in the Faculty of Science

University of Pretoria

Pretoria

SEPTEMBER 1998

KRUGER, ANNALIZE

THE WET-PROCESS FOR PHOSPHORIC ACID PRODUCTION

Ph.D. UP 1998

ACKNOWLEDGEMENTS

I would like to express my sincere gratitude to the following people, departments, companies and institutions for their support throughout my studies:

- My supervisor, Professor Anton M. Heyns, for his guidance, inspirational vision and financial support.
- Rob Fowles for his valuable advice, enthusiasm and support throughout this project.
- My parents and family for their support. A special thanks to my husband for his encouragement, patients and understanding.
- The rest of the research group for their advice.
- Foskor, and the Foundation of Research and Development for financial support.
- Foskor and Avmin for ICP analyses of samples.
- The Department of Electron Microscopy for electron microscope photographs.

SUMMARY

The wet-process for phosphoric acid production

by

Annalize Kruger

Presented for the degree Ph.D. (Chemistry)

Supervisor

Professor Anton M. Heyns

Institute of Applied Materials

University of Pretoria

Project Purephos was initiated by Foskor, to investigate some aspects of the phosphoric acid industry, in particular, the effect of impurities in phosphate rock, commonly found by their clients, on the crystallisation of calcium sulphate dihydrate and the produced phosphoric acid.

The saturation and supersaturation curve for Palfos 88P rock was determined. This will assist producers to optimise, and understand the impact of the free sulphate level on the crystallisation of calcium sulphate dihydrate, and the co-precipitation, and thus loss, of P_2O_5.

The influence of sodium, potassium, magnesium and the aluminium/fluoride ratio were investigated. It was found that although sodium and potassium promote crystal growth, the filtration rates could decrease with elevated levels, as a result of the precipitation of hexafluorosilicates.

Elevated levels of magnesium and aluminium increase acid viscosity and thus reduce filtration rates. The effect of aluminium can however be reduced, by controlling the aluminium/fluoride ratio.

This study attempts to readdress the misconception that igneous rock is more difficult to process, and show that by using high-grade igneous rock, under controlled conditions, the benefits of igneous rock can be enjoyed.

OPSOMMING

The wet-process for phosphoric acid production

deur

Annalize Kruger

Voorgelê vir die graad Ph.D. (Chemie)

Promotor

Professor Anton M. Heyns

Instituut vir Toegepaste Materiale

Universiteit van Pretoria

Die doel van Projek Purephos, in samewerking met Foskor, was om sekere aspekte van die produksie van fosforsuur te ondersoek, spesifiek die invloed van sekere onsuiwerhede in fosfaat rots, wat algemeen deur die kliënte ondervind word, op die kristallisering van kalsium sulfaat dihidraat en fosforsuur.

Versadiging en superversadiging kurwes is bepaal vir Palfos 88P rots. Dit sal produseerders help om die vrye-sulfaat konsentrasie te optimaliseer, en om die invloed van die konsentrasie op die kristallisering van die kalsium sulfaat dihidraat beter te begryp.

Natrium, kalium, magnesium en die aluminium/fluoried verhouding, is van die onsuiwerhede wat ondersoek is. Daar is gevind dat, alhoewel verhoogde konsentrasies van natrium en kalium kristalgroei bevorder, die fitrasie tempo vertraag word as gevolg van die presipitasie van hexafluorosilikate.

Verhoogde konsentrasies van magnesium en aluminium beïnvloed die viskositeit van die suur, en die filtrasie tempo word gevolglik benadeel. Die effek van aluminium kan beperk word deur die aluminium/fluoried verhouding te beheer.

Die studie poog om miskonsepsies oor die gebruik van stollingsgesteente vir die produksie van fosforsuur uit die weg te ruim, en wys dat, met die korrekte beheer van konsentrasies, die voordele van die rots benut kan word.

CONTENTS

CHAPTER 1

INTRODUCTION

1.1 HISTORICAL BACKGROUND:

The discovery of phosphorus is generally attributed to Henning Brand of Hamburg, who in 1669 obtained it by distilling urine. It was subsequently named 'Phosphorus' meaning light bearing. During the first half of the nineteenth century, notably Liebig and Lawes made significant advances in the science of plant nutrition, and the value of phosphate as fertilisers was soon realised.

Although urine remained the only source of the element for nearly hundred years after its discovery, it was replaced with bones by the end of the eighteenth century. Supplies of the latter soon proved to be inadequate, however, but fortunately, substantial phosphate mineral deposits were quickly found. Serious commercial production commenced in Europe at about 1850.

The development and exploitation of the countercurrent decantation process during the period 1915–1930, established wet-process phosphoric acid as an industrial commodity. Significant technological contributions by Weber in the United States and Nordengren in Sweden during the early 1930's are milestones on the road to maturity in the commercialisation of the process. Electric furnace phosphorus was first produced in England in 1890, and in the United States in 1897.

1.1.1 WET PROCESS:

Wet-process phosphoric acid for fertiliser use was first produced commercially in Germany between 1870 and 1872, and in the United States, at Baltimor, Maryland, for a short period at the beginning of 1880. The phosphoric acid in these early operations was made by digesting ground low-grade phosphorite in 16 per cent sulphuric acid.

In Europe there were about twelve companies in 1900, making wet-process phosphoric acid for the use in concentrated superphosphate. Importation from the Unites States of high-grade rock for single superphosphate, however, made the operation uneconomical and wet-process phosphoric acid production declined for several years.

Among the pioneers in wet-process phosphoric acid was the Shauffer Chemical Company, where a process was developed in 1897 for acidulating bones. In 1912 Shauffer converted the process to phosphate rock and developed a method for producing acid meeting food grade standards. Other early producers were Virginia-Carolina Chemical Company and American Agricultural Chemical Company.

The batch process for phosphoric acid underwent some improvements, but it was not until the introduction of the continuous process in 1915 that any significant technology of economical improvements were made. The Dorr Company developed an airlift agitation system that involved reaction of the rock-acid mixture in a series of preliminary digesters followed by countercurrent washing of the gypsum in a series of thickeners. By 1920, the Oliver Company replaced the last few thickeners in the wash train by continuous filters. The development of the continuous process, which might now be considered as a technological breakthrough, created a significant commercial interest in wet-process phosphoric acid.

In 1932, Dorr built the largest wet-process phosphoric acid plant up to that time. This plant consisted of three trains, each capable of processing 150 tons of phosphate rock per day. This process marked the second major commercial advance in wet-process phosphoric acid technology. It involved recycling of gypsum slurry for better control of crystal growth, thereby giving larger crystals and improved filterability, and separation and countercurrent washing of the gypsum on Oliver continuos filters. The product acid from the filters contained 30-32 per cent P_2O_5, which led to the term 'strong acid

process' for this type of installation. The strong acid process, as developed in the 1930-1950 period, was widely adopted and is still the standard method. Subsequent changes have been minor in nature, consisting largely of incremental modifications in the design of reactors, cooling equipment, and filters.

Other methods have been developed, involving the precipitation of calcium sulphate hemihydrate or anhydrite and recrystallisation of hemihydrate to dihydrate. Processes substituting sulphuric acid with hydrochloric acid or nitric acid were also developed.

1.1.2 FURNACE PROCESS:

The first elemental phosphorus process was developed in Europe in 1867 and in the United States in 1897.Today the industry is large and well developed, located mainly in areas where electric power is relative low in cost. Furnace phosphoric acid plants are normally built primarily for chemical rather than the fertiliser trade.

1.2 DISTRIBUTION OF PHOSPHATE DEPOSITS:

Phosphorus is not found free in nature and usually occurs in the fully oxidised state as phosphate. More than two hundred different phosphate minerals are known, but only those in the apatite group occur in sufficient abundance and concentration to serve as commercial sources of the element. The commonest apatite deposits consist mainly of fluorapatite $Ca_{10}(PO_4)_6F_2$, but chlorapatite, $Ca_{10}(PO_4)_6Cl_2$,hydroxylapatite $Ca_{10}(PO_4)_6(OH)_2$ and carbonate-apatite $Ca_5[(PO_4)_{3-x}(CO_3,F)_x](F, OH, Cl)$ can also occur.

Apatitic phosphate rock occurs mostly as a sedimentary deposit called phosphorite. The largest and most important phosphorite deposits are found in Morocco (Khourigba, Youssoufia, Bu Craa), USA (Florida, North Carolina), USSR (Kazakhstan),

China and Tunisia. Important commercial deposits also occur in Togo, Brazil, Nauro and other Pacific islands.

Apatite also occurs (less commonly) as igneous phosphate rock, which is highly crystalline and much purer than sedimentary phosphorite. Commercial important igneous rock formations of crystalline fluoroapatite are found in the Kola peninsula of USSR, the Northern Province of the Republic of South Africa, and Brazil, but these account for only 15 per cent of the world total of mined rock. There are, in addition, substantial deposits of aluminous phosphates, but satisfactory technological development of these has not yet taken place. The natural and artificial cycles of phosphorus are shown in Figure 1.1.

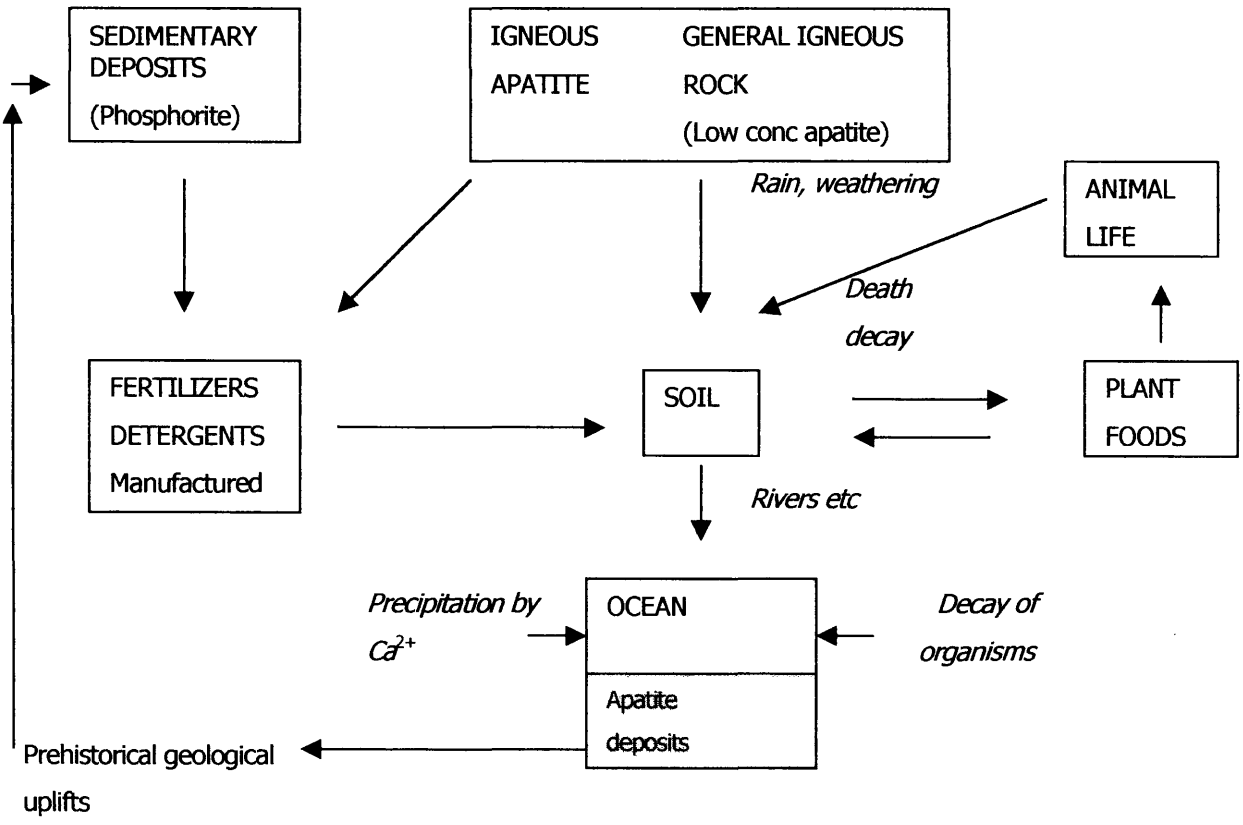

Figure 1.1. The natural and artificial cycles of phosphorus.

1.3 PRODUCTION:

Phosphoric acid is an important chemical intermediate, used mainly in the fertiliser field but also in other areas of chemical technology. In fertiliser production, it serves as an intermediate between phosphate ore and major end products such as ammonium phosphate, triple superphosphate, liquid mixed fertiliser, high-analysis solid mixed fertiliser, and some types of nitric phosphate. In the chemical field, phosphoric acid is an intermediate in the production of materials such as detergents, water treatment chemicals, surface treatment chemicals, and animal feed supplements.

On a tonnage basis, the inorganic compounds remain the most important; with fertilisers constituting the largest single application (85-90 per cent). Living creatures supply their phosphate needs by food, and phosphates in the food arise from biological phosphorus uptake from available soil components.

Since phosphates are unevenly distributed and not available to plants at the current levels of farming, it is the goal of the phosphate industry to supply phosphate fertilisers of the necessary quality and quantity to farmland areas throughout the world.

The worldwide phosphate market amounts to about 50Mt phosphate rock per annum. The growth in demand has been phenomenal during this century, and the industry has contributed substantially towards the improvement in living standards worldwide. From the beginning of this decade, the phosphate market has been facing a critical period. In the industrialised countries, the standstill of the population, and the worsening environmental conditions have caused domestic phosphate markets to contract.

Phosphoric acid can be produced from raw materials via two major process routes:

1. The wet process, using sulphuric acid attack, and
2. The electric furnace process, using electrical energy to produce elemental phosphorus as a first stage.

Because of current energy prices, the wet process accounts for over 90 per cent of the current phosphoric acid production.

Wet process phosphoric acid technology essentially comprises sulphuric acid attack and separation of the phosphoric acid from the calcium sulphate crystals resulting from the reaction:

$$Ca_9(PO_4)_6.CaF_2 + 10H_2SO_4 + 10xH_2O \rightarrow 10CaSO_4.xH_2O\downarrow + 6H_3PO_4 + 2HF\uparrow \quad (1.1)$$

With varying temperature and acid concentration either anhydrite (AH, x=0), hemihydrite (HH, x=1/2) or dihydrite (DH, x=2) is crystallised from the acidic solution.

The product acid is usually relative low in concentration and needs to be concentrated to 40 or 54 per cent P_2O_5, depending on the process in which it is to be used.

1.4 PHOSPHATE IN SOUTH AFRICA:

1.4.1 OCCURRENCE:

The commercial important phosphate deposits in South Africa are confined to igneous and marine sedimentary geological environments. The former environment is by far the most important in South Africa, and roughly 95 per cent of the country's production comes from the Phalaborwa Complex in the northern province.

The marine sedimentary deposits are mainly confined to the western and southern coastal regions and comprise both on-shore and off-shore deposits. The on-shore deposits occur intermittently from Saldanha Bay in the south to Lambert's Bay in the north and the off-shore deposits occur on the continental shelf at Agulhas Bank, stretching from Cape Town eastwards as far as Port Elizabeth. Deposits on the shelf off the west coast extend from Cape Town northwards as far as Lambert's Bay.

Carbonatite-peralkalina complexes, of which the Phalaborwa complex is by far the most important, represent the major type of host rock for phosphate in South Africa. Besides Phalaborwa, there are a number of other carbonatitic complexes in South Africa and its neighbouring territories that have been mined for phosphate, or are potential phosphate sources.

1.4.2 MINING:

The mining activities at Phalaborwa involve conventional open-pit methods for hard rock, namely drilling, blasting, and hauling of the broken rock to the crushers in 92 to 152 ton rear-dumper trucks.

The complex genesis from a series of concentric volcanic intrusions over a time span of about 1300 million years. It has left a legacy of extreme variability in the mineralogy, especially in the transition zones of contact between the successive volcanic pipes. Foskor produces copper concentrate and various grades of phosphate and baddeleyite for different market sectors.

The phosphate reserves at Phalaborwa are vast. Theoretically, the complex contains 2159Mt of ore, which could yield 298 Mt of merchant-grade phosphate rock per 100m of depth; that is, every 100m could sustain the current production, which is approximately three times the current domestic demand, for a century.

Economical and practical mining considerations would reduce the theoretical reserves considerably.

1.4.3 BENEFICATION:

Foskor can produce phosphate rock from three main sources, namely pyroxenite ore, foskorite ore and PMC tailings. The phosphate rock goes through different stages of crushing, milling and flotation.

Palfos 80M results from a four-stage flotation circuit comprising rougher, scavenger, cleaner, and recleaner stages, with the recirculation of middlings. The concentrate analysing 36.5 per cent P_2O_5 represents 87 per cent pure apatite. The Palfos 80M product contains mainly calcite, dolomite, diopside, and phlogopite as diluent minerals. The magnesium-bearing minerals give it a MgO content of about 1.5 per cent on the average. All the other phosphate rocks available on the world market have MgO contents of less than 0.4 per cent and in order to render the Phalaborwa rock acceptable to overseas customers, the content of gangue minerals has to be reduced. This is done by reflotation and cyclone classification of the Palfos 80M rock to produce: Palfos 86S with 39.3 per cent P_2O_5 and 0.65 per cent MgO, and Palfos 88P with 40.0 per cent P_2O_5 and less than 0.5 per cent MgO.

1.5 PROJECT PUREPHOS:

As the availability of high grade and good quality sedimentary phosphate rock diminishes, the utilisation of igneous rock for all types of phosphoric acid production will progressively increase. This fact, together with its inherent advantages, such as the by-production of high quality gypsum, will see the introduction of igneous rock phosphate, either in a blend or singularly on many plants throughout the world.

Igneous rock, not containing any organic matter, behaves very differently from rock of sedimentary origin, showing different physical qualities and some variation in chemical composition. Phosphoric acid technologies have to rely on raw materials of great variety and fluctuating composition. This means constant re-adaption of operating conditions and constant experimentation.

The crystallography of gypsum dihydrate produced from igneous rock is very often quite different to the cluster type crystals produced from sedimentary rock sources. Normally, the crystals are flat, needle-like in appearance and are affected by factors such as uncomplexed ("free") sulphate variations, phosphoric acid concentration, temperature, and soluble impurities. Such impurities may be present in low grade (low P_2O_5 content) material, since lower grades will contain contaminating minerals other than quartz, which may be soluble in a phosphoric and sulphuric acid environment. In some instances, the impurities may originate from other rock sources used in a blend. Depending on the level of the impurity, the rate of crystal growth and morphology might be affected, such that filtration rates are retarded and production capacity hindered. Alternatively, the ions produced upon dissolution may have a positive effect on crystallisation by increasing the size and thickness of the crystal.

In addressing these issues, a significant amount of work has been published on specific impurities and their effects. Most work has been done on pure reagents, that is, pure phosphoric acid and calcium phosphate, but little work has been done in the area of using actual plant raw materials and simulation of plant conditions. This is presumably so since it is difficult to duplicate dihydrate crystallisation processes in a laboratory environment.

Project purephos was initiated by Foskor, in co-operation with the Institute of Applied Materials –UP, to address these issues. Novel apparatus and plant raw materials were used to simulate actual wet process plant conditions.

The main objectives were:

1. Determine the influence of 'free sulphate' concentrations on the solubility of calcium sulphate dihydrate, that is, determine the saturation and supersaturation diagrams for 88P rock.

2. Investigate the influence of different levels of soluble impurities introduced into the system, on the crystal growth and morphology of the calcium sulphate dihydrate by-product, as well as the influence of the impurities on the produced phosphoric acid. The impurities being K^+, Na^+, Mg^{2+}, Al^{3+} and F^-, which are the most common impurities found by Foskor's clients.

1.6 LITERATURE CITED:

1. Chang L.L.Y., Howie R.A., and Zussman J., **"Rock forming minerals Sulphates, Carbonates, Phosphates and Halides**." Volume 5B:Non-silicates, Second edition, Longman Group Limited, (1996).

2. Becker P., **"Phosphates and phosphoric acid"**, Fertiliser Science and Technology, Series 3, (1989).

3. Corobridge D.E.C., **"Phosphorus An outline of its chemistry, biochemistry and technology"**, Second edition, Elsevier, (1980).

4. Slack A.V., **"Phosphoric acid"**, Fertilizer Science and Technology Series, Part 1, Marcel Dekker, (1968).

5. Roux E.H., De Jager D.H., Du Plooy J.H., Nicotra A., Van Der Linde G.J. and De Waal P., **"Phosphate in South Africa"**, Journal of South African Institute of Mining and Metallurgy, volume 89, no.5, pp. 129-139, (1989).

6. Kruger A. and Fowles R.G., **"The Effect of Extraneous Soluble Ions in Igneous Rock Phosphate on Crystallography of Gypsum Dihydrate and Thus Phosphoric Acid Production"**, To be published, IFA proceedings, September (1998).

CHAPTER 2

FROM INDUSTRIAL PLANT TO BENCH-SCALE

2.1 THE DIHYDRATE SYSTEM:

In the early development stages, dihydrate systems showed very dissimilar design features. Intense investigation of dihydrate process chemistry has thoroughly established the basic principles governing the process. Unfortunately, several drawbacks of the dihydrate processes remain, some of them inherent in the system itself. Relative weak product acid (27-30 per cent P_2O_5) and consequently high downstream energy consumption, and 4-6 per cent P_2O_5 losses, most of them co-crystallised P_2O_5 within the crystal lattice of calcium sulphate dihydrate, that are disposed of, are a few.

The advantages of dihydrate systems are:

1. There is no phosphate rock quality limitation.
2. On-line time is high.
3. Operation temperatures are low.
4. Start-up and shutdown are easy.
5. Large units can be built.
6. Wet rock can be used (saving drying costs for phosphate rock).

A dihydrate process can be considered to be made up of the following section:

1. A phosphate grinding section (for most cases).
2. Metering of the raw materials and recycled wash acid from the filter.
3. A phosphoric acid reaction section, where gypsum is formed.
4. A filtration section, where 28-30 per cent P_2O_5 product acid is separated from the gypsum crystals.

2.1.1 PHOSPHATE GRINDING SECTION:

Some grades of commercial rock do not need grinding, their particle size distribution being acceptable for a dihydrate reaction section. Most phosphate rock, however, needs particle size reduction, generally by ball or rod mills, with roller mills used for small units. The particle size distribution currently required for a dihydrate reaction system is 60-70 per cent below 150μm.

2.1.2 METERING OF RAW MATERIALS:

Phosphate rock feed, sulphuric acid flow, and recycle acid from the filtration section must continuously be fed, and precisely controlled by the weight belts of flow meters. Variations within the feed ratio are likely to disturb regular crystal growth. They are responsible for coating, increasing co-crystallised losses, as well as producing variable filtration characteristics of the gypsum cake that could result in higher soluble losses.

2.1.3 PHOSPHORIC ACID REACTION SECTION:

The reactor is the heart of a phosphoric acid unit. Whether single- or multi-tank, it contains an agitated reaction volume in circulation. Often a buffer tank, out of the circulation and installed before the filter, is suppose to give an additional correction to the total retention time of the phosphate particles. The cooling necessary to maintain a temperature of 70-80°C in the reactor, and 70-75°C at the filter, is provided either by a cooling airflow, or by a vacuum cooling system of pumped slurry cycle.

2.1.4 FILTRATION SECTION:

Filtration rate is a function of phosphate quality; however, the use of additives (flocculent) can sometimes improve the filtration rates. Three filter types are currently used for wet process phosphoric acid production: belt filter, pan- filters, and table filters.

Filter operation usually involves three continuous stages. The product acid, containing 28-32 per cent P_2O_5, is separated from the gypsum in the first stage, and the remaining phosphoric acid is washed from the gypsum residue during the second and third stages. Fresh water is used as the wash on the third stage, and the filtrate from this is then circulated over the gypsum in the second stage, where the acid concentration reaches about 20 per cent P_2O_5. This filtrate is pumped back to the premixing tank. The recycling acid flow varies as a function of the P_2O_5/CaO ratio in the phosphate; the lower the ratio, the more P_2O_5 has to be recycled to keep the slurry composition within the necessary standards. This is one of the most important factors to consider when assessing a new rock versus the adapted process technology.

Product acid resulting from dihydrate operations currently yields 27-30 per cent P_2O_5 , but it can be lower when very low-grade rock is consumed. Calcium sulphate resulting from the reaction is calcium sulphate dihydrate, which is for most cases pumped to tailings dams.

2.2 DESIGN CONSIDERATIONS:

The slurry reactor is the most important part of the phosphoric acid unit. The design and the way it will be operated determine its functional reliability, the yield of recovery, and the final product quality.

The size of the reactor has to be large enough to [1]:

1. Provide sufficient retention time for the phosphate rock to be completely converted (the remaining unreacted rock should be economically negligible, ≤0.1 per cent).
2. Provide enough reaction and retention time for regular crystal growth, and adequate crystal size.
3. Permit breaking of foam and emulsion of the slurry, during and after the reaction section.

Most attention is generally paid to the first point. There is often the fear of unreacted rock, short-cutting the reaction section, especially when undivided single-tank reactors are to be used.

Agitation in the reactor tank has to provide good mixing of the slurry and the introduced reaction components, in order to achieve the reaction conditions between the phosphate rock and the sulphuric acid. Agitation also has to ease the release of the gases from the slurry, and break down the foam.

2.3 THE NEED FOR BENCH-SCALE OPERATIONS:

Phosphoric acid technology has to rely on raw materials of such a great variety and permanently fluctuating composition, that it has to readapt itself constantly. In terms of phosphoric acid producers, this constant re-adaptation of operating technology means experimentation.

Each type of ore has to be tested, bearing in mind the various possible beneficiation techniques, in order to choose the most economical one with a marketable product quality. New construction materials have to be tested for corrosion resistance and the different phosphoric acid processes have to be tested with the individual ores. It is

obvious that, for economical and technical reasons, this experimentation can not be operated with large industrial-sized units. This is where bench-scale and pilot-plant units can play an important role. Their small size offers the required economical and technical flexibility and the proven reliability gives the rock producer and consumer the necessary information and confidence to implement their future developments.

2.4 DEFINITION OF A BENCH-SCALE UNIT:

A bench-scale unit is too small to be built as a reduced equivalent. Some of the dominating extrapolation factors necessitate different technical concepts. To give an example, a large reactor has to be cooled; a bench-scale unit has to be heated.

It can be installed in a laboratory room equipped with a good air hood, with a relative low capital investment. Relative small amounts of ore sample are necessary and operating is quick and flexible.

2.5 DESIGN OF BENCH-SCALE UNIT:

With the foregoing in mind, Foskor designed a bench-scale unit in co-elaboration with the Institute of Applied Materials to be used for Project Purephos.

2.5.1 APPARATUS:

A schematic diagram of the apparatus set-up is presented in Figure 2.1.
The bench-scale unit is composed of three main units:

1. Reaction/mixing section.
2. Filtration unit.
3. Receiver/holding vessel.

The reaction section is the section into which reagents, namely: sulphuric acid, commercial grade phosphoric acid and calcium hydroxide, were pumped, using peristaltic pumps. The function of this unit is to simulate the reaction/crystal formation section of a full- scale plant. It consists of a three-litre glass vessel, which is sealed with a multi-necked, removable flanged head. Provision is also made to pump slurry to the next section through a Teflon drainage tap at the bottom. Evaporation is controlled with a condenser, and the temperature of the unit is controlled with a water jacket around the vessel. Slurry is agitated with an overhead stirrer through a sealed shaft, and to ensure that the reagents are adequately mixed, the inner wall of the vessel is baffled.

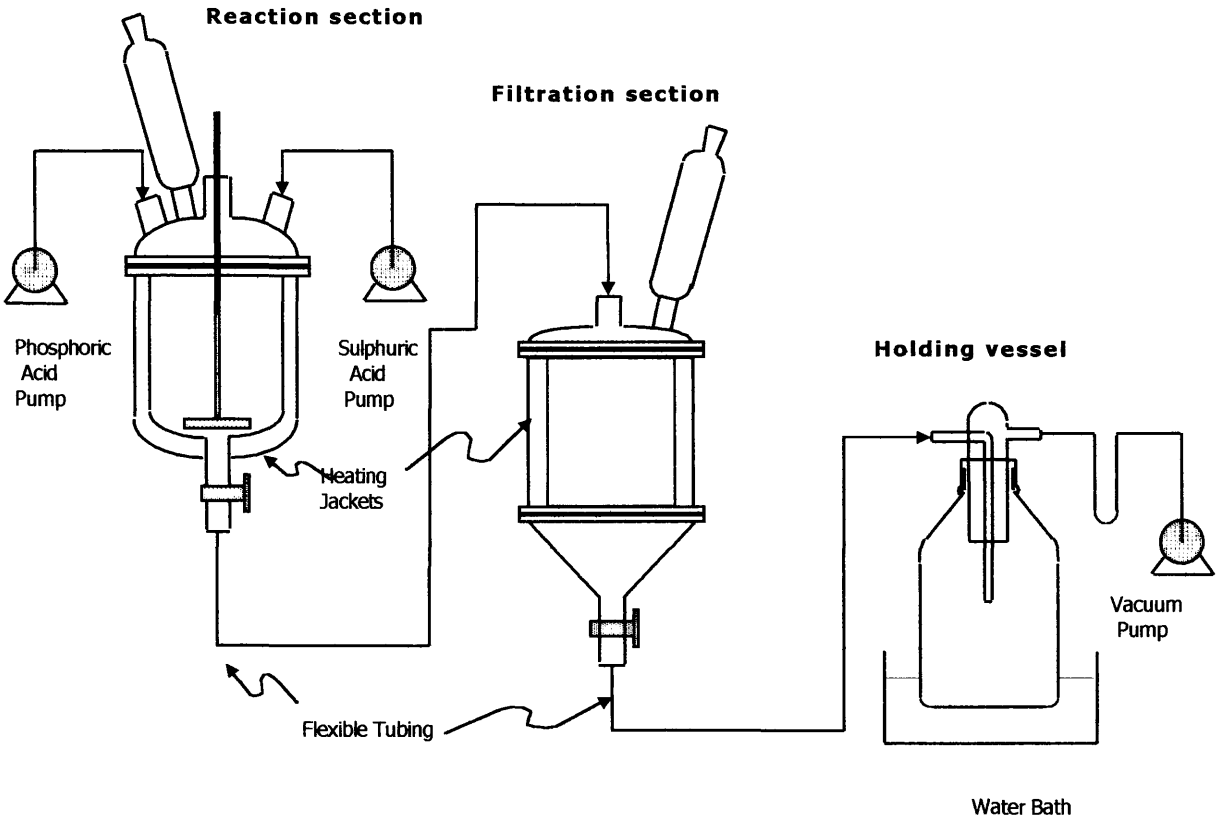

Figure 2.1. Schematic diagram of crystallisation test apparatus

The reaction unit leads, via sealed tubing, into the filtration section. The inside diameter is 110 mm, that is, an effective surface area of 38028.6 mm^2 (0.0380 m^2). The design of the filtration vessel is such that the drum of the filter can be removed from the bottom funnel (in a flanged set-up). This makes the insertion of filter cloth, and removal of filtrated gypsum, possible. The top of the vessel is also multi-necked and evaporation is controlled with a condenser. The top of the vessel can be removed as well. Temperature control is the same as for the reaction vessel, that is, by means of a heating jacket around the drum.

The receiving vessel is a simple glass vessel of two-litre capacity. It receives the filtrated acid via flexible tubing and is connected to a vacuum pump and manometer in order to maintain a vacuum of 500 mm Hg during filtration.

2.5.2 EXPERIMENTAL PROCEDURE:

Reagents were pumped at precise measured flow-rates into the reaction vessel, which was heated to a nominal temperature of 80 °C and stirred at a suitable rate. Various effects were measured at this point, such as the rate of pumping, adding the sulphuric acid to the phosphoric acid, crystal nucleation, and growth rate. Provision was made for sampling of the slurry formed during this stage. The sampling system incorporated a vacuum drawn system through a fine, porous, glass frit into a pre-weighed container. The sample was then completely digested with concentrated nitric acid. Sulphate, calcium, and other elements were then analysed at leisure.

Upon complete addition of the reagents, and after a predetermined retention time was allowed, the contents of the reactor was drained into the filtration section in which the solids was totally separated from the acid. The rate of filtration was determined from the time taken until all visible liquid was removed (in reality the cake would still

contain a significant amount of phosphoric acid). The filtrate was not circulated, and to compensate for this, a percentage gypsum (mass per mass) was added into the reaction slurry at the beginning of the experiments.

The weight and concentration of the phosphoric acid, collected in the receiving vessel, were determined. The mass, and the density of the total slurry and produced phosphoric acid, was recorded and the percentage solids calculated according to:

$$\% \text{ Solids} = \left[\frac{2.32\ (\text{Slurry density} - \text{acid density})}{\text{Slurry density}\ (2.32 - \text{acid density})} \right] \times \frac{100}{1} \qquad (2.1)$$

Where: 2.32 is the density of gypsum dihydrate

The cake was then thoroughly washed and sampled for further analyses and tests, e.g. recording of crystal quality and size, SEM (scanning electron microscope), IR (Infrared spectra), and other characteristics.

The rate of post-precipitation (and the characteristics of the precipitate) was also determined as a function of time. Produced phosphoric acid was left to stand for a minimum of four weeks before the post-precipitate was collected by means of filtration. The acid was then concentrated to 54 per cent P_2O_5, using a rotary evaporator. After two weeks, the acid was filtrated once more to collect the precipitated sludge.

2.6 LITERATURE CITED:

1. Becker P., **"Phosphates and phosphoric acid"**, Fertilizer Science and Technology, Series 3, (1989).

2. Slack A.V., **"Phosphoric acid"**, Fertilizer Science and Technology Series, Part 1, Marcel Dekker, (1968).

3. Kruger A. and Fowles R.G., **"The Effect of Extraneous Soluble Ions in Igneous Rock Phosphate on Crystallography of Gypsum Dihydrate and Thus Phosphoric Acid Production"**, To be published, IFA proceedings, September (1998).

CHAPTER 3

SATURATION AND SUPERSATURATION OF GYPSUM

3.1 INTRODUCTION:

The basic principle of wet process phosphoric acid production is usually described as the reaction of phosphate rock with sulphuric acid (H_2SO_4), to produce phosphoric acid (H_3PO_4) in solution and a calcium sulphate precipitate that is removed by filtration. In fact, when it enters the reaction medium, the phosphate rock does not come in contact with sulphuric acid at all, but rather a re-circulating stream of phosphoric acid that contains just a few per cent of free sulphuric acid [1].

It is in this way that the phosphate rock is best solubilized and made to give up its P_2O_5 content most effectively. The sulphuric acid present in the solution must be able to react effectively with the phosphate containing rock, so that little remains unreacted. Calcium sulphate crystals must be grown of a form that will give adequate filtration with minimum P_2O_5 loss. Thus, it is often said that the primary objective of any phosphoric acid unit is to make good gypsum/calcium sulphate [2]. This does not necessarily imply making large crystals, but it does mean that small crystals must be avoided in the production process.

The reaction conditions must be maintained, so that the sulphuric acid reacts with the phosphate rock as efficiently as possible. Stability of reaction conditions is needed above all else since the essence of the process is one of crystal growth. Maintaining such stability depends on the control of a number of interrelated parameters in the re-circulating reaction slurry, the most important of which are: solid content, acid strength (P_2O_5 percentage), temperature and sulphate (free sulphate level) [1, 2].

Once the control of the first three is well established, then successful day-to-day operation should only be a matter of sulphate control. However, the control of sulphate levels becomes practically impossible if P_2O_5 strength and solids content are

not controlled. Prayon likens the instability inherent in sulphate control to the analogy of a ball at rest on top of a hill – move it in any direction and it will begin to roll out of control [1].

Excess sulphate in the reaction slurry is the most effective factor in governing the crystallisation quality of gypsum, and therefore its filtration characteristics. Not only are the shape and size of crystals affected, but also the extent to which co-crystallised P_2O_5 is retained within the gypsum lattice.

Such co-crystallised losses are often the greater part of P_2O_5 losses, amounting to as much as 2-3.5 per cent of the total P_2O_5 input [2]. The tendency for co-crystallisation of P_2O_5 and consequent filter losses to occur, is increased when free sulphate levels are too low. Co-crystallisation, however, is also affected by many other factors, including the CaO/P_2O_5 ratio in the rock feed (reduced for igneous and hard rock) as well as the impurity levels in the rock. Optimum free sulphate levels vary for individual rock types and reaction systems, and are known by process developers for all main rock types, that are commercially used.

With the foregoing in mind, the first goal of project Purephos was to determine the optimum free sulphate levels for 88P rock, that is, determine the saturation and supersaturation diagram of calcium sulphate dihydrate. The influence of different sulphate levels on the crystallisation of the calcium sulphate dihydrate and the produced phosphoric acid was also determined.

3.2 EXPERIMENTAL:

3.2.1 APPARATUS:

The apparatus set-up is discussed in Chapter 2 (Section 2.5).

3.2.2 METHODOLOGY:

Phosphoric acid and gypsum (~5 per cent m/m), from Foskor's pilot plant, were first fed into the jacket-heated reactor to compensate for the absence of return-acid. The slurry was stirred and heated until the required temperature of 80 °C was reached. This temperature was maintained throughout the experiment.

Calcium hydroxide[1] (analytical reagent) and sulphuric acid (analytical reagent) were then fed into the reactor at specific rates[2], and gypsum was formed according to equation 3.1:

$$Ca(OH)_2 + H_2SO_4 \rightarrow CaSO_4 . 2H_2O \qquad (3.1)$$

It is clear that no dilution of the slurry took place, but in some cases, water was added to compensate for the volume that may have evaporated. Crystal habit modifier (Nanso SS 65) (~0.01g / 1500 g slurry) was dissolved in the water of experiments 9 - 11 to determine the influence of the modifier on the saturation and supersaturation diagram.

Either two (~5 min. and 1.5 hours), or three (0 min., ~5 min. and 1.5 hours) samples of slurry were taken during the retention time, as indicated in Table 3.2A and Table 3.2B. Sampling was done by submerging a porous glass frit (fitted on a glass tube) into the slurry and applying vacuum. The samples were diluted with nitric acid, to prevent the precipitation of calcium sulphate dihydrate, and then analysed for calcium and total sulphate.

---

[1] Calcium hydroxide was used instead of phosphate rock, the principle of calcium sulphate formation however, stays the same.

[2] It is important to note that the introduction of calcium hydroxide was not necessarily at a constant rate, the rate is however described in Table 3.1.

After a retention time, that varied for experiments, the slurry was pumped into the jacket heated filtration section where the solids were totally separated from the acid. Permeability of the gypsum was determined as the rate of filtration from the time taken until all visible liquid was removed, in reality the cake still contained a significant amount of phosphoric acid. The weight and volume of slurry were recorded in order to calculate the slurry density. Weight and volume of phosphoric acid produced were also recorded, and the percentage solids calculated according to equation 2.1. The cake was then thoroughly washed with acetone and sampled for analyses, infrared spectra and optical and electron microscope photographs.

Postprecipitate of the different samples was collected with filtration, after the phosphoric acid was allowed to stand for a minimum of four weeks. The mass postprecipitate per litre acid was calculated. Acid and postprecipitate samples were collected for further analyses, infrared spectra and optical and electron microscope photographs.

Reaction conditions for the experiments are presented in Table 3.1A and Table 3.1B.

3.2.3 ANALYSES OF SOLUTIONS AND SOLIDS:

Total sulphate determination of the three samples was done by titration with barium chloride and sulphonanzo III indicator, while the calcium was determined with ICP analyses. Acid samples were analysed for P_2O_5 and gypsum samples for total P_2O_5 only, by the colour development - UV spectrophotometric method.

Gypsum and postprecipitate samples were dried and IR spectra were recorded between 400 and 4000 cm^{-1} and between 50 and 650 cm^{-1} (Appendix I). The gypsum, postprecipitate and acid samples were analysed for different compounds as summarised in Table 3.3 and Table 3.4, with ICP analyses.

	EXP.1	EXP.2	EXP.3	EXP.4	EXP.5	EXP.6	EXP.7	EXP.8
Date	18/3/97	24/3/97	7/4/97	8/4/97	9/4/97	10/4/97	14/4/97	15/4/97
Phosphoric acid	1002.3 g.	1005.5 g.	1005.0 g.	1002.3 g.	1007.6 g.	1009.1 g.	1000.8 g.	1004.0 g.
Gypsum	50.0 g.	50.0 g.	100.0 g.	100.0 g.	50.0 g.	50.0 g.	50.0 g.	50.0 g.
Reagent addition Time	120 min.	180 min.	240 min.	240 min.	240 min.	150 min.	120 min.	120 min.
Water	109 ml.	203 ml.	75 ml.	30 ml.	25 ml.	20 ml.	10 ml.	0 ml.
Calcium hydroxide	198 g. (16.5g / 10min)	198 g. (11g / 10min)	175 g. (3.7g / 5min)	175 g. (1.8g / 2.5min)	197 g. All in first 20 min.	197 g. (13.2g / 10min)	198 g. (16.5g / 10min)	178 g. (14.8g / 10min)
Sulphuric acid	140 ml. (1.16ml / min)	140 ml. (0.80ml / min)	122 ml. (0.50ml / min)	122 ml. (0.50ml / min)	140 ml. (0.50ml / min)	140 ml. (0.90ml / min)	140 ml. (1.17ml / min)	140 ml. (1.17ml / min)
Retention time	80 min.	120 min.	108 min.	125 min.	80 min.	120 min.	180 min.	180 min.
Mass samples	66.9 g.	61.5 g.	83.5 g.	60.6 g.	78.8 g.	98.2 g.	81.7 g.	86.5 g.
Mass slurry	1367.8 g	1605.2 g	1457.9 g	1454.1 g	1390.3 g	1312.4 g	1290.7 g	1274.0 g
Total mass	1434.7 g.	1666.7 g.	1541.4 g.	1514.7 g.	1496.1 g.	1410.6 g.	1372.4 g.	1360.5 g.
Volume slurry	1000 ml.	1000 ml.	1000 ml.	800 ml.	750 ml.	800 ml.	750 ml.	780 ml.
Permeabi-Lity	2.2 min.	-	1 min.	1 min.	2.2 min.	1.2 min.	>3 min.	>4 min.
Mass gypsum *	642 g.	604 g.	723 g.	767 g.	1039 g.	938 g.	911 g.	913 g.
Volume acid	600 ml.	800 ml.	600 ml.	590 ml.	300 ml.	400 ml.	350 ml.	400 ml.
Acid density (Kg/L)	1.27	1.27	1.27	1.28	1.28	1.28	1.32	1.32
% Solids	33.8%	33.8%	33.8%	32.7%	32.7%	32.7%	28.0%	28.0%
Postprecipi-tate (Kg/L)	0.01	0.01	0.017	0.01	0.015	0.01	0.004	0.004

Table 3.1A. Reaction conditions and results.

* *Gypsum with unfiltrated acid*

	EXP.9	EXP.10	EXP.11
Date	28/5/97	29/5/97	2/6/97
Phosphoric acid	1000.5 g.	1006.2 g.	1004.8 g.
Gypsum	50.0 g.	50.0 g.	50.0 g.
Reagent addition Time	180 min.	180 min.	180 min.
Water + CHM	80 ml.	80 ml.	80 ml.
Calcium hydroxide	198.0 g. (11g / 10min)	198.0 g. (11g / 10min)	198.0 g. (11g / 10min)
Sulphuric acid	140 ml. (0.78ml/ min)	145 ml. (0.80ml/ min)	150 ml. (0.83ml/ min)
Retention time	110 min.	120 min.	120 min.
Mass samples	72.4 g.	63.7 g.	63.3 g.
Mass slurry	1347.1 g.	1504.5 g.	1488.8 g.
Total mass	1419.5 g.	1568.2 g.	1552.1 g.
Volume slurry	860 ml.	900 ml.	900 ml.
Permeabi-Lity	2.24 min.	2.08 min.	2.41 min.
Mass gypsum *	903.5 g.	908.0 g.	901.2 g.
Volume acid	400 ml.	480 ml.	500 ml.
Acid density (Kg/L)	1.3	1.28	1.28
% Solids	30.0%	32.7%	32.7%
Postprecipi-tate (Kg/L)	0.006	0.010	0.009

Table 3.1B. Reaction conditions and results.

** Gypsum with unfiltrated acid*

3.3 RESULTS:

3.3.1 ANALYSES:

The different results are summarised as follows:

Table 3.2A and Table 3.2B

Calcium and sulphate analyses of the samples taken during the retention time, acid samples after one day, and acid samples after four weeks. Analyses of the acid samples (after four weeks) for:Al_2O_3, Cu, K_2O, MgO and SiO_2.

Table 3.3

Analyses of the gypsum samples taken, after the cake was washed with acetone, for: fixed P_2O_5%, CaO%, MgO%, Al_2O_3%, Fe_2O_3%, F^-%, SiO_2%, Na_2O%, K_2O%, SrO%, CeO_2 ppm, La_2O_3 ppm, Y_2O_3 ppm, and Nb_2O_3 ppm.

Table 3.4

Analyses of postprecipitate samples taken, after it was washed with acetone, for: fixed P_2O_5%, CaO%, MgO%, Al_2O_3%, F^-%, SiO_2%, SO_4%, Na_2O ppm, K_2O ppm, Fe_2O_3 %, and SrO%. Not all the postprecipitate samples were analysed, in some cases the postprecipitate was not enough.

The Tables are presented below.

Experiment	1	2	3	4	5	6	7	8
Sulphate analyses *Sample 1*	5.9%	6.4%	2.1%	3.0%	2.5%	2.3%	6.4%	8.7%
Sample 2	5.9%	6.7%	2.1%	2.8%	2.2%	2.3%	6.4%	8.6%
Sample 3	6.1%	6.8%	2.2%	2.2%	2.0%	2.5%	6.4%	7.8%
Sample 4 (1 day)	4.5%	5.6%	1.4%	1.9%	1.3%	1.8%	5.8%	7.7%
acid (30 days)	4.0%	5.0%	1.2%	1.6%	1.4%	1.6%	5.7%	7.7%
Calcium analyses *Sample 1*	0.18%	0.18%	0.54%	0.28%	0.24%	0.27%	0.08%	0.07%
Sample 2	0.15%	0.17%	0.31%	0.30%	0.27%	0.25%	0.09%	0.07%
Sample 3	0.15%	0.19%	0.30%	0.25%	0.28%	0.25%	0.09%	0.08%
Sample 4 (1 day)	0.09%	0.08%	0.17%	0.13%	0.13%	0.13%	0.03%	0.03%
Acid (30 days)	0.05%	0.06%	0.08%	0.05%	0.06%	0.05%	0.02%	0.01%
CaO% *Sample 1*	0.25%	0.25%	0.49%	0.39%	0.33%	0.39%	0.11%	0.11%
Sample 2	0.21%	0.25%	0.43%	0.41%	0.38%	0.35%	0.13%	0.11%
Sample 3	0.21%	0.27%	0.43%	0.35%	0.39%	0.35%	0.13%	0.11%
Sample 4 (1 day)	0.13%	0.12%	0.24%	0.18%	0.18%	0.19%	0.037%	0.04%
Acid (30 days)	0.07%	0.09%	0.12%	0.07%	0.10%	0.07%	0.02%	0.02%
P_2O_5 *Gypsum*	3.63 ppm	4.55 ppm	10.68 ppm	11.8 ppm	11.6 ppm	15.5 ppm	9.1 ppm	12.1 ppm
P_2O_5 *acid*	25.9%	24.9%	29.7%	28.9%	28.4%	34.2%	34.1%	39.1%
Al_2O_3 *acid*	0.02%	0.02%	0.02%	0.02%	0.02%	0.02%	0.01%	0.01%
Cu *acid*	0.002%	0.002%	0.002%	0.002%	0.002%	0.002%	0.002%	0.002%
K_2O *acid*	0.02%	0.02%	0.02%	0.02%	0.02%	0.02%	0.29%	0.01%
MgO *acid*	0.35%	0.36%	0.37%	0.37%	0.41%	0.39%	0.29%	0.27%
SiO_2 *acid*	0.95%	0.93%	0.94%	0.83%	0.87%	0.84%	0.96%	0.95%

Table 3.2A. Analyses of samples taken during retention time and acid analyses.

Experiment	9	10	11
Sulphate analyses *Sample 1*	4.6%	2.5%	3.0%
Sample 2	4.1%	2.45%	2.9%
Sample 3 (1 day)	3.6%	1.9%	2.58%
acid (30 days)	3.6%	1.9%	2.3%
Calcium analyses *Sample 1*	0.16%	0.26%	0.22%
Sample 2	0.15%	0.24%	0.20%
Sample 3 (1 day)	0.05%	0.14%	0.12%
Acid (30 days)	0.02%	0.04%	0.04%
CaO% *Sample 1*	0.22%	0.36%	0.30%
Sample 2	0.21%	0.34%	0.28%
Sample 3 (1 day)	0.07%	0.20%	0.17%
Acid (30 days)	0.03%	0.06%	0.05%
P_2O_5 *acid*	22.3%	26.5%	26.0%
Al_2O_3 *acid*	0.02%	0.02%	0.01%
Cu *acid*	0.002%	0.002%	0.002%
K_2O *acid*	0.012%	0.012%	0.013%

Table 3.2B. Analyses of samples taken during retention time and acid analyses.

	Exp.1	Exp.2	Exp.3	Exp.4	Exp.5	Exp.6	Exp.7	Exp.8	Exp.9	Exp.10	Exp.11
Fixed P_2O_5 %	2.1	7.0	8.5	6.8	10.5	10.6	8.2	3.6	1.7	6.3	3.8
CaO%	26	30	26	31	20	41	52	30	29	29	27
MgO %	0.01	0.01	0.01	0.03	0.01	0.03	0.03	0.01	<0.01	<0.01	<0.01
Al_2O_3 %	0.01	0.01	0.01	0.01	0.01	0.01	0.01	0.01	<0.01	0.03	0.01
Fe_2O_3 %	0.14	0.03	0.02	0.03	0.04	0.03	0.03	0.01	<0.01	<0.01	<0.01
F^- %	0.05	0.22	0.28	0.25	0.42	0.38	0.32	0.12	<0.01	0.03	<0.01
SiO_2 %	0.02	0.23	0.10	0.14	0.24	0.17	0.17	0.03	<0.01	0.03	0.01
Na_2O %	0.23	0.16	0.16	0.13	0.14	0.12	0.12	0.10	0.01	0.01	0.01
K_2O %	0.02	0.03	0.04	0.05	0.06	0.05	0.03	0.04	<0.01	0.01	0.02
SrO %	0.028	0.026	0.036	0.039	0.019	0.022	0.027	0.034	0.080	0.040	0.070
CeO_2 ppm	154	176	194	277	62	158	220	237	265	263	271
La_2O_3 ppm	80	85	107	122	40	74	100	110	88	74	77
Y_2O_3 ppm	28	30	30	31	21	25	39	42	11	21	14
Nb_2O_3 ppm	138	166	166	171	80	133	195	197	202	191	205

Table 3.3. Analyses of gypsum samples.

	Exp. 3	Exp. 4	Exp. 5	Exp. 6	Exp. 7	Exp. 8
Fixed P_2O_5 %	3.22	5.94	3.34	3.00	1.32	1.31
CaO %	25.96	24.34	22.77	23.28	22.81	23.83
MgO %	0.08	0.07	0.13	0.07	0.01	0.19
Al_2O_3 %	0.004	0.003	0.008	0.004	0.001	0.004
F %	<1	<1	<1	<1	I/S	I/S
SiO_2 %	0.012	0.011	0.027	0.005	0.005	0.014
SO_4 %	49.0	46.0	44.0	49.0	48.0	56.0
Na_2O ppm	794	678	687	539	558	576
K_2O ppm	278	182	204	229	74	125
Fe_2O_3 %	0.03	0.02	0.03	0.02	0.01	0.01
SrO %	0.07	0.07	0.05	0.04	0.03	0.02

Table 3 4. Analyses of postprecipitate samples.

3.4 DISCUSSION:

3.4.1 REACTION AND CRYSTALLISATION:

Phosphoric acid is produced by reacting sulphuric acid with naturally occurring phosphate rock. The reaction combines calcium from the phosphate rock with sulphate from sulphuric acid, and the resulting calcium sulphate is separated from the reaction solution by precipitation. Most of the time, it is calcium sulphate with two molecules of water – dihydrate. If $CaSO_4.{}^1/_2\ H_2O$ is precipitated, it is a hemihydrate process.

A simplified reaction equation for the dihydrate process can be depicted as follows:

$$Ca_3(PO_4)_2 + 3H_2SO_4 + 6H_2O \rightarrow 2H_3PO_4 + 3CaSO_4.2H_2O \qquad (3.2)$$

The reaction occurs in the presence of an excessively large amount of phosphoric acid. Reaction 3.2 is an oversimplification of what actually takes place. The real occurrences within the reaction medium is better described by dividing it into three parallel and simultaneous reaction [2]:

1. When sulphuric acid dispersed in the reaction medium:
$$H_2SO_4 \rightarrow 2H^+ + SO_4^{2-} \qquad (3.3)$$

2. The attack of H^+ ions on the phosphate rock particles, which are introduced and dispersed in the slurry:
$$nH^+ + Ca_3(PO_4)_2 \rightarrow 2H_3PO_4 + (n\text{-}6)H^+ + 3Ca^{2+} \qquad (3.4)$$

The H^+ ions participating in this reaction belong to the sulphuric acid, as well as to the excess phosphoric acid, in the slurry. There are about 25 times more H_3PO_4 than H_2SO_4 molecules.

3. Ca^{2+} ions encounter SO_4^{2-} with consequent crystallisation:

$$Ca^{2+} + SO_4^{2-} + 2H_2O \rightarrow . CaSO_4.2H_2O \qquad (3.5)$$

The first reaction, that is ionisation of sulphuric acid, is instantaneous when the acid is dispersed within the slurry.

The second reaction, to separate the calcium ion, Ca^{2+}, from the rock particles, takes more time and is slow enough to be measurable. Most rock, however, react 95 per cent in less than 5 minutes. As the rock phosphate is introduced into the reaction medium, the particles are dispersed and impregnated by phosphoric acid. Hydrogen ions from the acid medium then attack the tri-calcium phosphate to liberate P_2O_5 into solution. Calcium ions from the rock are also liberated into solution. The chemical and physical mechanisms that occur depend heavily on the solubility characteristics of calcium sulphate, that is the behaviour of Ca^{2+} and SO_4^{2-} ions in the solution [1].

As for the third reaction, once the Ca^{2+} ion diffuses from the solid into the liquid phase, a crowd of SO_4^{2-} ions, as well as the liquid itself, which contains a large number of crystals, will surround it. Both SO_4^{2-} ions and the crystal surfaces will offer the Ca^{2+} ion some sort of attachment. The third reaction, being the slowest of the three, tends to let the sulphate and calcium ions accumulate in the liquid phase.

The sulphate ions in solution is a function of the sulphate fed to the reactor, both sulphuric acid feed and return acid, less the sulphate precipitated by the calcium released from the rock by dissolution of the phosphate. The amount of calcium ion in the solution is a function of the amount of phosphate solubilized, which is also a

function of the total sulphate. Calcium and sulphate ions in fact come to equilibrium, governed by the solubility of the calcium sulphate.

When calcium sulphate crystals are suspended in a phosphoric acid solution, the solubility product can be written:

$$SO_4^{2-} \text{ X } Ca^{2+} = K^1 \qquad (3.6)$$

As a matter of convenience, instead of the traditional molar concentration, the percentages of sulphate ions and CaO can be used [2]. At 75°C, with crude wet process acid, this gives:

$$K_s = SO_4\% \text{ x } CaO\% = 0.83 \qquad (3.7)$$

In reacting slurry, K_s increase substantially because of a state of supersaturation.

3.4.2 THE CaO/SO_4 SATURATION AND SUPERSATURATION DIAGRAM:

The CaO/SO_4 saturation and supersaturation diagram for 88P rock, as determined by experimentation, is presented in Figure 3.1. The CaO/SO_4 diagram shows Ca^{2+} and SO_4^{2-} solubility concentration lines, in a 30 per cent P_2O_5 wet process phosphoric acid and calcium sulphate dihydrate suspension. As a matter of convenience, the

---

[1] Kurteva and Brustus [13] found that
$C_{ca}(C_{SO4})^n = K_s$
Where n = 1.25 – 0.01t (t=temperature)
K_s = 0.460 x (2.40-log t)/0.912 x $(C_{P2O5})/100$
C_{ca} = concentration of Ca^{2+} wt.
C_{SO4} = concentration of SO_4^{2-}, wt.
C_{P2O5} = concentration of P_2O_5, wt.
Similar values could not be found for crude acid. The solubility product, however, can be applied with accuracy acceptable for industrial purposes.

concentrations on the diagram are expressed as a percentage weight of CaO and SO_4 in the phosphoric acid (values from Table 3.2A and Table 3.2B).

The y-axis represents the CaO concentration and the x-axis the SO_4 concentration. Thus, 1 per cent of SO_4 on the diagram is equivalent to 13g of SO_4 per litre of phosphoric acid (1000g acid = 0.767l acid), and 9.1g of SO_4 per litre of slurry (because of the 30 per cent solids in the slurry).

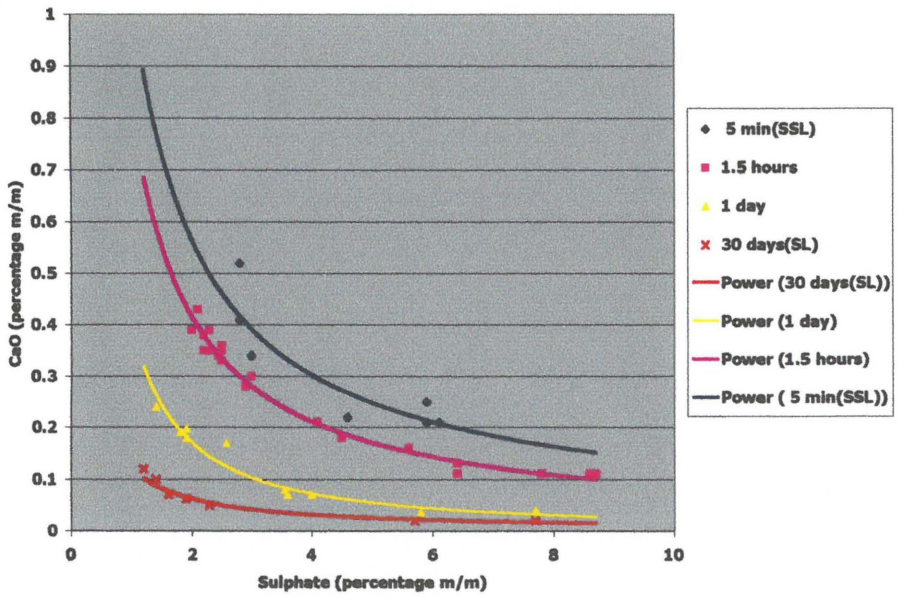

Figure 3.1. Supersaturation and saturation diagram of calcium sulphate dihydrate in 30 per cent P_2O_5 phosphoric acid[1].

When there is no reaction, the crystals and the solution are in equilibrium:

$$Ca^{2+} + SO_4^{2-} + 2H_2O \leftrightarrow CaSO_4.2H_2O \qquad (3.8)$$

The solubility product of Ca^{2+} and SO_4^{2-} can be written: $SO_4\% \times CaO\% \approx 0.83$ [2], at 75°C, in 30 per cent P_2O_5 phosphoric acid, when calcium sulphate crystals are in agitated suspension, but no reagents are added. At 25°C, the temperature at which

[1] 5 min. $y = 1.054x^{-0.897}$ $R^2 = 0.835$
1.5 hours $y = 0.818x^{-0.973}$ $R^2 = 0.981$
1 day $y = 0.399x^{-1.228}$ $R^2 = 0.946$
30 days $y = 0.1214x^{-0.965}$ $R^2 = 0.963$

the produced phosphoric acid were kept for four weeks before filtration, the solubility can be written: $SO_4\%$ x $CaO\% \approx 0.12$[1] This is shown by the SL line.

When SO_4^{2-} or Ca^{2+} ions are introduced into the system, which is in equilibrium, their concentrations will increase, and so will the co-ordinates of the solubility product. Simultaneously, SO_4^{2-} and Ca^{2+} ions will build up the crystals in what is called a regular crystal growth reaction (RCG) [2]. The solution is then in a state of supersaturation.

The more ions appear, the higher the supersaturation will be up to a level where spontaneous nucleation will take place [2, 3]. The SSL (supersaturation limit) line shows this limit. It is clear that whatever is beyond the boundary of the SSL line, will be exposed primarily to spontaneous nuclei formation (SNF).

The experimental results plotted on the SSL line can be mathematically represented as follows:

$$K_{SSL} = [CaO] \times [SO_4] \approx 1.06, \qquad (3.9)$$

with CaO and SO_4 expressed as a percentage weight in 30 per cent P_2O_5 phosphoric acid, at 80°C.

Reactants added beyond the SSL line are so quickly transferred into the solid crystal phase that no SO_4 or CaO value exceeding the SSL line can be detected. That means higher nucleation rates, but higher growth rates as well. The higher growth rates will compensate somewhat for the increased nucleation rate. Going beyond the SSL line is however avoided as far as possible.

[1] A value of 0.126 can be calculated at 25°C, using the equation of Kurteva and Brustus [2].

Below the SSL line, the crystallisation speed slows down and a number of parallel isokinetic lines can be drawn, the SL line having the speed ratio of zero. The crystallisation speed is a linear function of the difference of the solubility product of the isokinetic line under consideration and the SL line [2].

$$\phi(K_{ss} - K_s) = Q \qquad (3.10)$$

where:

K_{ss} = solubility product of the supersaturated solution (in percentage weight CaO and SO_4).

K_s = solubility product of the saturated solution (in percentage weight CaO and SO_4).

Q = quantity of gypsum, kg/m^3 slurry per hour, crystallised without spontaneous formation of nuclei (RCG reaction).

ϕ = Crystallisation mass transfer constant equivalent to 214 kg $(m^3)^{-1}$ when 30 per cent solids by volume in 30 per cent acid slurry at 75°C.

Using equation 3.10, with K_s = 0.83 and K_{ss} = 1.06, a crystallisation rate of ≈49 kg/m^3 slurry per hour, can be calculated for calcium sulphate dihydrate on the SSL line. This relationship is very important because it can be utilised for sizing reaction tanks and recycling volumes.

Beyond the SSL line, the calcium sulphate formation is too fast to be measured. While nucleation will take place, regular crystal growth should also be present, however, at a higher speed than what had been measured on the SSL line.

3.4.3 INTERPRETATION OF THE CaO /SO_4 DIAGRAM:

To illustrate the application of the CaO/SO_4 diagram, consider a phosphoric acid slurry with saturation and supersaturation diagram as depicted in Figure 3.2[1]. With all constituents held constant, the addition of sulphuric acid will result in a hypothetical horizontal move of the sulphate percentage, to the right along the abscissa.

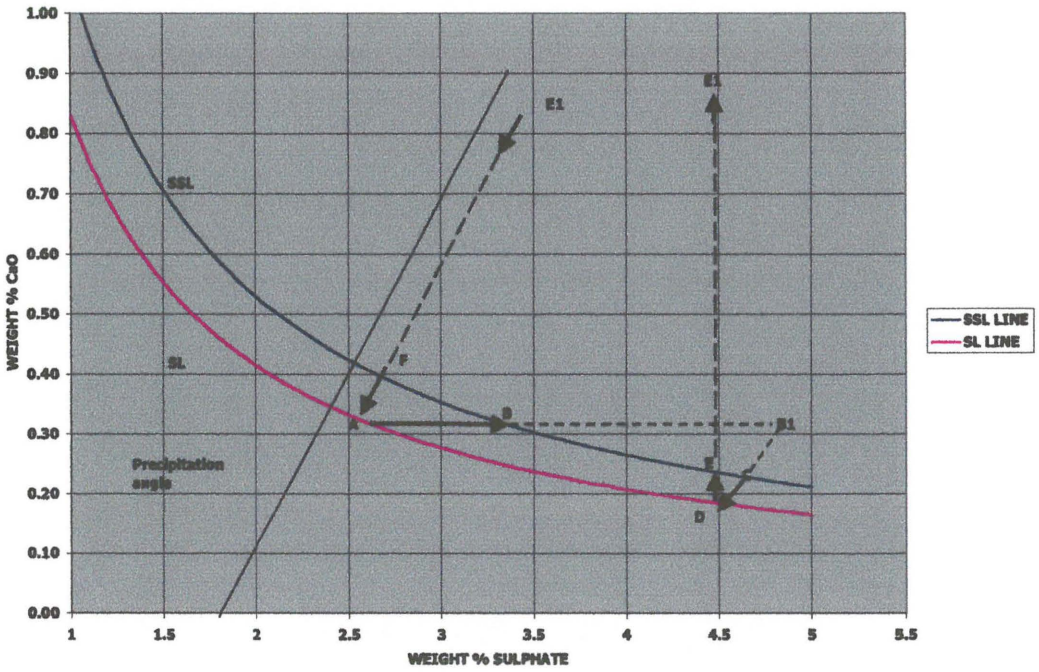

Figure 3.2. Interpretation of a supersaturation and saturation diagram of calcium sulphate dihydrate.

In Figure 3.2, if one starts from point A on the saturation line SL, and adds 2.25 per cent of SO_4 to the slurry all at once, the resulting CaO/SO_4 co-ordinates, assuming no precipitation, can be defined by the point B_1. Once the solution exceeds supersaturation beyond the SSL line, however, spontaneous precipitation will occur in addition to the regular crystal growth reaction, in this case at point B along the locus of line AB_1.

---

[1]The SL line represents the theoretical solubility product of 0.83, while the SSL line represents the experimentally determined supersaturation line.

Beyond B, with the continued addition of SO_4 the concentration will be deflected along the SSL line to point C, instead of proceeding to B_1, because of spontaneous precipitation of the calcium sulphate above the SSL line. Point C can be defined as the point where the theoretical $CaSO_4.2H_2O$ precipitation line, drawn through point B_1, intersects the SSL line. The slope of this line is the stoichiometric ratio 56:96, the respective molar weights of CaO and SO_4.

The amount of precipitating calcium sulphate dihydrate can be calculated, either from the CaO level of B and C on the SSL line, or from the SO_4 level of B_1 and C (in Figure 3.2 it is 0.10 per cent CaO, or 0.20 per cent SO_4, corresponding to 3.25kg of gypsum per cubic meter of slurry). In general, the amount of precipitation or crystallisation related to a move on the diagram between, for example point a and point b, is calculated with the weight balance of either the SO_4^{2-} or the Ca^{2+} ions between a and b [2]. The quantity of calcium sulphate precipitated during that move is proportional to the sum of the ions fed into the system, minus the concentration increase between point a and point b, on the diagram, for the respective ions.

At point C, continued precipitation will proceed along the extension of line B_1C to D. Line CD depicts the crystallisation and crystal growth of calcium sulphate from the SSL line, through the supersaturated area, to the SL line. At point D, CaO and SO_4 are in equilibrium.

With the addition of phosphate rock, amounting to 1.3 per cent CaO (equivalent to 2.25 per cent SO_4), added at once to the slurry and assuming that all the rock dissolve instantaneously, there will be a vertical rise of the CaO concentration from point D, to a hypothetical point E_1, crossing the supersaturation zone, and intersecting the SSL line at E. Instead of following the dashed line to point E_1 at 1.3 + 0.18 = 1.48 per cent CaO, once again the locus of changing concentration will go along the SSL line from E to F, with the resulting spontaneous precipitation of gypsum. Point F is where the

$CaSO_4$ precipitation line drawn through point E_1 intersects line SSL. The gypsum precipitated can be calculated from the different sulphate levels at point E and point F, or from the theoretical CaO level at point E_1 and point F. Finally, with continued precipitation and regular crystal growth beyond point F on line E_1F, the solution concentration will return to point A, on the saturation line, and the cycle will be completed, all of the 2.25 per cent added sulphate being precipitated as calcium sulphate.

3.4.4 INTRODUCTION OF SULPHURIC ACID:

To illustrate the introduction of sulphuric acid into the slurry, consider a sulphuric acid dispersion within saturated slurry at a ratio of 8.66 g of H_2SO_4 per litre of slurry. It corresponds to a 0.95 percentage weight change of SO_4 on the diagram.

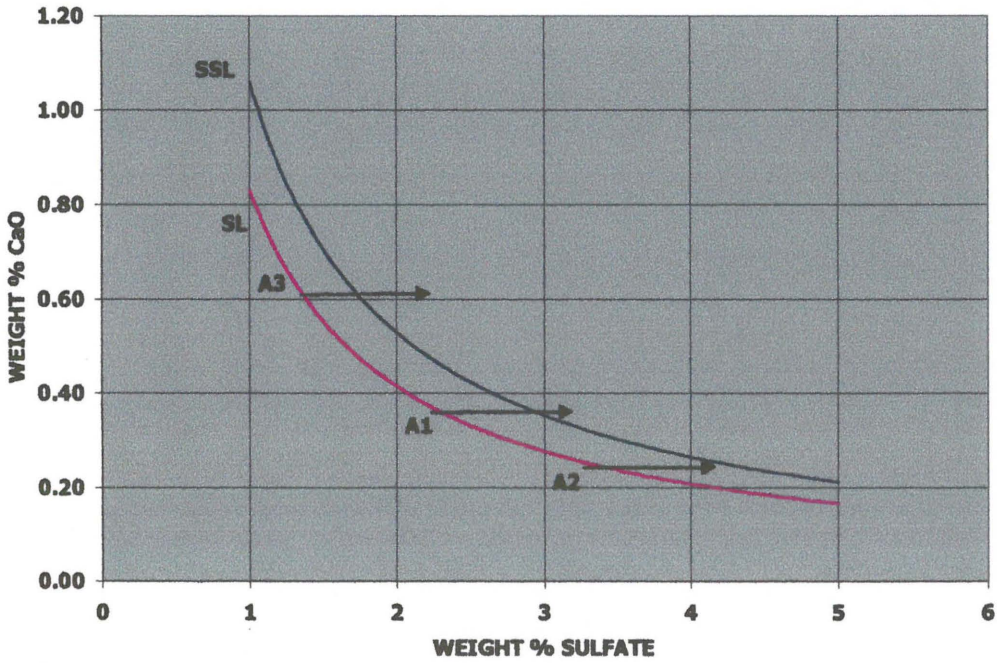

Figure 3.3. Effect of the introduction of 0.95 per cent sulphuric acid on the saturation and supersaturation diagram of calcium sulphate dihydrate.

If one starts from point A_1 on the SL line (Figure 3.3), 0.95 per cent of SO_4 will be added to the 2.2 per cent SO_4 already existing in the slurry. If the mixing is done at once, the SSL line will be exceeded with a margin of 0.29 per cent SO_4 and will promote spontaneous nucleation.

If one starts at point A_2, with 3.2 per cent initial SO_4 instead of the two per cent at A_1, the total amount of sulphuric acid can be fed into the slurry without exceeding the SSL line, and no spontaneous nucleation will occur. Starting at point A_3 however, most of the sulphuric acid added will contribute to spontaneous nucleation. This is because of the narrowing range of orderly crystallisation, the region between the S and SSL lines, when approaching low SO_4 concentrations.

The more nuclei produced, the smaller will be the mean size of the final crystals, and the poorer the filtration rates. This illustration shows why it is important to add sulphuric acid to a medium where the existing sulphate level is at a certain minimum [2].

3.4.5 INTRODUCTION OF PHOSPHATE ROCK:

The introduction of phosphate rock into the slurry will promote a vertical move of the operating point, due to the liberation of calcium from the raw material. In spite of the great speed of attack by the H^+ ions, the Ca^{2+} ions will not appear instantaneously in the slurry as the SO_4^{2-} ions do. The phosphate particles have to be dispersed, and impregnated by the phosphoric acid.

The phosphate rock attack kinetics is slow enough to be measured. Ground rock (70-80 per cent > 152μm) is generally decomposed by more than 90 per cent in less than 5-min. [2]. The initial reaction speed is always high, but it is the asymptotic final stage of the decomposition that characterises individual rock behaviour.

This is due mainly to the coating phenomenon, which is an over-vigorous crystallisation, completely enveloping the phosphate rock particle and protecting it from further rapid action by the attacking H^+ ions. Coating is emphasised by particle size, sulphuric acid concentration, as well as temperature [1].

The Ca^{2+} entities in solution, which are small compared even to finely ground phosphate rock, can infiltrate cavities in the rock particles. Since the H^+ ions are about four to five times faster than the SO_4^{2-} ions, it can be expected that the rock particles will have their porous cavities filled with a liquor containing many Ca^{2+} ions. Insoluble calcium sulphate can precipitate within an individual rock particle or around it as an impervious coating, if there is a large enough concentration of sulphate ions nearby. If allowed to happen, this would hinder further reaction of the phosphate rock [2].

3.4.6 THE EFFECT OF CRYSTAL HABIT MODIFIER ON THE SATURATION AND SUPERSATURATION DIAGRAM:

Dissolved organic and inorganic impurities interfere with the crystallisation of calcium sulphate dihydrate [4]. Such materials may change the nucleation conditions, the crystal growth rate, or the crystal habit. The activation energy for nucleation may be altered, and thereby the nucleation rate. If there is adsorption of impurities on the crystal surface, the growth rate is reduced, and if there is selective adsorption on some crystal surfaces, the crystal habit is influenced. As the name suggests, crystal habit modifier is used to alter the crystal habit and thereby improve filtration rates.

The calcium and sulphate analyses of the samples taken during Experiments 9 to 11 (Table 3.2B), compares well with that obtained for the other experiments. It can therefore be concluded that the crystal habit modifier added (0.01 per cent m/m) had no major effect on the saturation and supersaturation diagram.

3.4.7 INFRARED SPECTROSCOPY FOR DETECTING CO-PRECIPITATED P_2O_5 IN THE CRYSTAL LATTICE OF CALCIUM SULPHATE DIHYDRATE:

The P_2O_5 losses in the manufacture of wet-process phosphoric acid can be divided into three categories [4]:

1. Due to incomplete washing.
2. Due to unreacted phosphate rock (coating phenomenon).
3. Due to P_2O_5 incorporation into the calcium sulphate crystals.

The magnitude of the first type of loss depends on the strength of acid produced, filtration temperature, number of washes, crystal shape and size, and how much water, determined by the water balance, may be added for washing. With the proper process design, the second type of loss can be neglected.

The third kind, that is the incorporation of P_2O_5 into the crystal lattice of calcium sulphate dihydrate, was of special interest to this project. According to Elmore et. al. [5] the predominant ions in the phosphoric acid solutions are the H^+, $H_5P_2O_8^-$ and HSO_4^- ions. In the crystal lattice, however, it is more likely that an HPO_4^{2-} ion will replace an SO_4^{2-} ion [6, 7]. The problem has been closely studied by Fröchen and Becker [8], who found that all P_2O_5 in the calcium sulphate dihydrate crystal lattice is present as HPO_4^{2-} They verified this substitution by X-ray, thermogravimetric analysis, and differential thermal analysis

The HPO_4^{2-} ion can easily substitute for a sulphate ion, since these two ions are almost similar in size and share an affinity towards calcium ions. The similarity of these anions is also reflected by the existence of two comparable salts: $CaHPO_4.2H_2O$ and $CaSO_4.2H_2O$, which both crystallise in the monoclinic system with very similar unit cells. Both have a layered structure with alternating sheets of water molecules and anionic tetrahedra parallel to the (010) planes [9]. Ivanchenko et al. used infrared

spectroscopy for the qualitative analyses of co-precipitated P_2O_5, during the investigation of the influence of impurities on the co-precipitation [10].

Infrared spectra of all the gypsum and postprecipitate samples were recorded. The spectra of the gypsum sample of Experiment 1 are shown in Figure 3.4 and Figure 3.5, and that of Experiment 5 in Figure 3.6 and Figure 3.7. The spectra of the other samples are presented in Appendix I.

According to the gypsum analyses (Table 3.3), the infrared spectra depicted in Figure 3.4 and Figure 3.5 should indicate the presence of calcium sulphate dihydrate only, while the spectra in Figure 3.6 and Figure 3.7 should indicate the presence of co-precipitated P_2O_5 as well.

The observed frequencies and assignments are presented in Table 3.5. The infrared spectra reflect the similarity of the two ions. A comparison between the frequencies for $CaSO_4.2H_2O$ and $CaHPO_4.2H_2O$ in Table 3.5 shows the frequencies are very similar indeed. When calcium sulphate dihydrate and calcium hydrogen phosphate precipitate together, the result is very broad bands, making it difficult to distinguish between the bands of gypsum and that of co-precipitated phosphorus.

According to the analyses of the gypsum sample of Experiment 5 (Table 3.3), there is 10.5 per cent m/m co-precipitated P_2O_5 in the sample. As a result of the broadness and overlapping of peaks as explained above, this can not clearly be seen in the spectra. It is therefore concluded that the use of infrared spectroscopy for the quantitative analysis of co-precipitated P_2O_5 will only be possible if large amounts of P_2O_5 co-precipitated.

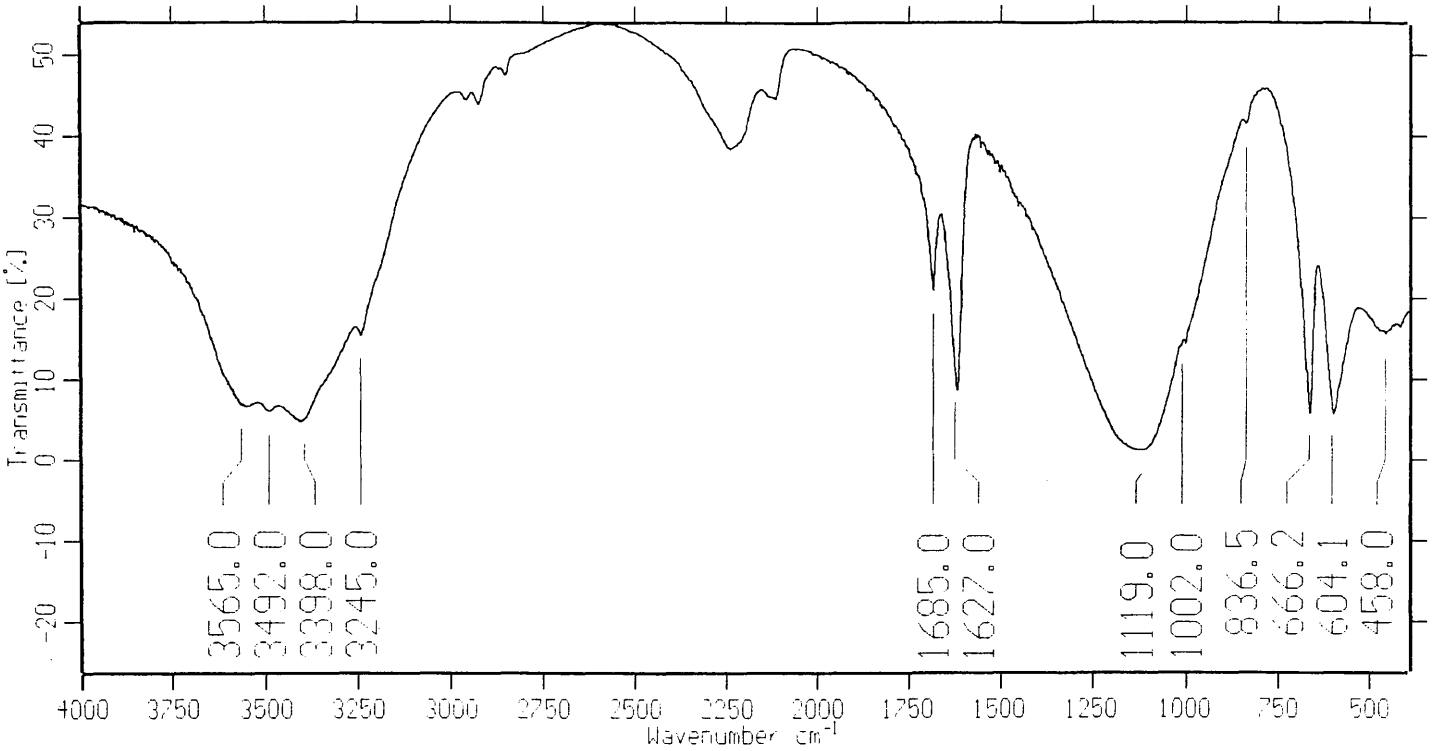

Figure 3.4. The Mid infrared spectrum of gypsum (Experiment 1).

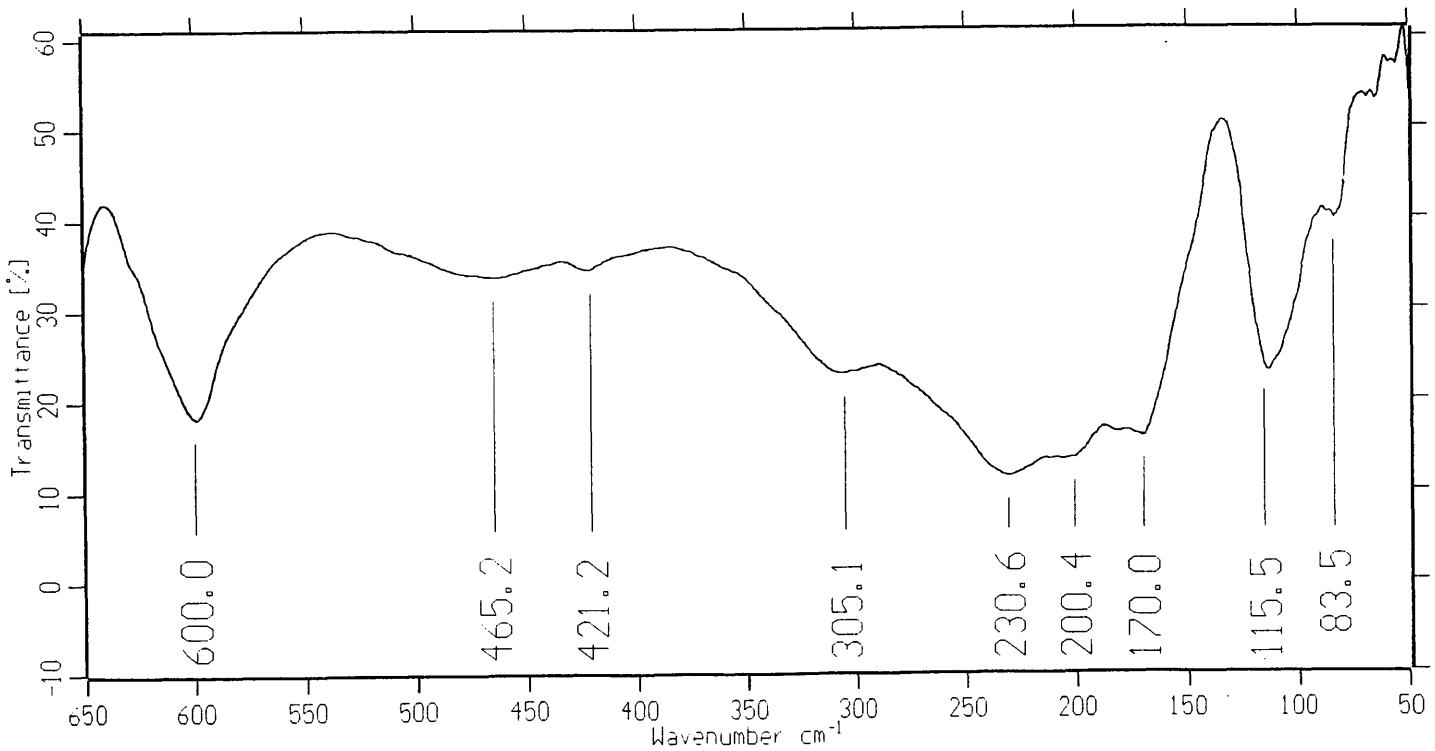

Figure 3.5. The Far infrared spectrum of gypsum (Experiment 1).

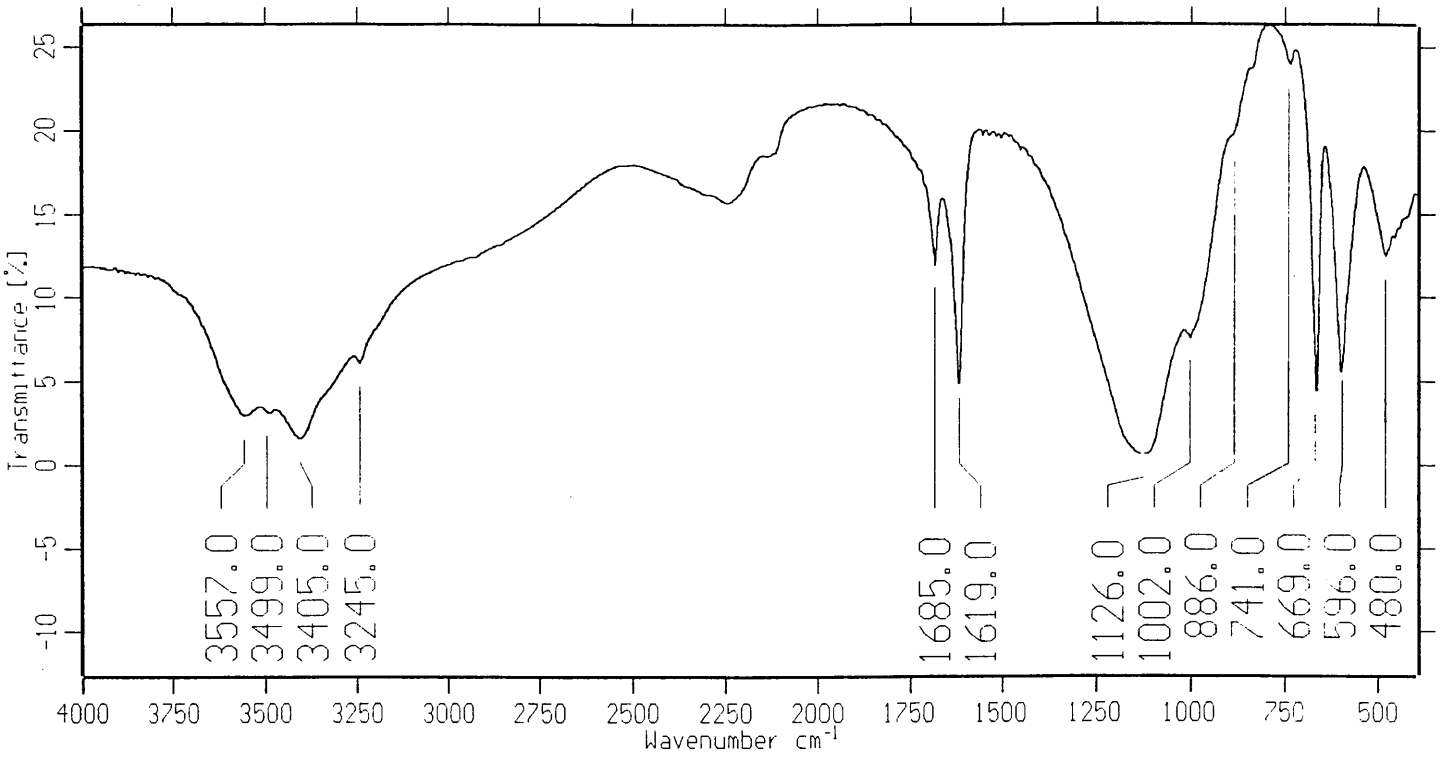

Figure 3.6. The Mid infrared spectrum of gypsum (Experiment 5).

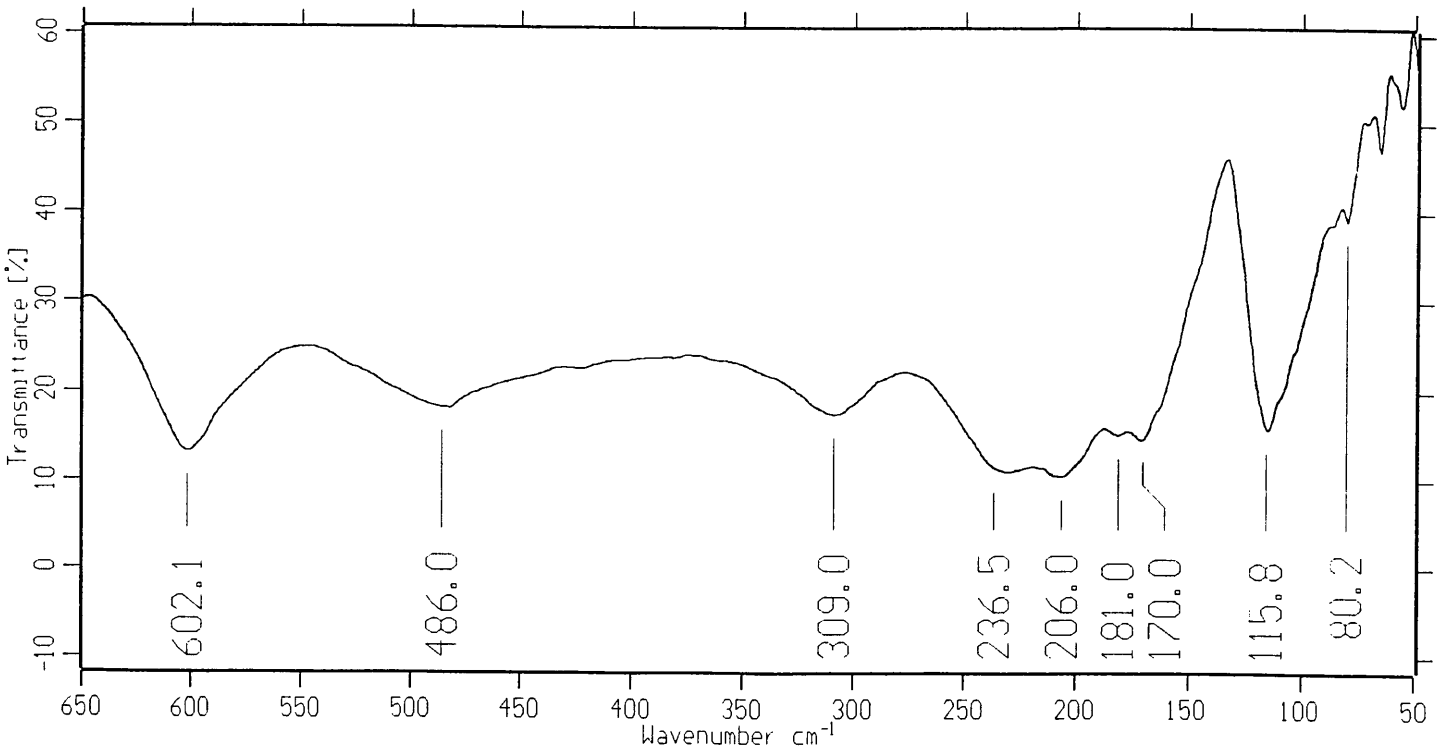

Figure 3.7. The Far infrared spectrum of gypsum (Experiment 5).

	$CaSO_4.2H_2O$	$CaHPO_4.2H_2O$	Experiment 1	Experiment 5
ν_1	1000 *Au* 1006 *Ag*	1005	1003	1002
ν_2	492, 413 *Ag*	418 400	465 421	480
ν_3	1131*Au* 1142 1118*Bu* 1144*Ag* 1138 1117*Bg*	1135 1075	1130(very broad)	1126(Very broad)
ν_4	602*Au* 674 604*Bu* 621*Ag* 669 624*Bg*	557	666 600	669 596
ν_{H2O}	3555 3500 3408 3250	3548 3490 3281 3163 2950	3567 3492 3398 3245	3557 3499 3405 3245
δ_{H2O}	1690 1629	1217 750	1685 1627	1685 1619

Table 3.5. Infrared frequencies (cm^{-1}) for $CaSO_4.2H_2O$ and $CaHPO_4.2H_20$ [11], and the assignment of the observed frequencies of Experiment 1 and Experiment 5.

3.4.8 CRYSTALLISATION OF GYPSUM AND POSTPRECIPITATE:

The importance of good quality gypsum for the production of phosphoric acid was already emphasised in the introduction.

When the concentration of CaO and/or SO_4^{2-} go beyond the supersaturation line for calcium sulphate dihydrate, there will be crystal nucleation as well as crystal growth. This will result in small crystals with poor filtration rates. In order to obtain crystalline precipitates having good filtration properties, mass crystallisation from solutions must be conducted at moderately low supersaturations [12].

Photographs were taken of the calcium sulphate dihydrate and postprecipitate samples, to investigate the influence of the sulphuric acid and calcium hydroxide addition rates on the crystal size and filtration rates obtained. All the calcium sulphate dihydrate crystals obtained were needle type crystals, typically of igneous rock. As a best case scenario, a photograph of a sample of the calcium sulphate dihydrate obtained in Experiment 3 is presented in Figure 3.8.

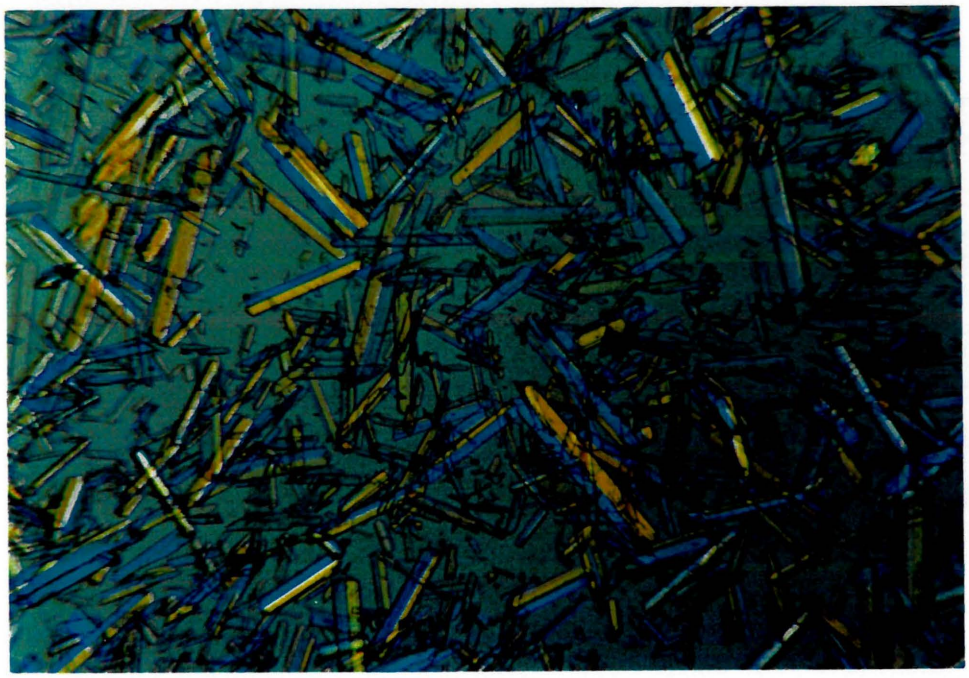

Figure 3.8 Calcium sulphate dihydrate obtained in Experiment 3 (100x

The best filtration rate was obtained for this experiment, that is one minute (Table 3.1A). Table 3.2A shows that the sulphate analyses never exceeded 2.1 per cent. It must be stated that this does not mean the sulphate percentage never exceeded this value, but that the value was the highest value obtained. The gypsum in Figure 3.8 is of a good quality with the resulting filtration rate.

On the other hand, a filtration rate of more than four minutes (Table 3.1A) was obtained for Experiment 8. The sulphate analyses in Table 3.2A show that a free sulphate level of 8.7 per cent was obtained. With the addition of calcium, the supersaturation level would certainly have been passed. The resulting small gypsum crystals and poor filtration rate is expected. A photograph of the poor quality calcium sulphate dihydrate obtained in Experiment 8 is shown in Figure 3.9.

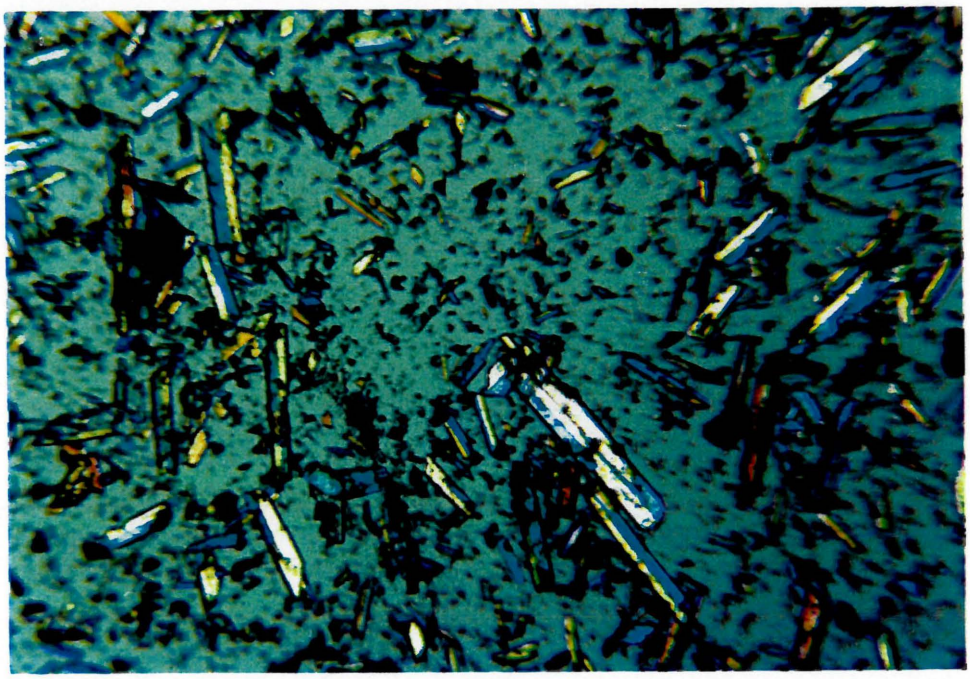

Figure 3.9 Calcium sulphate dihydrate obtained in Experiment 8 (100X magnified).

Although a decrease in free sulphate level usually results in an increase in co-precipitated P_2O_5 [1, 2, 4], at first it seems like this was not the case in this study. The free sulphate level is however not the only factor influencing the co-precipitation of P_2O_5.

It is also influenced by the following [4]:

1. P_2O_5 concentration of the phosphoric acid (the higher the concentration the more the co-precipitation, which is in accordance with mass action).
2. Solid content in the slurry (substitution decreases with increasing solid content). Within the 20 to 40 per cent solid content range normally found in practice, this has little effect on the substitution [8].
3. Reaction temperature (an increase in temperature, resulting in a decrease in supersaturation, decreases the substitution).
4. Changes in retention time (this has little effect as explained by the automatic self-adjustment of the supersaturation, so that nucleation and crystal growth create a balance against the addition of reactants).

When all of the above is taken into consideration, the co-precipitation analyses obtained can easily be explained.

The postprecipitate analyses (Table 3.4) show that the precipitates were mainly calcium sulphate dihydrate. There was no drastic change in impurity concentrations with different sulphate and/or calcium hydroxide addition rates. It can therefore be concluded that the precipitation of postprecipitate was not influenced by the rate of addition of sulphuric acid and/or calcium hydroxide.

3.5 CONCLUSIONS:

The necessity of the control of free sulphate levels for the production of calcium sulphate crystals with an adequate filtration rate is well known. It is important for the phosphoric acid producer to know the optimal free sulphate levels, that is the supersaturation and saturation solubility diagram for calcium sulphate dihydrate. This diagram is influenced by different factors, such as the temperature of the reacting

slurry, the strength of phosphoric acid, and soluble impurities contained in the reacting slurry. The only way to determine the diagram for a specific type of rock and operation conditions is by means of experimentation.

The calcium sulphate dihydrate saturation and supersaturation diagram was determined for 88P rock in the presence of 30 per cent P_2O_5 phosphoric acid at 80°C. The experimental results plotted on the SSL line can mathematically be represented as follows:

$K_{SSL} = [CaO] \times [SO_4] \approx 1.06.$

Interpretation of such a diagram was discussed, as well as the influence of the addition of sulphuric acid and phosphate rock. It was found that the added crystal habit modifier, Nanso SS 65, (Experiments 9-11) had no influence on the saturation and supersaturation diagram.

Infrared spectra were interpreted and the possibility of using this method for the quantitative analyses of co-precipitated P_2O_5 was investigated. It was concluded, however, that this method is not sensitive enough.

Analyses of free sulphate levels, filtration rates obtained, and photographs of the precipitated calcium sulphate dihydrate clearly showed that there is a relationship between high free sulphate levels, small crystals and poor filtration rates.

3.6 REFERENCES:

1. **"Automation aids sulphate control",** Phosphoric acid processing, Phosphorus and Potassium, no. 210, July-August (1997).

2. Becker P., **"Phosphates and Phosphoric acid"** Raw Materials, Technology and Economics of the wet process, Fertilizer science and technology series - Vol. 6., 2nd edition, (1989).

3. Potts L.W., **"Quantitative analyses: Theory and Practice"**, Harper and Row publishers, pp. 315-317, (1987).

4. Slack A.V., **"Phosphoric acid"** Part 1 Fertilizer science and technology series – Vol. 1., Marchel Dekker publishers, (1968).

5. Elmore K.L., Hatfield J.D., Dunn R.L., Jones A.D., **"Journal of Physical Chemistry"**, 69, (1965), 3520.

6. Van Der Sluis S., Witkamp G.J., Van Rosmalen G.M., **"Crystallization of calcium sulphate in concentrated phosphoric acid",** Journal of crystal growth, 79, pp. 620, (1986).

7. Waggaman W.H., **"Phosphoric acid, Phosphates and Phosphatic Fertilizers"**, 2nd edition, Reinhold publishers, (1952).

8. Fröchen J. and Becker P., **"Crystallization and Co-crystallization in the Manufacture of Wet-process Phosphoric acid"**, Paper presented at the Technical Meetings of the International Superphosphate Manufacturers' Association, Stockholm, (1959).

9. Rinaudo C., Lanfranco A.M., Franchini-Angela M., **"The system $CaHPO_4.2H_2O$-$CaSO_4.2H_2O$: crystallizations from phosphate solutions in the presence of SO_4^{2-} "**, Journal of Crystal Growth, 142, pp. 184-192, (1994).

10. Ivanchenko L. G., Guller B. D., Yu. Zinyuk R., and Vashkevich N. G., **"Co-precipitation of phosphates during crystallization of gypsum from phosphoric acid solutions",** Zhurnal Prikladnoi Khimii, Vol. 54, pp. 1001-1006, May (1981).

11. Farmer V. C., **"The Infrared Spectra of Minerals"**, Adlard and son publishers, p.393, 427, (1974).

12. Ivanov E.V., Ya Zinyuk R., Pozin M.E., **"Production Of Wet-Process Phosphoric Acid With Stepwise Feeding Of Apatite Concentrate"**, Zhurnal Prikladnoi Khimii, Vol. 54, No. 3, pp. 483-489, March (1981).

13. Kurteva, Brustus, Zhurnal Prikladnoi Khimii, Vol. 34, p. 1714, (1961).

CHAPTER 4

CALCIUM SULPHATE DIHYDRATE

4.1 INTRODUCTION:

The morphology of gypsum (calcium sulphate dihydrate) can be influenced by the following [1]:

1. Differences between the concentrations of the reaction solutions, that is the saturation levels of the solutions.
2. Temperature fluctuations.
3. Influence of foreign ions, impurities, on the crystallisation process.

The effect of saturation and supersaturation levels on the crystallisation of calcium sulphate dihydrate and the produced phosphoric acid was discussed in Chapter 3. The main objective of the second part of the study was, however, to investigate the influence of different impurities, commonly found by Foskor's clients, on the production of phosphoric acid.

Before the influence of specific impurities can be understood and discussed, it is necessary to look at a few aspects of calcium sulphate dihydrate from a theoretical point of view. In particular, the morphology and structure of calcium sulphate dihydrate, the crystallisation and growth processes involved, as well as the effect of impurities on the crystallisation process and phosphoric acid in general.

4.2 CRYSTAL STRUCTURE AND MORPHOLOGY:

Calcium sulphate dihydrate ($CaSO_4.2H_2O$) crystallises in the space group I 2/a, with the lattice constants a = 5.679 Å, b = 15.202 Å, c = 6.522 Å, $\beta = 118.43^0$ and Z = 4 [2]. The crystal structure of calcium sulphate dihydrate is presented in Figure 4.1.

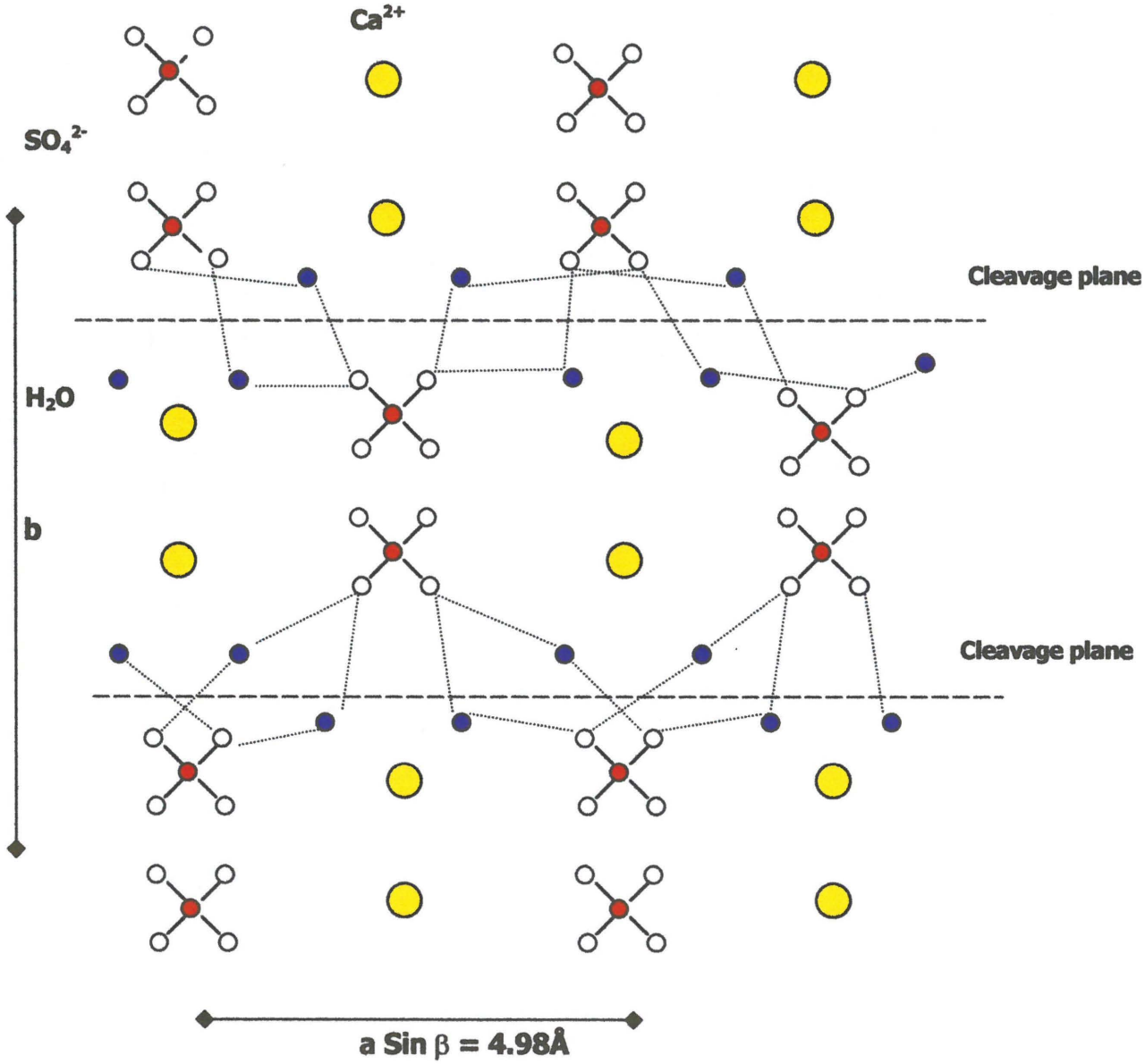

Figure 4.1. The structure of calcium sulphate dihydrate viewed along the z-axis, showing the way in which the (010) cleavage planes intersect hydrogen bonds between water molecules and sulphate tetrahedra.

The crystal structure of gypsum consists of layers of sulphate tetrahedra bound to calcium ions, parallel to the (010) plane. Sheets of water molecules separate the layers. The water molecules are directed with their hydrogen atoms towards the

oxygen atoms of the adjacent sulphate ions, and form hydrogen bonds with them. The weak bonding in the layers containing the water of crystallisation accounts for the perfect cleavage of gypsum [3].

Figure 4.2 depicts the morphology of a calcium sulphate dihydrate single crystal with commonly observed forms, where {xyz} refers to the set of planes symmetry related to (xyz), and <xyz> refers to the set of directions symmetry related to [xyz].

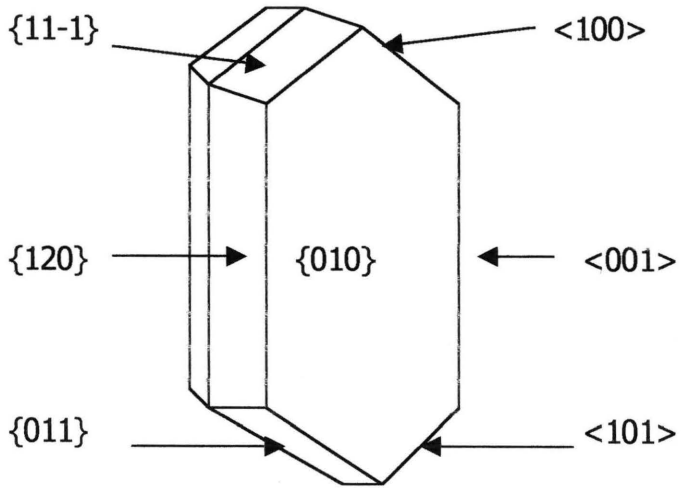

Figure 4.2. Gypsum crystal morphology with forms {010}, {120}, {011} and {11-1}.

4.3 CRYSTAL FORMATION:

The first stage, nucleation, corresponds to the production of new centres from which growth can occur. Nucleation is a very complicated phenomenon that has led to many theories. There is, however, a common driving force - saturation.

Several types of nucleation have been reported [4]:

1. Primary nucleation:

The nuclei form spontaneously out of the mother liquor. Nucleation is essentially effected by the level of supersaturation, but can also be effected by external influences such as agitation.

2. Secondary nucleation:

Nucleation is effected by the presence of solids in a supersaturated medium.

In a solution, there occur local, statistically governed variations in the concentration called fluctuations. The simplest fluctuation is the conjunction of two molecules to form a complex [5]. Of the many such complexes formed, some split apart again while others catch a third molecule. In this way, the building continues until small complexes are formed. Some of the complexes reach a critical size; those smaller than this size tends to split, while those greater have a predominant tendency to grow. A nucleus can be defined as a molecular complex or fluctuation, which has reached this critical size.

These aggregates of varying size may be depicted by minute, spherical droplets to which well-established theoretical considerations can be applied. The creation of a new surface requires energy, which is provided by the tendency of the supersaturated solution to deplete itself. There is therefore an energy balance between the creation of solid surfaces, nuclei, and the deposition process [6].

Another mechanism for the formation of large crystals and particles that precipitate from solution, is aggregation and coagulation of the crystallites that were initially formed in the supersaturated solution. In these processes, the charge at the solid/liquid interface plays an important part. Similar charged particles will tend to

remain dispersed in the aqueous phase due to electrostatic repulsion. Ions or molecules of opposite charge, which may be absorbed at the surface of these crystals, can therefore reduce the surface charge and induce agglomeration or aggregation. In the overall precipitation process, it is important to separate crystal growth and aggregation since both lead to the production of larger sized particles.

The different steps of precipitation are presented in Figure 4.3.

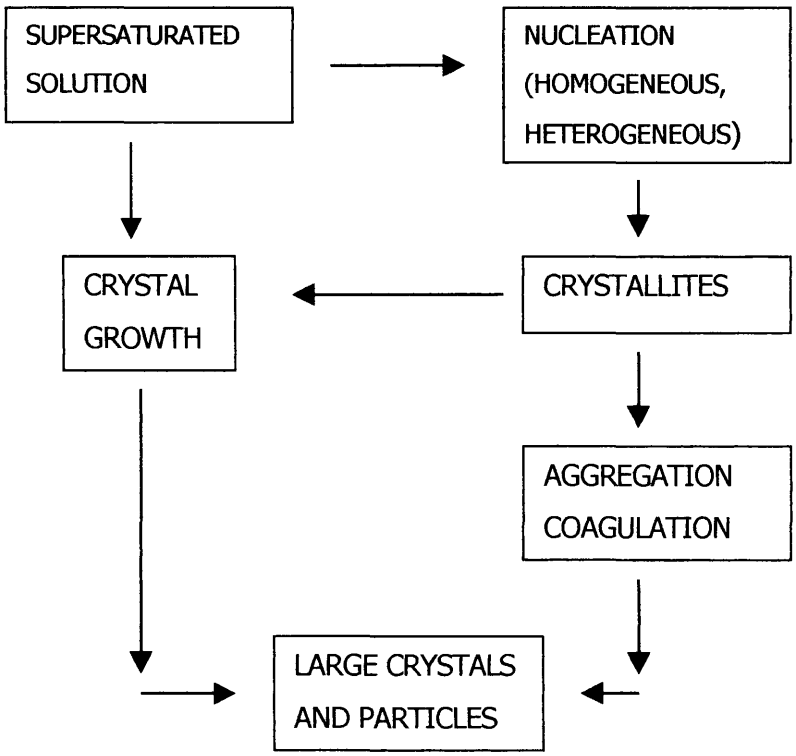

Figure 4.3. The different steps of the precipitation process.

The proportionality between the degree of supersaturation and the precipitation rate can be expressed in a semi-quantitative way by the Von Weimarn equation [4],

$$\text{Rate} \propto (Q - S)/S \qquad (4.1)$$

Where Q = actual concentration

S = equilibrium solubility.

4.4 CRYSTAL GROWTH:

4.4.1 THE GROWTH PROCESS:

During growth, the step front advances to the corner of the crystal and completes a molecular layer. When all the steps are eliminated through formation of complete layers, additional growth is only possible if new steps are formed [5, 6]. This model has a particularly unfavourable energy requirement and predicts a stepwise energy barrier as each layer is completed and new surface nucleation is required. The model implies the inability of a crystal to grow at supersaturations lower than the threshold value for nucleation. However, the most regular and well-built crystals are obtained at low supersaturations [5].

In reality, crystals are imperfect and contain dislocations. The theory of stepwise growth not only proposes the formation of monomolecular layers in a layer-by-layer growth mechanism, it also recognises the non-equivalence of sites on the crystal surface, i.e. Frenkel kinks [5]. The formation of a screw dislocation on the crystal surface offers perpetual steps for crystal growth and avoids the necessity for two-dimensional nucleation

The deposition of new material takes place through a number of simple, step-wise events [6], that are depicted in Figure 4.4. The emergence of a screw dislocation is also shown.

1. The diffusion of ions or molecules, within the bulk solution phase (position A), up to the crystal surface.

2. At the surface, a process of adsorption can attach the unit to the crystal surface (position C).
3. The unit can then undergo two-dimensional diffusion to a neighbouring site, position D, offering an energetically more favourable position at an edge or step on the crystal surface.
4. A one-dimensional diffusion along the step to a kink, position E, places the seed unit in an even more energetically favourable position, with three of its planes in contact with the crystal surface.
5. Attachment at the kink, with concomitant dehydration, completes the process of incorporation into the crystal lattice.

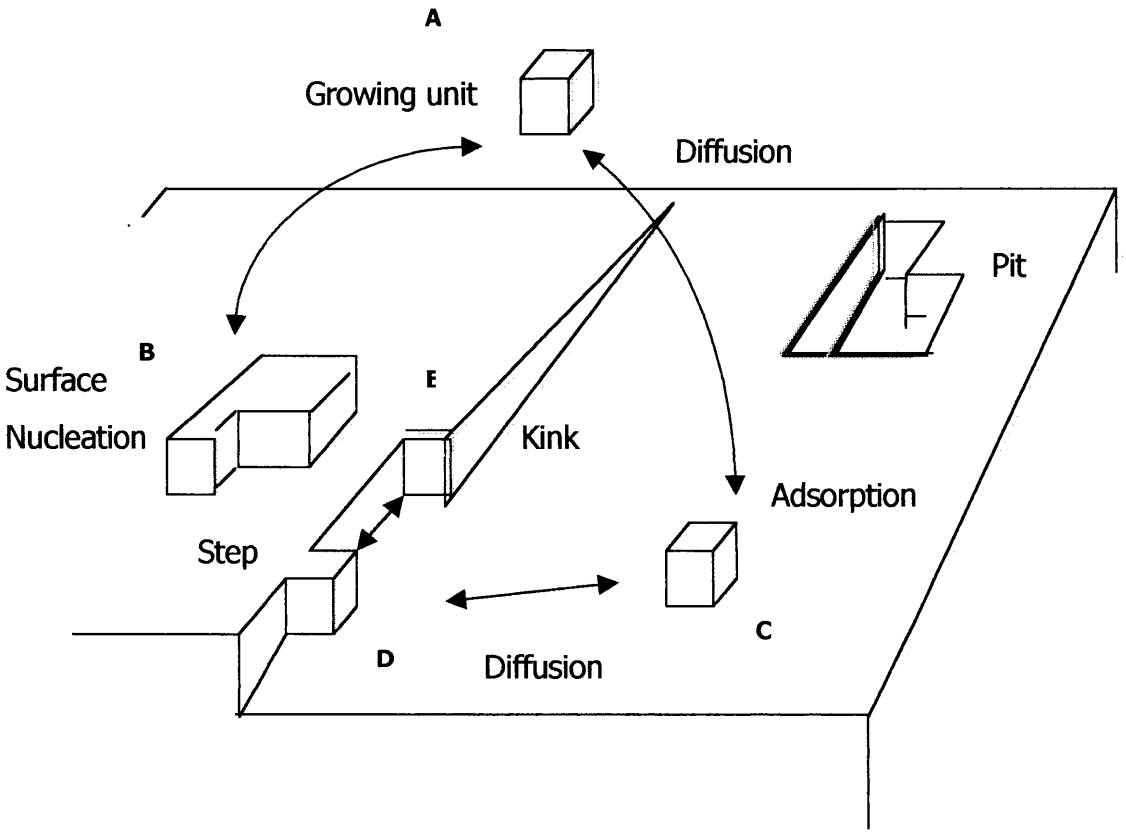

Figure 4.4. Representation of a crystal surface.

4.4.2 THE GROWTH RATE:

Volume diffusion, surface reactions [7], or a combination of volume diffusion and surface reactions [8] can control the growth rate of a crystal. It should be noted, however, that the rate controlling process might change with the shape of the crystal, the degree of saturation of the solution, and defect density on the crystal surface.

The following surface controlled kinetics have been identified:

1. Linear, related to the adsorption process.
2. Parabolic, related to the integration of ions in screw dislocation centred spiral steps, and
3. Exponential, related to the formation and growth of surface nuclei [8].

Sparingly soluble electrolytes mostly grow by a parabolic or exponential rate law at small or moderate supersaturations, that can change to transport control at higher levels of supersaturations [9].

Crystal growth of gypsum proceeds by a combined spiral and layer growth mechanism [10, 11]. The average growth rate of gypsum is determined by the contributions of the different growth rates of individual crystal surfaces. It is known that the (010) surface of calcium sulphate dihydrate contains no screw dislocations [7], and growth thus always proceeds according to the exponential rate law, that is surface nucleation and growth. At relative low levels of supersaturation, the parabolic rate law best describes the overall growth of gypsum, while it changes to the exponential rate law at higher levels of supersaturation [12]. It is therefore concluded, that the contribution of the (010) surface to the overall growth of gypsum increases with increasing levels of supersaturation.

The rate of growth of a single crystal is proportional to the level of supersaturation. Furthermore, the solid deposited per unit of time is proportional to the available crystal

surface area. Thus, for a given quantity of seed material, growth is proportional to the level of supersaturation, as well as the specific surface area of the crystal mass [5]. The growth kinetics can be interpreted in terms of an empirical equation [13]:

$$- dC/dt = kS(C - C_s)^n \quad (4.2)$$

Where: C = The solution concentration.

C_s = The saturation at the particular ionic strength.

k = The growth rate constant.

S = The surface area of the crystals or even the number of growing sites, and

n = The growth order of the process, n = 2 for the parabolic rate law.

When the influence of different additives is investigated, however, it is better to plot the mean linear growth rate R, as a function of the relative supersaturation σ, defined by $((C-C_s)/C_s)$ [13]. The influence of the additives will then be self-evident.
The mean linear growth rate R, can be expressed as follows:

$$R = -d\sigma/dt \times L \times 1/\rho \times 1/S \text{ cm/min} \quad (4.3)$$

Where: L = Solubility at equilibrium for the particular ionic strength in g/cm^3.

ρ = Density in g/cm^3.

S = Surface of the crystal in cm^2 per cm^3 solution.

To estimate the surface area of the crystals during the growth process, isomorphous growth of the crystals can be assumed, that is the crystal morphology does not change during growth. The surface area S is expressed as follows:

$$S = S_0 [((\sigma_0 - \sigma)L + A_0)/A_0]^{2/3} \quad (4.4)$$

Where: S_0 = S at t = 0 and $\sigma_0 = \sigma$ at t = 0.

A_0 = mass of seed crystals at t = 0 in g per cm^3.

The dehydration of the cations, calcium, is generally considered to be the rate determining step for integration and absorption, as the anions are more easily dehydrated [8, 14]. However, although less hydrated, the bulky SO_4^{2-} ions may have to overcome considerable rotational energy barriers to integrate into the crystal lattice. Moreover, the presence of hydration water in calcium sulphate dihydrate may facilitate the integration of calcium ions. Thus, both factors favour smaller integration and absorption frequencies for the sulphate ion [10].

4.4.3 THE GROWTH AFFINITY:

The driving force for crystallisation, the growth affinity β, is the difference between the chemical potential of a mole growth units of the crystallising substance in its supersaturated solution, and the chemical potential of the mole growth units in its crystalline form, divided by RT. The choice of one molecule $CaSO_4.2H_2O$ as a growth unit for calcium sulphate dihydrate seems reasonable, because association into molecules already occurs in solution.

$$\beta = - \Delta\mu/RT = \ln (a(Ca^{2+})a(SO_4^{2-})/a(Ca^{2+})_{eq}a(SO_4^{2-})_{eq}) \qquad (4.5)$$

At low concentrations, it can be assumed that the activities of Ca^{2+} and SO_4^{2-} are equal, while the activity of the H_2O molecule remains practically constant [15]. At higher concentrations, however, the activities of the ions must be calculated. This procedure becomes very complex, especially when foreign ions, impurities, is added to the crystallising solution.

4.5 IMPURITIES IN PRECIPITATES:

Dissolved organic and inorganic impurities interfere with the crystallisation of calcium sulphate dihydrate. Such materials may change the nucleation conditions, the crystal growth rate, or the crystal habit. The activation energy for nucleation may be altered, and thereby the nucleation rate and the final crystal size. If there is adsorption of impurities on crystal surfaces, the growth rate is reduced; and if there is selective adsorption on some crystal surfaces, the crystal habit is influenced [5, 17].

Apparently, the incorporation reaction of crystal growth is promoted by background electrolyte in the solution [18]. The electrolyte might also influence the surface charge of the crystals, thus facilitating the transport of either Ca^{2+} or SO_4^{2-} ions towards the surface. The effect of electrolyte on the growth rate could also be imposed through the influence of the ions on the surface diffusion, transport along the steps or the final incorporation of the units at the kink sites. Electrolyte in the solution has the effect of screening the Ca^{2+} and SO_4^{2-} ions and of lowering the H_2O activity by their hydration. The ions also have their specific interaction with the calcium and sulphate ions. Both effects result in a change in the activities of the calcium and sulphate ions.

4.5.1 THERMODYNAMICS:

As already mentioned, in reality all crystals at temperatures above absolute zero contain some defects, which are generally vacant atomic sites or substituted impurity ions. Up to a certain concentration, the presence of point defects actually reduces the free energy, G, of a crystal and is therefore energetically favourable.

The Gibbs free energy, G, of a crystal is that thermodynamic quantity which is a minimum when a crystal is in equilibrium with its surroundings. It can be defined as follow [16]:

$$\Delta G = \Delta H - \Delta TS \qquad (4.6)$$

Where: The enthalpy, H, is the internal energy at constant pressure. The internal energy is the sum of all the electrostatic energy terms due to interatomic forces and the kinetic energy terms due to vibrational motions.

The entropy, S, is a measure of the state of disorder in the crystal.

T is the temperature in Kelvin.

The creation of a vacancy or other point defect not only requires energy; it distorts the local structure as well. This increase in the enthalpy, ΔH, however, is accompanied by an increase in the entropy, ΔS, since the defects increase the disorder in an otherwise perfect crystal. For small defect concentrations, the $-T\Delta S$ term dominates at all temperatures above 0 K, and the change in free energy, ΔG, is negative. The enthalpy and entropy terms are not very temperature dependent, and so at higher temperatures, the $T\Delta S$ term becomes more dominating and the free energy minimum occurs at a higher defect concentration. It can therefore be concluded that at higher temperatures there are more vacancies, and a larger accommodation of impurities.

4.5.2 CONTAMINATION OF PRECIPITATES:

The exact mechanism, by which a precipitate becomes contaminated, can be highly complex.

1. Co-precipitation by adsorption:

Contamination of colloidal surfaces involves both physical (electrostatic) and chemical interaction [4]. There are four chemical factors that favour the adsorption of one ion rather than another of the same charge at a surface site:

1. *Solubility:* The ion that forms the less soluble compound with one of the ions of the precipitate will be preferentially adsorbed. (Paneth-Fajans-Hahn rule)

2. *Concentration:* The ion that is present at higher concentration will be adsorbed.

3. *Ionic charge:* The higher the charge on an ion, the more readily it is adsorbed.

4. *Ionic size:* Precipitates prefer to adsorb ions that are similar in size to those making up the precipitate crystal lattice.

2. Co-precipitation by occlusion:

In this form of contamination impurities (foreign ions and solvent) are trapped either in cavities within crystals or in cavities within aggregates of small crystals [4]. Interstitial uptake is difficult to identify, and the dependence of uptake as a function of process conditions is hard to predict.[18].

The most probable interstitial positions for foreign ions in gypsum are among the water molecules. The water molecules are arranged in layers perpendicular to the b-axis. This structure leaves high openings among the water molecules, with radii as large as 1 Å (Figure 4.1). Furthermore, a cation in this site will be stabilised by the dipole – ion interaction with water [15].

3. Co-precipitation by isomorphous replacement:

Isomorphous replacement occurs when one compound is able to fit into the crystal lattice of another compound with little or no distortion of the lattice, as was observed when phosphate co-precipitated with calcium sulphate dihydrate. It is necessary that the ions making up the two compounds have about the same ionic radius, and that the chemical bonds of the two compounds have about the same degree of covalence [4, 15]. The replacement tends to be uniform throughout the precipitate, in contrast to the highly localised contamination that results from occlusion. For isomorphous substitution, a partition coefficient D can be defined which takes into account the competition between the impurity and substituted ions [18].
For cation X, D is given by:

$$D = \{[X^+]/[Ca^{2+}](crystal)\} / \{[X^+]/[Ca^{2+}](solution)\} \quad (4.7)$$

When the D-value is experimentally found to be constant over a wide range of calcium and foreign ion, X, concentrations, the incorporation most likely proceeds by isomorphous substitution.

The mechanism of co-precipitation:

The following proposed mechanism of co-precipitation is based on the effect of growth rate on the incorporation of foreign cations into gypsum [15]. In a surface controlled

mechanism, the extent to which a foreign cation will enter the crystal, depends on the relative fluxes of adsorption and desorption, of the co-precipitating ion, to and from the growing surface. The partition coefficient, D, will depend in part on the relationship between the rate of exchange of the co-precipitating ion at adsorption sites, and the rate of growth. The foreign cations adsorb to, and desorb from, the surface of the growing crystal. As the flux of the major precipitating species (calcium, sulphate and water) is increased, more foreign ions are trapped within the crystal structure. The partition coefficient will therefore increase with increasing growth rate.

The incorporation of the foreign cations, however, also depends on its concentration in solution and on the availability of adsorption sites on the surface. As the growth rate of gypsum is increased, the flux of calcium ions to the surface increases and the number of available sites for the adsorption of the foreign cation decrease. Thus, the partition coefficient approaches a limiting value at high growth rates, due to the competition with calcium ions on available adsorption sites.

The effect of temperature on the change of the partition coefficient with growth rate also supports this mechanism. At higher temperatures, the rate of exchange of ions on adsorption sites is faster and the desorption flux of the co-precipitating ion can more easily compete with the counter flux of the major precipitating species. The amount of foreign ions trapped in the crystal during its growth is thus smaller, and consequently the partition coefficient is less affected by the growth rate.

4. Postprecipitation:

The second precipitate develops after the first precipitation and covers the first precipitate. In this study, however, postprecipitate refers to the precipitate that formed while the produced phosphoric acid stood for a minimum of four weeks.

4.6 INTERFERENCE BY IMPURITIES IN PHOSPHORIC ACID:

In anhydrous orthophosphoric acid, neighbouring PO_4 tetrahedra are held together by hydrogen bonds in a macromolecular structure. Introduction of water tetrahedra, which have considerable larger dimensions than the PO_4 tetrahedra, causes distortion of the lattice for geometric reasons and accordingly, a reduction of the lattice rigidity and the viscosity. As dilution with water proceeds, the liquid is considered to be built up by a mixture of fragments of phosphoric acid structure and water structure. The phosphoric acid and the water are bound together by a complicated hydrogen bridge system.

Phosphate ions possess a tendency to associate even in weak solution. The lattice has a tetrahedral co-ordination and a very open structure [5]. In general, four hydrogen bonds link each molecule to the remainder of the lattice. The interstitial space between the co-ordination tetrahedra is sufficient large to accommodate free, non-associated molecules without greatly disturbing the structural arrangement. Introduction of foreign matter, such as electrolytes, affects equilibrium conditions and the number of lattice defects. Furthermore the electric field around an ion polarises the surrounding molecules and strengthens the hydrogen bonds, thus stabilising the lattice. Therefore, an increase in charge increases the viscosity. Ions larger than the interstitial space, however, can distort the lattice with a resulting decrease in viscosity.

The interstitial space in the water lattice is considered larger than in the orthophosphoric acid lattice. It is therefore assumed, that foreign ions added to the system preferably enter into the water lattice fragments in a phosphoric acid solution, as long as enough water is present in relation to the amount of foreign ions added [5].

When ionic impurities are added to the solution, however, the relative concentration of "free" water will drop during hydration of the impurity, with the resulting increase in viscosity [19].

When the viscosity of the solution is increased, the transport of material becomes more difficult, that leads to local over-concentrations of extended duration during the reactions. This in turn results in an increase in nucleation frequency. Thus, a greater number of smaller crystals form, with the resulting effect on the filtration properties. Moreover, the filtration rate is inversely proportional to the viscosity of the liquid phase, with all other factors constant. Hence, the increase in viscosity caused by impurities affects filtration adversely in two ways, one direct and one indirect [17].

4.7 REFERENCES:

1. Hunger K.J., Henning O., **"On the Crystallisation of Gypsum from Supersaturated Solutions"**, Crystallisation and Research Technology, Vol. 23, No. 9, pp. 1135 – 1143, (1988).

2. Bartels H., Follner H., **"Crystal Growth and Twin Formation of Gypsum"**, Crystallisation and Research Technology, Vol. 24, No. 12, pp. 1191 – 1196, (1989).

3. Williams S.H., **"The Shear Strength of Gypsum Single Crystals on Three Cleavage Planes"**, Tectonophysics, Vol.148, pp. 163 – 173, (1988).

4. Potts L.W., **"Quantitative analyses: Theory and Practice"**, Harper and Row publishers, pp. 315-317, (1987).

5. Slack A.V., **"Phosphoric acid",** Part 1 Fertilizer science and technology series – Vol. 1., Marchel Dekker publishers, (1968).

6. Nriagu J.O., Moore P.B., **"Phosphate Minerals"**, Springer-Verlag, (1984).

7. Bosbach D., Jordan G., Rammensee W., **"Crystal Growth and Dissolution Kinetics of Gypsum and Fluorite: An in Situ Scanning Force Microscopy Study"**, European Journal of Minerals, Vol. 7, pp. 267 – 276, (1995).

8. Nielsen A.E., Toft J.M., **"Electrolyte Crystal Growth Kinetics"**, Journal of Crystal Growth, vol. 67, pp. 278 – 288, (1984).

9. Nielsen A.E., **"Electrolyte Crystal Growth Mechanisms"**, Journal of Crystal Growth, Vol. 67, pp. 289 – 310, (1984).

10. Zhang J. Nancollas G.H., **"Influence of calcium/sulphate molar ratio on the growth rate of calcium sulphate dihydrate at constant supersaturation."**, Journal of Crystal Growth, vol. 118, pp. 287– 294, (1992).

11. Van Rosmalen G.M., Daudey P.J., Marchee W.G.J., **"An Analysis of Growth Experiments of Gypsum Crystals in Suspension"**, Journal of Crystal Growth, Vol. 52, pp. 801 – 811, (1981).

12. Bosbach D., Junta-Rosso J.L., Becker U., Hochella M.F., **"Gypsum Growth in the Presence of Background Electrolytes Studied by Scanning Force Microscopy"**, Geochimica et Cosmochimica Acta, Vol. 60, No. 17, pp. 3295 – 3304, (1996).

13. Brandse W.P., van Rosmalen G.M., Brouwer G., **"The Influence Of Sodium Chloride On The Crystallisation Rate Of Gypsum"**, Journal of Inorganic Nucleation Chemistry, Vol. 39, pp. 2007-2010, (1977).

14. Christoffen M.R., Christoffen J., Weijnen M.P.C., Van Rosmalen G.M., **"Crystal Growth of Calcium Sulphate Dihydrate at Low Supersaturation"**, Journal of Crystal Growth, Vol. 58, pp. 585 – 595, (1982).

15. Kushnir J., **"The Co-precipitation of Strontium, Magnesium, Sodium, Potassium and Chloride Ions with Gypsum. An Experimental Study"**, Geochimica et Cosmochimica Acta, Vol. 44, pp. 1471 – 1482, (1980).

16. Putnis A., **"Introduction to Mineral Science"**, Cambridge University Press, (1992).

17. Becker P., **"Phosphates and Phosphoric acid"** Raw Materials, Technology and Economics of the wet process, Fertilizer science and technology series - Vol. 6., 2nd edition (1989).

18. Witkamp G.J., van Rosmalen G.M., **"Continuous Crystallisation of Calcium Sulphate Phases from Phosphoric Acid Solutions"**, American Chemical Society Symposium Series, Chapter 29, pp. 381-394, (1990).

19. Kir'yanova E.V., **"Effect of Organic Impurities on Crystallisation Processes in Systems Containing Phosphoric Acid"**, Neorganicheskie Materialy, Vol. 28, No. 6, pp. 1236 – 1240, (June 1992).

CHAPTER 5

THE EFFECT OF SODIUM IMPURITY

5.1 INTRODUCTION:

It is well known that foreign ions play an important role in the crystallisation of gypsum, as well as the produced phosphoric acid. In order to understand this process, the influence of different impurities, starting with sodium, are investigated and the results interpreted in accordance with the theoretical principles discussed in Chapter 4. All these studies adopted the "free – drift" method, in which the seed crystals were added to the non-equilibrium solutions, and allowed to react towards equilibrium. The extent of the reaction was determined by monitoring the variation of solution composition as a function of time.

5.2 EXPERIMENTAL:

5.2.1 APPARATUS:

The apparatus set-up is discussed in Chapter 2 (Section 2.5).

5.2.2 METHODOLOGY:

Phosphoric acid (~1005 g.) and gypsum (50.0 g.) were fed into the reactor and heated, with continuous stirring, until the required temperature of 80 °C was reached. The temperature was maintained throughout the experiment. Sulphuric acid (145 ml. diluted with 60 ml. water) was continuously pumped into the reactor, at a specific rate, while portions of calcium hydroxide were added to the slurry every 10 minutes. Sodium hydroxide was either dissolved in the sulphuric acid, or added with the calcium hydroxide at intervals of ten minutes.

After the reagents' addition time (three hours), the slurry was stirred for another two hours (retention time), during which two samples of slurry were collected by instant filtration. The samples, diluted with nitric acid, were analysed for total sulphate and calcium. The mass of the samples was reported.

After two hours retention time, the slurry was pumped into the filtration section where the phosphoric acid was separated from the gypsum. From this point on, the methodology, that is sampling, calculation of the percentage solids, infrared spectra, and optical and electron microscope photographs, proceeded in the same manner as the methodology discussed in Chapter 3 (Section 3.2.2).

Reaction conditions for the experiments are presented in Table 5.1.

5.2.3 ANALYSES OF SOLUTIONS AND SOLIDS:

Total sulphate determination of the three samples was done by titration with barium chloride and sulphonanzo III indicator, while calcium was determined with ICP analyses. Acid samples were analysed for P_2O_5 and gypsum samples for total P_2O_5 only, by the colour development - UV spectrophotometric method.

Gypsum and postprecipitate samples were dried and infrared spectra were recorded between 400 and 4000 cm^{-1} (Appendix I). Optical and electron microscope photographs were taken.

The acid, gypsum, and postprecipitate samples were analysed for different compounds, as summarised in Table 5.3 and Table 5.4, with ICP analyses.

	EXP.0 0.05% Na	EXP.1 0.25%Na	EXP.2 0.50% Na	EXP.3 2.50% Na	EXP.4 3.75% Na	EXP.5 0.05% Na	EXP.6 0.25% Na	EXP.7 0.50% Na
Date	20/8/97	21/8/97	28/8/97	4/9/97	8/9/97	15/9/97	16/9/97	18/9/97
Phosphoric acid	1009.7 g.	1005.1 g.	1006.2 g.	1006.2 g.	1005.0 g.	1005.5 g.	1008.9 g.	1005.0 g.
Gypsum	50.0 g.	50.0 g.	50.0 g.	50.0 g.	50.0 g.	50.0 g.	50.0 g.	50.0 g.
Reagent addition Time	180 min.	180 min.	180 min.	180 min.	180 min.	180 min.	180 min.	180 min.
Water	60 ml.	60 ml.	60 ml.	60 ml.	60 ml.	60 ml.	60 ml.	60 ml.
Calcium hydroxide	198 g. (11g / 10min)	198 g. (11g / 10min)	198 g. (11g / 10min)	198 g. (11g / 10min)	198 g. (11g / 10min)	198 g. (11g / 10min)	198 g. (11g / 10min)	198 g. (11g / 10min)
Sulphuric acid	145 ml. (0.8ml / min)	145 ml. (0.8ml / min)	145 ml. (0.8ml / min)	145 ml. (0.8ml / min)	145 ml. (0.8ml / min)	145 ml. (0.8ml / min)	145 ml. (0.8ml / min)	145 ml. (0.8ml / min)
Sodium hydroxide	1.3g dissolved in acid	6.5g dissolved in acid	13.0g dissolved in acid	65.0g (3.6g /10min)	97.5g (5.4g /10min)	1.3g dissolved in acid	6.5g dissolved in acid	13.0g (0.7g /10min)
Retention time	120 min.	120 min.	120 min.	120 min.	120 min.	120 min.	120 min.	120 min.
Mass samples	42.9 g.	49.6 g.	44.3 g.	37.8 g.	38.3 g.	36.3 g.	48.3 g.	40.7 g.
Mass slurry	1506.3 g.	1513.0 g.	1486.1 g.	1501.7 g.	1581.4 g.	1473.4 g.	1414.0 g.	1461.0 g.
Total mass	1549.2 g.	1562.6 g.	1530.4 g.	1539.5 g.	1619.6 g.	1509.7 g.	1462.3 g.	1501.7g
Volume slurry	950 ml.	950 ml.	950 ml.	900 ml.	900 ml.	900 ml.	950 ml.	900 ml.
Permeability	1.14 min.	1.17 min.	1.53 min.	4.70 min.	5.00 min.	1.14 min.	1.33 min.	1.59 min.
Mass gypsum *	766 g.	769 g.	1022 g.	1047 g.	1050 g.	954 g.	789 g.	894 g.
Volume acid	600 ml.	600 ml.	400 ml.	400 ml.	400 ml.	540 ml.	520 ml.	490 ml.
Acid density (Kg/L)	1.27	1.26	1.26	1.30	1.31	1.27	1.26	1.27
Solids %	33.8	35.0	35.0	30.3	29.1	33.8	35.0	33.8
Postprecipi-tate (Kg/L)	0.009	0.014	0.017	0.005	0.007	0.009	0.013	0.011

Table 5.1. Reaction conditions and results.

* *Gypsum with unfiltrated acid*

5.3 RESULTS:

5.3.1 ANALYSES:

The different results are summarised as follows:

Table 5.2

Calcium and sulphate analyses of the samples taken during the retention time, acid samples after one day, and acid samples after four weeks. Analyses of the acid samples (after four weeks) for: Al_2O_3, Cu, K_2O, MgO and SiO_2.

Table 5.3

Analyses of the gypsum samples taken, after the cake was washed with acetone, for: fixed P_2O_5%, CaO%, MgO%, Al_2O_3%, Fe_2O_3%, SO_4%, F^-%, SiO_2%, Na_2O%, K_2O%, SrO%, CeO_2 ppm, La_2O_3 ppm, Y_2O_3 ppm, and Nb_2O_3 ppm.

Table 5.4

Analyses of postprecipitate samples taken, after it was washed with acetone, for: fixed P_2O_5%, CaO%, MgO%, Al_2O_3%, F^-%, SiO_2%, SO_4%, Na_2O %, K_2O %, Fe_2O_3 %, SrO%, CeO_2 ppm, La_2O_3 ppm, Y_2O_3 ppm, and Nb_2O_3 ppm.

The Tables are presented below.

Experiment	0	1	2	3	4	5	6	7
Sulphate analyses *Sample 1*	2.7%	3.4%	3.5%	3.4%	3.2%	3.8%	2.8%	2.8%
Sample 2	2.4%	3.1%	3.2%	3.2%	2.6%	3.7%	2.5%	2.6%
Sample 3 (1 day)	2.2%	2.6%	2.5%	2.7%	2.4%	3.4%	1.9%	1.9%
acid (4 weeks)	1.9%	2.3%	2.3%	2.1%	2.12%	3.16%	1.6%	1.8%
Calcium analyses *Sample 1*	0.26%	0.21%	0.21%	0.20%	0.18%	0.27%	0.25%	0.23%
Sample 2	0.23%	0.18%	0.19%	0.16%	0.16%	0.25%	0.23%	0.18%
Sample 3 (1 day)	0.13%	0.10%	0.09%	0.10%	0.12%	0.13%	0.12%	0.11%
Acid (4 weeks)	0.06%	0.05%	0.05%	0.06%	0.06%	0.04%	0.06%	0.06%
CaO% *Sample 1*	0.37%	0.29%	0.30%	0.28%	0.25%	0.39%	0.35%	0.32%
Sample 2	0.32%	0.26%	0.26%	0.23%	0.23%	0.35%	0.32%	0.25%
Sample 3 (1 day)	0.18%	0.15%	0.12%	0.14%	0.17%	0.19%	0.17%	0.16%
Acid (4 weeks)	0.09%	0.07%	0.07%	0.09%	0.09%	0.05%	0.09%	0.08%
P_2O_5 *acid*	26.7%	28.0%	30.3%	26.5%	25.9%	23.6%	25.5%	29/8%
Al_2O_3 *acid*	0.05%	0.06%	0.07%	0.07%	0.06%	0.07%	0.05%	0.06%
Cu *acid*	0.002%	0.002%	0.002%	0.002%	0.002%	0.002%	0.002%	0.002%
K_2O *acid*	0.021%	0.023%	0.025%	0.043%	0.033%	0.021%	0.023%	0.028%
MgO *acid*	0.50%	0.55%	0.57%	0.56%	0.56%	0.60%	0.67%	0.44%
SiO_2 *acid*	0.72%	0.37%	0.12%	0.02%	0.014%	0.70%	0.36%	0.02%

Table 5.2. Analyses of samples taken during retention time and acid analyses.

	Exp.0	Exp.1	Exp.2	Exp.3	Exp.4	Exp.5	Exp.6	Exp.7
Fixed P_2O_5 %	5.14	3.66	6.64	8.88	11.56	8.14	9.56	9.82
CaO%	21.1	21.7	25.3	24.5	23.3	25.5	24.4	24.6
MgO %	0.16	0.17	0.19	0.21	0.25	0.16	0.17	0.24
Al_2O_3 %	0.01	0.01	0.01	0.03	0.04	0.01	0.01	0.01
Fe_2O_3 %	0.03	0.03	0.05	0.06	0.07	0.04	0.04	0.05
F %	0.55	0.85	1.50	1.90	1.80	0.45	0.85	1.45
SO_4%	40.2	30.9	31.6	30.9	30.9	33.3	31.7	31.3
SiO_2 %	0.11	0.13	0.07	0.08	0.12	0.10	0.04	0.07
Na_2O %	0.09	0.58	1.07	3.30	4.91	0.25	0.50	1.09
K_2O %	0.02	0.02	0.02	0.03	0.04	0.02	0.02	0.03
SrO %	0.04	0.04	0.02	0.03	0.03	0.03	0.03	0.02
CeO_2%	0.05	0.05	0.04	0.05	0.05	0.06	0.05	0.04
La_2O_3 %	0.03	0.02	0.02	0.02	0.02	0.02	0.02	0.02
Y_2O_3 ppm	65.9	64.9	58.7	77.9	86.7	56.7	68.3	60.9
Nb_2O_3%	0.04	0.04	0.04	0.04	0.044	0.04	0.04	0.03

Table 5.3. Analyses of gypsum samples.

	Exp. 0	Exp. 1	Exp. 2	Exp. 3	Exp. 4	Exp. 5	Exp.6	Exp.7
Fixed P_2O_5 %	5.32	6.28	3.92	2.96	9.80	1.50	0.76	3.04
CaO %	23.5	14.6	18.2	24.1	17.9	16.1	17.2	16. 8
MgO %	0.12	0.12	0.12	0.11	0.20	0.08	0.60	0.20
Al_2O_3 %	0.09	0.17	0.15	0.03	0.07	0.08	0.21	0.17
F %	10.4	28.0	18.8	3.7	2.6	11.7	27.6	27.6
SiO_2 %	0.02	<0.01	<0.01	<0.01	0.03	<0.01	<0.01	<0.01
SO_4 %	32.9	18.9	25.1	30.9	31.0	34.6	21.6	20.8
Na_2O %	6.4	14.0	11.4	4.7	5.9	6.3	13.7	14.2
K_2O %	0.05	0.08	0.06	0.04	0.03	0.04	0.07	0.08
Fe_2O_3 %	0.04	0.04	0.04	0.05	0.06	0.02	0.18	0.05
SrO%	0.06	0.04	0.05	0.05	0.02	0.04	0.04	0.05
CeO_2%	0.04	0.03	0.04	0.04	0.01	0.04	0.03	0.05
La_2O_3%	0.02	0.02	0.02	0.02	0.01	0.02	0.01	0.02
Y_2O_3ppm	47.7	33.4	40.1	61.3	17.0	35.8	24.9	38.2
Nd_2O_3%	0.03	0.02	0.03	0.03	0.01	0.03	0.02	0.03

Table 5.4. Analyses of postprecipitate samples.

5.4 DISCUSSION:

5.4.1 GROWTH RATE:

The effect of increasing concentrations of sodium impurity on the growth rate is presented in Figure 5.1. Values of relative supersaturation and growth rate were calculated using equation 4.3 and 4.4[1] (Chapter4, Section 4.4.2). Although the solutions were filtrated after the retention time (2 hours), and therefore did not reach absolute equilibrium, the trend shown in Figure 5.1 agrees well with that observed in the literature [1]. The higher the concentration of sodium impurity in the supersaturated solution, the faster the growth rate of calcium sulphate dihydrate.

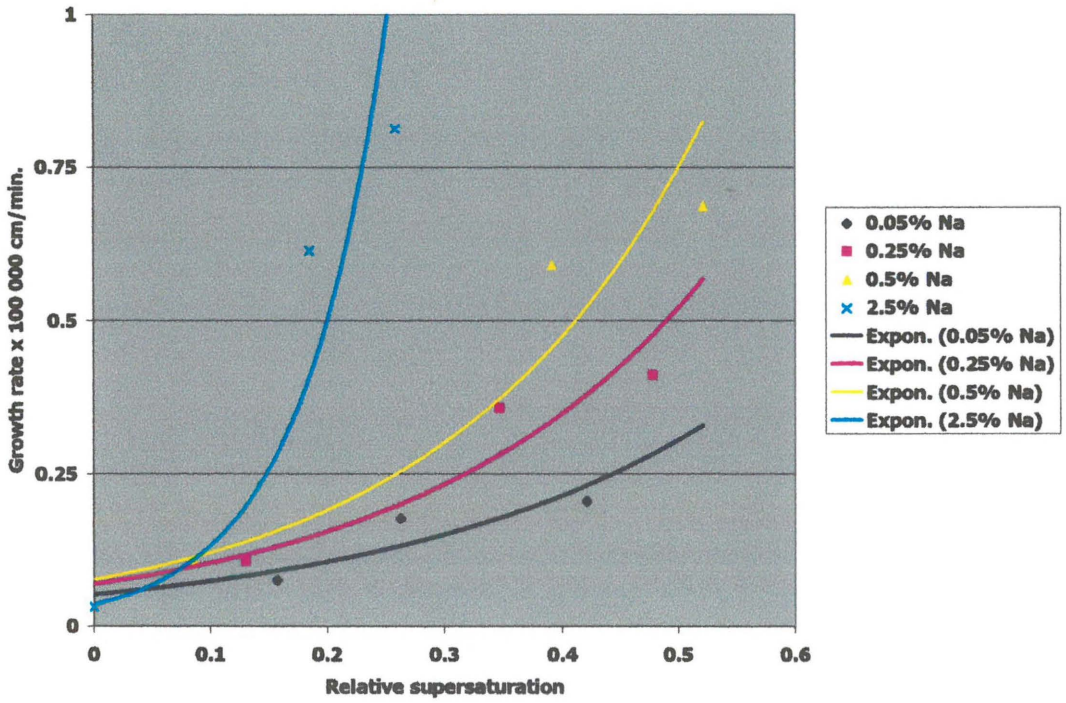

Figure 5.1. The effect of elevated levels of sodium impurity on the growth rate of calcium sulphate dihydrate.

[1] The calculation procedure for Figure 5.1. is explained in Appendix II.

It is reported that the solubility of calcium sulphate dihydrate is enhanced by increasing levels of sodium [1]. The concentration of calcium and sulphate are therefore higher at the same levels of relative supersaturation, resulting in an increase in growth rates.

The relative increase in growth rate, however, is larger than should be expected from the relative increase of the solubility of gypsum. Sodium therefore not only increased the solubility of calcium sulphate dihydrate; the growth process is promoted as well. It was found that the incorporation reaction is promoted by the presence of background electrolyte in the solution [2]. Sodium ions can influence the surface charge of the gypsum crystals, thus facilitating the transport of either Ca^{2+} or SO_4^{2-} ions towards the surface. The surface diffusion process, transport along the steps, or the final incorporation of the building units at the kink sites, can also be influenced.

5.4.2 CO-PRECIPITATION OF SODIUM:

The ion radius of sodium ions is very similar to that of calcium (1.24 Å and 1.20 Å respectively [3]), and it is therefore expected that sodium ions will be incorporated into the crystal lattice by means of isomorphous substitution. The partition coefficient, D, for sodium ions is given by:

$$D = \{[Na^+]/[Ca^{2+}](crystal)\}/\{[Na^+]/[Ca^{2+}](solution)\} \quad (5.1)$$

Unfortunately, the produced phosphoric acid was not analysed for sodium and the distribution coefficient for sodium, could therefore not be calculated.

The gypsum analyses (Table 5.3) show that not only the co-precipitated sodium concentration increased with elevated levels of sodium impurity, but also the concentrations of P_2O_5, calcium, magnesium, aluminium, iron, fluorine and potassium.

According to the co-precipitation mechanism discussed in Chapter 4, an increase in growth rate of calcium sulphate dihydrate will result in increasing impurity concentrations. The elevated levels of impurities in the precipitated calcium sulphate dihydrate thus confirm the enhanced growth rate in the presence of sodium impurity.

The infrared spectrum of gypsum (Experiment 4) is presented in Figure 5.2. Presence of co-precipitated P_2O_5 (11.56% Table 5.3) is confirmed by the band at 966 cm^{-1} [4].

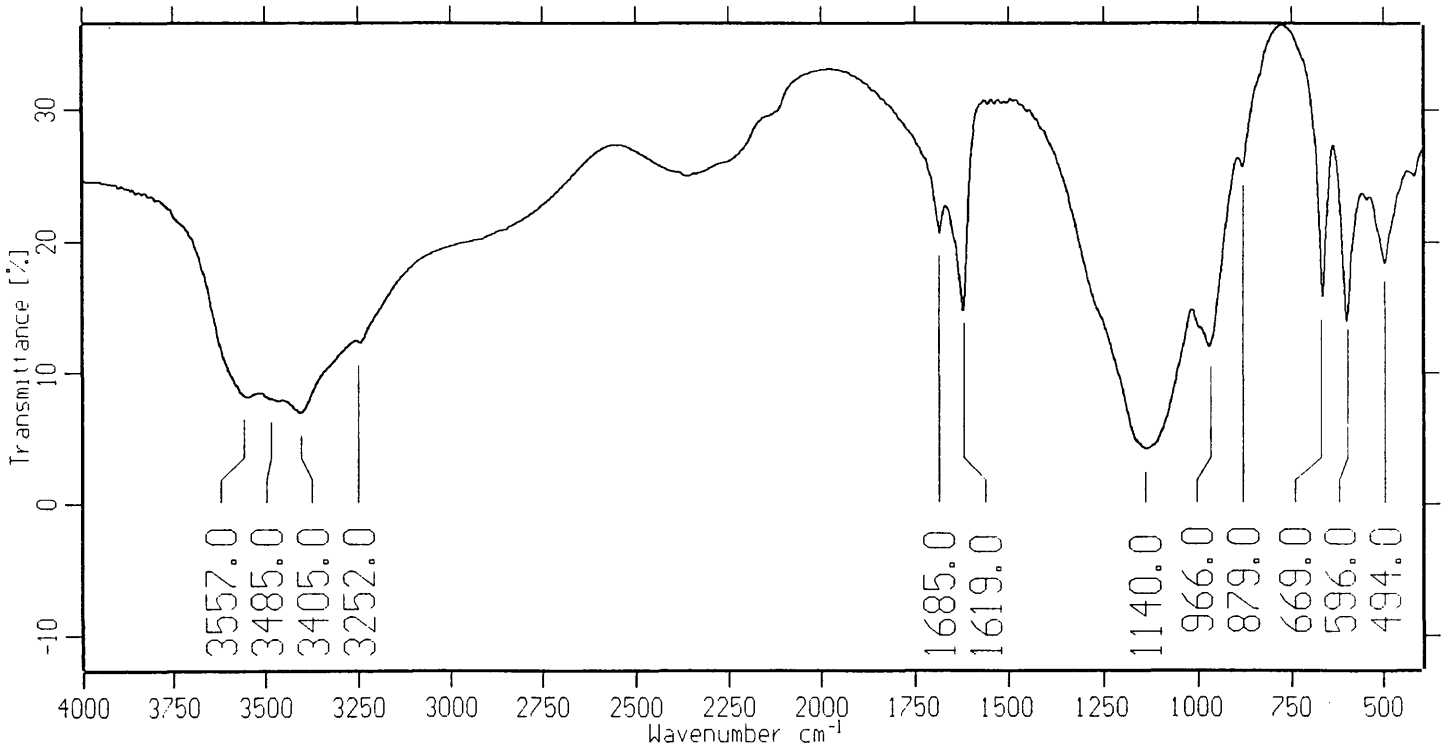

Figure 5.2. The infrared spectrum of gypsum precipitated in the presence of 3.75 percent added sodium impurity (Experiment 4).

5.4.3 GYPSUM MORPHOLOGY:

The increase in growth rate results in larger calcium sulphate dihydrate crystals that will promote the filtration rate[1]. A photograph of a gypsum sample (Experiment 4) is presented in Figure 5.3. It is evident that the growth rate of the precipitated gypsum was enhanced by the presence of sodium impurity (3.75 per cent added).

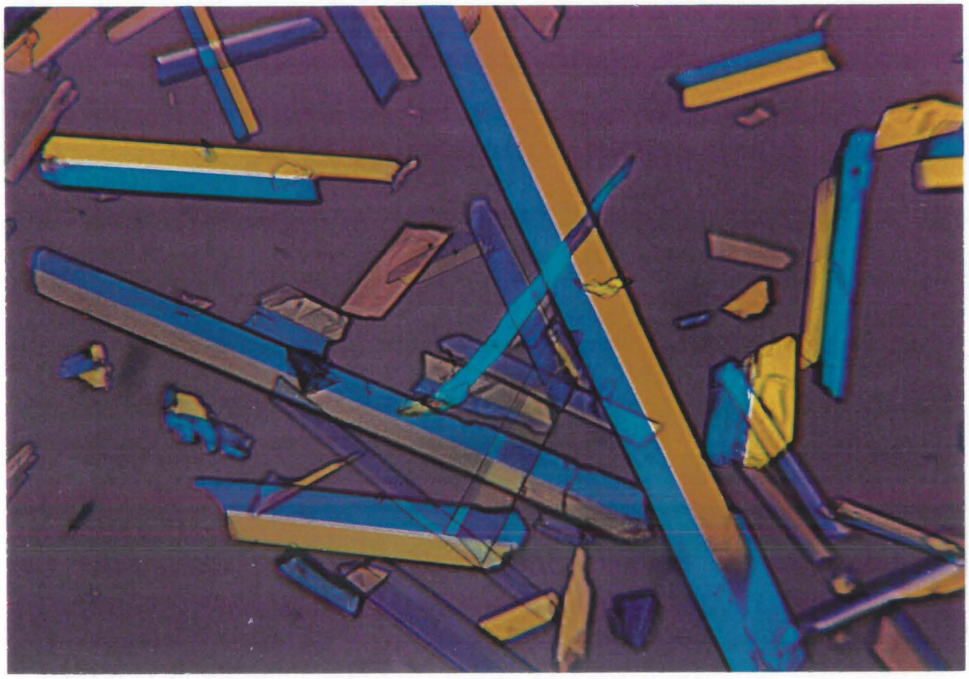

Figure 5.3. Photograph of a gypsum sample (Experiment 4) illustrating the enhanced growth rate of gypsum in the presence of sodium impurity (3.75 per cent added) (100X magnified).

Increasing solubility of calcium sulphate dihydrate, however, will also specifically promote growth of the (010) surface. Growth of this surface proceeds according to the exponential rate law, that is, surface nucleation and growth. At elevated levels of saturation, the energy barrier of surface nucleation is passed more frequently and growth of this crystal surface is thus promoted.

[1] The filtration rate is also influenced by other factors, that will be discussed later, resulting in a decrease in filtration rate with increasing levels of sodium impurity.

5.4.4 CO-DEPOSITIONING OF HEXAFLUOROSILICATES:

Precipitation of hexafluorosilicate occurs in the presence of sodium ions:

$$2\ Na^{+} + SiF_6^{2-} \rightarrow Na_2SiF_6 \qquad (5.2)$$

An advantage of this reaction, is the reduction of the fluorine content of the produced phosphoric acid. When the slurry cooled during filtration, however, sodium hexafluorosilicate precipitated as very minute crystals, which blinded the filter cloth and thus reduced filtration. It can be seen (Table 5.1) that the permeability of the gypsum increased with increasing concentrations of added sodium, despite the increase in crystal size.

The solubility of sodium hexafluorosilicate decreased even further when the filtrated phosphoric acid cooled to room temperature. Co-depositioning of sodium hexafluorosilicate was evident in electron micrographs of postprecipitate samples, even at small concentrations of added sodium impurity. An electron micrograph, showing the precipitated sodium hexafluorosilicate, is presented in Figure 5.4.

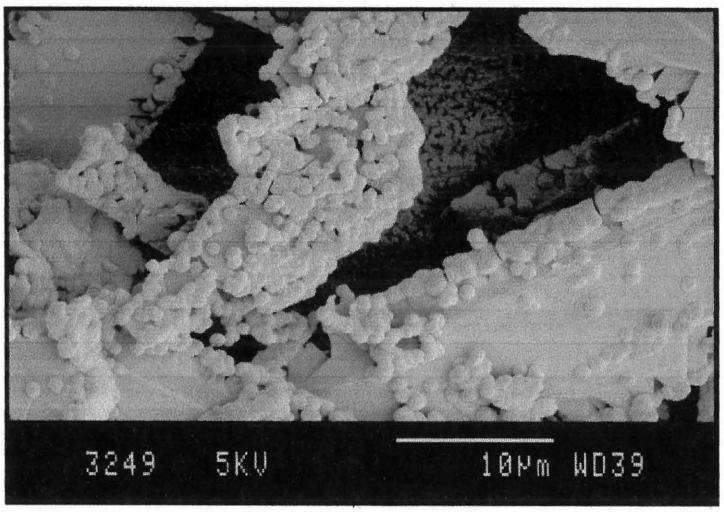

Figure 5.4. Electron micrograph of postprecipitate, showing the co-deposition of sodium hexafluorosilicate.

While analyses of the produced phosphoric acid (a reduction in SiO_2 concentration) confirmed the precipitation of sodium hexafluorosilicate, analyses of the postprecipitate samples seems to be contradicting. The co-depositioning of sodium hexafluorosilicate, however, is not homogeneous (Figure 5.4) and the analyses will thus be a function of the sample taken.

Infrared spectra of postprecipitate samples confirmed the presence of co-deposited sodium hexafluorosilicate. The infrared spectrum of a postprecipitate sample (Experiment 3) is presented in Figure 5.5. The band at 734 cm^{-1} indicates the presence of hexafluorosilicate [5].

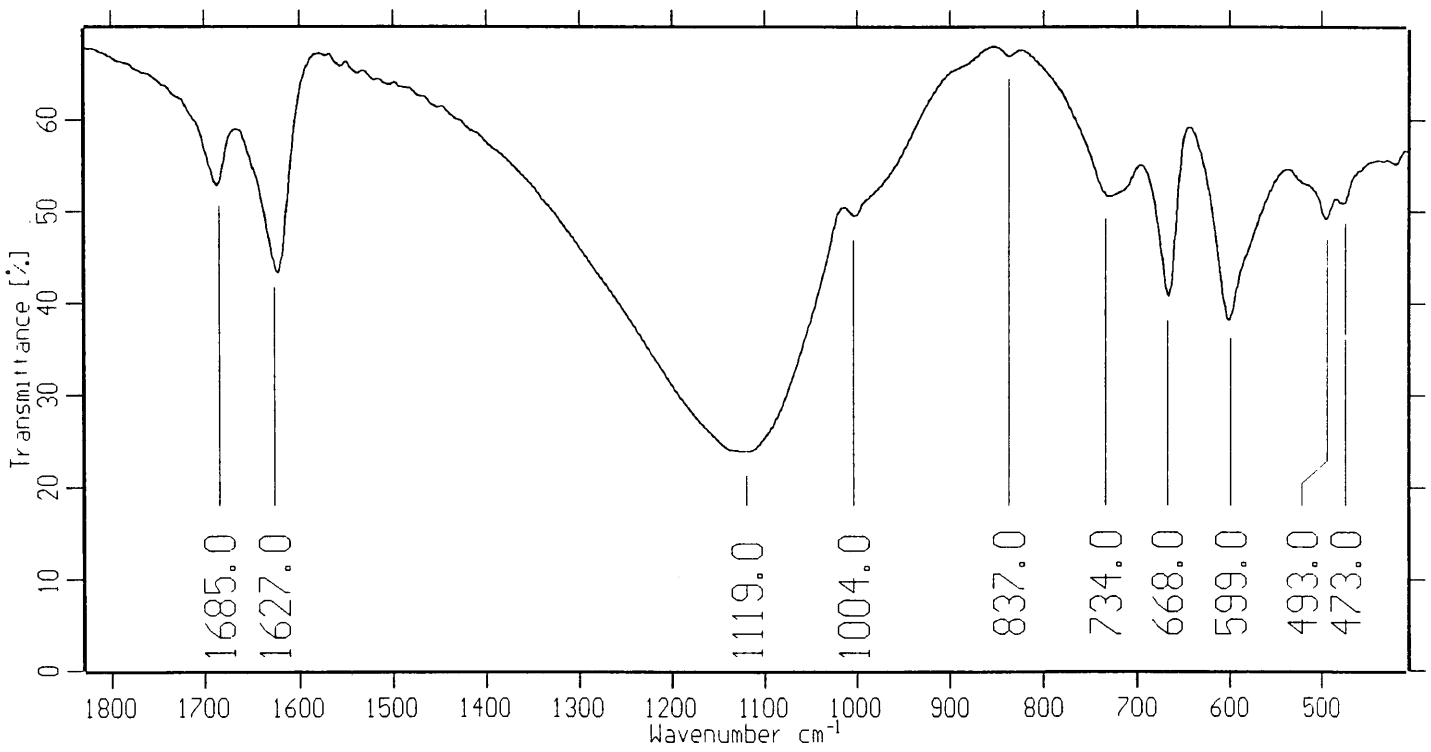

Figure 5.5. Infrared spectrum of postprecipitate showing the presence of hexafluorosilicate.

5.4.5 POSTPRECIPITATE MORPHOLOGY:

Electron micrographs of postprecipitate samples are presented in Figure 5.6 (a) and (b). It is evident that the presence of sodium promoted the formation of 'swallow tail' and 'saw tooth' crystals. The observed effects are the result of 'twinning' of the precipitating calcium sulphate dihydrate.

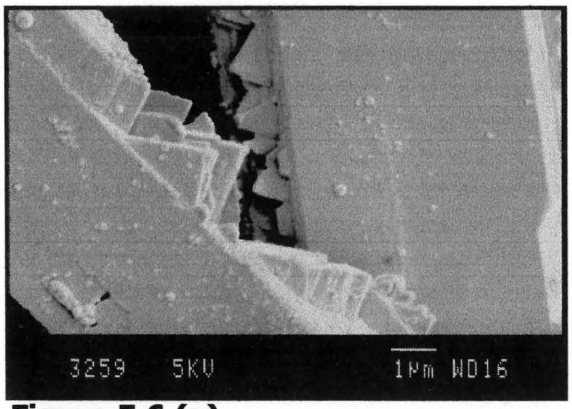

Figure 5.6 (a).

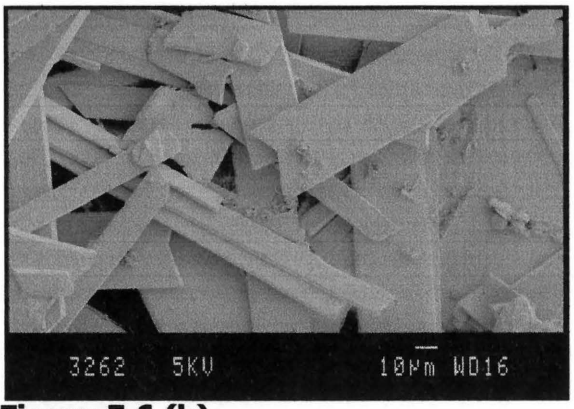

Figure 5.6 (b).

The effect of sodium impurity on the morphology of postprecipitate.

Although twinning of calcium sulphate dihydrate is common, the occurrence of a{100} penetration twins (Figure 5.6 (b)) is not. It is reported that the presence of sodium decreased the formation of broad d{101} twins and increased formation of a{100} twins[1] [6,7].

Glauberite is the only stable Ca-Na double sulphate. Analyses of the geometrical relationships between glauberite and gypsum reveals two-dimensional coincidence-cells between the (010) plane of gypsum and the (001), (110) and (100) planes of glauberite [8].

[1] The difference between a{100) twins and d{101} twins being that a{101} twins have parallel sides and d{101} twins have sloping sides.

Epitaxial two-dimensional growth of glauberite on gypsum is thus geometrically possible. After the depositioning of glauberite on gypsum, the crystals are more likely to grow as twins. The same effect was observed where sulphate ions promoted twin formation of brushite ($CaHPO_4.2H_2O$) [9]. In spite of the strict similarity of the two anionic groups, only a small percentage of the sulphate ions were incorporated into the crystal lattice.

An increase in growth rate due to twinning were indicated by growth experiments; when single crystals and twins formed simultaneously, the twins were always larger [10, 11]. The growth rate is a function of relative supersaturation and the available crystal surface area. Twinning of calcium sulphate crystals increases the available surface area and thus the growth rate as well. Twinning was not observed in gypsum samples. It can be argued, however, that the retention time was too short to allow the crystals to reach their equilibrium form.

5.4.6 PHOSPHORIC ACID:

Analyses of the produced phosphoric acid are presented in Table 5.2. It is evident that the P_2O_5 percentage of the produced phosphoric acid decreased with elevated levels of sodium impurity. This is in accordance with the increasing levels of co-precipitated P_2O_5, as a result of the increasing growth rate of gypsum.

5.5 CONCLUSIONS:

Influence of sodium on the production of phosphoric acid can be summarised as follows:

1. The influence of sodium on the growth rate.
2. The precipitation of sodium hexafluorosilicates.

Sodium promoted the growth rate in three ways. It increased the solubility of calcium sulphate dihydrate, resulting in higher concentrations of calcium and sulphate at the same levels of relative supersaturation. Sodium also promoted the surface reactions of crystal growth, and the formation of a{100} twins. The increase in growth rate with elevated levels of sodium impurity was confirmed by the increased impurity concentrations of gypsum.

Precipitation of sodium hexafluorosilicate has the advantage of lowering the fluorine content of the produced phosphoric acid. When the slurry cools during filtration, however, sodium hexafluorosilicate precipitate as minute crystals which blinds the filter cloth, and thus reduce the filtration rate.

5.6 REFERENCES:

1. Brandse W.P., van Rosmalen G.M., Brouwer G., **"The Influence Of Sodium Chloride On The Crystallisation Rate Of Gypsum"**, Journal of inorganic and nucleation Chemistry, Vol. 39, pp. 2007-2010, (1977).

2. Witkamp G.J., Van Der Eerden J.P., Van Rosmalen G.M., **"Growth of Gypsum. I. Kinetics"**, Journal of Crystal Growth, Vol. 102, pp. 281 – 289, (1990).

3. Whittaker E.J.W., Muntus R., **"Ionic Radii for the Use in Geochemistry"**, Geochimica et Cosmochimica Acta, Vol.43, pp. 945 – 956.

4. Farmer V. C., **"The Infrared Spectra of Minerals"**, Adlard and son publishers, p. 427, (1974).

5. Naulin C., Bougon R., **"Journal of Chemical Physics"**, Vol. 64, p. 4155, (1976).

6. Cody A.M., Cody R.D., **"SEM and Polarization Analyses Updating Early Light Microscope Studies Related To {101} Twin Formation in Gypsum"**, Journal of Crystal Growth, Vol. 98, pp. 731 – 738, (1989).

7. Rinaudo C., Franchini – Angela M., **"Curvature of Gypsum Crystals by Growth in the Presence of Impurities"**, Mineralogical Magazine, Vol. 53, pp. 479 – 482, (September 1989).

8. Rinaudo C., Franchini-Angela M., **"Influence of Sodium and Magnesium on the Growth Morphology of Gypsum"**, Neues Jarbuch Miner. Adh., Vol. 160, No. 1, pp. 105-115, (January 1989).

9. Rinaudo C., Lanfranco A.M., Franchini-Angela M., **"The system $CaHPO_4.2H_2O$-$CaSO_4.2H_2O$: crystallizations from phosphate solutions in the presence of SO_4^{2-}"**, Journal of Crystal Growth, 142, pp. 184-192, (1994).

10. Rinaudo C., Robert M.C. Lefaucheux F., **"Growth and Characterization of Gypsum Crystals"**, Journal of Crystal Growth, Vol. 71, pp. 803 – 806, (1985).

11. Van Rosmalen G.M., Daudey P.J., Marchee W.G.J., **"An Analysis of Growth Experiments of Gypsum Crystals in Suspension"**, Journal of Crystal Growth, Vol. 52, pp. 801 – 811, (1981).

CHAPTER 6

THE EFFECT OF POTASSIUM IMPURITY

6.1 INTRODUCTION:

Only a limited amount of work has been done regarding the influence of potassium on the production of phosphoric acid, since potassium is not generally found in phosphate rock. It is, however, one of the impurities commonly found by Foskor's clients. Since potassium and sodium are similar, it was expected that the effects of potassium on the production of phosphoric acid would be very much the same as that found for sodium.

6.2 EXPERIMENTAL:

6.2.1 APPARATUS:

The apparatus set-up is discussed in Chapter 2 (Section 2.5).

6.2.2 METHODOLOGY:

The methodology was the same as that discussed for sodium (Chapter 5 Section 5.2.2), with the following modifications:

1. Potassium hydroxide was added instead of sodium hydroxide.
2. The produced phosphoric acid was concentrated[1].

After four weeks, the phosphoric acid was concentrated to 54 per cent P_2O_5. Concentration was done with a Buchi rotary evaporator (applied vacuum 70 KPa, water temperature 100 °C). The concentrated acid was left to stand for another two

[1] Acid was concentrated to ~54% P_2O_5, the usual concentration of phosphoric acid sold for production of fertilisers.

weeks, before the sludge was separated from the acid with filtration. Samples of the acid and sludge were collected for analyses, infrared spectra, and electron microscope photographs.

Reaction conditions for the experiments are presented in Table 6.1.

6.2.3 ANALYSES OF SOLUTIONS AND SOLIDS:

Total sulphate determination of the acid samples was done by titration with barium chloride and sulphonanzo III indicator, while calcium was determined with ICP analyses.

Acid samples were analysed for P_2O_5 and gypsum samples for total P_2O_5 only, by the colour development - UV spectrophotometric method.

Gypsum, postprecipitate, and sludge samples were dried and infrared spectra were recorded between 400 and 4000 cm^{-1} (Appendix I). Optical and electron microscope photographs were taken of the solid samples.

Acid, gypsum, postprecipitate and sludge samples were analysed for different compounds with ICP analyses.

6.3 RESULTS:

6.3.1 ANALYSES:

The different results are summarised as follows:

Table 6.2:

Calcium and sulphate analyses of the samples taken during the retention time, acid samples after one day, and acid samples after four weeks. Analyses of the acid samples (after four weeks) for: Al_2O_3%, Cu%, K_2O%, MgO% and SiO_2%.

Table 6.3:

Analyses of the gypsum samples taken, after the cake was washed with acetone, for: fixed P_2O_5%, CaO%, MgO%, Al_2O_3%, Fe_2O_3%, SO_4%, F^-%, SiO_2%, Na_2O%, K_2O%, SrO%, CeO_2 %, La_2O_3 %, Y_2O_3 ppm, and Nb_2O_3 %.

Table 6.4:

Analyses of postprecipitate samples taken, after it was washed with acetone, for: fixed P_2O_5%, CaO%, MgO%, Al_2O_3%, F^-%, SiO_2%, SO_4%, Na_2O %, K_2O %, Fe_2O_3 %, SrO%, CeO_2 %, La_2O_3 %, Y_2O_3 ppm, and Nb_2O_3 %.

Table 6.5:

Concentration and analyses of acid samples for: SO_4%, CaO%, Al_2O_3%, Cu%, K_2O%, MgO% and SiO_2%.

Table 6.6:

Analyses of sludge samples for: fixed P_2O_5%, CaO%, MgO%, Al_2O_3%, F^-%, SiO_2%, SO_4%, Na_2O %, K_2O %, Fe_2O_3 %, SrO%, CeO_2 %, La_2O_3 %, Y_2O_3 ppm, and Nb_2O_3 %. The Tables are presented below.

	EXP.20 0.01% K	EXP.21 0.01%K	EXP.22 0.05% K	EXP.23 0.05% K	EXP.24 0.10% K	EXP.25 0.10% K	EXP.26 0.50% K	EXP.27 0.50% K	EXP.28 0.75%K	EXP. 29 0.75%K
Date	12/01/98	15/01/98	19/01/98	20/01/98	21/01/98	22/01/98	27/01/98	28/01/98	29/01/98	2/02/98
Phosphoric acid	1006.5 g.	1005.8 g.	1005.2 g.	1005.1 g.	1006.2 g.	1005.3 g.	1006.8 g.	1005.7 g.	1005.4 g.	1007.1g.
Gypsum	50.0 g.	50.0 g.	50.0 g.	50.0 g.	50.0 g.	50.0 g.	50.0 g.	50.0 g.	50.0 g.	50.0 g.
Reagent add. Time	180 min.	180 min.	180 min.	180 min.	180 min.	180 min.	180 min.	180 min.	180 min	180 min.
Water	60 ml.	60 ml.	60 ml.	60 ml.	60 ml.	60 ml.	60 ml.	60 ml.	60 ml.	60 ml.
Calcium hydroxide	198 g. (11g / 10min)	198 g. (11g / 10min)	198 g. (11g / 10min)	198 g. (11g / 10min)	198 g. (11g / 10min)	198 g. (11g / 10min)	198 g. (11g / 10min)	198 g. (11g / 10min)	198 g. (11g / 10min)	198 g. (11g / 10min)
Sulphuric acid	145 ml. (0.8ml / min)	145 ml. (0.8ml / min)	145 ml. (0.8ml / min)	145 ml. (0.8ml / min)	145 ml. (0.8ml / min)	145 ml. (0.8ml / min)	145 ml. (0.8ml / min)	145 ml. (0.8ml / min)	145 ml. (0.8ml / min)	145 ml. (0.8ml / min)
Potassium Hydroxide	0.2g. dissolved in acid	0.2g. dissolved in acid	1.2g. dissolved in acid	1.2g. dissolved in acid	2.5g. dissolved in acid	2.5g. dissolved in acid	12.6g. (0.7g/ 10min.)	12.6g. (0.7g/ 10min.)	18.0g (1.0g/ 10min.)	18.0g (1.0g/ 10min.)
Reten. Time	120 min.	120 min.	120 min.	120 min.	120 min.	120 min.	120 min.	120 min.	120 min.	120 min.
Samples	40.4 g.	48.6 g.	42.4 g.	41.5 g.	54.0g	53.2 g.	45.9 g.	41.2 g.	44.0 g.	42.2 g.
Mass slurry	1476.4 g	1165.0 g	1469.0 g.	1412.6 g	1475.9 g	1400.0 g	1461.8 g	1450.0 g	1508.0 g.	1484.8 g.
Total mass	1516.8 g.	1213.6 g.	1511.4 g.	1454.1 g.	1529.9 g.	1453.2 g.	1507.7 g.	1491.2 g.	1552.0 g.	1527.0 g.
Vol. Slurry	950ml.	900 ml.	900 ml.	900 ml.	900 ml.	900 ml.	900 ml.	900 ml.	900 ml	930 ml.
Permeabi-Lity	2.25 min.	1.00 min.	50 sec.	48 sec.	1.11 min.	1.11 min.	1.05 min.	1.20 min.	1.25min.	1.50 min.
Mass gypsum*	961 g.	750 g.	775 g.	763 g.	771 g.	759 g.	809 g.	865 g.	873 g.	876 g.
Vol. Acid	580 ml.	550 ml.	550 ml.	550 ml.	550 ml.	550 ml.	550 ml.	530 ml.	520 ml.	500 ml.
Acid density (Kg/L)	1.25	1.27	1.27	1.27	1.27	1.27	1.26	1.26	1.26	1.26
Solids %	36.1	33.8	33.8	33.8	33.8	33.8	35.0	35.0	35.0	35.0
Postprecipi -tate (Kg/L)	0.010	0.008	0.008	0.010	0.011	0.010	0.011	0.013	0.008	0.010

Table 6.1. Reaction conditions and results.

** Gypsum with unfiltrated acid*

Experiment	20	21	22	23	24	25	26	27	28	29
Sulphate analyses *Sample 1*	1.80%	3.05%	2.96%	2.88%	2.80%	2.75%	2.60%	2.17%	2.50%	2.40%
Sample 2	1.60%	2.60%	2.93%	2.46%	2.55%	2.50%	2.60%	2.15%	2.50%	2.35%
Sample 3 (1 day)	0.75%	1.75%	2.16%	1.69%	2.00%	1.90%	1.89%	1.78%	1.72%	1.75%
acid (4 weeks)	0.65%	1.66%	2.13%	1.80%	1.88%	1.88%	1.77%	1.69%	1.64%	1.67%
Calcium analyses *Sample 1*	0.45%	0.24%	0.21%	0.24%	0.21%	0.20%	0.19%	0.20%	0.22%	0.21%
Sample 2	0.42%	0.22%	0.21%	0.22%	0.22%	0.20%	0.17%	0.20%	0.17%	0.18%
Sample 3 (1 day)	0.34%	0.14%	0.12%	0.13%	0.12%	0.12%	0.11%	0.11%	0.08%	0.11%
Acid (4 weeks)	0.24%	0.08%	0.06%	0.07%	0.07%	0.07%	0.06%	0.07%	0.07%	0.06%
CaO% *Sample 1*	0.63%	0.35%	0.30%	0.34%	0.30%	0.28%	0.28%	0.28%	0.31%	0.30%
Sample 2	0.59%	0.32%	0.29%	0.31%	0.30%	0.28%	0.25%	0.28%	0.24%	0.25%
Sample 3 (1 day)	0.47%	0.20%	0.17%	0.18%	0.17%	0.17%	0.16%	0.16%	0.11%	0.16%
Acid (4 weeks)	0.33%	0.11%	0.09%	0.10%	0.10%	0.09%	0.09%	0.10%	0.10%	0.09%
P_2O_5 *acid*	34.1%	28.2%	28.02%	29.1%	27.0%	31.0%	31.6%	32.4%	27.7%	31.2%
Al_2O_3 *acid*	0.04%	0.04%	0.04%	0.04%	0.04%	0.04%	0.04%	0.04%	0.04%	0.04%
Cu *acid*	0.09%	0.07%	0.10%	0.10%	0.15%	0.09%	0.18%	0.14%	0.08%	0.07%
K_2O *acid*	0.037%	0.055%	0.047%	0.045%	0.052%	0.047%	0.098%	0.093%	0.279%	0.274%
MgO *acid*	0.416%	0.445%	0.441%	0.444%	0.437%	0.453%	0.435%	0.444%	0.437%	0.440%
SiO_2 *acid*	0.786%	0.944%	0.848%	0.785%	0.703%	0.729%	0.200%	0.206%	0.050%	0.047%

Table 6.2. Analyses of samples taken during retention time and acid analyses.

	Exp.20	Exp.21	Exp.22	Exp.23	Exp.24	Exp.25	Exp.26	Exp.27	Exp.28	Exp.29
Fixed P_2O_5 %	4.25	3.15	3.88	2.55	2.65	3.48	3.45	3.43	4.05	4.58
CaO%	27.39	28.94	27.18	30.69	30.73	28.85	27.82	27.81	26.55	26.02
MgO %	0.22	0.20	0.19	0.15	0.17	0.20	0.16	0.19	0.21	0.21
Al_2O_3 %	0.03	0.04	0.02	0.02	0.03	0.03	0.02	0.02	0.03	0.02
Fe_2O_3 %	0.07	0.06	0.06	0.04	0.04	0.06	0.05	0.05	0.07	0.07
F^- %	<0.01	<0.01	<0.01	<0.01	<0.01	<0.01	1.3	1.3	1.8	1.8
SO_4%	40.8	40.9	40.1	41.1	41.3	40.5	37.7	38.0	36.6	35.3
SiO_2 %	0.11	0.13	0.16	0.10	0.09	0.15	0.200	0.17	0.16	0.15
Na_2O %	0.08	0.08	0.08	0.07	0.08	0.06	0.11	0.08	0.08	0.11
K_2O %	0.06	0.06	0.07	0.06	0.13	0.14	1.09	1.14	1.43	1.49
SrO %	0.02	0.02	0.03	0.02	0.02	0.02	0.02	0.03	0.02	0.02
CeO_2%	0.03	0.04	0.04	0.02	0.02	0.04	0.03	0.05	0.02	0.03
La_2O_3 %	0.02	0.02	0.02	0.02	0.02	0.02	0.02	0.02	0.02	0.02
Y_2O_3 ppm	69	69	67	64	69	62	62	59	72	67
Nb_2O_3%	0.02	0.03	0.02	0.02	0.02	0.02	0.03	0.03	0.02	0.03

Table 6.3. Analyses of gypsum samples.

	Exp. 20	Exp. 21	Exp. 22	Exp. 23	Exp. 24	Exp. 25	Exp. 26	Exp. 27	Exp. 28	Exp. 29
Fixed P_2O_5 %	9.80	3.70	1.25	3.95	2.60	3.65	3.70	8.25	0.90	2.50
CaO %	23.95	27.80	23.56	22.75	18.21	16.62	16.23	14.24	17.81	16.32
MgO %	0.19	0.12	0.08	0.11	0.06	0.08	0.08	0.15	0.05	0.08
Al_2O_3 %	0.02	0.01	0.05	0.04	0.13	0.13	0.13	0.14	0.13	0.14
F %	<0.01	<0.01	I/S	7.0	18.0	18.0	19.0	19.0	19.5	19.6
SiO_2 %	0.16	0.06	0.02	0.08	0.03	0.03	0.04	0.12	0.03	0.04
SO_4 %	33.8	41.3	44.4	37.0	32.0	34.4	32.0	31.4	42.1	42.7
Na_2O %	0.06	0.04	0.16	0.15	0.24	0.25	0.25	0.26	0.25	0.25
K_2O %	0.03	0.04	6.29	5.47	11.69	12.55	16.36	11.65	13.08	14.0
Fe_2O_3 %	0.06	0.04	0.02	0.03	0.03	0.03	0.03	0.04	0.02	0.03
SrO%	0.04	0.11	0.10	0.10	0.07	0.05	0.05	0.03	0.07	0.05
CeO_2	0.03	0.05	0.05	0.05	0.04	0.03	0.03	0.03	0.05	0.05
La_2O_3	0.01	0.02	0.02	0.02	0.02	0.01	0.01	0.01	0.01	0.01
Y_2O_3	53	45	38	38	31	32	30	34	30	31
Nd_2O_3	0.03	0.04	0.04	0.04	0.03	0.03	0.03	0.03	0.03	0.03

Table 6.4. Analyses of postprecipitate samples.

	Exp.21	Exp.22	Exp.24	Exp.26	Exp.28
P_2O_5 *acid*	53.9%	53.4%	53.5%	51.2%	53.5%
Density (Kg/L)	1.60	1.55	1.65	1.62	1.65
Postprecipi-tate (Kg/L)	0.015	0.019	0.026	0.052	0.052
SO_4^{2-} %*acid*	2.69%	3.37%	3.4%	3.22%	3.06%
CaO% *acid*	0.009	0.011	0.006	0.005	0.007
Al_2O_3% *acid*	0.089	0.07	0.086	0.073	0.073
Cu% *acid*	0.0000	0.0006	0.0007	0.0006	0.0007
K_2O% *acid*	0.068	0.055	0.088	0.145	0.540
MgO% *acid*	0.926	0.746	0.834	0.835	0.950
SiO_2% *acid*	0.322	0.315	0.098	0.051	0.05

Table 6.5. Concentration and analyses of acid samples.

	Exp. 21	Exp. 22	Exp. 24	Exp. 26	Exp. 28
Fixed P_2O_5 %	4.90	14.70	10.00	20.20	26.40
CaO %	21.4	16.3	21.6	17.2	17.2
MgO %	1.88	0.69	0.45	1.10	0.75
Al_2O_3 %	0.23	0.26	0.24	0.26	0.20
F %	<0. 1	11.2	6.6	6.8	0.07
SiO_2 %	6.46	0.07	0.05	0.13	0.40
SO_4 %	34.5	28.1	36.9	25.9	25.1
Na_2O %	5.66	5.35	4.69	3.21	0.82
K_2O %	2.79	2.65	2.21	2.9	2.73
Fe_2O_3 %	0.19	0.14	0.12	0.26	0.23
SrO%	0.47	0.42	0.43	0.20	0.29
CeO_2%	0.87	1.76	2.18	1.52	1.72
La_2O_3%	0.41	0.93	1.19	0.86	0.93
Y_2O_3%	260 ppm	0.03	0.06	0.06	0.05
Nd_2O_3%	0.58	1.15	1.53	1.06	1.19

Table 6.6. Analyses of sludge samples.

6.4 DISCUSSION:

6.4.1 GROWTH RATE:

The influence of elevated levels of potassium on the growth rate is depicted in Figure 6.1. Values of relative saturation and growth rate were calculated, using equations 4.3 and 4.4 (Chapter 4, Section 4.4.2)[1].

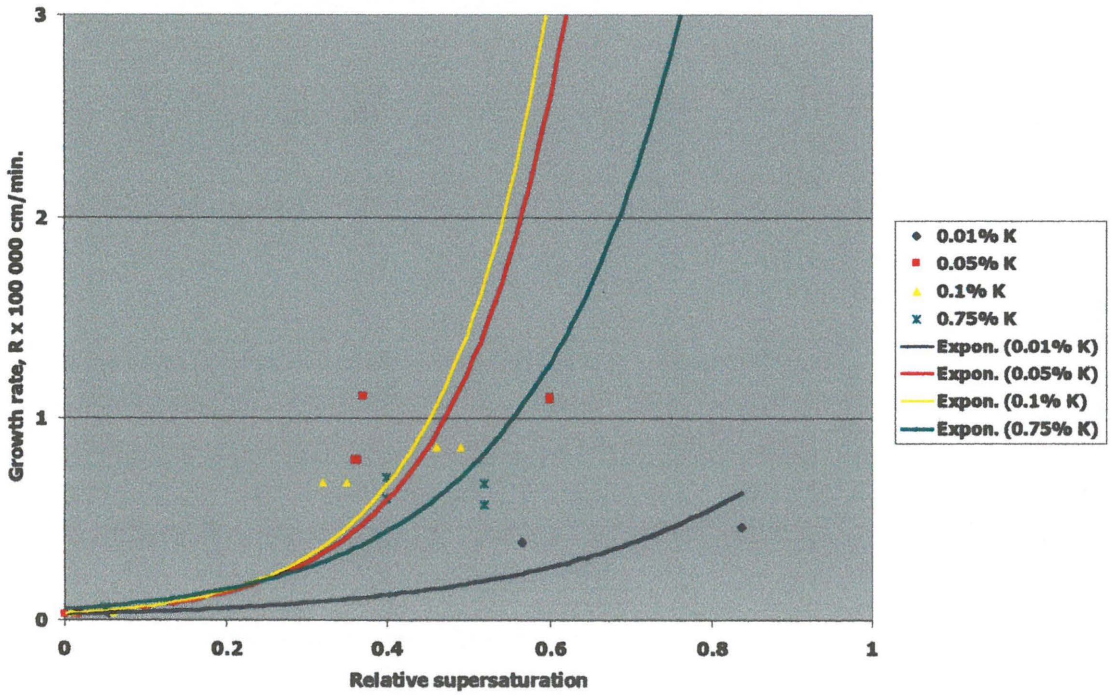

Figure 6.1. The influence of elevated levels of potassium impurity on the growth rate of calcium sulphate dihydrate.

At first, the effect of elevated levels of potassium on the growth rate of calcium sulphate dihydrate appears to be the same as that of sodium; the higher the level of added impurity, the higher the growth rate.

[1] Details of calculation procedures are presented in Appendix II.

Elevated levels of potassium did initially increase the growth rate of calcium sulphate dihydrate. Therefore, it could be concluded that the presence of potassium increased the solubility of calcium sulphate dihydrate, resulting in higher levels of calcium and sulphate and increased growth rates. With the addition of 0.75 per cent potassium, however, the growth rate of calcium sulphate dihydrate was reduced. This result was unexpected.

6.4.2 CO-PRECIPITATION OF POTASSIUM:

The partition coefficient, D, for potassium ions is given by:

$$D = \{[K^+]/[Ca^{2+}](crystal)\}/\{[K^+]/[Ca^{2+}](solution)\} \quad (6.1)$$

When the D-value is found to be constant over a range of calcium and potassium concentrations, it can be assumed that incorporation of potassium into the crystal structure of calcium sulphate dihydrate proceeded by isomorphous substitution. The calculated D-values were plotted graphically, as presented in Figure 6.2.

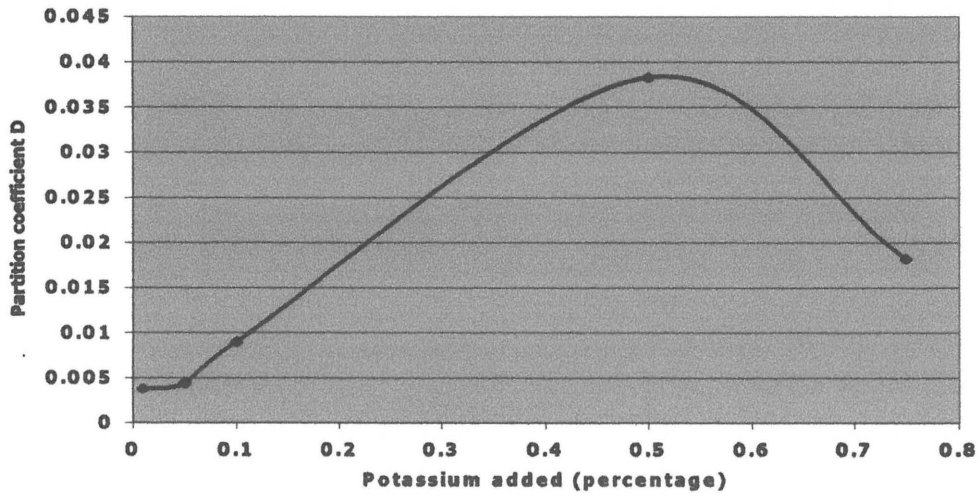

Figure 6.2. Distribution coefficients for potassium impurity.

It is evident that all of the co-precipitated potassium was not incorporated into the crystal structure by isomorphous substitution. This result could be expected since the ionic radius of potassium is larger that the ionic radius of calcium (138 pm. and 100 pm. respectively [1]). Substitution of calcium by potassium would have distorted the crystal structure, with the resulting increase in internal energy.

6.4.3 CO-DEPOSITIONING OF HEXAFLUOROSILICATES:

Precipitation of hexafluorosilicates occur in the presence of potassium as follows:

$$2K^+ + SiF_6^{2-} \rightarrow K_2SiF_6 \qquad (6.2)$$

Gypsum analyses (Table 6.3) and postprecipitate analyses (Table 6.4) show increasing concentrations of K_2O, SiO_2, and F^-, with elevated levels of potassium impurity. It is evident that potassium hexafluorosilicate precipitated with the calcium sulphate dihydrate. This is confirmed by electron micrographs (Figure 6.3) and infrared spectra (Figure 6.4 and Figure 6.5) of gypsum and postprecipitate samples.

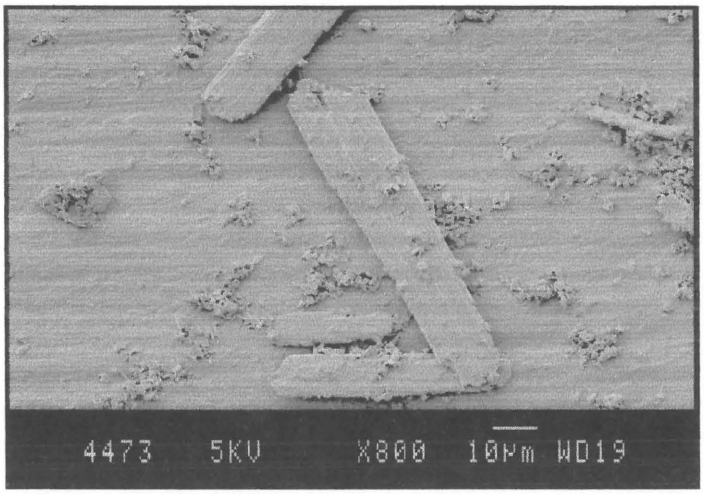

Figure 6.3. Electron micrograph of a gypsum sample (Experiment 26) showing the presence of potassium hexafluorosilicate.

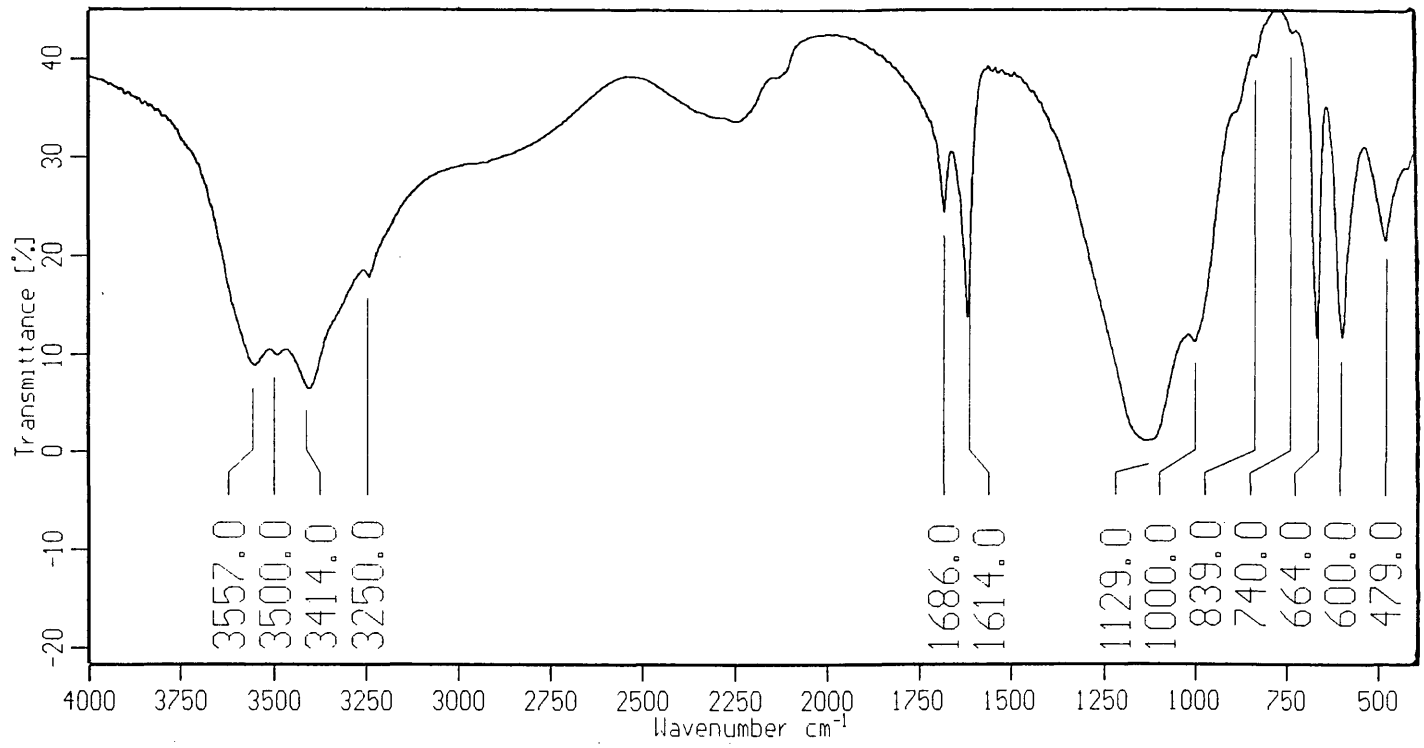

Figure 6.4. The infrared spectrum of gypsum (Experiment 29). Co-depositioning of K_2SiF_6 is confirmed by the bands at 740 cm^{-1} and 479 cm^{-1} [2].

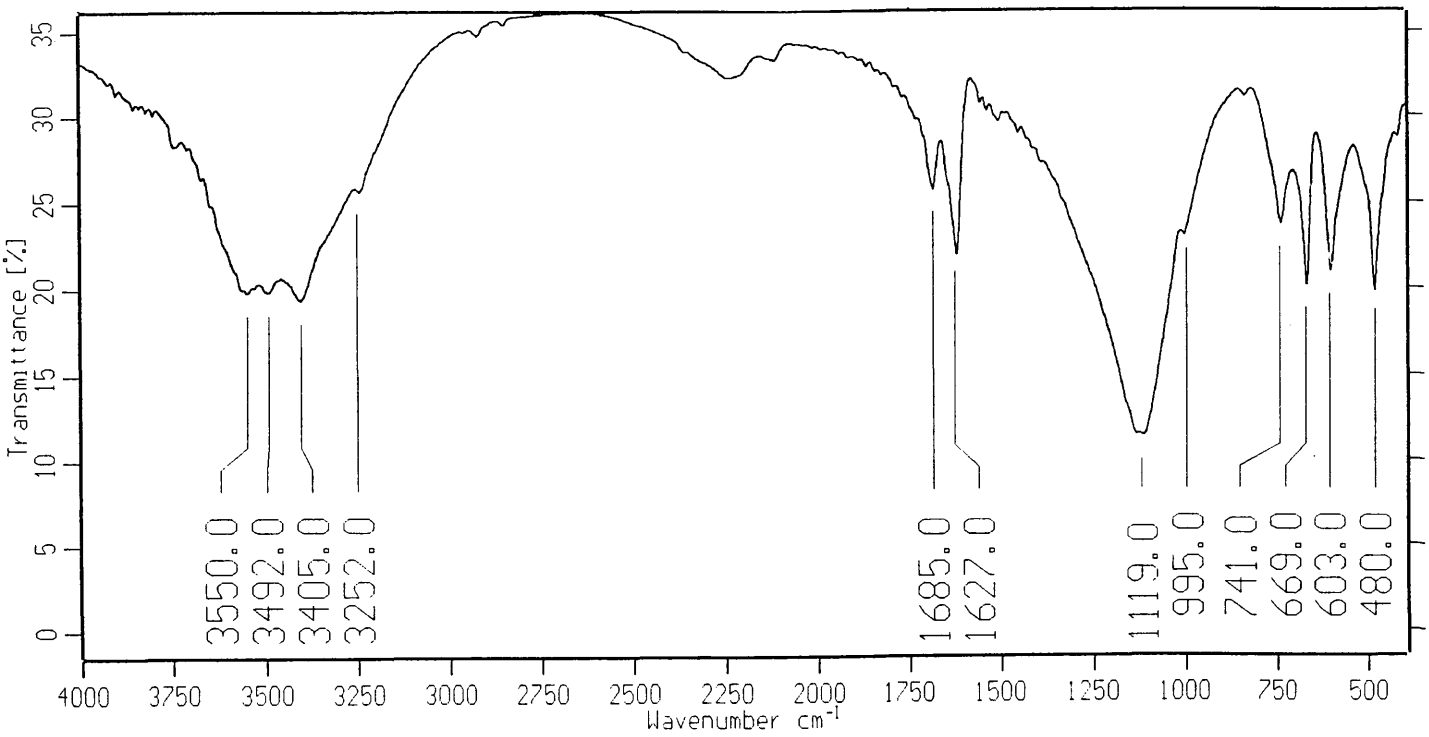

Figure 6.5. The infrared spectrum of postprecipitate (Experiment 24). Co-depositioning of K_2SiF_6 confirmed by the bands at 741 cm^{-1} and 480 cm^{-1} [2].

Potassium hexafluorosilicate is less soluble than sodium hexafluorosilicate in 30 per cent phosphoric acid [3]. Precipitation of potassium hexafluorosilicate thus already occurred with calcium sulphate dihydrate in the reaction unit, as confirmed by analyses, infrared spectra and electron micrographs.

Introduction of potassium increased the solubility of calcium sulphate dihydrate, and the growth rate accordingly. When the potassium concentration exceeded the solubility of potassium hexafluorosilicate, however, it started to precipitate. It is likely that potassium hexafluorosilicate precipitated on the surface of the calcium sulphate dihydrate crystals, reducing the available surface and thus the growth rate as well.

Although the precipitation of potassium hexafluorosilicate prevented the positive influence of potassium on the growth rate to proceed, the advantage of the precipitation is shown by the filtration rates (Permeability, Table 6.1). Since some of the potassium hexafluorosilicate precipitated with the gypsum, the amount of hexafluorosilicate that would have precipitate during filtration, blinding the filter cloth, was reduced. The influence of potassium on the filtration rate was thus not as severe as that of sodium.

6.4.4 PHOSPHORIC ACID:

The produced phosphoric acid was not influenced by the presence of potassium in the concentration range investigated (0.01 per cent - 0.75 per cent). Most of the potassium impurity precipitated with the gypsum, and the concentration left in the produced acid was relatively small compared to the concentration of potassium in the gypsum.

6.4.5 SLUDGE:

In 30 per cent P_2O_5, postprecipitate consists mainly of calcium sulphate dihydrate and alkaline fluorosilicates, but in concentrated acid more compounds precipitate, including complex phosphates. This reduces the overall soluble P_2O_5 yield in the final fertiliser products. The following list shows the most common compounds occurring in phosphoric acid with concentrations ranging from 40 to 50 per cent P_2O_5 [4]:

$CaSO_4.2H_2O$	Calcium sulphate dihydrate.
Na_2SiF_6	Precipitation starts wherever slurry cools down.
K_2SiF_6	Precipitate when K^+ content increases in acid.
$NaKSiF_6$	Scaling on filter and in pipes.
$CaSO_4.CaSiF_6CaAlF_6(Na)_{12}H_2O$	Chukhrovite, scales filter cloth.
$CaSO_4.{}^1/_2\ H_2O$	Hemihydrate. Precipitates during concentration of acid.
CaF_2	Precipitates during concentration of acid.
$MgAlF_6Na.6H_2O$	Ralstonite, precipitates in 40-50 per cent acid.
$Fe_3KH_{14}(PO_4)_8.4H_2O$	X-compound, precipitate in 50 per cent acid, when high Fe and Al containing phosphate ores are used. Precipitation is delayed, after ~14 days.
$Al_3KH_{14}(PO_4)_8.4H_2O$	X-compound.
$Fe(H_2PO_4)_2.2H_2O$	Precipitates with high iron.

The chemical composition and formation kinetics of sludge during the phosphoric acid concentration operation and storage period depend on the composition and amount of solids transferred from the original filter acid grade.

Calcium sulphate dihydrate is thermodynamically unstable in the concentrated acid and will decompose to form hemihydrate and anhydrate, thus releasing water for the precipitation of other compounds. Sodium fluorosilicate will complete its precipitation since it is less stable in higher concentrated acid, while potassium fluorosilicate will reach higher solubility rates [3]. The released K^+ ions will be involved in X compound formation [4].

Sludge analyses is presented in Table 6.6. Aluminium and iron concentrations are low, thus no x-compound formation was expected. The sludge most probably consists of calcium sulphate hemihydrate and anhydrite, as well as potassium and sodium hexafluorosilicates. An electron micrograph of a sludge sample (Experiment 21) is shown in Figure 6.6.

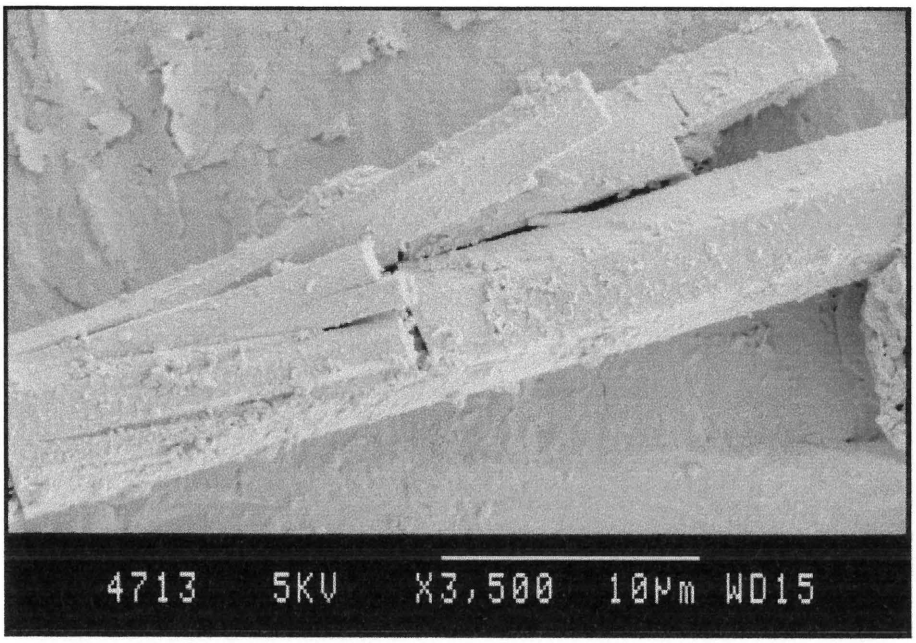

Figure 6.6. Electron micrograph of a sludge sample (Experiment 21), showing the precipitated hexafluorosilicates.

6.5 CONCLUSIONS:

Elevated levels of potassium initially enhanced the growth rate (up to 0.5 per cent added). With further addition of potassium, however, potassium hexafluorosilicate precipitated, most likely on the surface of calcium sulphate dihydrate, thus reducing the growth rate. The precipitated potassium hexafluorosilicate was confirmed by infrared spectra, electron micrographs and analyses of gypsum and postprecipitate samples. Although the precipitation of potassium hexafluorosilicate reduced the growth rate, it had the advantage of lowering the amount of potassium hexafluorosilicate that would have precipitate during filtration and blinded the filter cloth. The sludge most probably consists of calcium sulphate hemihydrate and -anhydrate, as well as potassium and sodium hexafluorosilicates.

6.6 REFERENCES:

1. Atkins P.W., " **Physical Chemistry"**, Fourth edition, Oxford University Press, p.959, (1990).

2. Prinsloo L.C., Heyns A.M., Ehrl R, Range K.J., **"The Vibrational Spectra of Potassium Hexafluorosilicate, K_2SiF_6"**, European Journal of Solid State Inorganic Chemistry, t 34, pp. 881-893, (1997).

3. Slack A.V., **"Phosphoric acid"** Part 1 Fertilizer science and technology series – Vol. 1., Marchel Dekker publishers, (1968).

4. Becker P., **"Phosphates and Phosphoric acid"** Raw Materials, Technology and Economics of the wet process, Fertilizer science and technology series - Vol. 6., 2nd edition (1989).

CHAPTER 7

THE EFFECT OF MAGNESIUM IMPURITY

7.1 INTRODUCTION:

Most types of phosphate rock contain 0.2 to 0.6 per cent magnesia, expressed as MgO, therefore the effect of magnesium impurity on the production of wet process phosphoric acid had been investigated [1]. It was concluded that magnesium ions impend filtration of wet process acid either by affecting the crystal shape and size of the precipitating calcium sulphate dihydrate, or by increasing the viscosity of the phosphoric acid. Besides the problems with filtration of the acid, however, the major concern for magnesium in phosphoric acid is the effect on downstream products, such as diammonium phosphate, where ammonium magnesium phosphate, ($MgNH_4PO_4$), precipitate instead. Analytical data of phosphoric acid show that magnesium is solubilized, and deports to the 30 per cent acid.

7.2 EXPERIMENTAL:

7.2.1 APPARATUS:

The apparatus set-up is discussed in Chapter 2 (Section 2.5).

7.2.2 METHODOLOGY:

The methodology was the same as that discussed for sodium (Chapter 5 Section 5.2.2), with the following modifications:

1. Magnesium sulphate heptahydrate[1] was added instead of sodium hydroxide.
2. The produced phosphoric acid was concentrated.

[1] The water and sulphuric acid were corrected with the amount of crystal water and sulphate added with magnesium sulphate heptahydrate.

After four weeks, the phosphoric acid was concentrated to 54 per cent P_2O_5. Concentration was done with a Buchi rotary evaporator (applied vacuum 70 kPa, water bath temperature 100 °C). The sludge was separated form the acid with filtration, after two weeks. Samples of the acid and sludge were collected for analyses, infrared spectra, and electron microscope photographs.

Reaction conditions for the experiments are presented in Table 7.1.

7.2.3 ANALYSES OF SOLUTIONS AND SOLIDS:

Total sulphate determination of the acid samples was done by titration with barium chloride and sulphonanzo III indicator, while calcium was determined with ICP analyses. Acid samples were analysed for P_2O_5 and gypsum samples for total P_2O_5 only, by the colour development - UV spectrophotometric method.

Gypsum, postprecipitate, and sludge samples were dried and infrared spectra were recorded between 400 and 4000 cm^{-1} (Appendix I). Optical and electron microscope photographs were taken of the solid samples.

Acid, gypsum, postprecipitate and sludge samples were analysed for different compounds with ICP analyses.

7.3 RESULTS:

7.3.1 ANALYSES:

The different results are summarised as follows:

Table 7.2:

Calcium and sulphate analyses of the samples taken during the retention time, acid samples after one day, and acid samples after four weeks. Analyses of the acid samples (after four weeks) for: P_2O_5%, Al_2O_3%, Cu%, K_2O%, MgO% and SiO_2%.

Table 7.3:

Analyses of the gypsum samples taken, after the cake was washed with acetone, for: fixed P_2O_5%, CaO%, MgO%, Al_2O_3%, Fe_2O_3%, SO_4%, F^-%, SiO_2%, Na_2O%, K_2O%, SrO%, CeO_2 %, La_2O_3 %, Y_2O_3 ppm, and Nb_2O_3 %.

Table 7.4:

Analyses of postprecipitate samples taken, after it was washed with acetone, for: fixed P_2O_5%, CaO%, MgO%, Al_2O_3%, F^-%, SiO_2%, SO_4%, Na_2O %, K_2O %, Fe_2O_3 %, SrO%, CeO_2 %, La_2O_3 %, Y_2O_3 ppm, and Nb_2O_3 %.

Table 7.5:

Concentration and analyses of acid samples for: SO_4%, CaO%, Al_2O_3%, Cu%, K_2O%, MgO% and SiO_2%.

Table 7.6:

Analyses of sludge samples for: fixed P_2O_5%, CaO%, MgO%, Al_2O_3%, F^-%, SiO_2%, SO_4%, Na_2O %, K_2O %, Fe_2O_3 %, SrO%, CeO_2 %, La_2O_3 %, Y_2O_3 ppm, and Nb_2O_3 %. The Tables are presented below.

	EXP.30 0.01% Mg	EXP.31 0.01% Mg	EXP.32 0.05% Mg	EXP.33 0.05% Mg	EXP.34 0.10% Mg	EXP.35 0.10% Mg	EXP.36 0.50% Mg	EXP.37 0.50% Mg	EXP.38 0.75% Mg	EXP. 39 0.75% Mg
Date	19/09/98	23/02/98	24/02/98	25/02/98	2/03/98	3/03/98	4/03/98	6/03/98	9/03/98	10/03/98
Phosphoric acid	1005.7 g.	1005.1 g.	1004.9 g.	1006.5 g.	1005.7 g.	1006.5 g.	1006.3 g.	1005.6 g.	1006.3 g.	1007.0g.
Gypsum	50.0 g.	50.0 g.	50.0 g.	50.0 g.	50.0 g.	50.0 g.	50.0 g.	50.0 g.	50.0 g.	50.0 g.
Reagent add. Time	180 min.	180 min.	180 min.	180 min.	180 min.	180 min.	180 min.	180 min.	180 min	180 min.
Water	60 ml.	60 ml.	54 ml.	54 ml.	52 ml.	52 ml.	20 ml.	20 ml.	0 ml.	0 ml.
Calcium hydroxide	198 g. (11g / 10min)	198 g. (11g / 10min)	198 g. (11g / 10min)	198 g. (11g / 10min)	198 g. (11g / 10min)	198 g. (11g / 10min)	198 g. (11g / 10min)	198 g. (11g / 10min)	198 g. (11g / 10min)	198 g. (11g / 10min)
Sulphuric acid	145 ml. (0.80ml / min)	145 ml. (0.80ml / min)	145 ml. (0.80ml / min)	145 ml. (0.80ml / min)	140 ml. (0.77ml / min)	140 ml. (0.77ml / min)	124 ml. (0.70ml / min)	124 ml. (0.70ml / min)	115 ml. (0.60ml / min)	115 ml. (0.60ml / min)
$MgSO_4$. $7H_2O$	1.52g dissolved in acid	1.52g dissolved in acid	7.60g (0.4g/ 10min.)	7.60g (0.4g/ 10 min.)	15.20g. (0.84g/ 10 min.)	15.20g. (0.84g/ 10 min.)	76.00g. (4.2g/ 10min.)	76.00g. (4.2g/ 10min.)	114.00g (6.3g/ 10min.)	114.00g (6.3g/ 10min.)
Reten. time	120 min.	120 min.	120 min.	120 min.	120 min.	120 min.	120 min.	120 min.	120 min.	120 min.
Samples	43.3 g.	42.4 g.	41.1 g.	51.2 g.	52.9 g.	48.3 g.	41.4 g.	37.0 g.	33.5 g.	33.1 g.
Mass slurry	1454.6 g.	1457.6 g.	1471.9 g.	1461.4 g.	1454.8 g.	1469.8 g.	1469.3 g.	1495.4 g.	1515.7 g.	1499.3 g.
Total mass	1497.9 g.	1500.0 g.	1513.0 g.	1512.6 g.	1507.7 g.	1518.1 g.	1510.7 g.	1532.4 g.	1549.2 g.	1532.4 g.
Vol. slurry	900 ml.	900 ml..	900 ml.	910 ml.	950 ml.	950 ml.	900 ml.	950 ml.	930 ml.	930 ml.
Permeabi-Lity	1.25 min.	1.3 min.	1.3 min.	1.13 min.	1.2 min.	1.25 min.	1.5 min.	1.2 min.	3.25 min.	2.25 min.
Mass gypsum*	822.7 g.	807.6 g.	806.0 g.	806.7 g.	778.9 g.	755.3 g.	939 3 g.	822.0 g.	957.2 g.	928.5 g.
Vol. acid	500 ml.	530 ml.	500 ml.	520 ml.	520 ml.	520 ml.	520 ml.	546 ml.	453 ml.	480 ml.
Acid density (Kg/L)	1.28	1.28	1.28	1.28	1.28	1.28	1.28	1.29	1.30	1.30
Solids %	32.7	32.7	32.7	32.7	32.7	32.7	32.7	31.5	30.3	30.3
Postprecipi -tate (Kg/L)	0.007	0.007	0.006	0.006	0.006	0.006	0.004	0.005	0.003	0.004

Table 7.1. Reaction conditions and results.

* *Gypsum with unfiltrated acid*

Experiment	30	31	32	33	34	35	36	37	38	39
Sulphate analyses *Sample 1*	2.70%	2.76%	2.75%	2.80%	2.70%	2.75%	2.65%	2.70%	2.80%	2.60%
Sample 2	2.48%	2.50%	2.72%	2.70%	2.50%	2.60%	2.56%	2.50%	2.50%	2.60%
Sample 3 (1 day)	2.00%	2.10%	2.29%	2.26%	2.10%	2.27%	2.05%	2.30%	2.10%	2.04%
acid (4 weeks)	1.82%	1.88%	2.05%	2.07%	1.90%	2.06%	1.85%	2.04%	1.80%	1.86%
Calcium analyses *Sample 1*	0.239%	0.279%	0.229%	0.315%	0.280%	0.310%	0.256%	0.240%	0.280%	0.255%
Sample 2	0.224%	0.136%	0.205%	0.221%	0.137%	0.230%	0.186%	0.225%	0.134%	0.190%
Sample 3 (1 day)	0.145%	0.233%	0.129%	0.131%	0.234%	0.218%	0.148%	0.150%	0.232%	0.130%
Acid (4 weeks)	0.074%	0.072%	0.064%	0.070%	0.074%	0.068%	0.072%	0.073%	0.074%	0.064%
CaO% *Sample 1*	0.334%	0.391%	0.321%	0.441%	0.392%	0.434%	0.358%	0.336%	0.392%	0.357%
Sample 2	0.313%	0.191%	0.286%	0.309%	0.192%	0.322%	0.260%	0.315%	0.187%	0.266%
Sample 3 (1 day)	0.20%	0.326%	0.181%	0.184%	0.323%	0.305%	0.207%	0.21%	0.324%	0.247%
Acid (4 weeks)	0.104%	0.101%	0.090%	0.099%	0.104%	0.095%	0.100%	0.102%	0.103%	0.098%
P_2O_5 *acid*	28.8%	28.8%	27.0%	26.1%	26.4%	27.7%	25.8%	28.7%	31.5%	28.5%
Al_2O_3*acid*	0.043%	0.052%	0.043%	0.055%	0.038%	0.038%	0.03%	0.038%	0.039%	0.04%
Cu *acid*	0.06%	0.05%	0.07%	0.08%	0.08%	0.12%	0.12%	0.09%	0.12%	0.12%
K_2O *acid*	0.027%	0.020%	0.022%	0.025%	0.027%	0.029%	0.024%	0.024%	0.023%	0.026%
MgO *acid*	0.474%	0.483%	0.566%	0.380%	0.642%	0.453%	1.579%	1.63%	1.49%	2.22%
SiO_2 *acid*	0.856%	0.887%	0.898%	0.892%	0.837%	0.729%	0.787%	0.845%	0.766%	0.769%

Table 7.2. Analyses of samples taken during retention time and acid analyses.

	Exp.30	Exp.31	Exp.32	Exp.33	Exp.34	Exp.35	Exp.36	Exp.37	Exp.38	Exp.39
Fixed P_2O_5 %	6.75	6.60	9.30	8.10	7.45	8.35	8.85	9.65	10.65	8.90
CaO%	28.25	27.85	26.09	27.19	26.41	28.50	27.15	26.16	26.71	27.81
MgO %	0.17	0.19	0.25	0.20	0.21	0.21	0.58	0.70	0.87	0.98
Al_2O_3 %	0.02	0.01	0.02	0.01	0.01	0.01	0.01	0.01	0.01	0.02
Fe_2O_3 %	0.05	0.05	0.05	0.05	0.04	0.04	0.06	0.05	0.05	0.06
F^-%	<0.1	<0.1	<0.4	<0.1	<0.1	<0.1	<0.1	<0.1	<0.1	<0.1
SO_4%	39.1	40.6	37.0	37.4	37.5	40.0	35.2	39.3	38.4	38.8
SiO_2 %	0.15	0.14	0.18	0.16	0.11	0.12	0.10	0.12	0.12	0.10
Na_2O %	0.09	0.08	0.10	0.08	0.08	0.08	0.07	0.08	0.09	0.08
K_2O %	0.05	0.04	0.04	0.04	0.04	0.03	0.04	0.05	0.04	0.04
SrO %	0.03	0.03	0.03	0.03	0.02	0.03	0.03	0.03	0.03	0.03
CeO_2%	0.04	0.04	0.05	0.04	0.03	0.04	0.04	0.04	0.04	0.04
La_2O_3 %	0.02	0.02	0.02	0.02	0.01	0.01	0.01	0.01	0.01	0.01
Y_2O_3 ppm	67	67	65	60	45	52	53	67	68	67
Nb_2O_3%	0.04	0.04	0.04	0.04	0.02	0.04	0.04	0.04	0.04	0.04

Table 7.3. Analyses of gypsum samples.

	Exp. 30	Exp. 31	Exp. 32	Exp. 33	Exp. 34	Exp. 35	Exp. 36	Exp. 37	Exp. 38	Exp. 39
Fixed P_2O_5 %	5.35	5.80	1.30	2.35	1.05	1.20	1.18	0.95	1.93	1.78
CaO %	31.45	30.37	33.63	31.39	33.24	30.91	29.88	34.01	32.82	33.95
MgO %	0.17	0.19	0.13	0.22	0.12	0.12	0.36	0.34	0.64	0.81
Al_2O_3 %	0.02	0.02	0.02	0.02	0.02	0.02	0.02	0.02	0.02	0.02
F %	<0.1	<0.1	<0.1	<0.1	<0.1	<0.1	<0.1	<0.1	<0.1	<0.1
SiO_2 %	0.05	0.02	0.02	0.02	0.02	0.02	0.02	0.05	0.12	0.12
SO_4 %	45.3	47.9	49.4	47.9	45.3	50.0	47.6	48.7	46.9	43.0
Na_2O %	0.05	0.05	0.03	0.06	0.03	0.03	0.03	0.03	0.06	0.05
K_2O %	0.02	0.02	0.01	0.01	0.01	0.01	0.01	0.01	0.02	0.02
Fe_2O_3 %	0.07	0.06	0.03	0.04	0.02	0.03	0.03	0.03	0.05	0.05
SrO%	0.09	0.16	0.12	0.12	0.07	0.10	0.11	0.11	0.05	0.12
CeO_2%	0.05	0.07	0.06	0.06	0.06	0.06	0.06	0.07	0.05	0.08
La_2O_3%	0.02	0.02	0.03	0.02	0.02	0.02	0.02	0.03	0.02	0.03
Y_2O_3ppm	61	56	60	61	42	42	39	51	58	51
Nd_2O_3%	0.04	0.05	0.05	0.05	0.05	0.05	0.05	0.06	0.04	0.06

Table 7.4. Analyses of postprecipitate samples.

	Exp.31	Exp.33	Exp.35	Exp.37	Exp.39
P_2O_5 *acid*	56.0%	56.2%	57.1%	51.9%	56.1%
Density	1.6	1.7	1.6	1.7	1.8
Postprecipi-tate (Kg/L)	0.042	0.037	0.025	0.015	0.016
SO_4^{2-} %*acid*	3.47	4.00	4.50	6.45	8.20
CaO%*acid*	0.008	0.005	0.008	0.007	0.013
Al_2O_3% *acid*	0.083	0.086	0.062	0.056	0.064
Cu% *acid*	0.0007	<0.0000	0.0003	<0.0000	<0.0000
K_2O% *acid*	0.053	0.055	0.049	0.052	0.054
MgO% *acid*	1.00	1.05	0.99	1.80	2.70
SiO_2% *acid*	0.14	0.18	0.35	0.22	0.18

Table 7.5. Concentration and analyses of acid samples.

	Exp. 31	Exp. 35	Exp. 39
Fixed P_2O_5 %	15.1	9.7	10.7
CaO %	19.7	23.2	20.9
MgO %	0.59	1.94	5.30
Al_2O_3 %	0.23	0.20	0.16
F %	4.8	11.7	9.8
SiO_2 %	0.12	0.01	0.06
SO_4 %	31.2	42.8	45.9
Na_2O %	3.91	6.47	2.16
K_2O %	0.11	0.16	0.14
Fe_2O_3 %	0.13	0.18	0.14
SrO%	0.54	0.51	0.58
CeO_2%	2.0	2.5	2.4
La_2O_3%	1.08	1.40	1.50
Y_2O_3ppm	0.034%	466	490
Nd_2O_3%	1.38	1.60	1.90

Table 7.6. Analyses of sludge samples.

7.4 DISCUSSION:

7.4.1 GROWTH RATE:

The influence of magnesium on the growth rate of calcium sulphate dihydrate is presented in Figure 7.1. Relative saturation and growth rate values were calculated using equations 4.3 and 4.4 (Chapter 4, Section 4.4.2)[1].

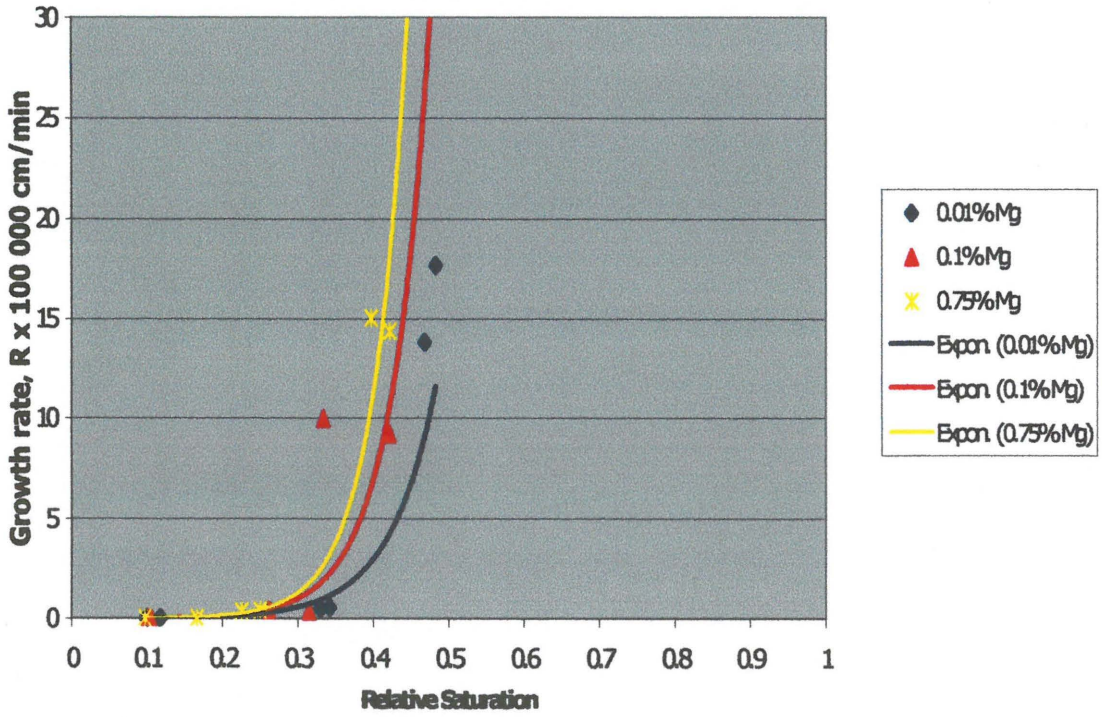

Figure 7.1. The influence of elevated levels of magnesium impurity on the growth rate of calcium sulphate dihydrate.

It is evident that elevated levels of magnesium had no on effect the growth rate of calcium sulphate dihydrate. Gypsum analyses, presented in Table 7.3, show no increase in impurity concentrations, and therefore confirm that the growth rate was not influenced.

[1] Details of calculation procedures are presented in Appendix II.

7.4.2 CO-PRECIPITATION OF MAGNESIUM:

It is reported that magnesium occurs as Mg^{2+} (seventy per cent), and as the complex $MgSO_4$ (thirty per cent) in the slurry [2]. Magnesium impurity can thus be adsorbed either as magnesium ions, or as magnesium sulphate. Although magnesium and calcium have the same ionic charge, the radius of magnesium ions is smaller than that of calcium, 72 pm and 100 pm respectively [3]. The partition coefficient for magnesium is given by:

$$D = \{[Mg^{2+}]/[Ca^{2+}](crystal)\}/\{[Mg^{2+}]/[Ca^{2+}](solution)\} \quad (7.1)$$

Calculated values of the partition coefficient, for increasing concentrations of added magnesium impurity, were plotted graphically as presented in Figure 7.2.

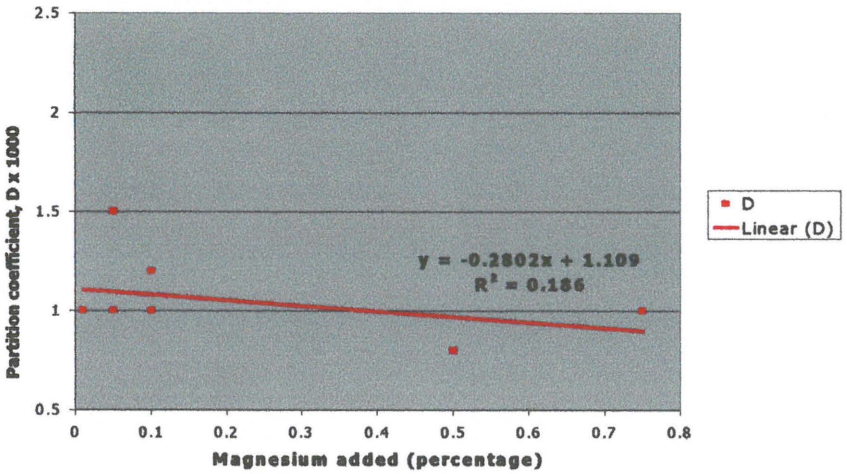

Figure 7.2. The distribution coefficient for elevated levels of added magnesium impurity.

The distribution coefficient, D, is small (~0.001). Although it is not evident in Figure 7.2 that magnesium was incorporated into the crystal lattice by isomorphous substitution of calcium ions, limited incorporation is confirmed by the gypsum analyses, and it is in agreement with the findings of Becker [1] and Ivanchenko et. al. [4].

It was found that co-precipitation of magnesium promoted curvature of the calcium sulphate dihydrate crystals [2]. No effect of magnesium on the morphology of the calcium sulphate dihydrate crystals could, however, be observed.

7.4.3 CO-PRECIPITATION OF P_2O_5:

Calcium sulphate dihydrate analyses, Table 7.3, indicate increasing concentrations of co-precipitated P_2O_5 with elevated levels of magnesium impurity. It is reported that co-precipitation is mainly caused by formation of magnesium phosphate compounds, $MgHPO_4$, although it is not incorporated into the crystal lattice in this form [4]. The infrared spectrum of a gypsum sample, Experiment 38, is presented in Figure 7.3. Co-precipitation of P_2O_5 is confirmed by the band at 886 and 1002 cm^{-1} [5].

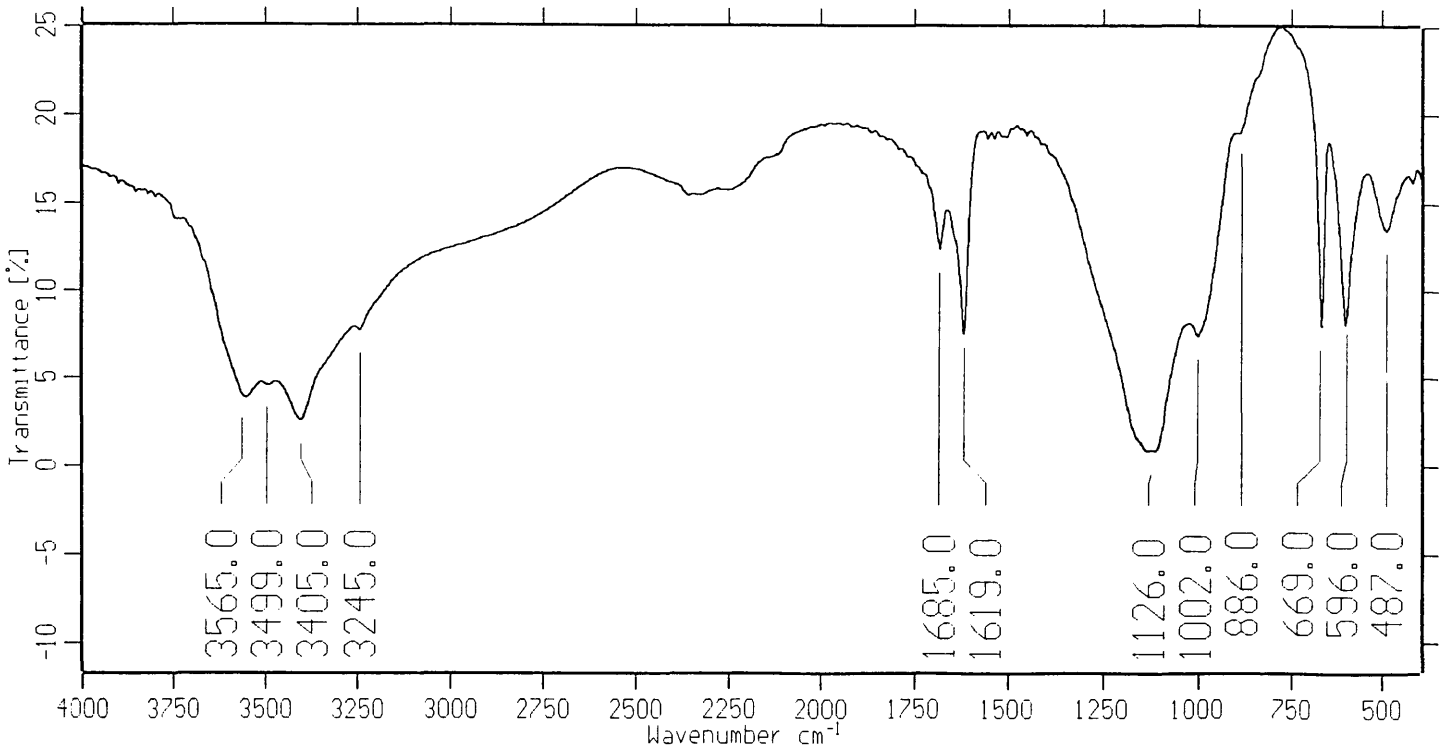

Figure 7.3. The infrared spectrum of gypsum (Experiment 38) showing the presence of co-precipitated P_2O_5.

7.4.4 PHOSPHORIC ACID:

Acid and gypsum analyses presented in Table 7.2 and Table 7.3, show that most of the magnesium deported to the acid. Magnesium ions, present in the acid, polarise the surroundings and increase the acid viscosity. This increase in acid viscosity not only effects the filtration rate directly, Permeability Table 7.1, but indirectly as well.

When viscosity is increased, it hinders the transport of ions, that leads to local supersaturations of extended duration (Chapter 4, Section 4.6). Spontaneous nucleation is thus promoted, with the resulting smaller crystals and reduced filtration rates. Electron micrographs of two gypsum samples (Experiment 31 and Experiment 39) are presented in Figure 7.4. The increased number of small crystals is evident.

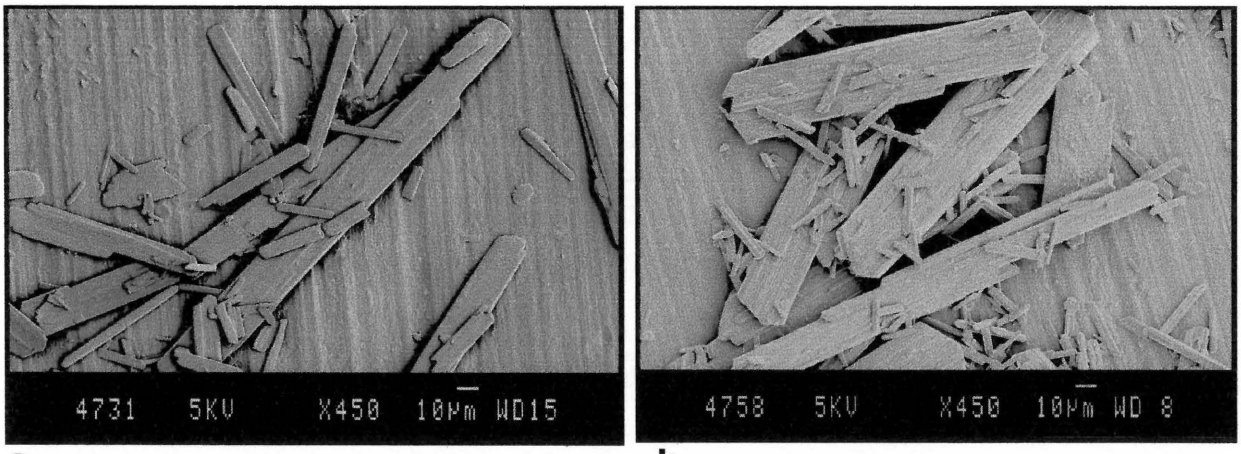

a b

Figure 7.4. Electron micrographs of gypsum samples, Experiment 31 Figure 7.4a and Experiment 39 Figure 7.4b, showing the influence of elevated levels of magnesium impurity on the number of small crystals.

7.4.5 SLUDGE:

Analyses of the precipitated sludge, presented in Table 7.6, suggest that samples mainly consist of calcium sulphate. The precipitation of ralstonite ($MgAlF_6Na.6H_2O$) is also a possibility, since the sodium concentrations are relatively high. Infrared spectra of the samples indicate the precipitation of a hexafluorosilicate, although it is not confirmed by the analyses. The electron micrograph of a sludge sample (Experiment 35) is presented in Figure 7.5.

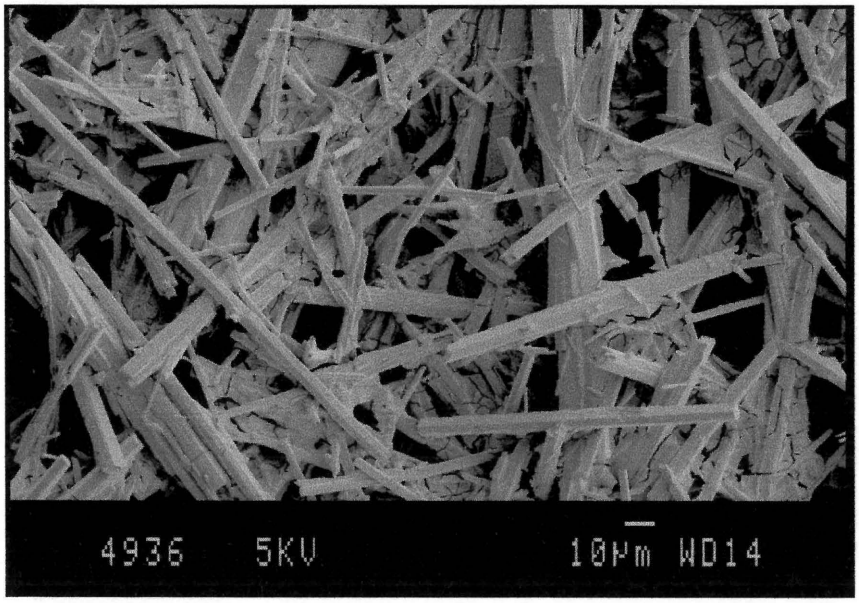

Figure 7.5. Electron micrograph of a sludge sample (Experiment 35).

7.5 CONCLUSIONS:

The incorporation of a small percentage of magnesium was indicated by gypsum analyses. Although it is reported that the incorporation of magnesium into the crystal lattice promoted curvature, no effect of magnesium on the morphology of the crystals could be observed.

Most of the added magnesium impurity deported to acid, however, where it increased the acid viscosity. The increased acid viscosity not only influenced the filtration rate directly, but indirectly as well by promoting the formation of small crystals.

The percentage of co-precipitated P_2O_5 increased with elevated levels of magnesium impurity. Magnesium apparently form magnesium phosphate compounds, and thus promotes the formation of HPO_4^{2-} ions that can be incorporated into the crystal lattice.

7.6 REFERENCES:

1. Becker P., **"Phosphates and Phosphoric acid"**, Raw Materials, Technology and Economics of the wet process, Fertilizer science and technology series - Vol. 6., 2nd edition (1989).

2. Franchini-Angela M., Rinaudo C., **"Influence of Sodium and Magnesium on the Growth Morphology of Gypsum, $CaSO_4.2H_2O$"**, Neues Jahrbuch Miner. Abh., Vol. 160, No. 1, pp. 105 – 115, (1989).

3. Atkins P.W., **" Physical Chemistry"**, Fourth edition, Oxford University Press, p.959, (1990).

4. Ivanchenko L.G., Guller B.D., Yu Zinyuk R., Vashkevich N G., **"Co-precipitation of Phosphates During Crystallization of Gypsum From Phosphoric Acid Solutions"**, Zhurnal Prikladnoi Khimii, Vol. 54, No. 5, pp.1001 – 1006, (May 1981).

5. Farmer V. C., **"The Infrared Spectra of Minerals"**, Adlard and Son Publishers, p. 427, (1974).

CHAPTER 8

THE EFFECT OF ALUMINIUM AND FLUORIDE IMPURITIES

8.1 INTRODUCTION:

The last effect of impurities investigated, was that of different ratios of aluminium and fluoride on the crystallisation of calcium sulphate dihydrate and the produced phosphoric acid.

8.1.1 ALUMINIUM:

The aluminium content of commercial rock can vary widely, from 0.2 per cent to three per cent (expressed as Al_2O_3). Most of the aluminium, seventy to ninety per cent, go into the solution during phosphate rock attack, where it increase the acid density and viscosity. It is reported that aluminium not only promotes regular crystal growth in al directions, but also has the benefit of reducing corrosion, probably due to the formation of AlF_6^{3-} from F^- and Al^{3+} ions [1].

The remainder stays with the gypsum, partially dissolving during the cake wash. It can therefore be concluded that aluminium precipitate as an aluminium hexafluoride, AlF_6^{3-}, possible AlF_6MgNa (ralstonite). With increasing P_2O_5 concentration, the filter cake contains more precipitated aluminium compounds.

8.1.2 FLUORIDE:

Fluorides generally occur with F/P_2O_5 ratios between 0.09 and 0.13, for sedimentary ores, and can fall to 0.04 for igneous ores [1].

Hydrofluoric acid is produced during phosphate rock attack:

$$Ca_{10}(PO_4)_6F_2 + 20H^+ \rightarrow 6\ H_3PO_4 + 10Ca^{2+} + 2HF \qquad (8.1)$$

HF is a weak acid, with $(H^+)(F^-)/HF = 10^{-3.2}$

Hydrofluoric acid has a strong tendency to react with silica:

$$6HF + SiO_2 \rightarrow H_2SiF_6 + 4H_2O \rightarrow SiF_6^{2-} + 2H^+ \quad (8.2)$$

H_2SiF_6 is a strong, totally dissociated acid.

To complete the reaction, enough reactive silica must be available. If the reaction is not completed, however, hydrofluoric acid will remain in the phosphoric acid, with the resulting high corrosion rates on all the stainless steel parts of the equipment. Hydrofluorosilicic acid, H_2SiF_6, reacts with available sodium and potassium, and precipitates as sodium and potassium hexafluorosilicates (Chapter 5 and 6). The fluoride, remaining in the phosphoric acid, is eventually deposited on the meadows through the application of phosphate fertilisers. This can give an enlarged fluoride content to the grass, which can cause fluorosis of e.g., cows [2].

8.2 EXPERIMENTAL:

8.2.1 APPARATUS:

The apparatus set-up is discussed in Chapter 2 (Section 2.5).

8.2.2 METHODOLOGY:

The methodology was the same as that discussed for sodium (Chapter 5, section 5.2.2), with the following modifications:

1. Calcium fluoride[1] and aluminium hydroxide, were added at different ratios, instead of sodium hydroxide.
2. The produced phosphoric acid was concentrated.

[1] The calcium hydroxide was corrected with the amount of calcium added with the calcium fluoride.

The produced acid was concentrated to 54 per cent P_2O_5 after four weeks, with a Buchi rotary evaporator (applied vacuum 70 kPa, water bath temperature 100 °C). After the acid stood for two weeks, the sludge was separated from the acid with filtration. Samples were collected for analyses, infrared spectra and electron microscope photographs.

Reaction conditions for the experiments are presented in Table 8.1.

8.2.3 ANALYSES OF SOLUTIONS AND SOLIDS:

Total sulphate determination of the acid samples was done by titration with barium chloride and sulphonanzo III indicator, while calcium was determined with ICP analyses. Acid samples were analysed for P_2O_5 and gypsum samples for total P_2O_5 only, by the colour development - UV spectrophotometric method.

Gypsum, postprecipitate and sludge samples were dried and infrared spectra were recorded between 400 and 4000 cm^{-1} (Appendix I). Optical and electron microscope photographs were taken of the solid samples

Acid, gypsum, postprecipitate and sludge samples were analysed for different compounds with ICP analyses.

8.3 RESULTS:

8.3.1 ANALYSES:

The different results are summarised as follows:

Table 8.2:

Calcium and sulphate analyses of the samples taken during the retention time, acid samples after one day, and acid samples after four weeks. Analyses of the acid samples (after four weeks) for: P_2O_5%, Al_2O_3%, Cu%, K_2O%, MgO% and SiO_2%.

Table 8.3:

Analyses of the gypsum samples taken, after the cake was washed with acetone, for: fixed P_2O_5%, CaO%, MgO%, Al_2O_3%, Fe_2O_3%, SO_4%, F^-%, SiO_2%, Na_2O%, K_2O%, SrO%, CeO_2 %, La_2O_3 %, Y_2O_3 ppm, and Nb_2O_3 %.

Table 8.4:

Analyses of postprecipitate samples taken, after it was washed with acetone, for: fixed P_2O_5%, CaO%, MgO%, Al_2O_3%, F^-%, SiO_2%, SO_4%, Na_2O %, K_2O %, Fe_2O_3 %, SrO%, CeO_2 %, La_2O_3 %, Y_2O_3 ppm, and Nb_2O_3 %.

Table 8.5:

Concentration and analyses of acid samples for: SO_4%, CaO%, Al_2O_3%, Cu%, K_2O%, MgO% and SiO_2%.

Table 8.6:

Analyses of sludge samples for: fixed P_2O_5%, CaO%, MgO%, Al_2O_3%, F^-%, SiO_2%, SO_4%, Na_2O %, K_2O %, Fe_2O_3 %, SrO%, CeO_2 %, La_2O_3 %, Y_2O_3 ppm, and Nb_2O_3 %. The Tables are presented below.

	EXP.40 1.0% F 0.0% Al	EXP.41 1.0% F 0.0% Al	EXP.42 0.75% F 0.25% Al	EXP.43 0.75% F 0.25% Al	EXP.44 0.5% F 0.5% Al	EXP.45 0.5% F 0.5% Al	EXP.46 0.25% F 0.75% Al	EXP.47 0.25% F 0.75% Al	EXP.48 0.0% F 1.0% Al	EXP.49 0.0% F 1.0% Al
Date	19/03/98	23/03/98	24/03/98	25/03/98	26/03/98	27/03/98	30/03/98	2/04/98	3/04/98	6/04/98
Phosphoric acid	1004.6 g.	1004.8 g.	1004.8 g.	1005.7 g.	1005.2 g.	1005.5 g.	1005.1 g.	1005.5 g.	1003.9 g.	1006.8 g.
Gypsum	50.0 g.	50.0 g.	50.0 g.	50.0 g.	50.0 g.	50.0 g.	50.0 g.	50.0 g.	50.0 g.	50.0 g.
Reagent add. Time	180 min.	180 min.	180 min.	180 min.	180 min.	180 min.	180 min.	180 min.	180 min	180 min.
Water	60 ml.	60 ml.	60 ml.	60 ml.	60 ml.	60 ml.	60 ml.	60 ml.	60 ml.	60 ml.
Calcium hydroxide	198 g. (11g / 10min)	198 g. (11g / 10min)	198 g. (11g / 10min)	198 g. (11g / 10min)	198 g. (11g / 10min)	198 g. (11g / 10min)	198 g. (11g / 10min)	198 g. (11g / 10min)	198 g. (11g / 10min)	198 g. (11g / 10min)
Sulphuric acid	145 ml. (0.8ml / min)	145 ml. (0.8ml / min)	145 ml. (0.8ml / min)	145 ml. (0.8ml / min)	145 ml. (0.8ml / min)	145 ml. (0.8ml / min)	145 ml. (0.8ml / min)	145 ml. (0.8ml / min)	145 ml. (0.8ml / min)	145 ml. (0.8ml / min)
CaF_2	30.8 g (1.7g/ 10 min)	30.8g (1.7g/ 10 min)	22.9 g (1.3g/ 10 min)	22.9 g (1.3g/ 10 min)	15.4g. (0.85g/ 10 min)	15.4g. (0.85g/ 10 min)	7.6g. (0.42g/ 10min.)	7.6g. (0.42g/ 10min.)	.	.
$Al(OH)_3$			11.3g (0.63g/ 10 min)	11.3 g (0.63g/ 10 min)	22.5g (1.25g/ 10 min)	22.5g (1.25g/ 10 min)	33.75g (1.875g/ 10 min)	33.75g (1.875g/ 10 min)	45.0g (2.5g/ 10 min)	45.0g (2.5g/ 10 min)
Reten. time	120 min.	120 min.	120 min.	120 min.	120 min.	120 min.	120 min.	120 min.	120 min.	120 min.
Samples	45.2 g.	59.0 g.	48.2 g.	41.2 g.	42.9 g.	45.7 g.	45.2 g.	49.0 g.	49.9 g.	46.0 g.
Mass slurry	1457.2 g.	1441.3 g.	1481.4 g.	1483.6 g.	1497.0 g.	1493.4 g.	1502.4 g.	1495.8 g.	1503.4 g.	1503.3 g.
Total mass	1503.0 g.	1500.3 g.	1529.6 g.	1524.8 g.	1539.9 g.	1539.1 g.	1547.6 g.	1544.8 g.	1553.3 g.	1549.3 g.
Vol. slurry	950ml.	950 ml.	950 ml.	950 ml.	950 ml.	950 ml.	950 ml.	950 ml.	920 ml	920 ml.
Permeabi-Lity	1.3 min.	43 sec.	1.0 min.	1.0 min.	1.2 min.	1.0 min	1.5 min.	1.5 min.	1.5 min.	1.5 min.
Mass gypsum*	694.2 g.	761.8 g.	790.0 g.	783.0 g.	920.0 g.	780.3 g.	950.3 g.	909.0 g.	931.4 g.	990.4 g.
Vol. acid	600 ml.	560 ml.	560 ml.	570 ml.	470 ml.	570 ml.	440 ml.	466 ml.	480 ml.	430 ml.
Density (Kg/L)	1.29	1.29	1.29	1.29	1.29	1.29	1.29	1.29	1.29	1.29
Solids %	31.5	31.5	31.5	31.5	31.5	31.5	31.5	31.5	31.5	31.5
Postprec. (Kg/L)	0.0060	0.0079	0.0050	0.0050	0.0057	0.0043	0.0072	0.0058	0.0070	0.0065

Table 8.1. Reaction conditions and results.

**Gypsum with unfiltrated acid*

Experiment	40	41	42	43	44	45	46	47	48	49
Sulphate analyses *Sample 1*	5.18%	4.30%	4.56%	4.70%	4.00%	4.10%	3.10%	3.44%	2.60%	2.60%
Sample 2	5.16%	3.80%	4.30%	4.50%	3.78%	3.90%	3.05%	3.20%	2.35%	2.34%
Sample 3 (1 day)	4.60%	2.90%	3.80%	3.90%	3.75%	3.74%	2.70%	2.80%	1.96%	2.07%
Sample 4 (4 weeks)	4.56%	2.67%	3.70%	3.80%	3.74%	3.68%	2.70%	2.80%	1.96%	1.98%
Calcium analyses *Sample 1*	0.192%	0.192%	0.154%	0.151%	0.162%	0.174%	0.200%	0.171%	0.263%	0.256%
Sample 2	0.164%	0.259%	0.860%	0.152%	0.146%	0.138%	0.174%	0.167%	0.202%	0.190%
Sample 3 (1 day)	0.093%	0.128%	0.129%	0.088%	0.086%	0.061%	0.086%	0.102%	0.109%	0.128%
Acid (4 weeks)	0.035%	0.054%	0.040%	0.039%	0.046%	0.043%	0.050%	0.049%	0.071%	0.071%
CaO% *sample 1*	0.269%	0.268%	0.215%	0.211%	0.227%	0.244%	0.280%	0.239%	0.369%	0.357%
Sample 2	0.229%	0.362%	0.233%	0.212%	0.205%	0.194%	0.243%	0.234%	0.282%	0.266%
Sample 3 (1 day)	0.130%	0.179%	0.122%	0.123%	0.121%	0.086%	0.119%	0.142%	0.153%	0.179%
Acid (4 weeks)	0.049%	0.076%	0.056%	0.055%	0.065%	0.060%	0.070%	0.069%	0.100%	0.100%
P_2O_5 *acid*	27.3%	26.5%	29.12%	29.7%	26.2%	26.0%	29.5%	25.9%	29.5%	25.9%
Al_2O_3 *acid*	0.023%	0.039%	0.576%	0.587%	1.123%	1.126%	1.720%	1.702%	2.358%	2.253%
Cu *acid*	0.0003%	0.0004%	0.0004%	0.0004%	0.0004%	0.0004%	0.0004%	0.0004%	0.0004%	0.0004%
K_2O *acid*	0.027%	0.030%	0.024%	0.028%	0.029%	0.028%	0.030%	0.030%	0.028%	0.028%
MgO *acid*	0.323%	0.332%	0.334%	0.333%	0.323%	0.341%	0.333%	0.327%	0.340%	0.340%
SiO_2 *acid*	0.906%	1.244%	0.786%	0.764%	0.424%	0.451%	0.314%	0.316%	0.197%	0.194%

Table 8.2. Analyses of samples taken during retention time and acid analyses.

	Exp.40	Exp.41	Exp.42	Exp.43	Exp.44	Exp.45	Exp.46	Exp.47	Exp.48	Exp.49
Fixed P_2O_5 %	2.08	4.43	7.03	7.15	10.80	7.98	8.70	9.80	11.30	8.55
CaO%	32.78	32.05	29.97	30.05	26.37	30.37	28.44	27.08	24.70	26.31
MgO %	0.15	0.18	0.19	0.17	0.19	0.16	0.14	0.15	0.19	0.12
Al_2O_3 %	0.05	0.06	0.36	0.31	0.57	0.49	0.66	0.69	1.19	0.74
Fe_2O_3 %	0.03	0.03	0.04	0.06	0.06	0.05	0.05	0.05	0.08	0.04
F^- %	1.6	0.7	1.3	1.4	1.3	1.2	0.8	0.8	0.4	0.2
SO_4%	44.7	40.7	38.6	38.8	34.2	39.3	40.6	38.0	38.3	39.7
SiO_2 %	0.39	0.33	0.34	0.45	0.38	0.27	0.12	0.15	0.11	0.07
Na_2O %	0.10	0.07	0.09	0.09	0.07	0.07	0.04	0.05	0.04	0.04
K_2O %	0.02	0.01	0.03	0.01	0.03	0.02	0.01	0.02	0.02	<0.01
SrO %	0.04	0.3	0.03	0.03	0.02	0.03	0.02	0.02	0.02	0.02
CeO_2%	0.05	0.05	0.05	0.04	0.04	0.05	0.05	0.05	0.05	0.05
La_2O_3 %	0.03	0.02	0.02	0.02	0.02	0.02	0.02	0.02	0.02	0.02
Y_2O_3 ppm	247	72	73	73	58	62	87	105	62	56
Nb_2O_3%	0.04	0.04	0.04	0.04	0.04	0.04	0.04	0.04	0.04	0.04

Table 8.3. Analyses of gypsum samples.

	Exp.40	Exp.41	Exp.42	Exp.43	Exp.44	Exp.45	Exp.46	Exp.47	Exp.48	Exp.49
Fixed P_2O_5 %	1.0	1.2	2.4	1.8	6.0	2.6	2.2	3.3	4.9	4.0
CaO %	35.2	37.7	34.0	33.2	31.8	31.5	29.9	28.9	30.9	28.6
MgO %	0.02	0.02	0.22	0.16	0.28	0.19	0.19	0.19	0.26	0.31
Al_2O_3 %	0.13	0.13	0.20	0.14	0.43	0.27	0.40	0.38	0.73	0.81
F %	<0.05	<0.05	<0.05	0.16	0.13	0.13	0.17	0.14	0.09	0.14
SiO_2 %	0.02	0.02	0.02	0.02	0.15	0.03	0.02	0.02	0.02	0.02
SO_4 %	52.0	54.4	44.7	50.0	44.2	49.7	49.0	48.7	47.1	47.9
Na_2O %	0.03	0.03	0.03	0.03	0.03	0.03	0.03	0.03	0.03	0.03
K_2O %	0.007	0.006	0.009	0.009	0.009	0.007	0.010	0.007	0.006	0.008
Fe_2O_3 %	0.01	0.01	0.02	0.02	0.04	0.03	0.02	0.03	0.37	0.38
SrO%	0.08	0.10	0.03	0.04	0.04	0.04	0.04	0.04	0.04	0.04
CeO_2%	0.07	0.07	0.03	0.03	0.03	0.03	0.03	0.025	0.023	0.024
La_2O_3%	0.06	0.08	0.01	0.01	0.01	0.01	0.01	0.01	0.01	0.01
Y_2O_3ppm	79	59	43	33	37	35	45	40.3	29.9	34.4
Nd_2O_3%	0.07	0.07	0.02	0.03	0.02	0.02	0.02	0.02	0.02	0.02

Table 8.4. Analyses of postprecipitate samples.

	Exp.41	Exp.43	Exp.45	Exp.47	Exp.49
P_2O_5 *acid*	54.3%	51.2%	56.0%	51.6%	53.8%
Density	1.75	1.72	1.81	1.84	1.86
Postprecipi-tate (Kg/L)	0.049	0.016	0.009	-	-
SO_4^{2-} %*acid*	5.58	7.60	8.10	6.35	4.22
CaO%*acid*	0.016	0.0057	0.015	0.0020	0.059
Al_2O_3 *acid*	2.38	0.084	2.70	1.21	9.40
Cu *acid*	<0.0000	0.0003	0.0014	<0.0000	<0.0000
K_2O *acid*	0.035	0.049	0.130	0.032	0.160
MgO *acid*	0.35	0.45	1.56	0.37	1.91
SiO_2 *acid*	0.017	0.150	0.380	0.017	0.200

Table 8.5. Concentration and analyses of acid samples.

	Exp. 41	Exp. 45	Exp. 49
Fixed P_2O_5 %	-	-	-
CaO %	23.1	19.3	26.7
MgO %	1.01	0.71	0.99
Al_2O_3 **%**	0.23	0.65	1.09
F %	12.5	-	-
SiO_2 **%**	0.02	0.02	0.01
SO_4 **%**	41.3	34.2	46.8
Na_2O **%**	6.61	9.85	3.81
K_2O **%**	0.18	0.28	0.14
Fe_2O_3 **%**	0.14	0.10	0.22
SrO%	0.42	0.26	0.26
CeO_2**%**	1.7	1.2	1.3
La_2O_3**%**	0.9	0.7	0.8
Y_2O_3**ppm**	574	719	466
Nd_2O_3**%**	1.3	0.9	1.0

Table 8.6. Analyses of sludge samples.

8.4 DISCUSSION:

8.4.1 GROWTH RATE:

The effect of different ratios of aluminium and fluoride, on the growth rate of calcium sulphate dihydrate, is presented in Figure 8.1. Relative saturation and growth rate values were calculated using equation 4.3 and 4.4 (Chapter 4, Section 4.4.2)[1].

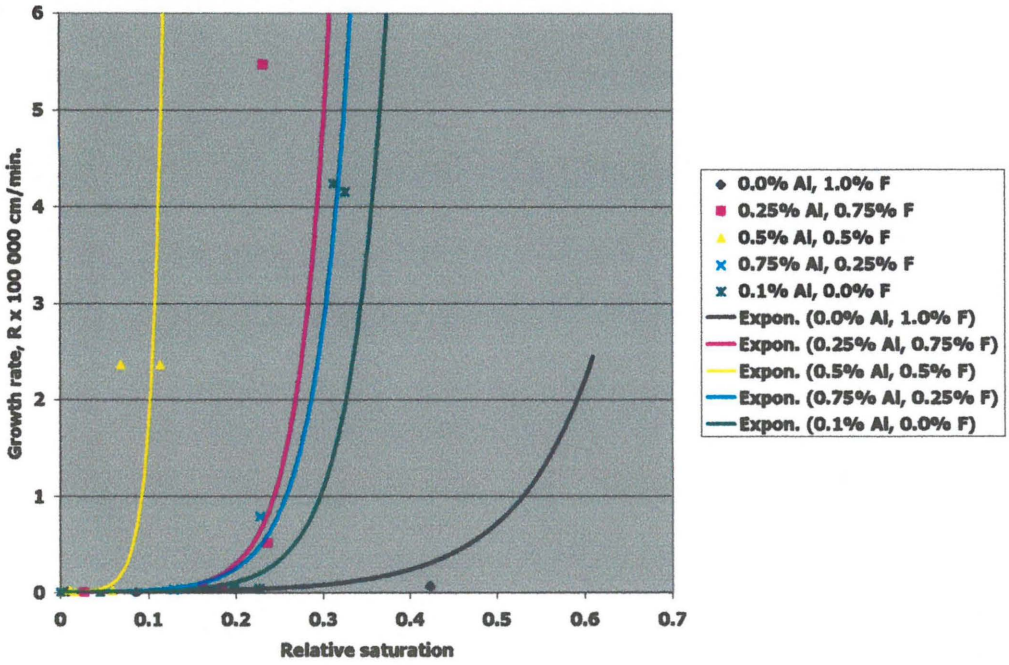

Figure 8.1. The influence of different ratios of aluminium and fluoride, on the growth rate of calcium sulphate dihydrate.

The growth rate was initially increased with elevated levels of aluminium impurity, up to 0.5 per cent added, but decreased with further additions. The growth rate was, however, higher than in the absence of added aluminium impurity.

[1] Details of calculation procedures are presented in Appendix II.

It is reported that the dependence of the solubility of calcium sulphate dihydrate on the aluminium/fluoride ratio, is the consequence of predominant formation of AlF^{2+} complexes under the given condition [3]. The AlF^{2+} complex lowers the stability of the phosphoric acid – water association, and raises the water activity. Increasing solubility results in increasing growth rates.

8.4.2 GYPSUM MORPHOLOGY:

Elevated ratios of aluminium/fluoride initially enhanced the growth rate, with the resulting increase in crystal size. Aluminium promotes growth in all directions, and improves the thickness – to – length ratio of the crystal [1,4]. At high ratios, however, the opposite trend was observed; decreasing growth rates with the resulting smaller crystals. Although twinning of the calcium sulphate dihydrate crystals is usually associated with sodium, the formation of a {100} penetration twins occurred with increasing ratios of aluminium/fluoride Electron micrographs of two gypsum samples are presented in Figure 8.2.

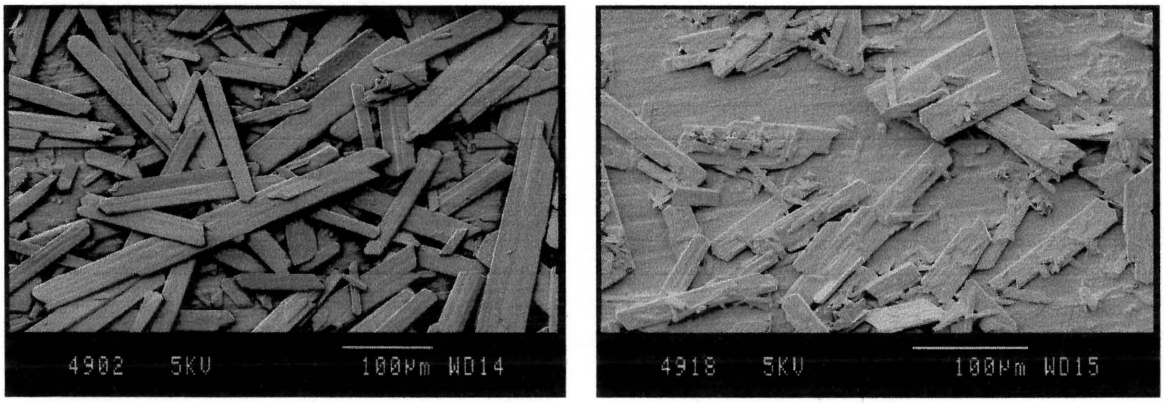

a **b**

Figure 8.2. Gypsum samples of Experiment 41 (Figure 8.2a) and Experiment 47 (Figure 8.2b), illustrating the effect of elevated ratios of aluminium/fluoride on the morphology of the crystals.

8.4.3 CO-PRECIPITATION OF P_2O_5:

Gypsum analyses (Table 8.3) show an increasing percentage of co-precipitated P_2O_5 with elevated ratios of aluminium/fluoride. It was found that polyvalent ions increase the substitution considerably, although it was not incorporated into the crystal lattice [5]. It was suggested that the polyvalent ions either decrease the concentration of hydronium ions, and thus favour the formation of HPO_4^{2-} ions in the solution, or adsorb at the crystal surface, forming a layer which unfavourably influences the passage of certain ions against others.

Fluoride probably formed a fluoroaluminate complex of the AlF_x^{3-x} type, reducing the effect of aluminium on the percentage of co-precipitated P_2O_5. This is in agreement with the findings of Ivancheko et. al. [6]. Infrared spectra of the gypsum samples confirmed the presence of co-precipitated P_2O_5.

8.4.4 PHOSPHORIC ACID:

Most of the added aluminium deported to the acid (acid and gypsum analyses, Table 8.2 and Table 8.3). Aluminium ions polarised the surrounding in a similar manner as magnesium ions, with the resulting increase in acid viscosity, that retards filtration. An increasing amount of small crystals, the result of increased acid viscosity, was also observed with elevated ratios of aluminium and fluoride (Figure 8.2).

Aluminium impurity enhances the degree of agglomeration [7]. The degree of agglomeration is proportional to the slurry density; that is, an increase in the density increases the probability that any two particles will collide. This modifying effect is much more pronounced in the static case, indicating the existence of a hydrodynamic influence on the growth process.

8.4.5 POSTPRECIPITATE MORPHOLOGY:

Agglomeration of gypsum was not observed, however, enhanced agglomeration with elevated ratios of aluminium/fluoride was evident in electron micrographs of postprecipitate samples. Electron micrographs of a postprecipitate sample (Experiment 47) are presented in Figure 8.3. Agglomeration of the crystals is evident.

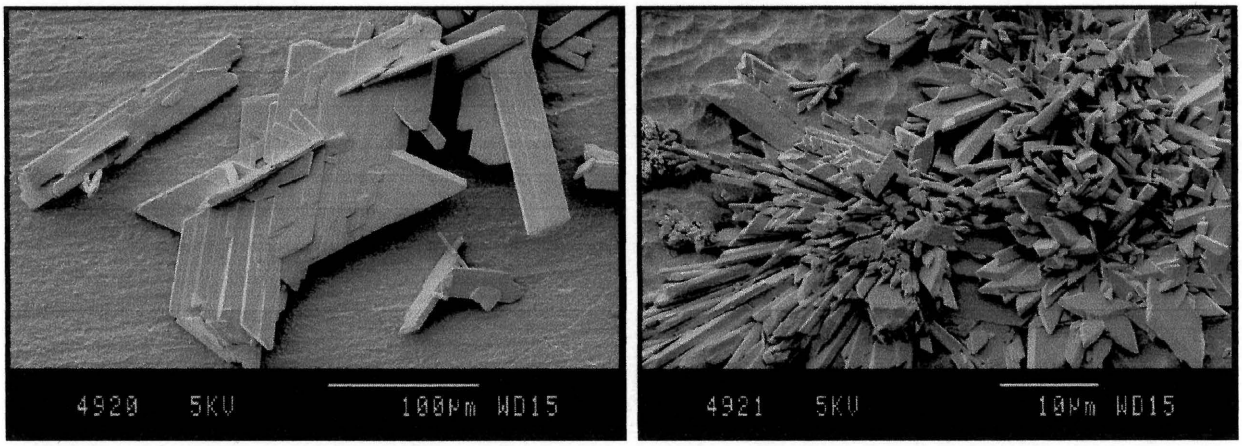

Figure 8.3. Electron micrographs of a postprecipitate sample (Experiment 47), illustrating the agglomeration of the crystals.

8.4.6 SLUDGE:

It is difficult to determine the exact composition of the sludge samples, however, it is probably a combination of calcium sulphate, ralstonite ($MgAlF_6Na.6H_2O$) and chukhrovite ($CaSO_4.CaSiF_6CaAlF_6(Na)_{12}H_2O$. Infrared spectra of the samples confirm the presence of hexafluorosilicate. The sludge analyses is presented in Table 8.6.

8.5 CONCLUSIONS:

Elevated levels of the aluminium/fluoride ratio initially promoted the growth rate, due to the formation of AlF^{2+} complexes that increased the water activity. Further elevation of the ratio resulted in increasing concentrations of aluminium impurity in the acid. Although aluminium promoted growth of calcium sulphate dihydrate, it also increased the acid viscosity (amount of small crystals), and density (agglomeration of the crystals). Elevated aluminium concentrations also resulted in increasing co-precipitation of P_2O_5.

Controlling the aluminium/fluoride ratio, can thus not only promote crystal growth and enhance filtration rates, but reduce the co-precipitation of P_2O_5 as well.

8.6 REFERENCES:

1. Becker P., **"Phosphates and Phosphoric acid"** Raw Materials, Technology and Economics of the wet process, Fertilizer science and technology series - Vol. 6., 2nd edition (1989).

2. Van der Sluis S., Schrijver A.H.M., Baak F.P.C., van Rosmalen G.M**., "Fluoride Distribution Coefficients in Wet Phosphoric Acid Processes"**, Industrial Engineering and Chemical Research, Vol. 27, pp. 527 – 536, (1988).

3. Glazyrina L.N., Savinkova E.I., Grinevich A.V., Akhmedova L.E., **"Solubility of Calcium Sulphate Hemihydrate and Dihydrate in Phosphoric Acid Containing Al^{3+}, F^-, and SiF_6^{2-} ions"**, Zhurnal Prikladnoi Khimii, Vol. 53, No. 11, pp. 2524 – 2527, (November 1980).

4. Hasson D., Addai-Mensah J., Metcalfe J., **"Filterability of Gypsum Crystallized in Phosphoric Acid Solutions in the Presence of Ionic Impurities"**, Industrial and Engineering Chemical Research, Vol. 29, pp. 867 – 875, (1990.)

5. Dahlgren S.E., **"Phosphate Substitution in Calcium Sulphate in Phosphoric Acid Manufacture"**, British Chemical Engineering, Vol. 10, No. 11, (November 1965).

6. Ivancheko L.G., Guller B.D., Yu Zinyuk R., Vashkevich N G., **"Co-precipitation of Phosphates During Crystallization of Gypsum From Phosphoric Acid Solutions"**, Zhurnal Prikladnoi Khimii, Vol. 54, No. 5, pp.1001 – 1006, (May 1981).

7. Budz J., Jones A.G., Mullin J.W., **"Effect of Selected Impurities on the Continuous precipitation of Calcium Sulphate (Gypsum)"**, Journal of Chemical Technology and Biotechnology, Vol. 36, pp. 153 – 161, (1986).

CHAPTER 9

CONCLUSIONS

9.1 SATURATION AND SUPERSATURATION OF CALCIUM SULPHATE DIHYDRATE:

The crystal morphology of calcium sulphate dihydrate is influenced by factors such as temperature, added impurities and the free sulphate concentration in the reacting solution. Since the production of small crystals must be avoided in order to maintain acceptable filtration rates, it is necessary to know the saturation and supersaturation diagram for the specific type of rock.

The saturation and supersaturation diagram was determined for 88P rock. It was found that the saturation line, at 25°C, could be expressed as follows:

$$K_{SL} = SO_4\% \times CaO\% \approx 0.12^{1}, \quad (9.1)$$

while the supersaturation line, at 80°C, can be expressed as:

$$K_{SSL} = [CaO] \times [SO_4] \approx 1.06. \quad (9.2)$$

When calcium and sulphate concentrations are between the saturation and supersaturation lines, the crystals will be subjected to regular crystal growth only, with the resulting larger crystals and good filtration rates. Going beyond the supersaturation line, however, will promote the formation of nuclei. Increasing numbers of small crystals hinder filtration rates.

It was illustrated why it is necessary to maintain a minimum percentage of free sulphate in the reacting slurry.

---

[1] The value is in good agreement with the calculated value, using the equation of Kurteva and Brustus.

9.2 THE EFFECT OF IMPURITIES:

The presence of extraneous impurities in the reacting slurry can influence different aspect of wet-process phosphoric acid production, such as: filtration rates, scaling and corrosion of the equipment, and the final concentration of impurities in the produced phosphoric acid.

Sodium, potassium, magnesium, and different ratios of aluminium and fluoride were added to the reaction slurry, while simulating actual plant conditions, in order to investigate the influence of these ions on the crystallisation of calcium sulphate dihydrate and the produced phosphoric acid.

9.2.1 SODIUM:

Elevated levels of sodium impurity promoted the growth of calcium sulphate in three ways: by enhancing the solubility of calcium sulphate dihydrate, by assisting the incorporation reaction of the building units, and by promoting the formation of a {101} twins. Sodium mainly precipitated with calcium sulphate dihydrate, and only a small percentage deported to the acid. Although analyses were not available to calculate the distribution coefficient, D, is can be assumed that some of the sodium would be incorporated into the crystal lattice by means of isomorphous substitution of calcium ions. The increased growth rate was confirmed by increasing concentrations of impurities in the precipitated gypsum.

When the slurry cooled during filtration, sodium hexafluorosilicate precipitated as minute crystals, which blinded the filter cloth and thus decreased the filtration rates. This reaction, however, has the advantage of lowering the fluoride concentration in the slurry, and thus the corrosion on stainless steel parts.

9.2.2 POTASSIUM:

Since sodium and potassium ions are very similar, it was expected that potassium would have the same effect as sodium. Elevated levels of potassium did indeed enhance the growth rate of calcium sulphate dihydrate, however, not as much as sodium did. Calculation of the distribution coefficient indicated that potassium was not incorporated into the crystal lattice by isomorphous substitution of calcium. This result must, however, be interpreted with caution since the analyses did not distinguish between co-precipitated potassium, and potassium hexafluorosilicate that precipitated on the crystal surface of the crystals. It is quite possible that some of the potassium was incorporated by means of isomorphous substitution.

Potassium hexafluorosilicate is less soluble than sodium hexafluorosilicate, at this particular temperature and acid strength. Precipitation of potassium hexafluorosilicate was evident in optical and electron microscope photographs of gypsum and postprecipitate samples, and was confirmed by infrared spectra and analyses. The precipitation of potassium hexafluorosilicate decreased the concentration of potassium in the reacting slurry, and thus the effect of potassium on the growth rate of calcium sulphate dihydrate. It is also suspected that some of the hexafluorosilicate precipitated on the crystal surface of calcium sulphate, decreasing the available crystal surface that in effect lowered the growth rate. Precipitation of hexafluorosilicate with calcium sulphate dihydrate, lowered the amount that would have precipitated when the slurry cools during filtration.

9.2.3 MAGNESIUM:

Elevated levels of magnesium had no effect on the growth rate of calcium sulphate dihydrate. Most of the added magnesium deported to the acid, while a small percentage was incorporated into the crystal lattice of calcium sulphate dihydrate.

Elevated levels of magnesium ions in the acid polarised the surroundings, strengthened the hydrogen bonds, and thus increased the acid viscosity. Transport of ions becomes more difficult with increasing acid viscosity, and leads to local supersaturations of extended duration. Nucleation is thus promoted, and the amount of small crystals increased.

Analyses show that the percentage of co-precipitated P_2O_5 increased with elevated levels of supersaturation. The presence of magnesium ions in the acid promotes the formation of HPO_4^{2-} by forming associate pairs with it.

9.2.4 ALUMINIUM AND FLUORIDE:

Augmenting ratios of aluminium and fluoride were added to the reacting slurry. It was found that the presence of aluminium and fluoride, in the ratio that promoted the formation of AlF^{2+}, increased the growth rate of calcium sulphate dihydrate. The AlF^{2+} complex apparently lowers the stability of the phosphoric acid – water association and rises the water activity.

Aluminium promoted growth of calcium sulphate dihydrate in all directions. Elevated levels of aluminium, however, also enhanced the acid viscosity and density that reduce filtration rates. Agglomeration of calcium sulphate dihydrate crystals, an indication of enhanced acid density, were evident in electron micrographs of postprecipitate samples.

9.3 FUTURE WORK:

The effect of different impurities on the growth rate of calcium sulphate was investigated, while simulating actual plant conditions. It was found that sodium and

potassium ions, both monovalent, and aluminium ions, trivalent, promoted growth of gypsum crystals. However, magnesium ions, divalent, had no effect on the growth rate. Impurities probably influence the surface charge, assisting the incorporation of building units, or the dehydration of the ions. The exact mechanism, however, is not understood.

A study of the crystal growth process, with the purpose of determining the exact mechanism by which impurities actually assist growth, would help to explain the effects of other impurities on the growth rate of calcium sulphate dihydrate.

APPENDIX I

INFRARED SPECTRA

1.1 INFRARED SPECTRA OF CHAPTER 3:

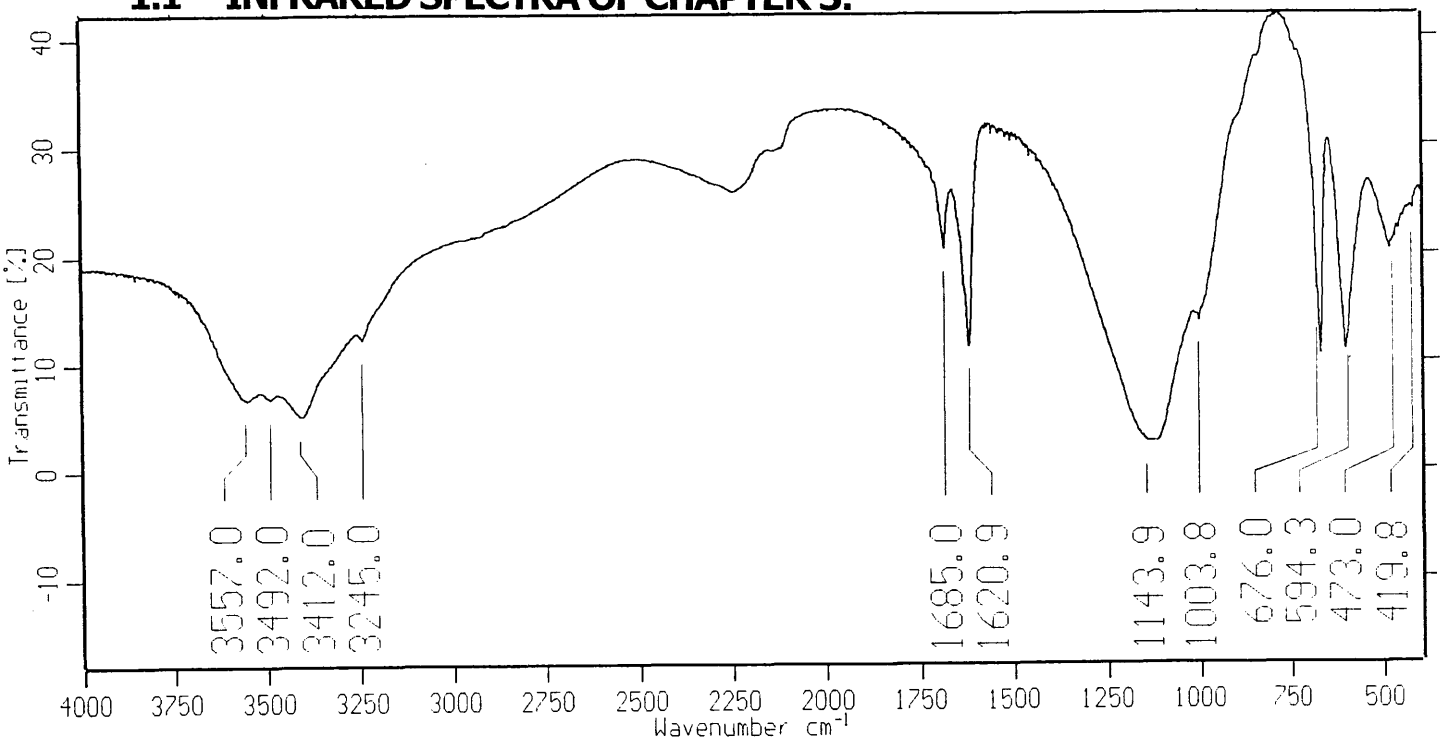

Figure 1.1. Mid-infrared spectrum of gypsum Experiment 2.

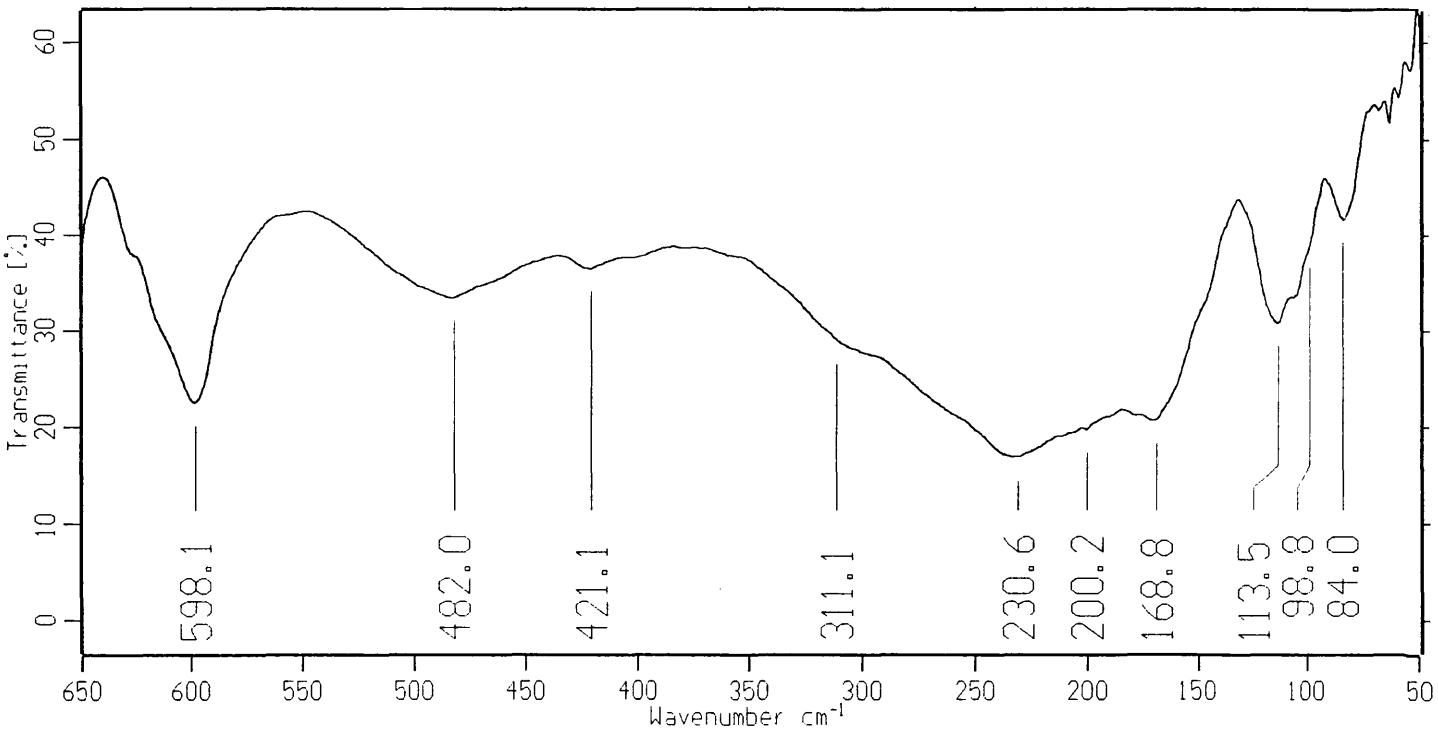

Figure 1.2. Far-infrared spectrum of gypsum Experiment 2.

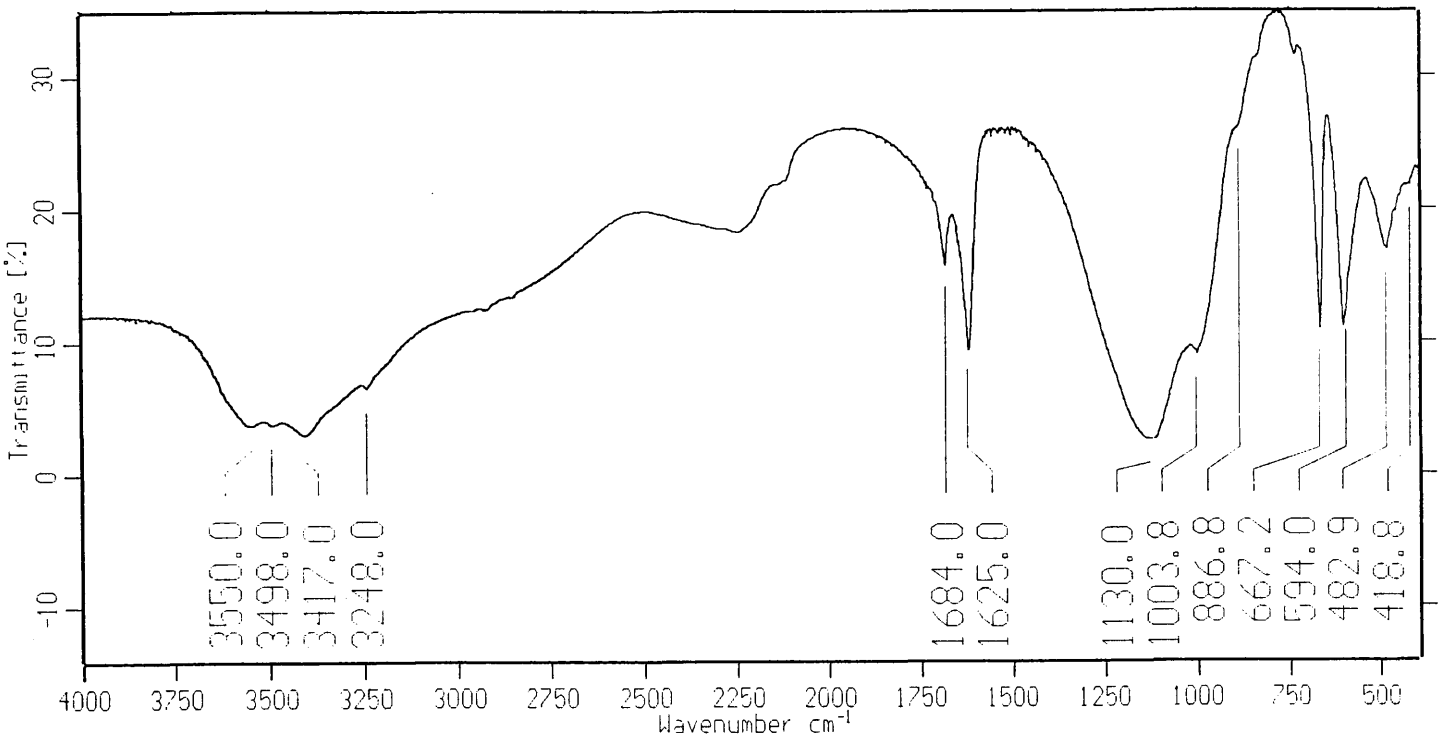

Figure 1.3. Mid-infrared spectrum of gypsum Experiment 3.

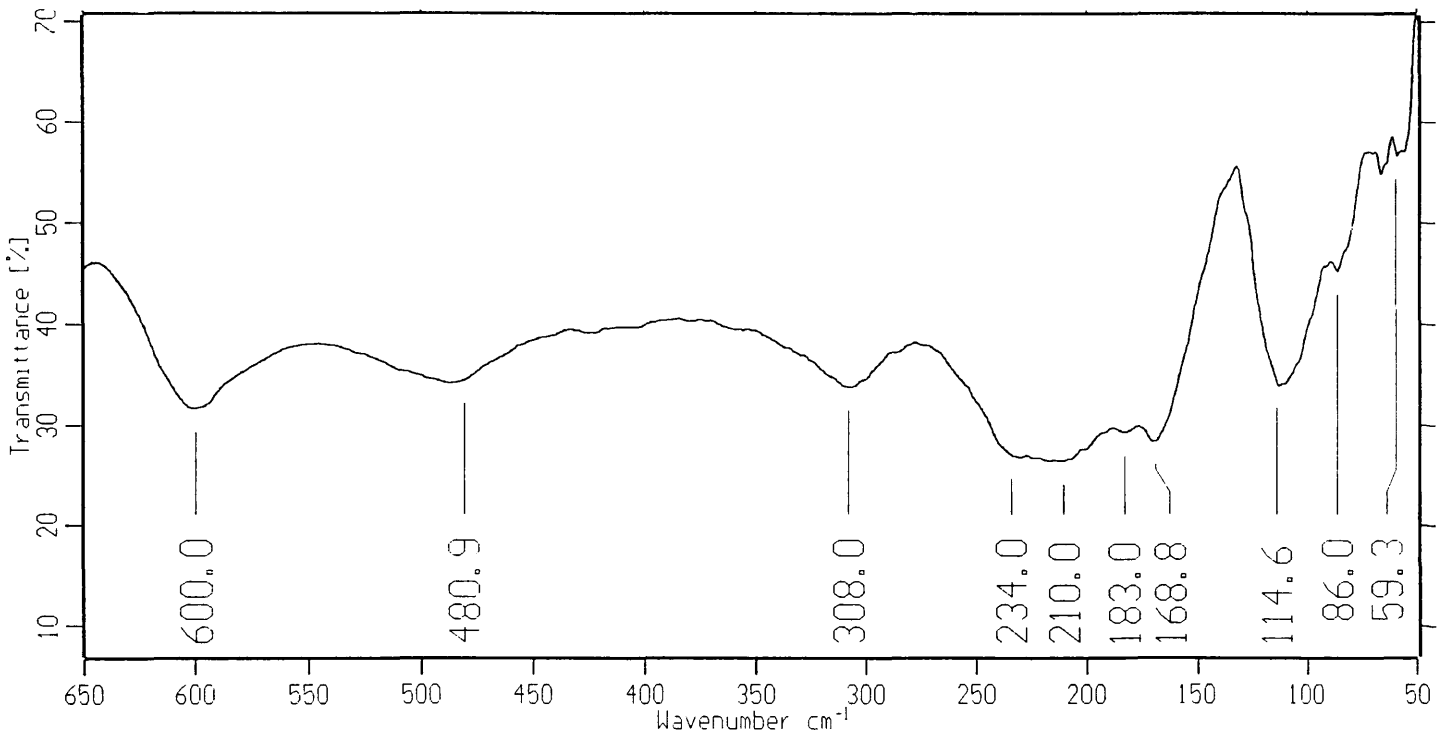

Figure 1.4. Far-infrared spectrum of gypsum Experiment 3.

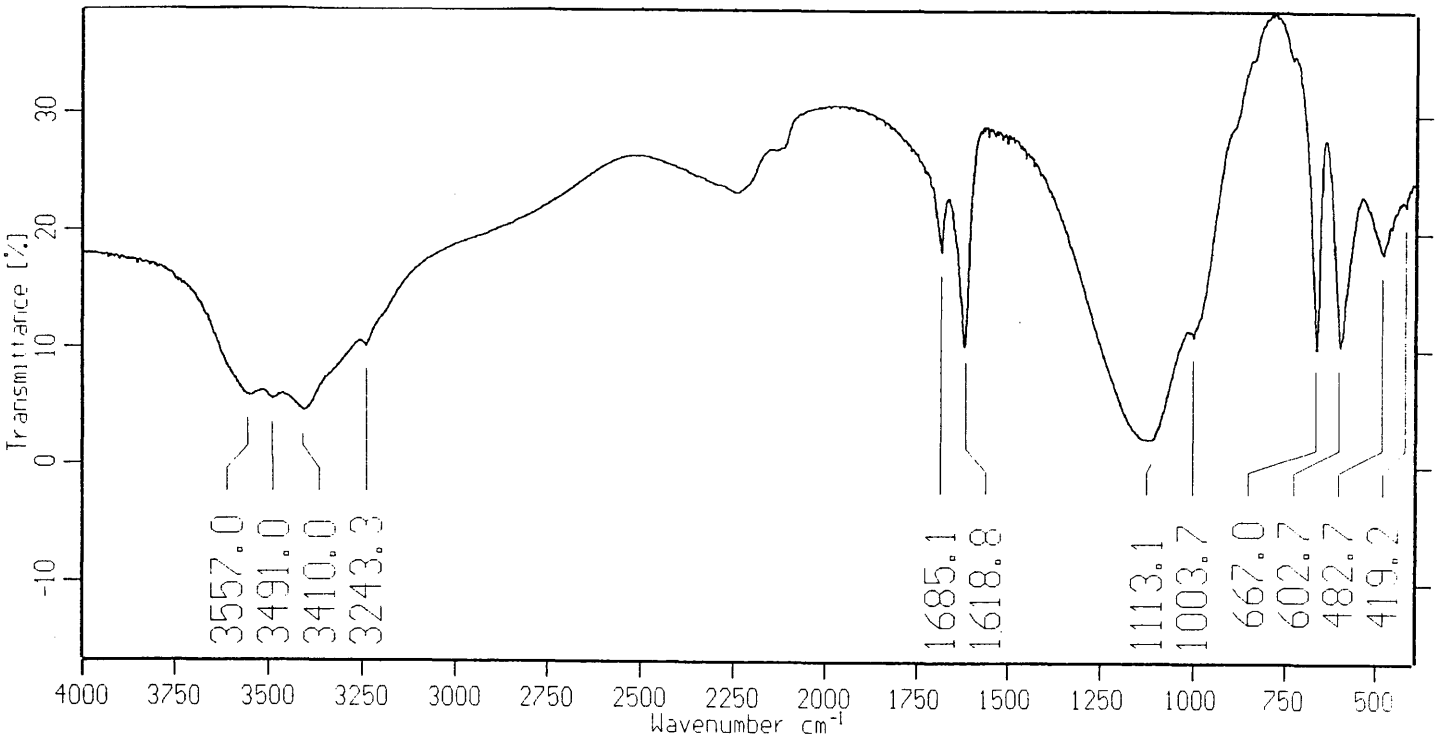

Figure 1.5. Mid-infrared spectrum of gypsum Experiment 4.

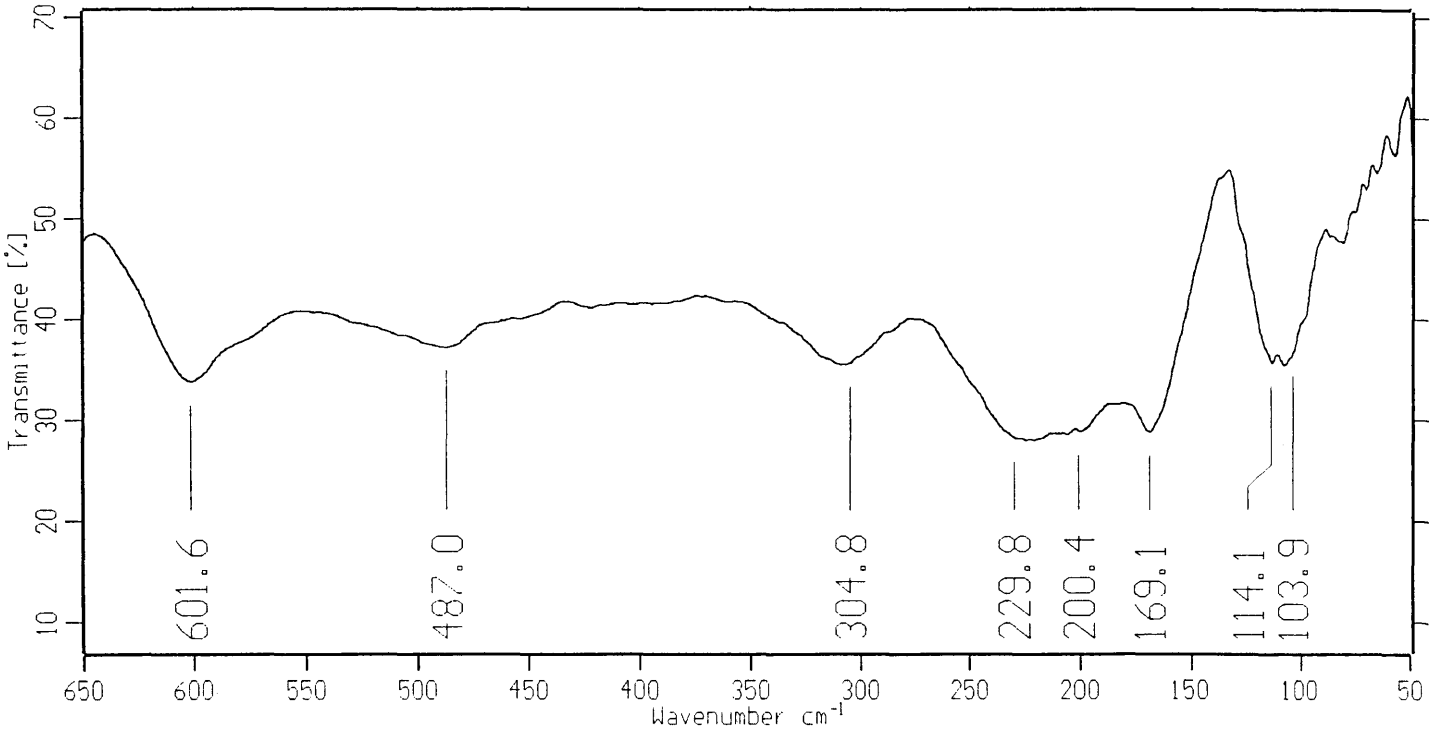

Figure 1.6. Far-infrared spectrum of gypsum Experiment 4.

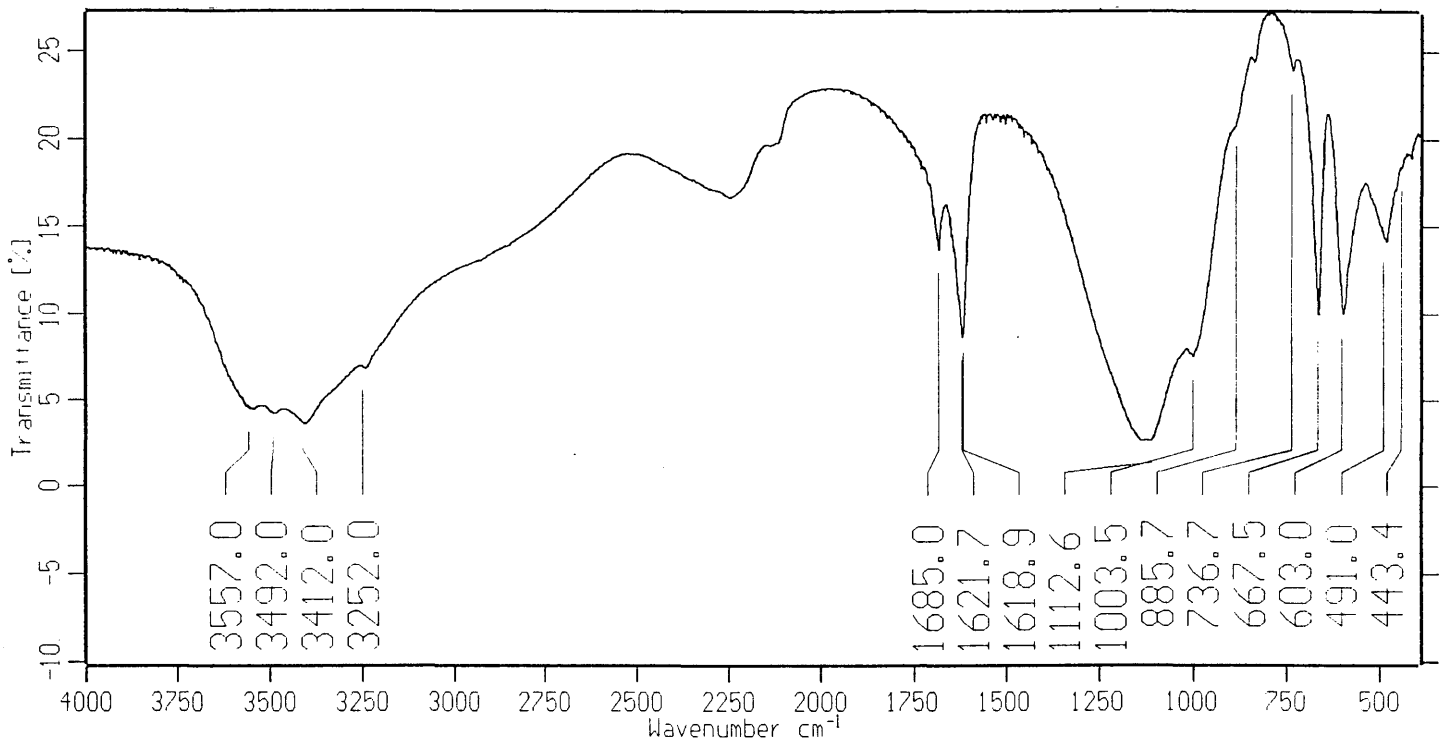

Figure 1.7. Mid-infrared spectrum of gypsum Experiment 6.

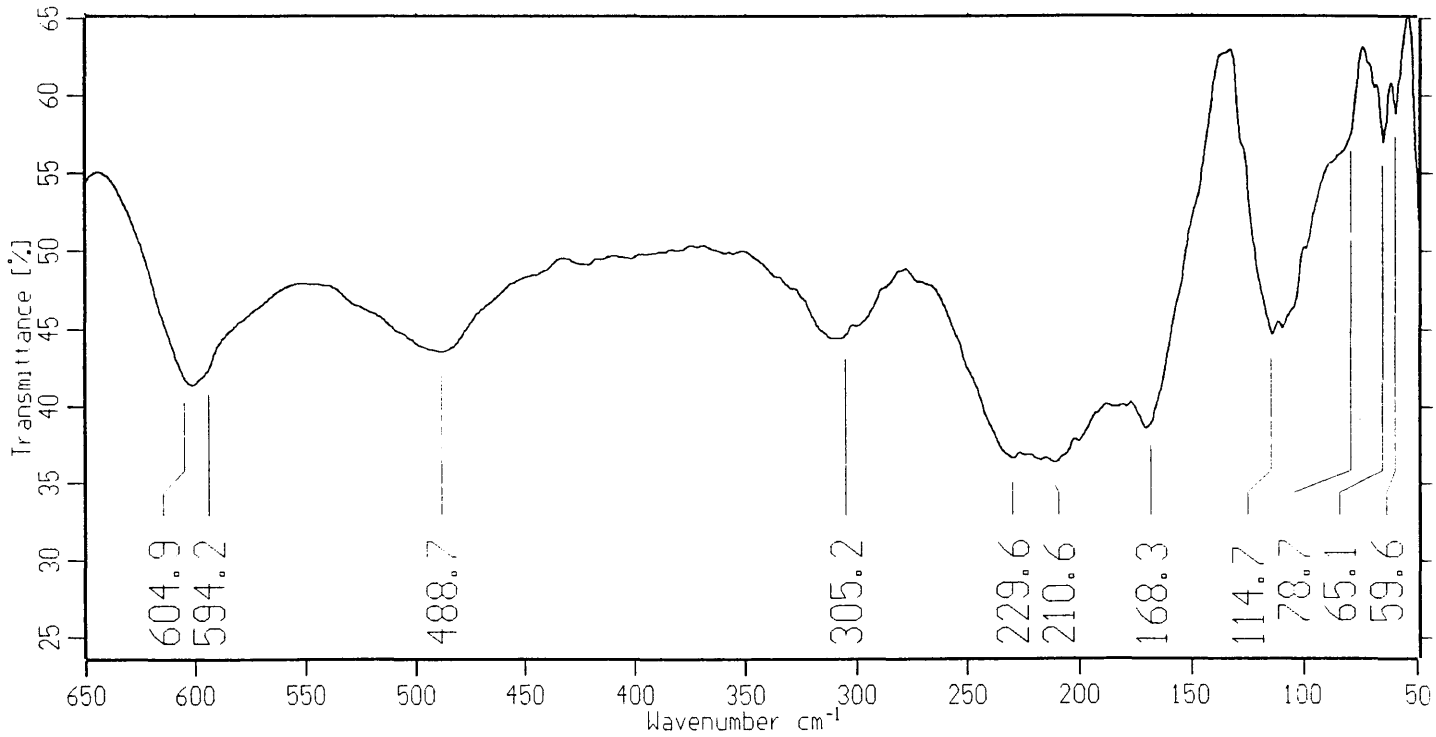

Figure 1.8. Far-infrared spectrum of gypsum Experiment 6.

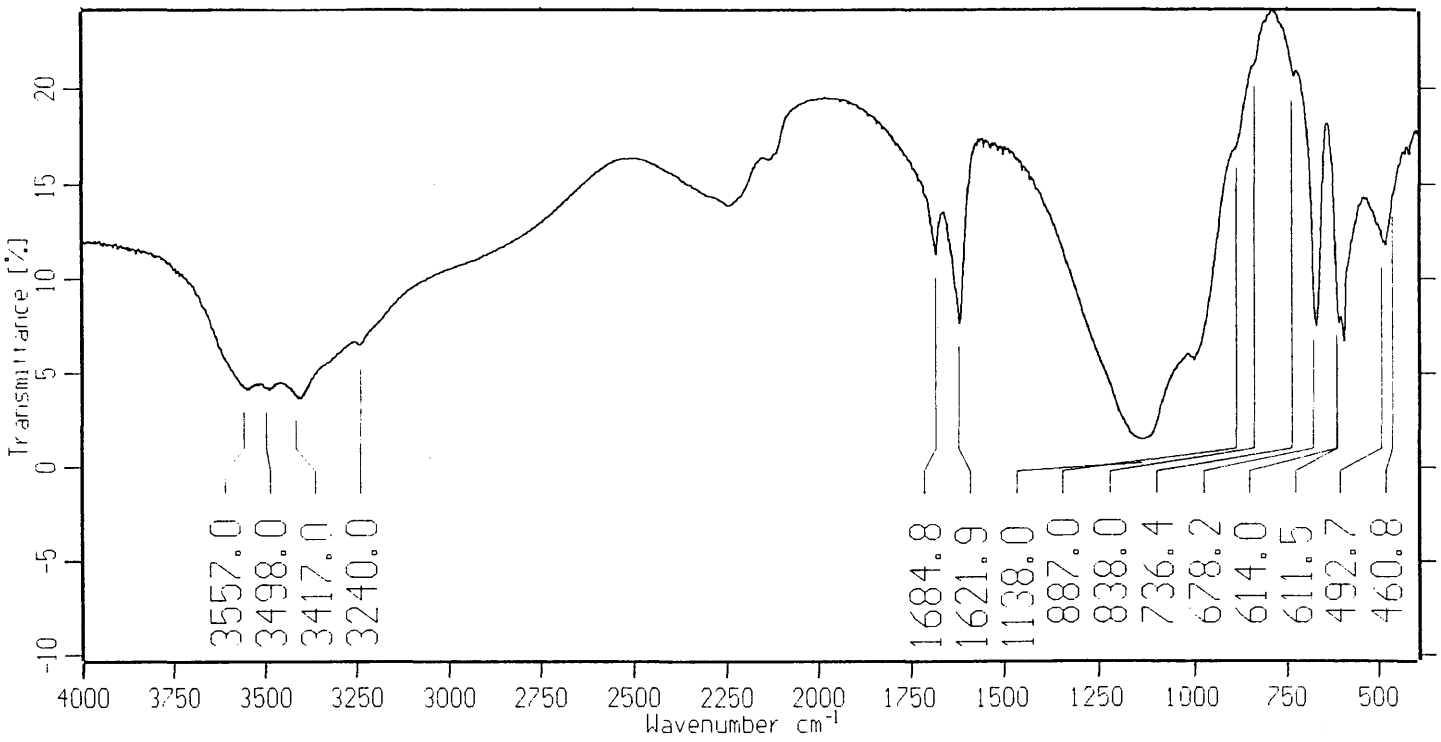

Figure 1.9. Mid-infrared spectrum of gypsum Experiment 7.

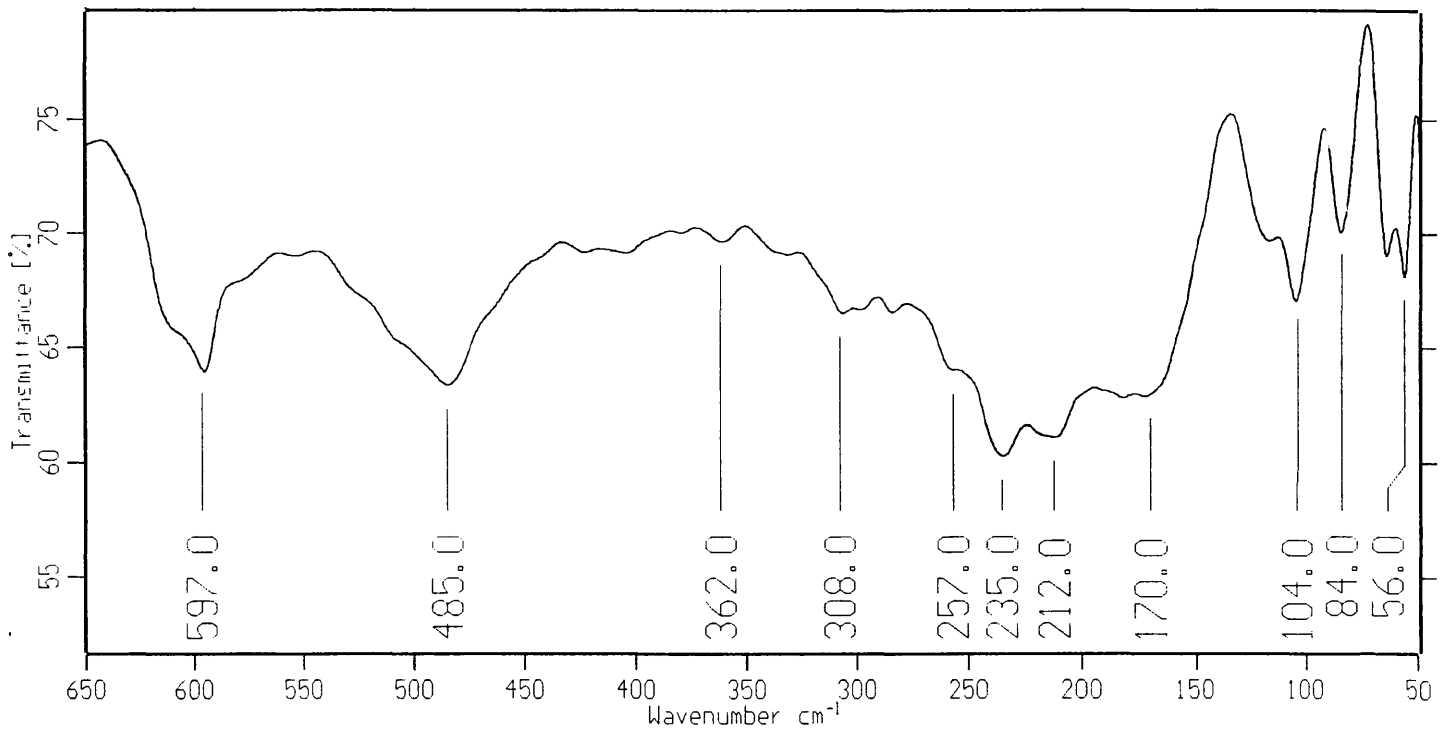

Figure 1.10. Far-infrared spectrum of gypsum Experiment 7.

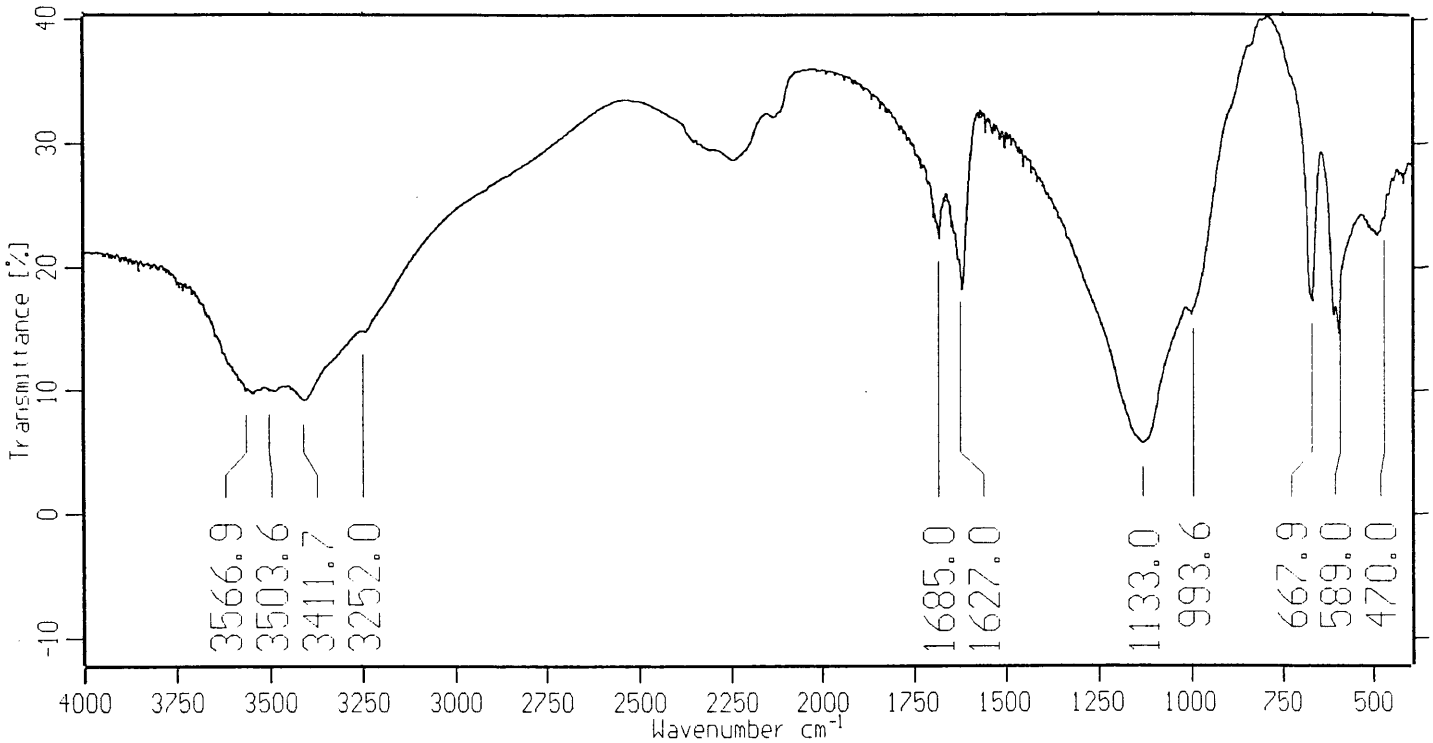

Figure 1.11. Mid-infrared spectrum of gypsum Experiment 8.

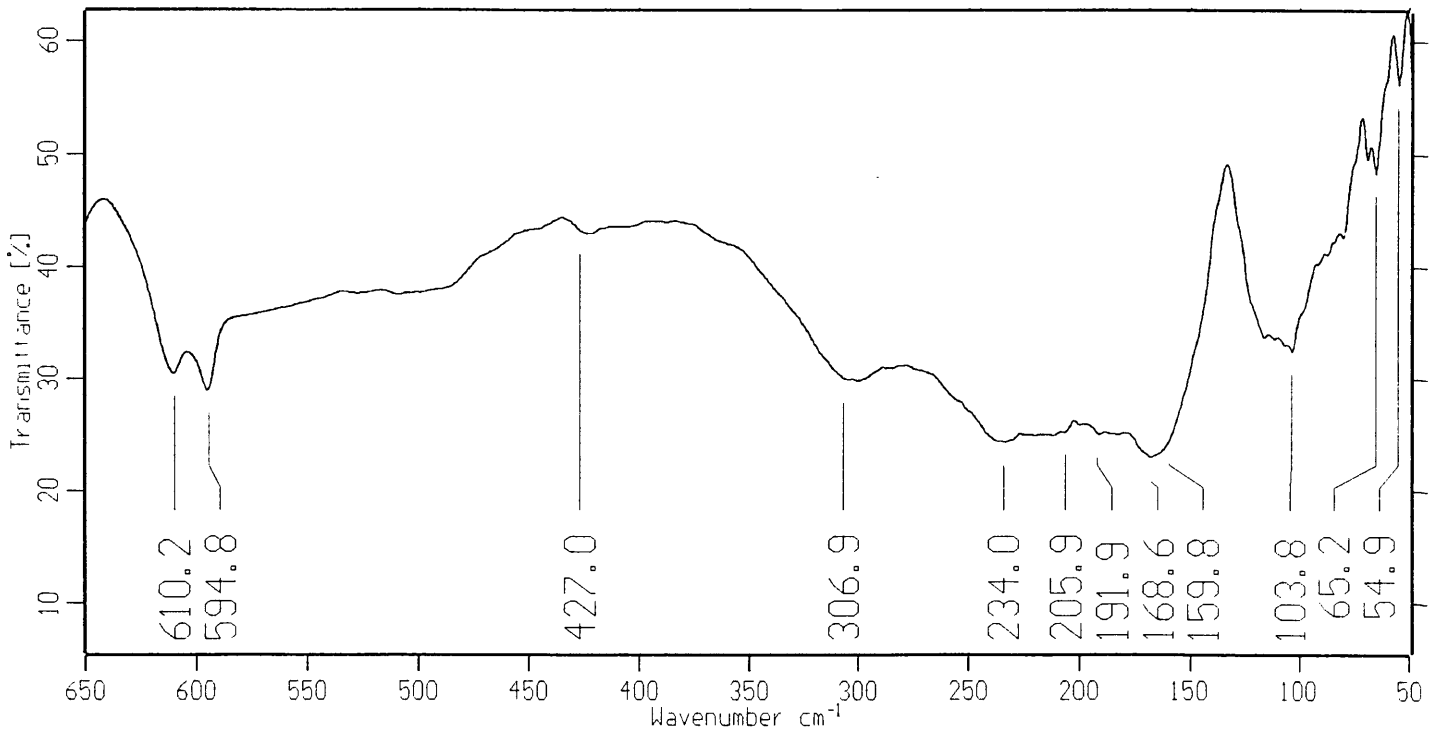

Figure 1.12. Far-infrared spectrum of gypsum Experiment 8.

1.2 INFRARED SPECTRA OF CHAPTER 5:

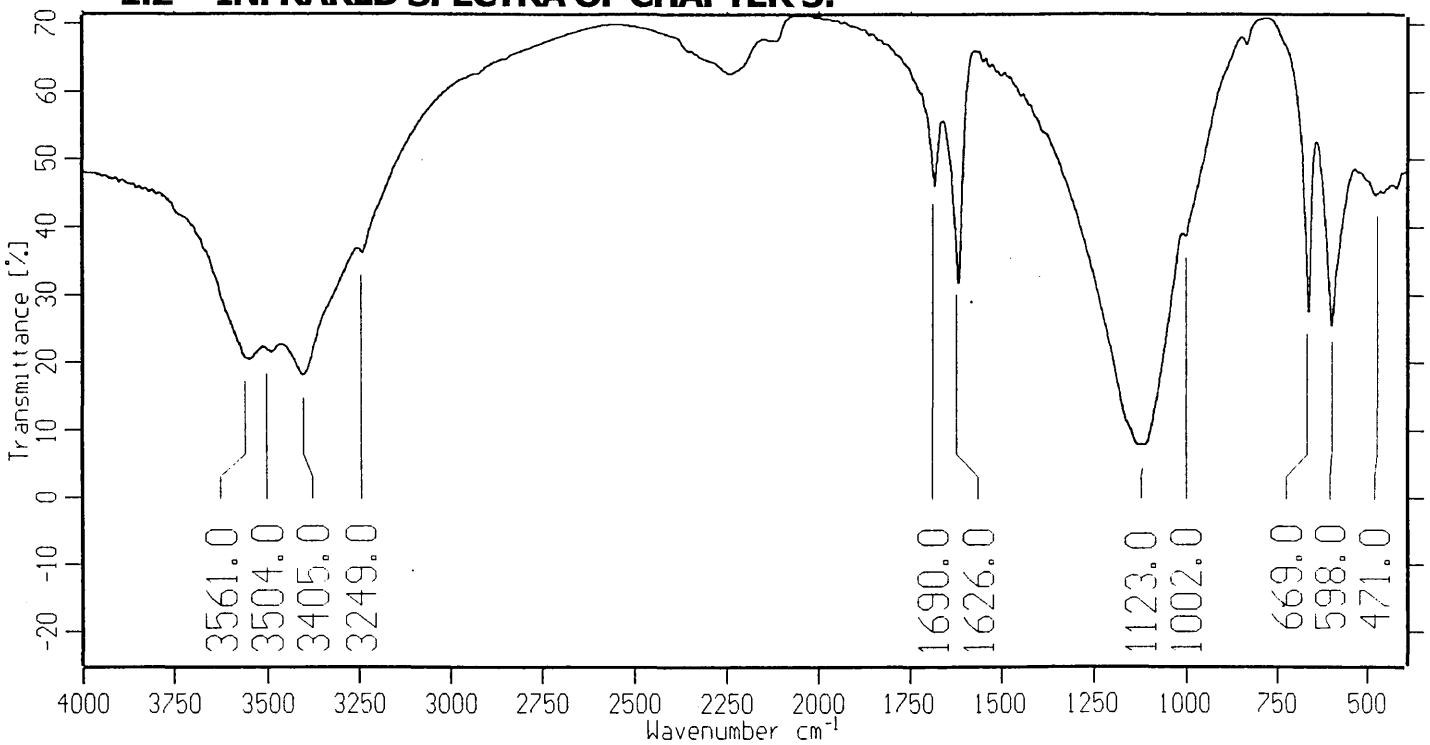

Figure 2.1. Infrared spectrum of gypsum Experiment 0.

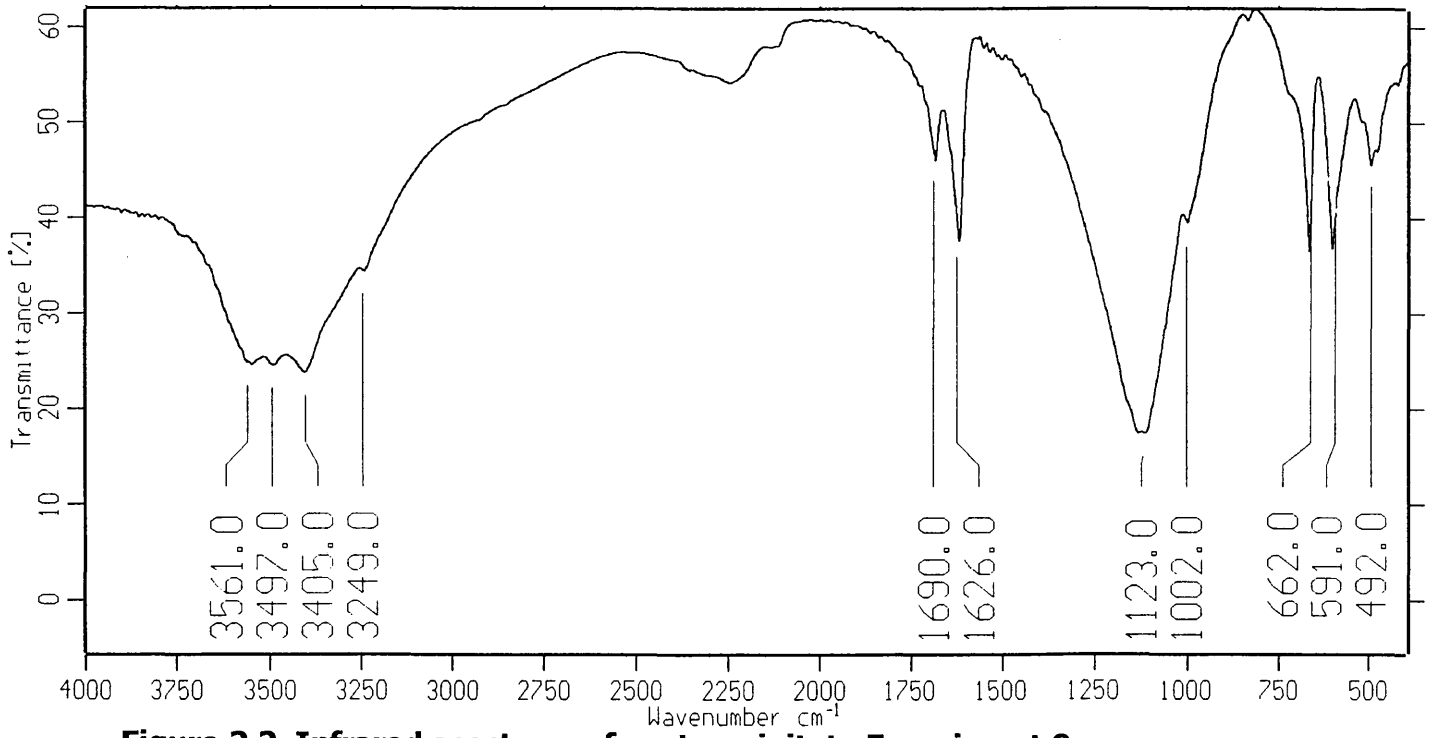

Figure 2.2. Infrared spectrum of postprecipitate Experiment 0.

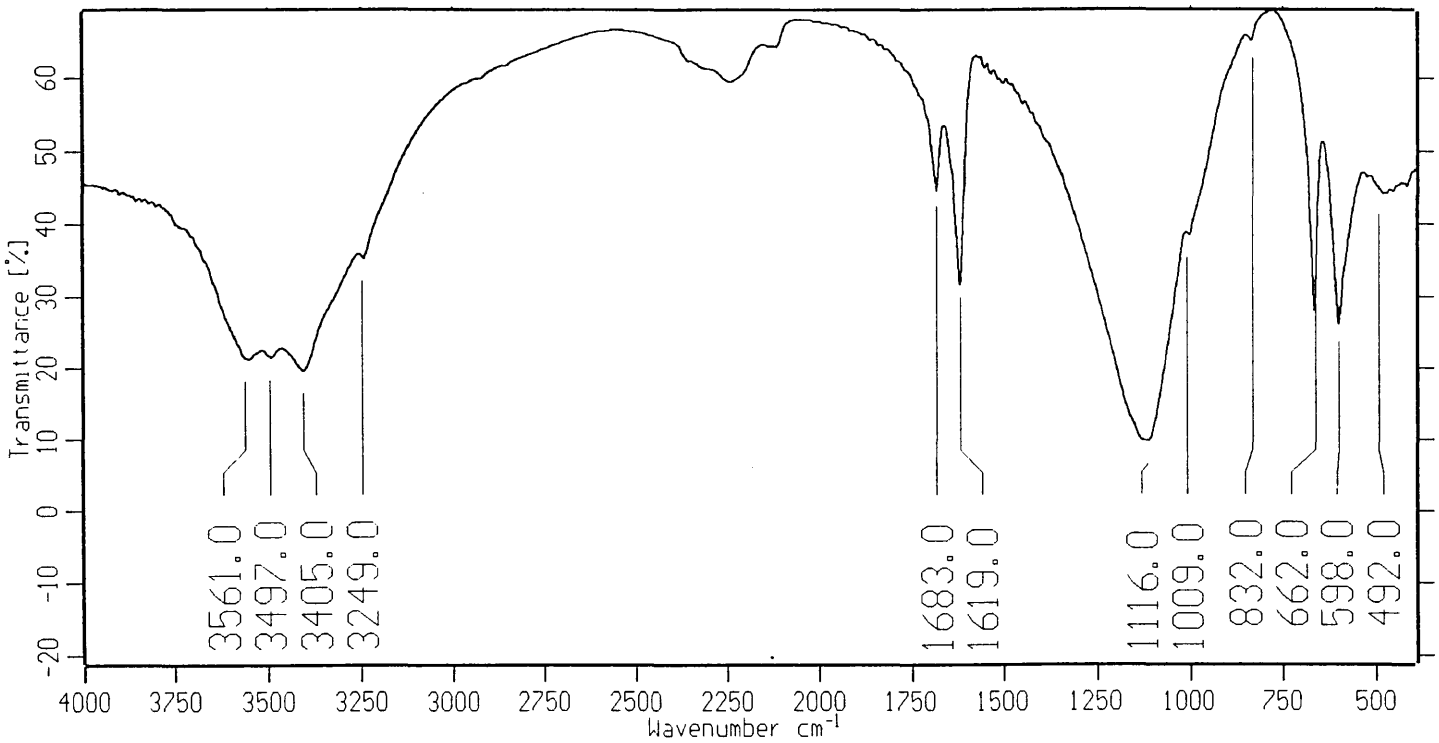

Figure 2.3. Infrared spectrum of gypsum Experiment 1.

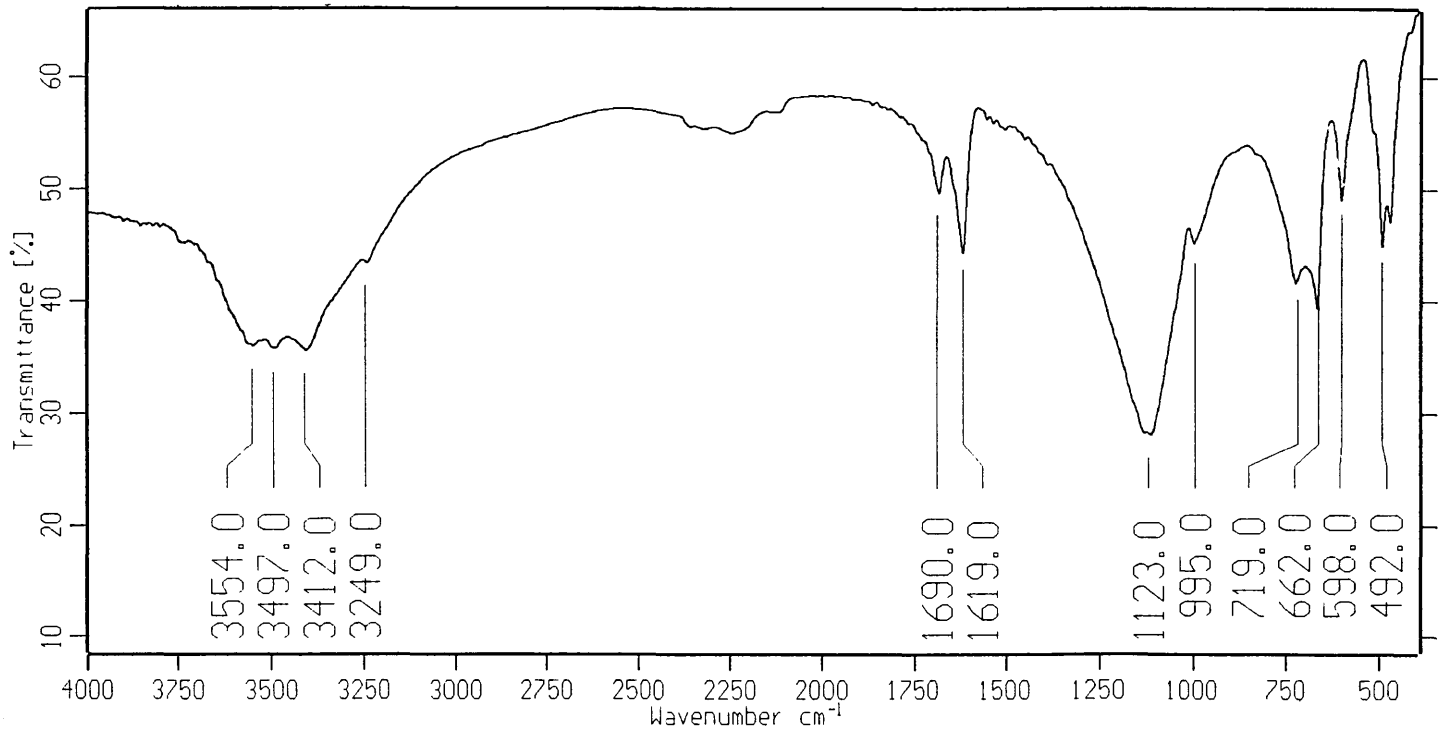

Figure 2.4. Infrared spectrum of postprecipitate Experiment 1.

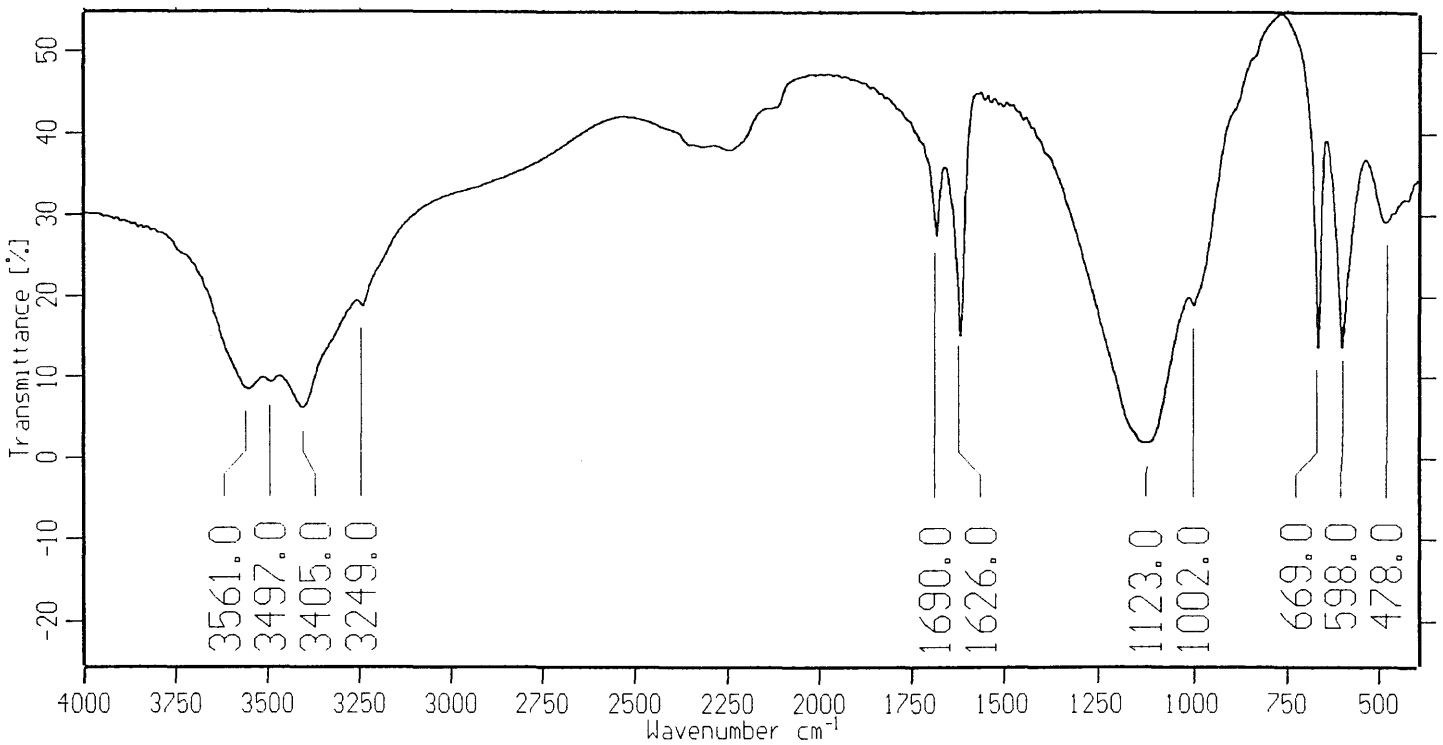

Figure 2.5. Infrared spectrum of gypsum Experiment 2.

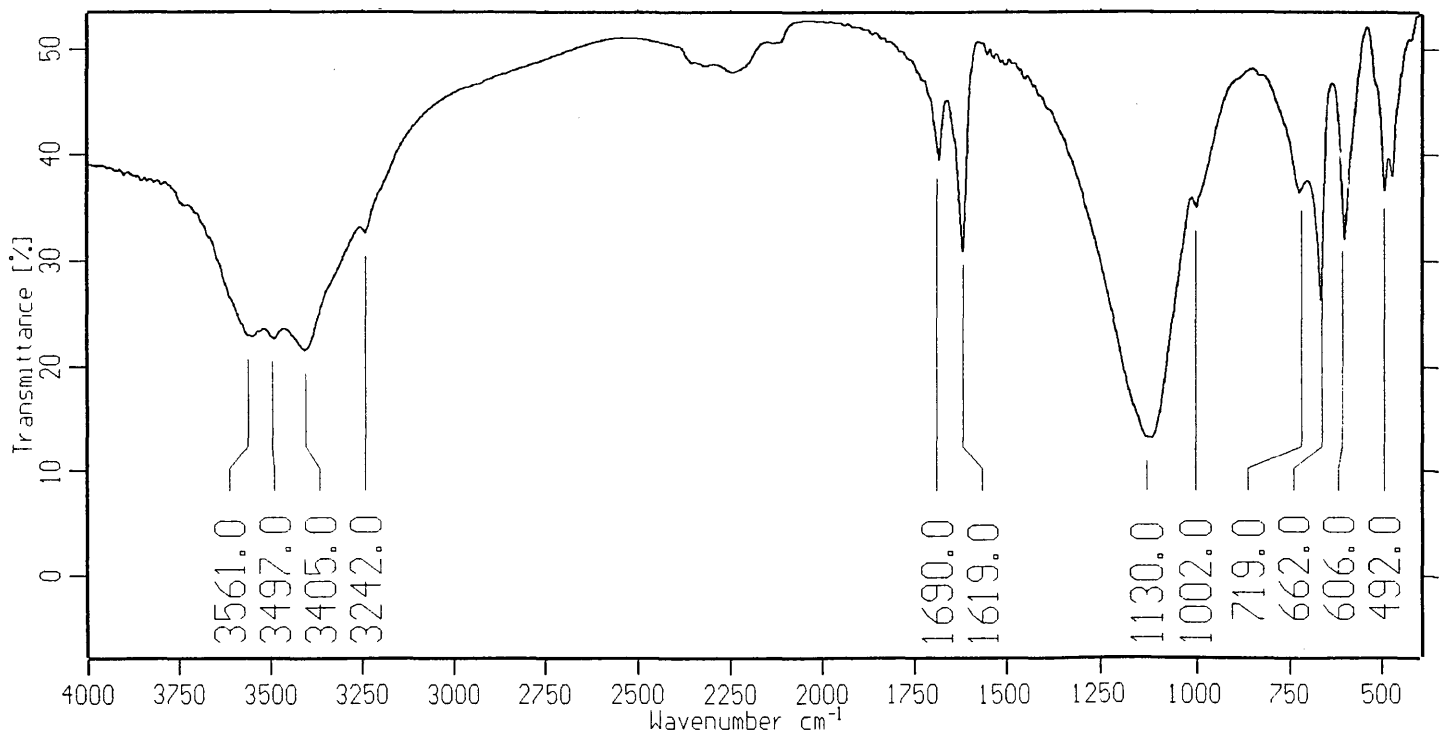

Figure 2.6. Infrared spectrum of postprecipitate Experiment 2.

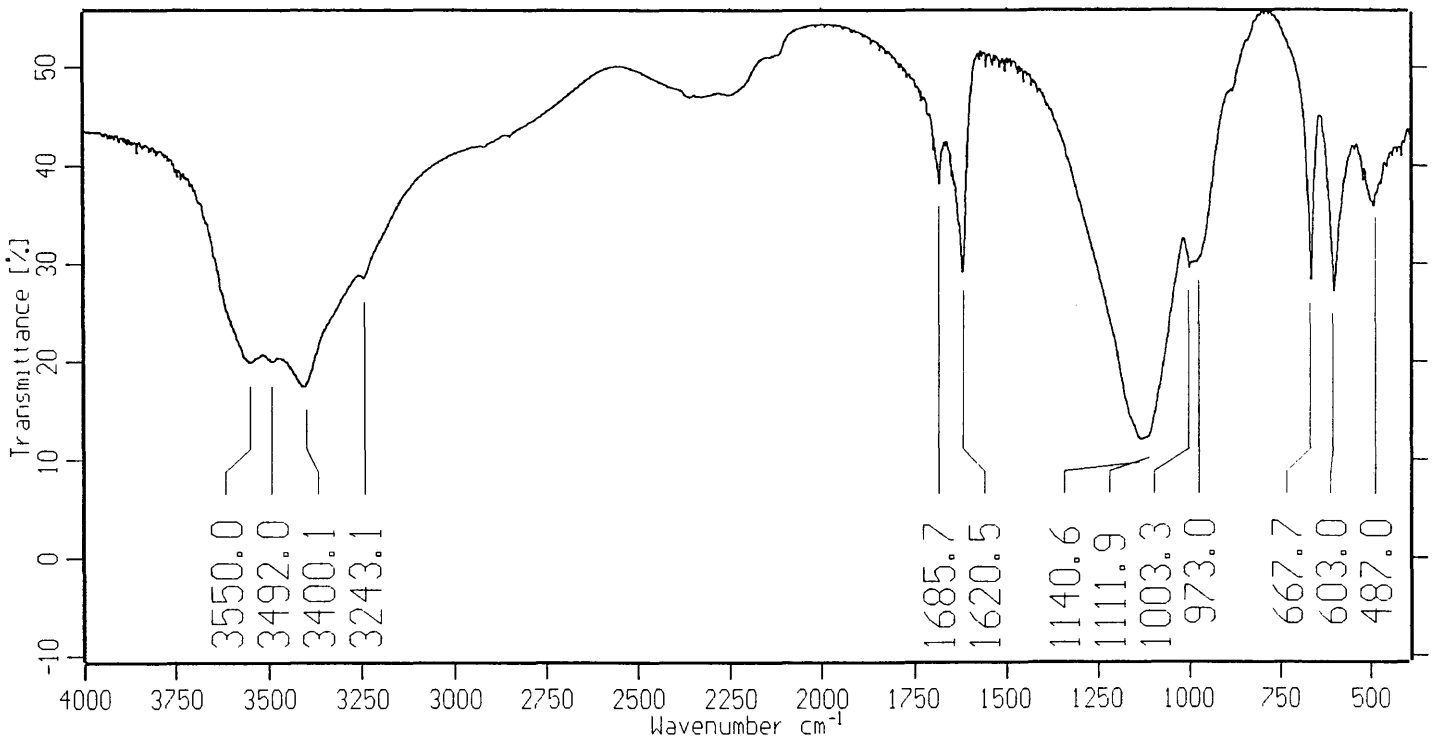

Figure 2.7. Infrared spectrum of gypsum Experiment 3.

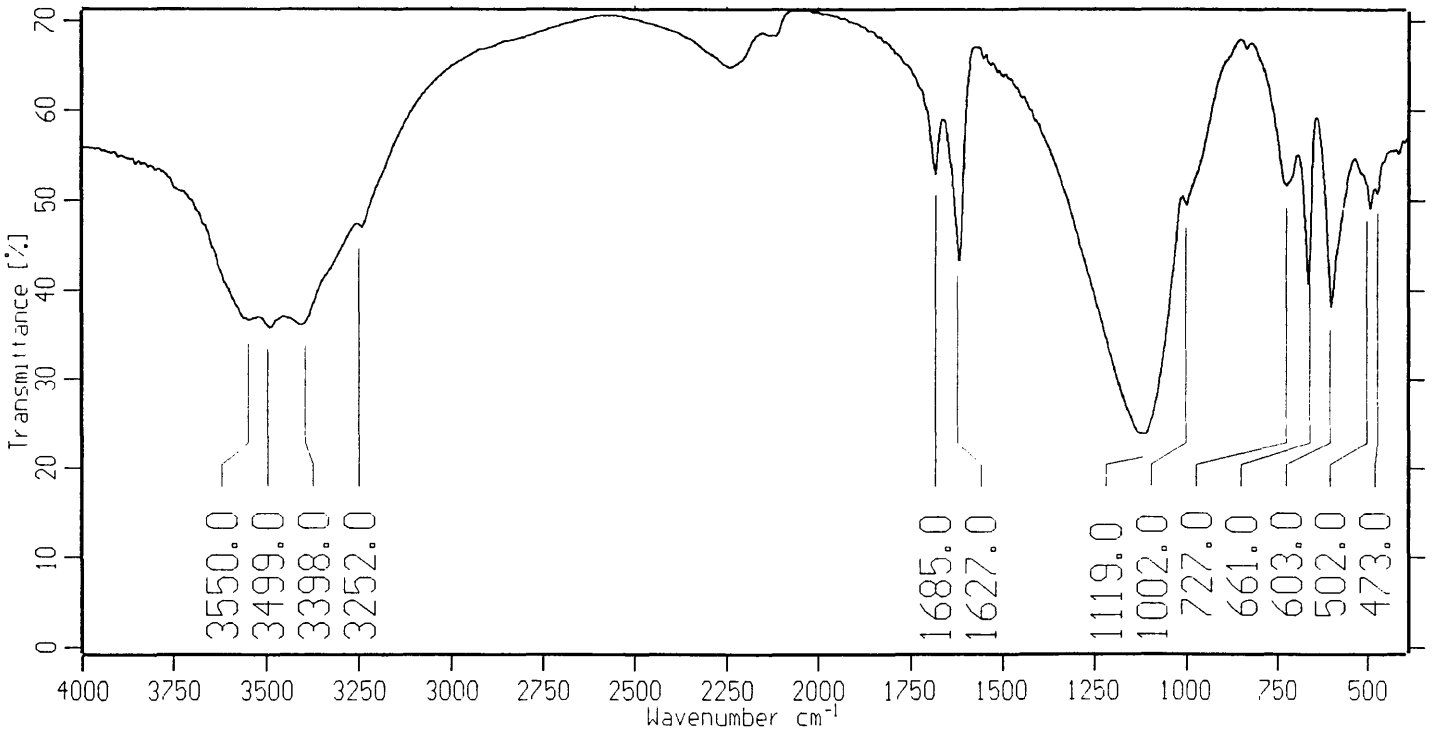

Figure 2.8. Infrared spectrum of postprecipitate Experiment 3.

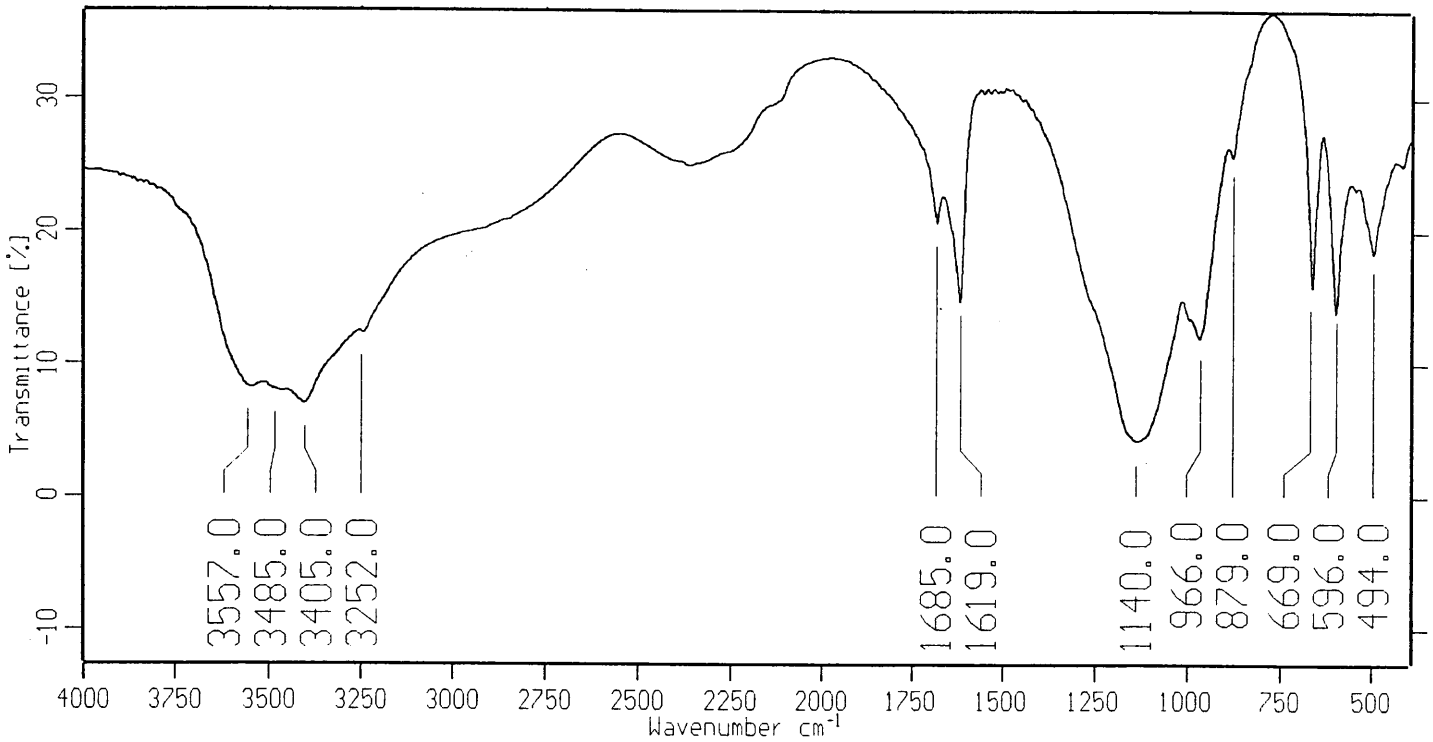

Figure 2.9. Infrared spectrum of gypsum Experiment 4.

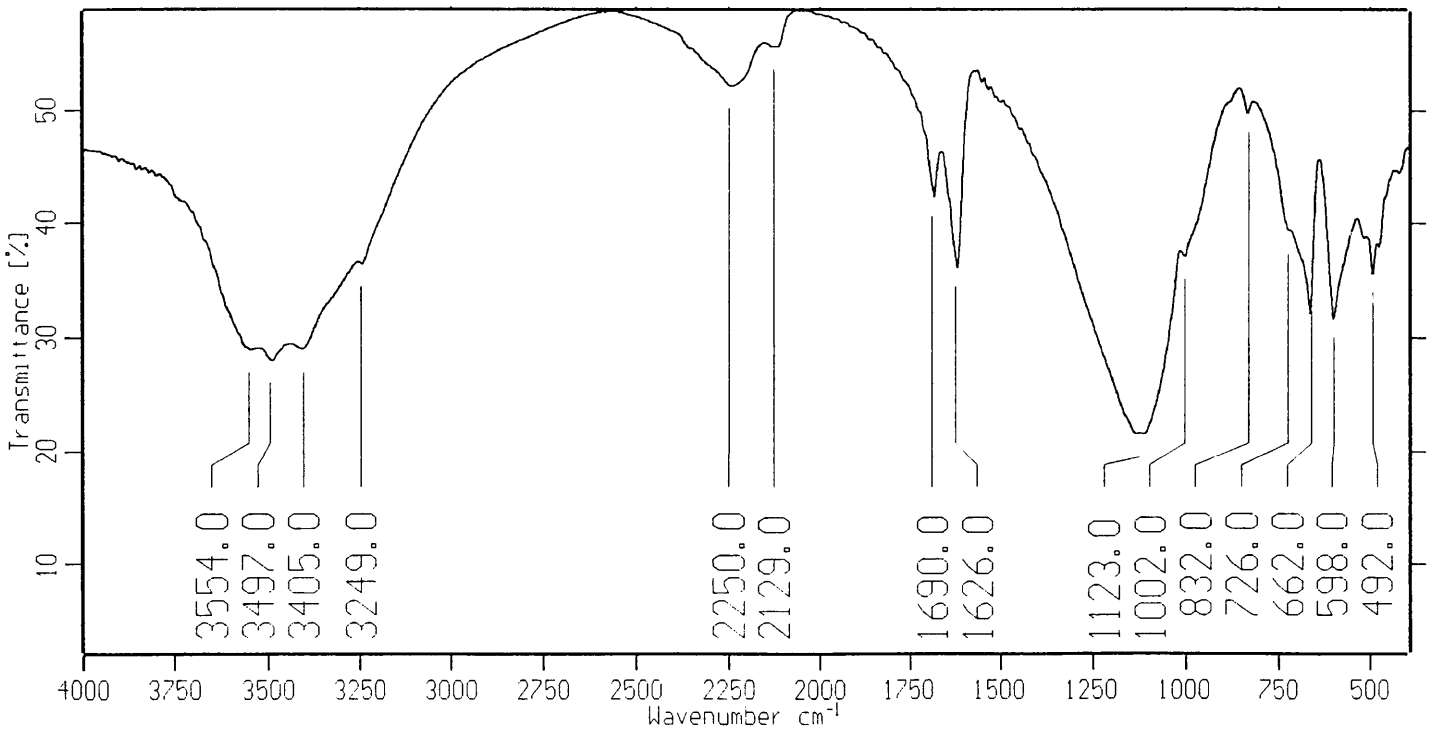

Figure 2.10. Infrared spectrum of postprecipitate Experiment 4.

1.3 INFRARED SPECTRA OF CHAPTER 6:

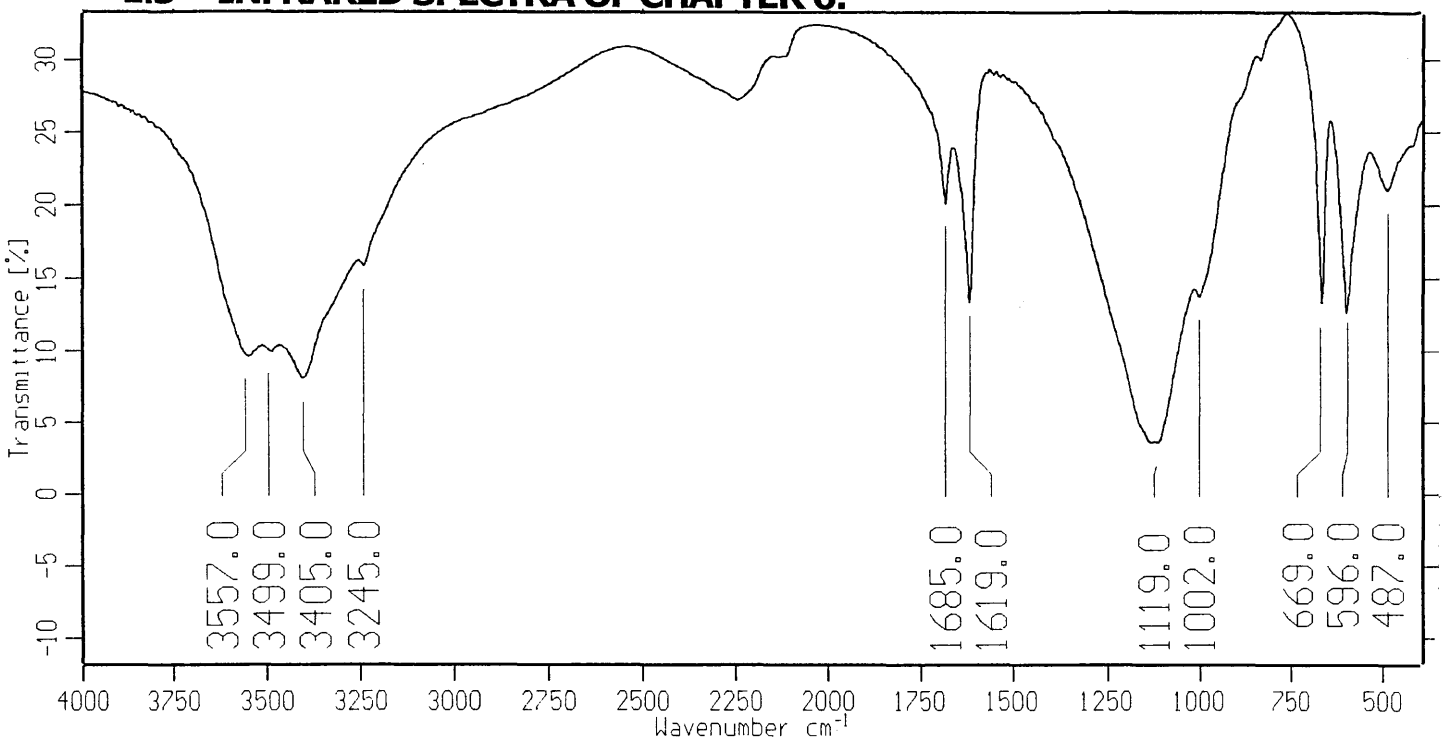

Figure 3.1. Infrared spectrum of gypsum Experiment 21.

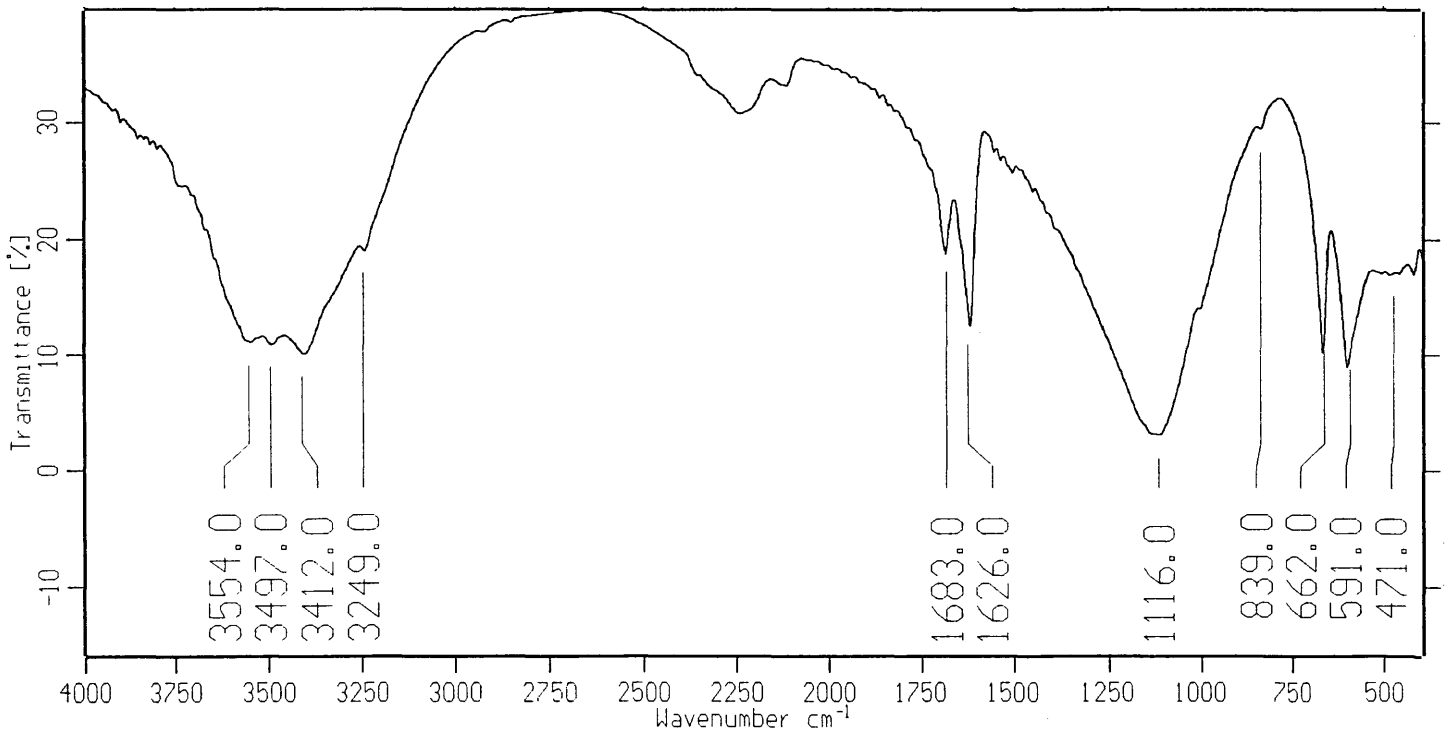

Figure 3.2. Infrared spectrum of postprecipitate Experiment 21.

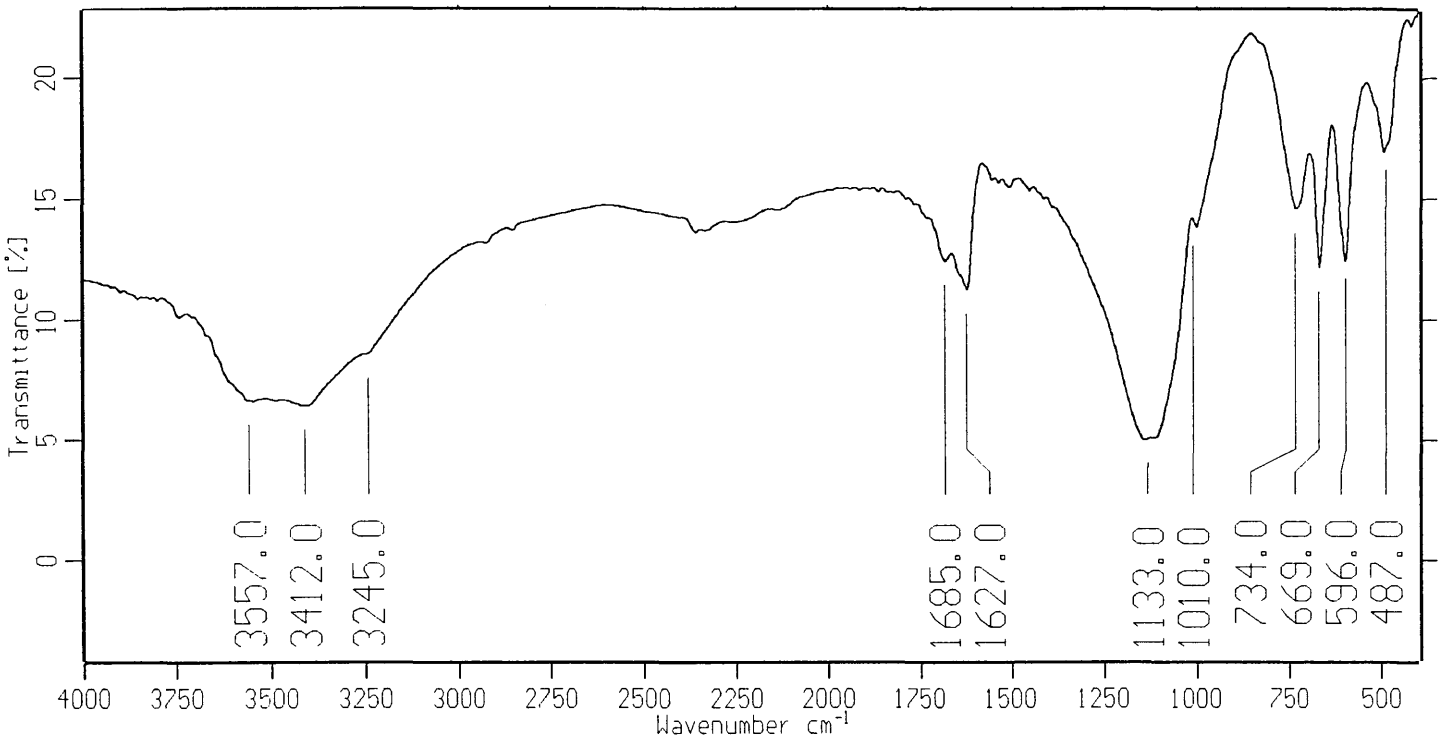

Figure 3.3. Infrared spectrum of sludge Experiment 21.

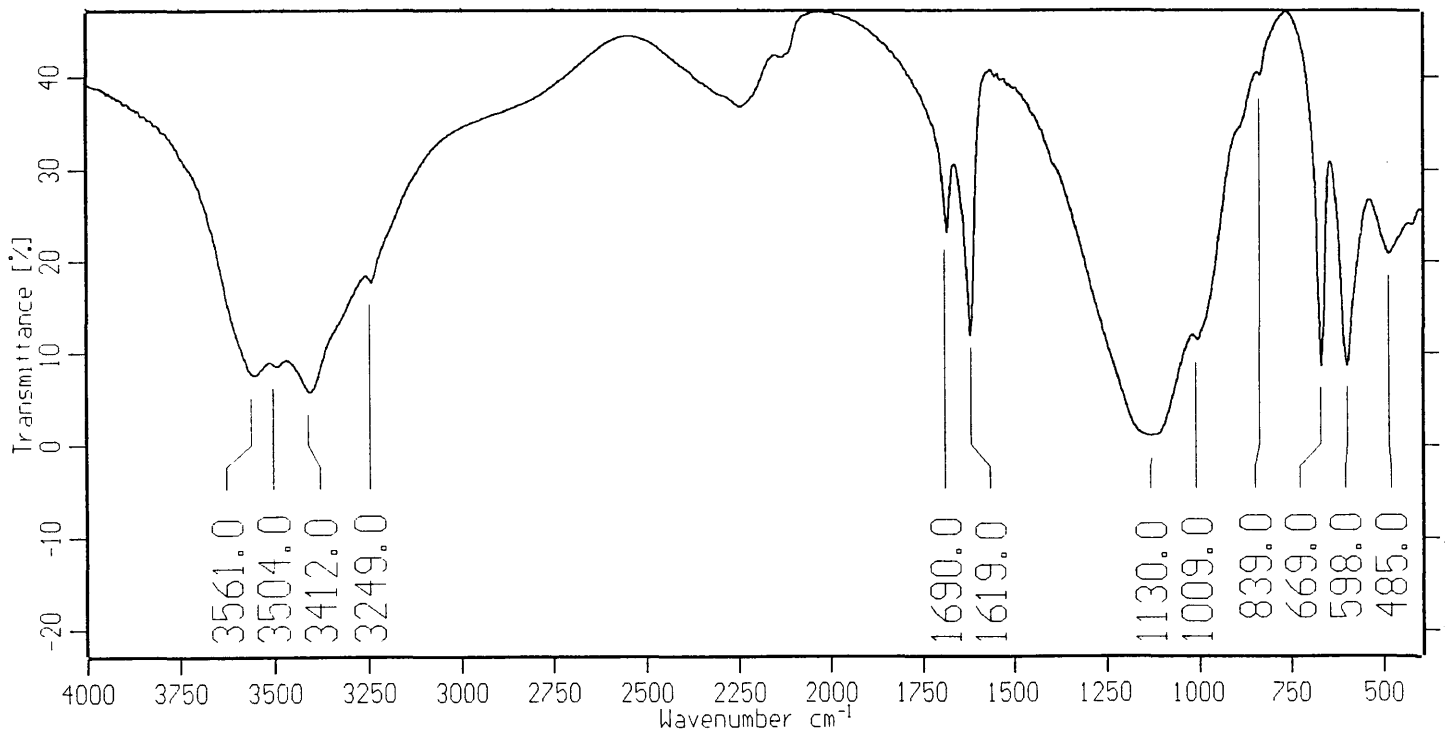

Figure 3.4. Infrared spectrum of gypsum Experiment 22.

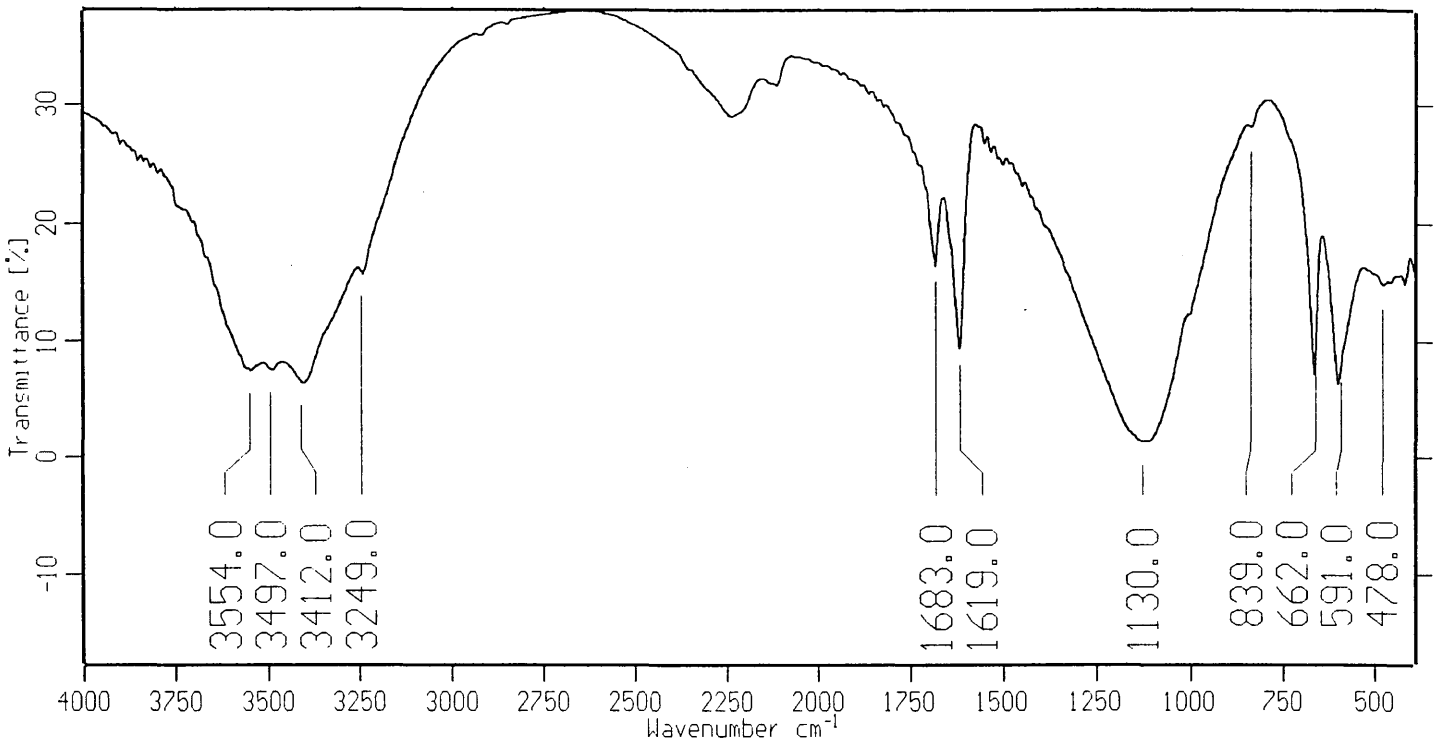

Figure 3.5. Infrared spectrum of postprecipitate Experiment 22.

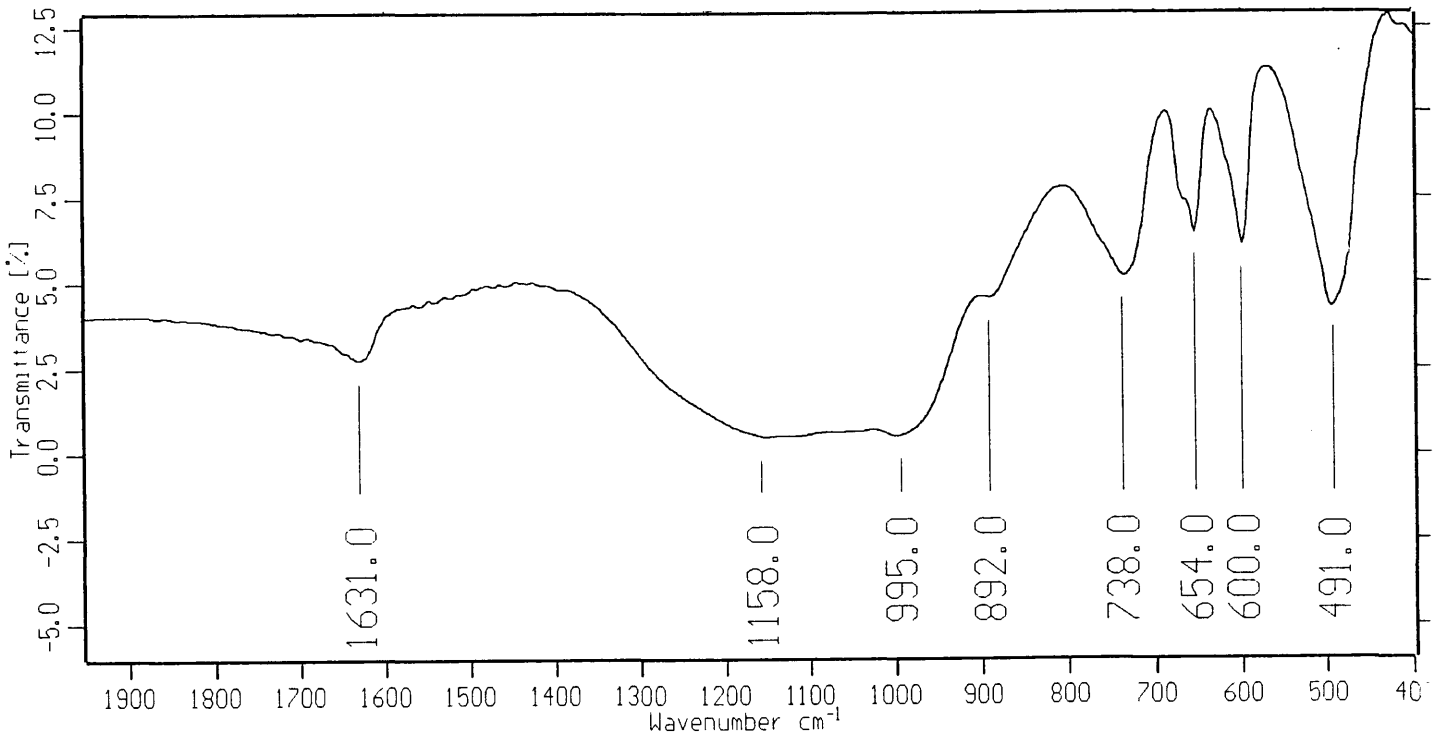

Figure 3.6. Infrared spectrum of sludge Experiment 22.

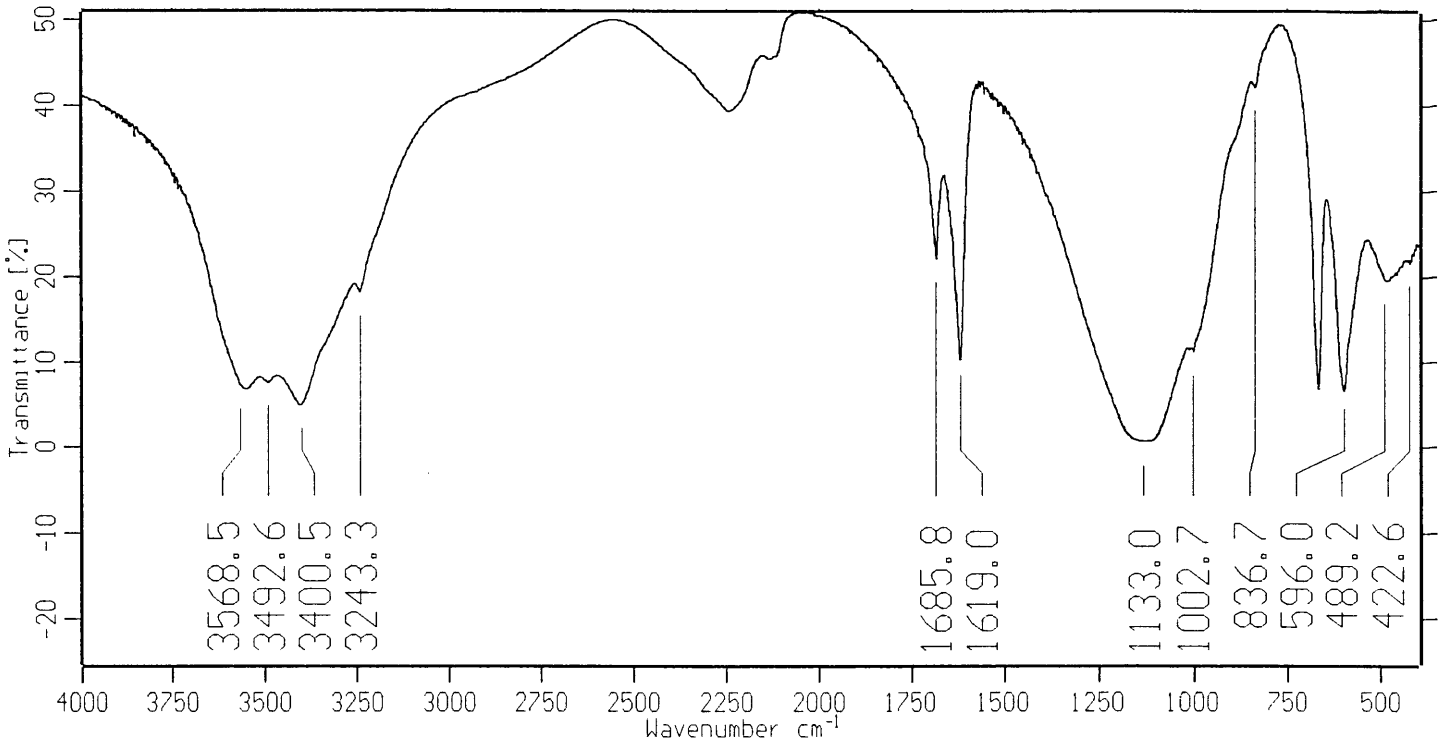

Figure 3.7. Infrared spectrum of gypsum Experiment 24.

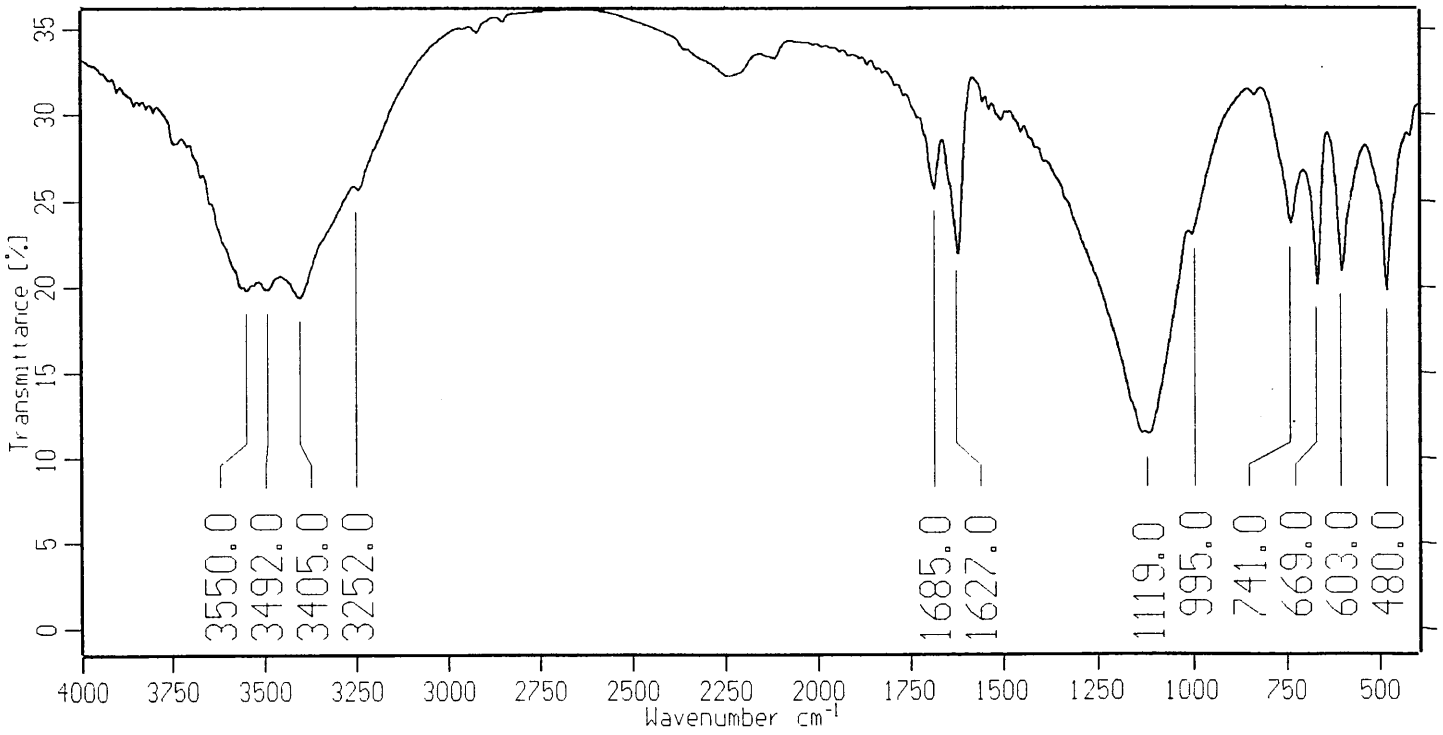

Figure 3.8. Infrared spectrum of postprecipiate Experiment 24.

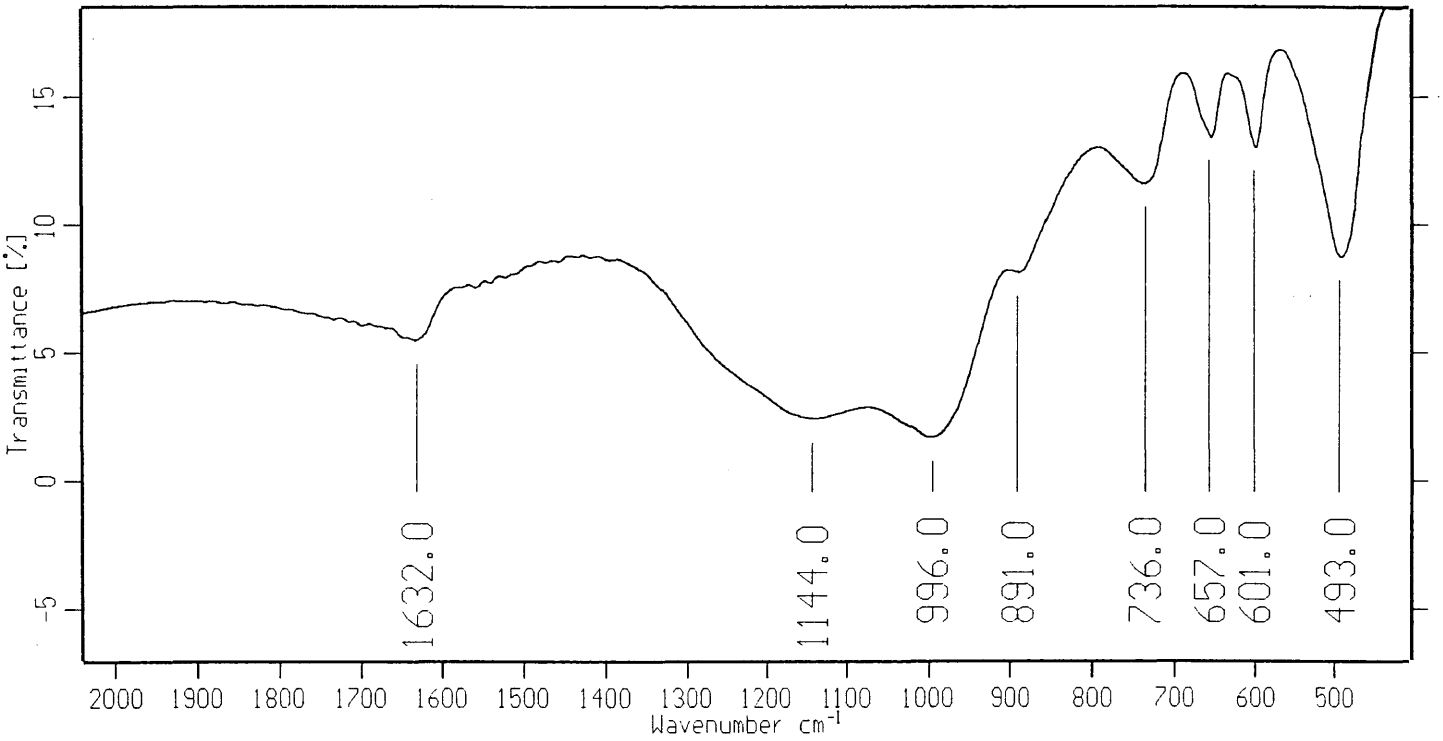

Figure 3.9. Infrared spectrum of sludge Experiment 24.

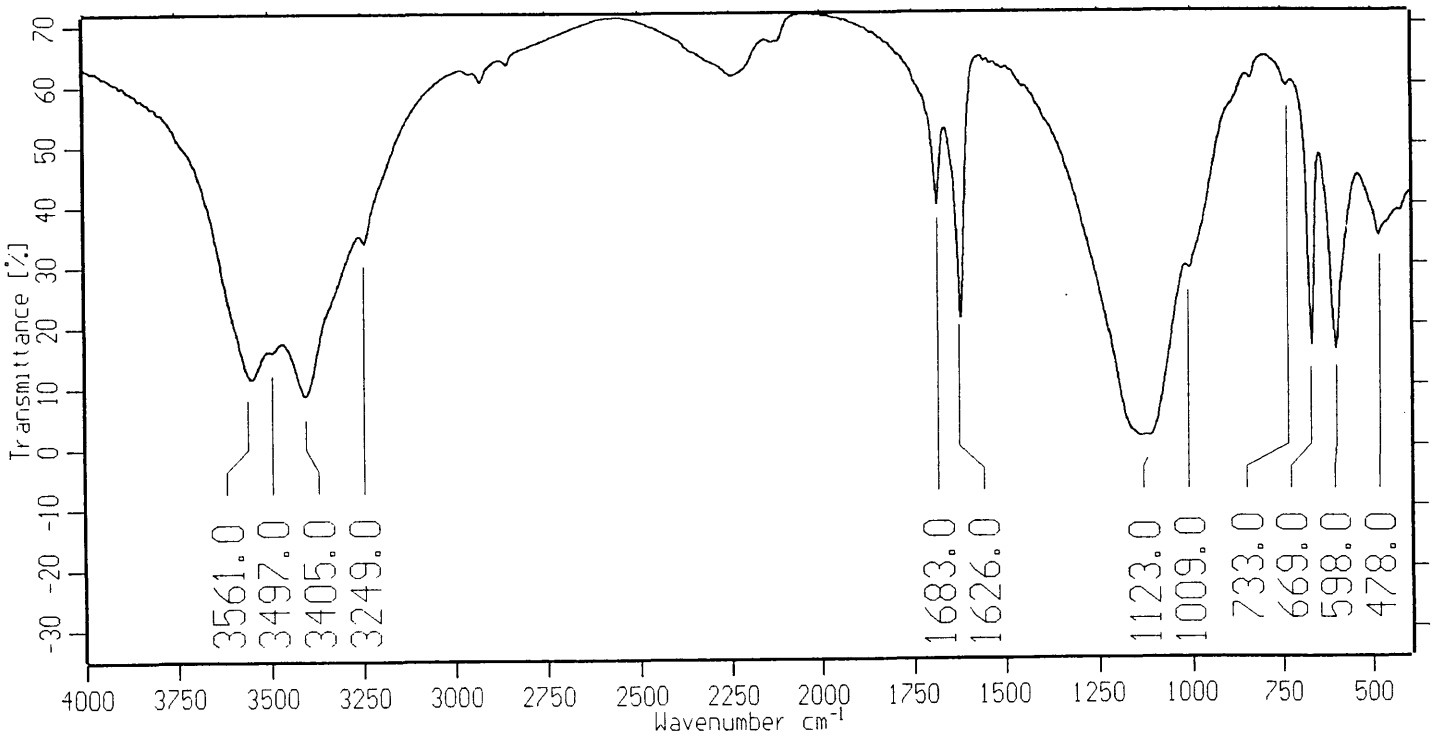

Figure 3.10. Infrared spectrum of gypsum Experiment 26.

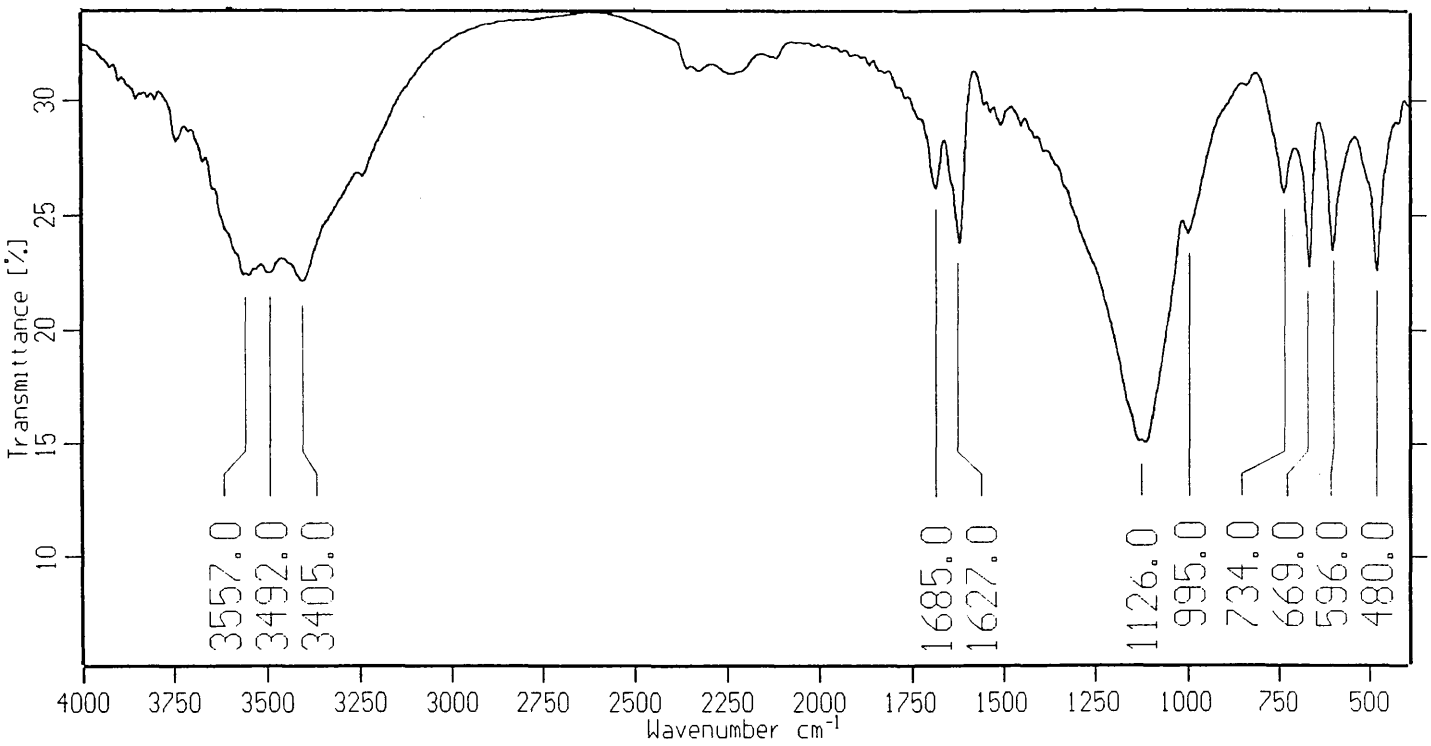

Figure 3.11. Infrared spectrum of postprecipitate Experiment 26.

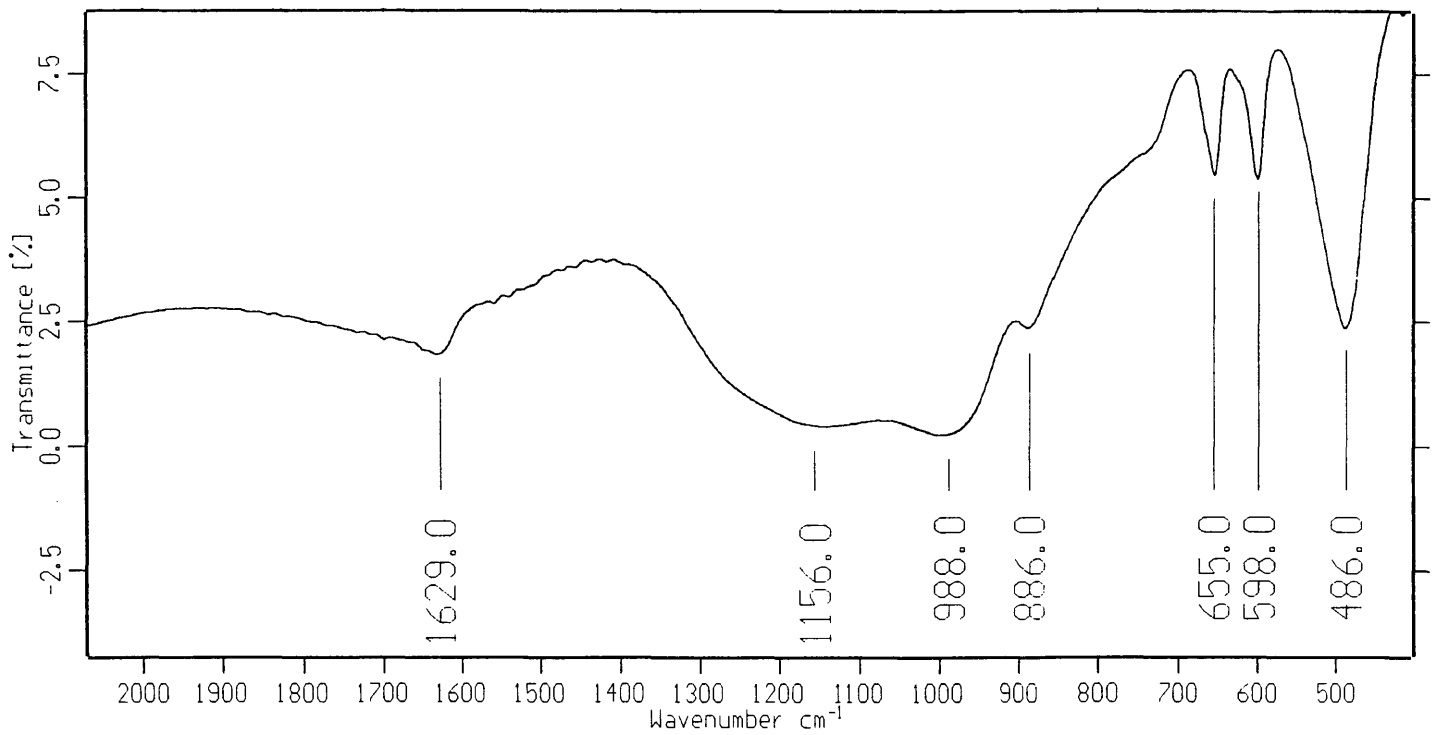

Figure 3.12. Infrared spectrum of sludge Experiment 26.

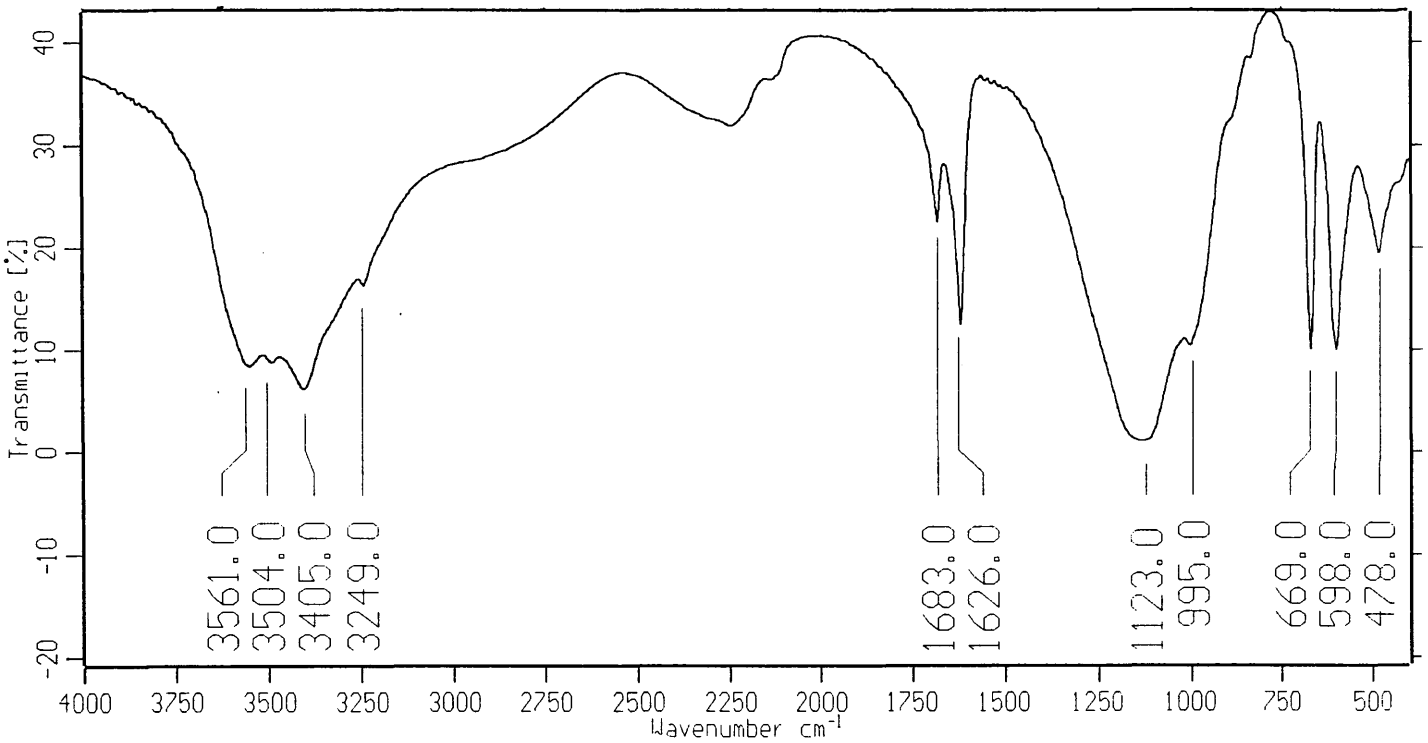

Figure 3.13. Infrared spectrum of gypsum Experiment 28.

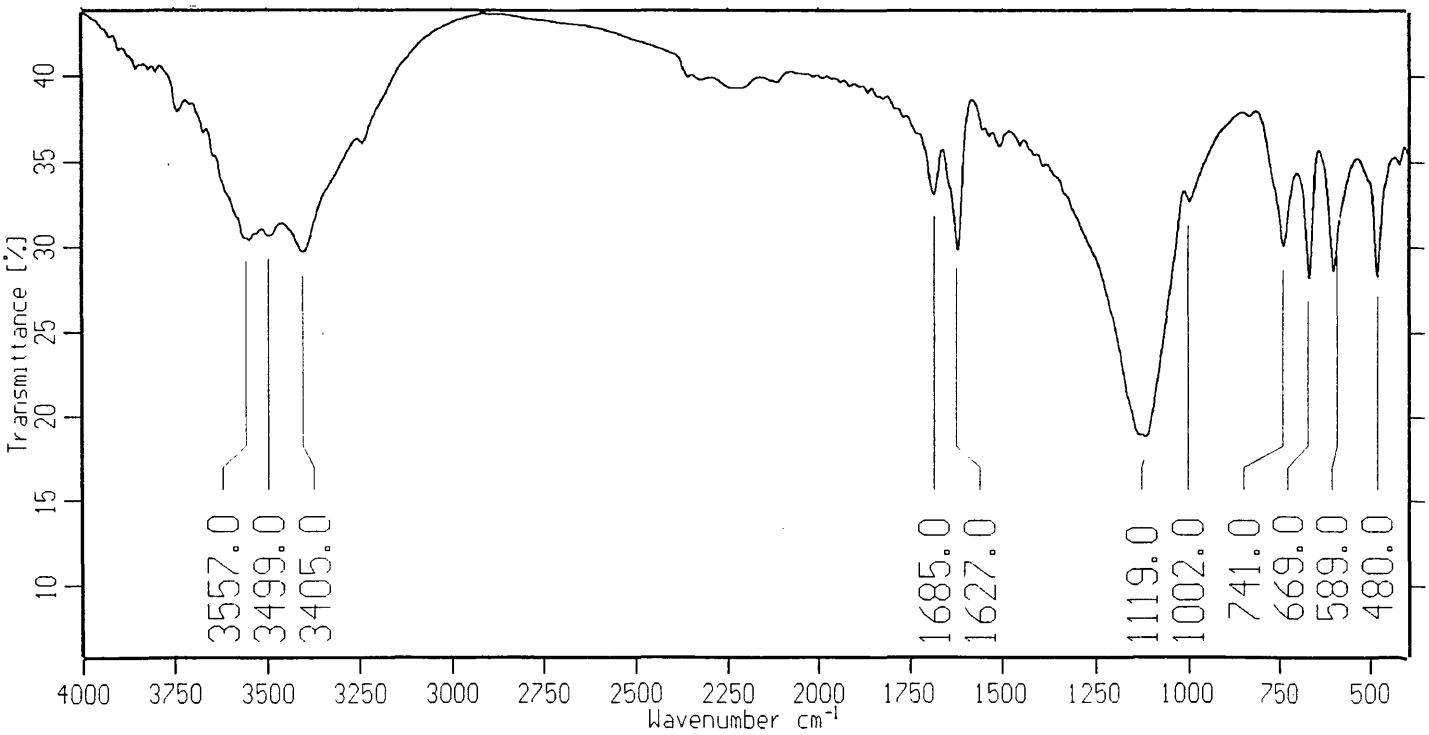

Figure 3.14. Infrared spectrum of postprecipitate Experiment 28.

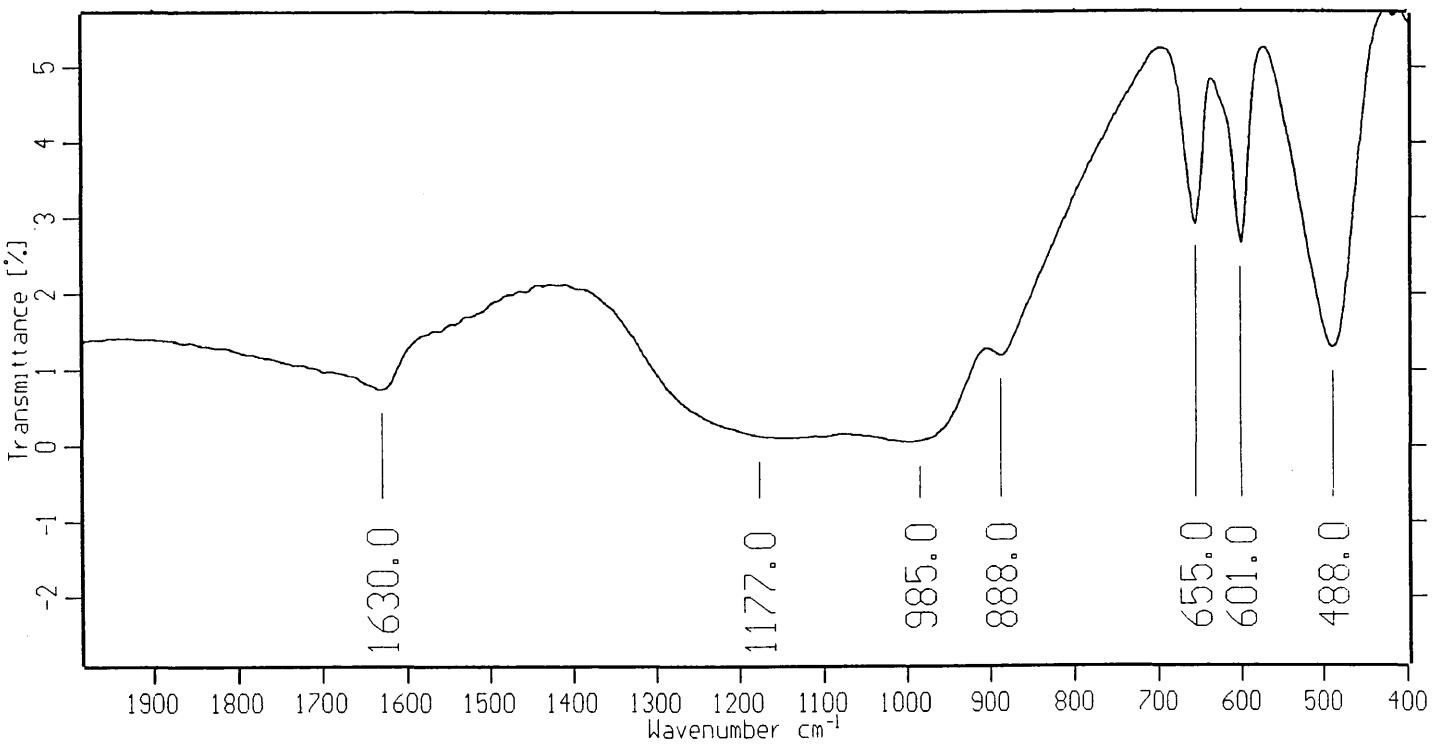

Figure 3.15. Infrared spectrum of sludge Experiment 28.

1.4 INFRARED SPECTRA OF CHAPTER 7:

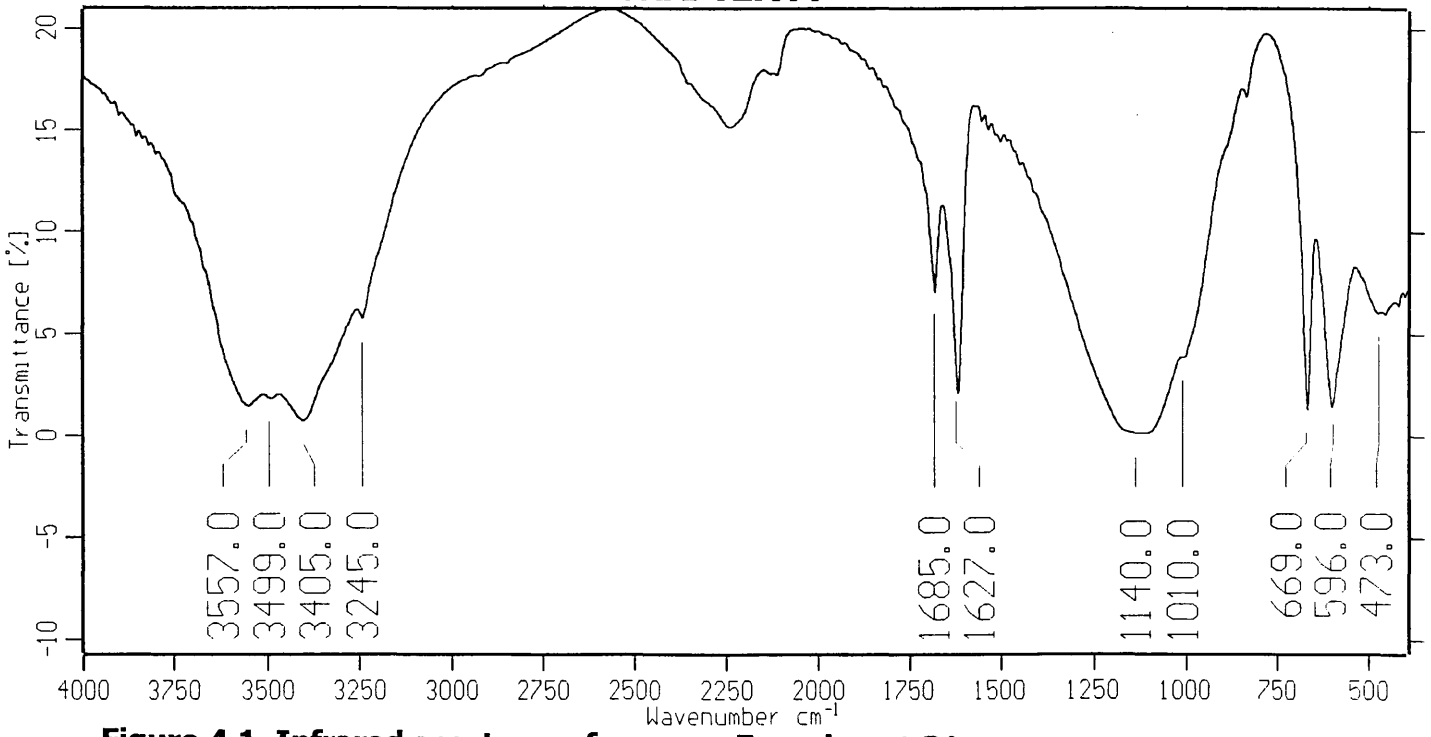

Figure 4.1. Infrared spectrum of gypsum Experiment 31.

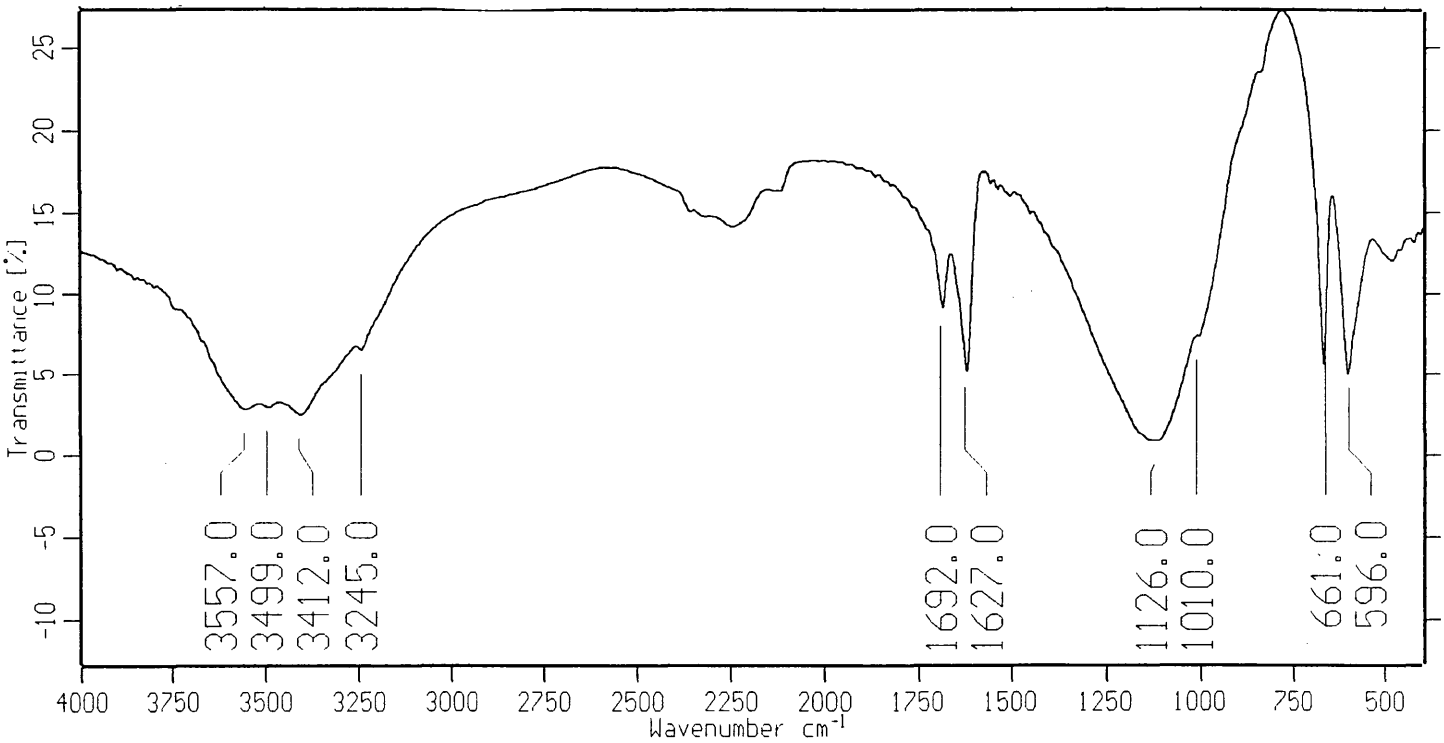

Figure 4.2. Infrared spectrum of postprecipitate Experiment 31.

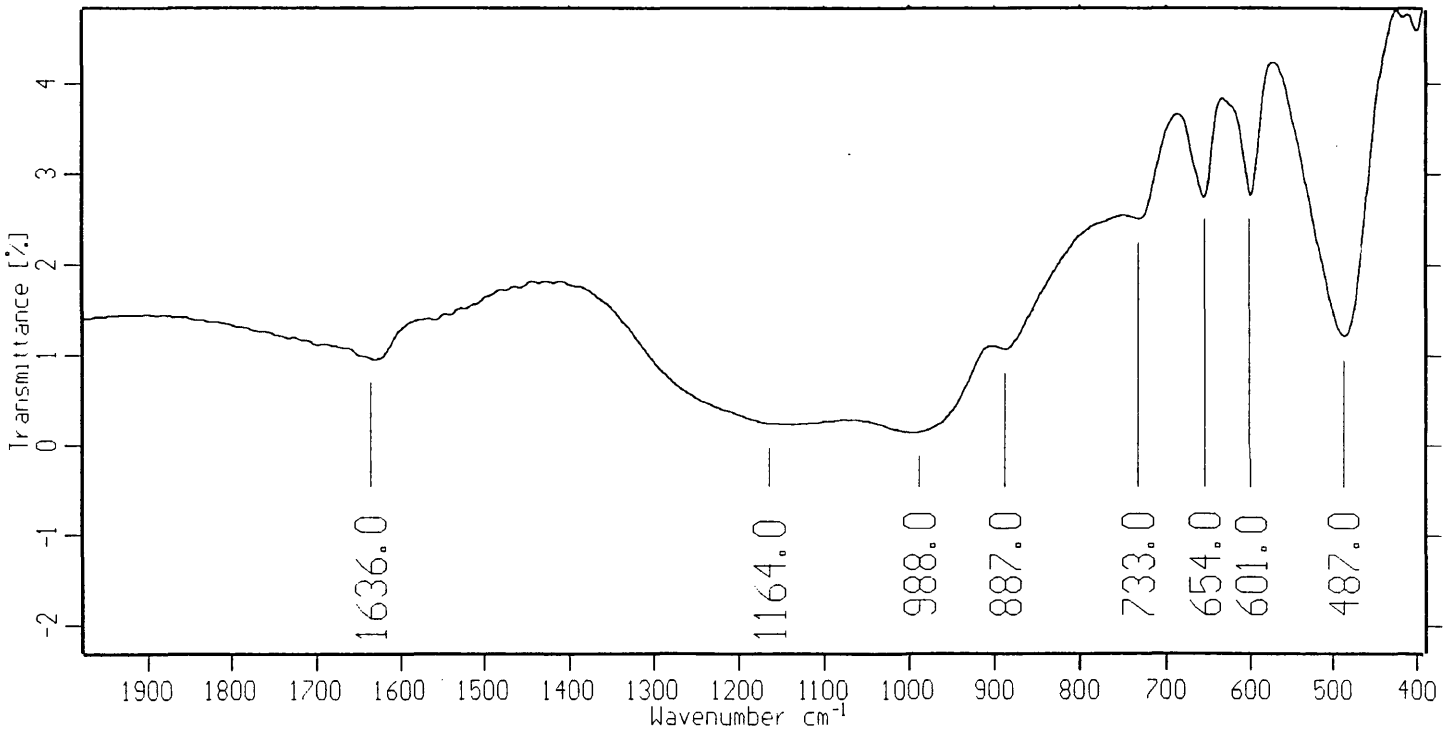

Figure 4.3. Infrared spectrum of sludge Experiment 31.

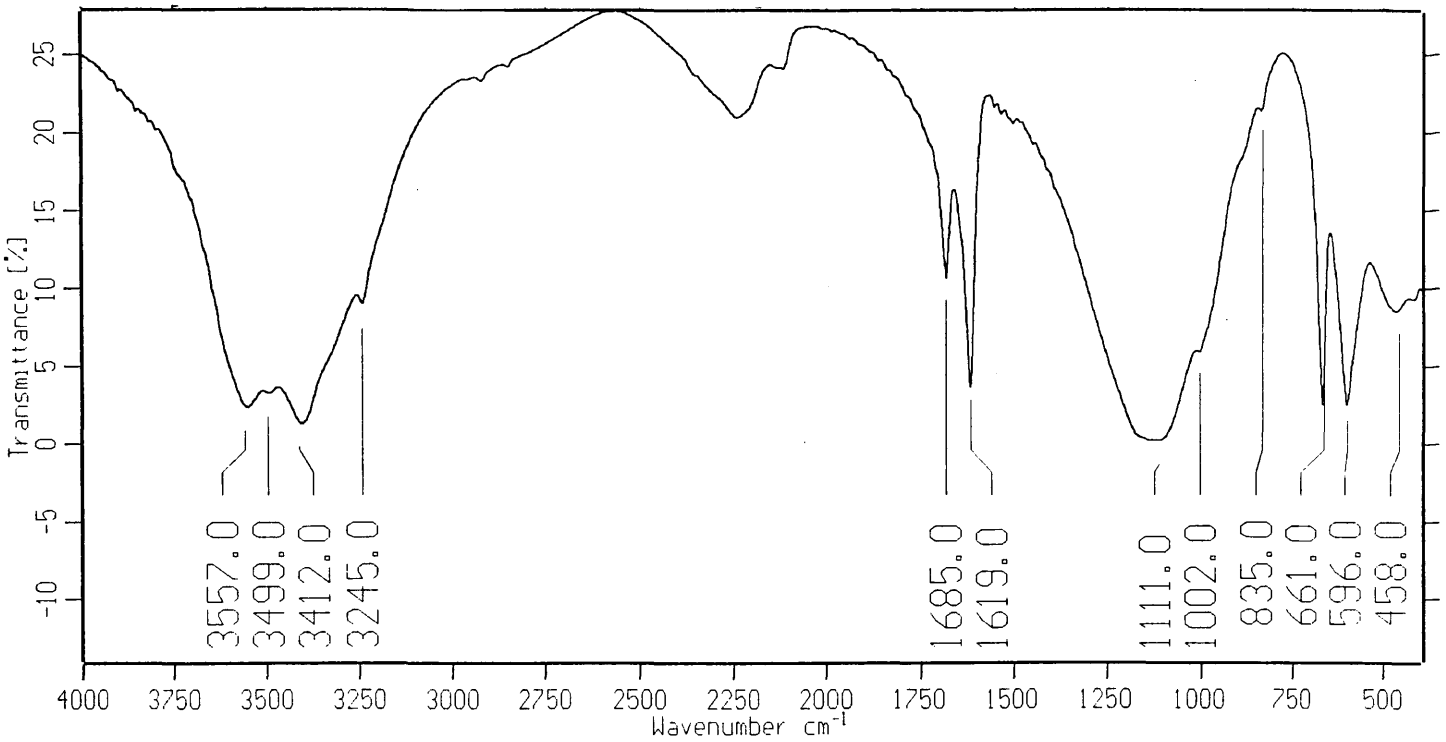

Figure 4.4. Infrared spectrum of gypsum Experiment 33.

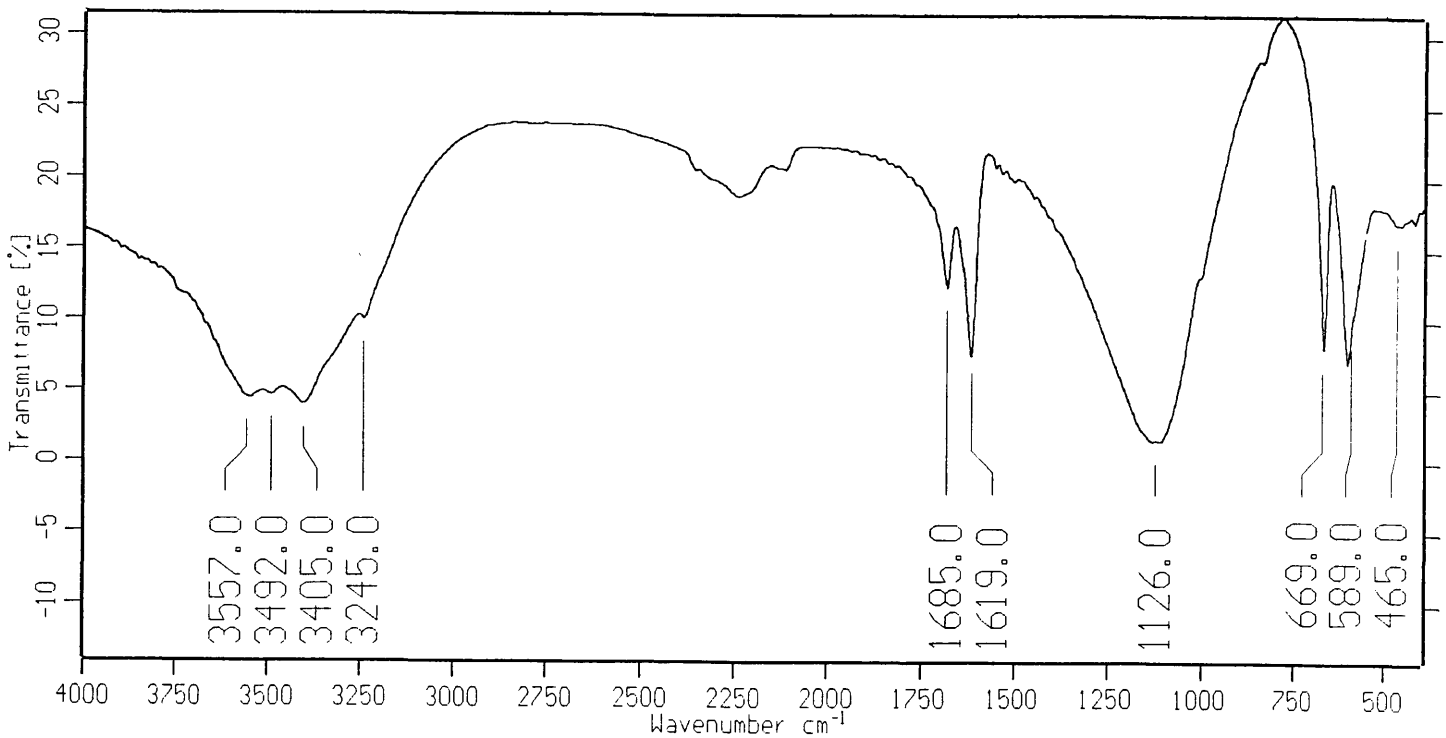

Figure 4.5. Infrared spectrum of postprecipitate Experiment 33.

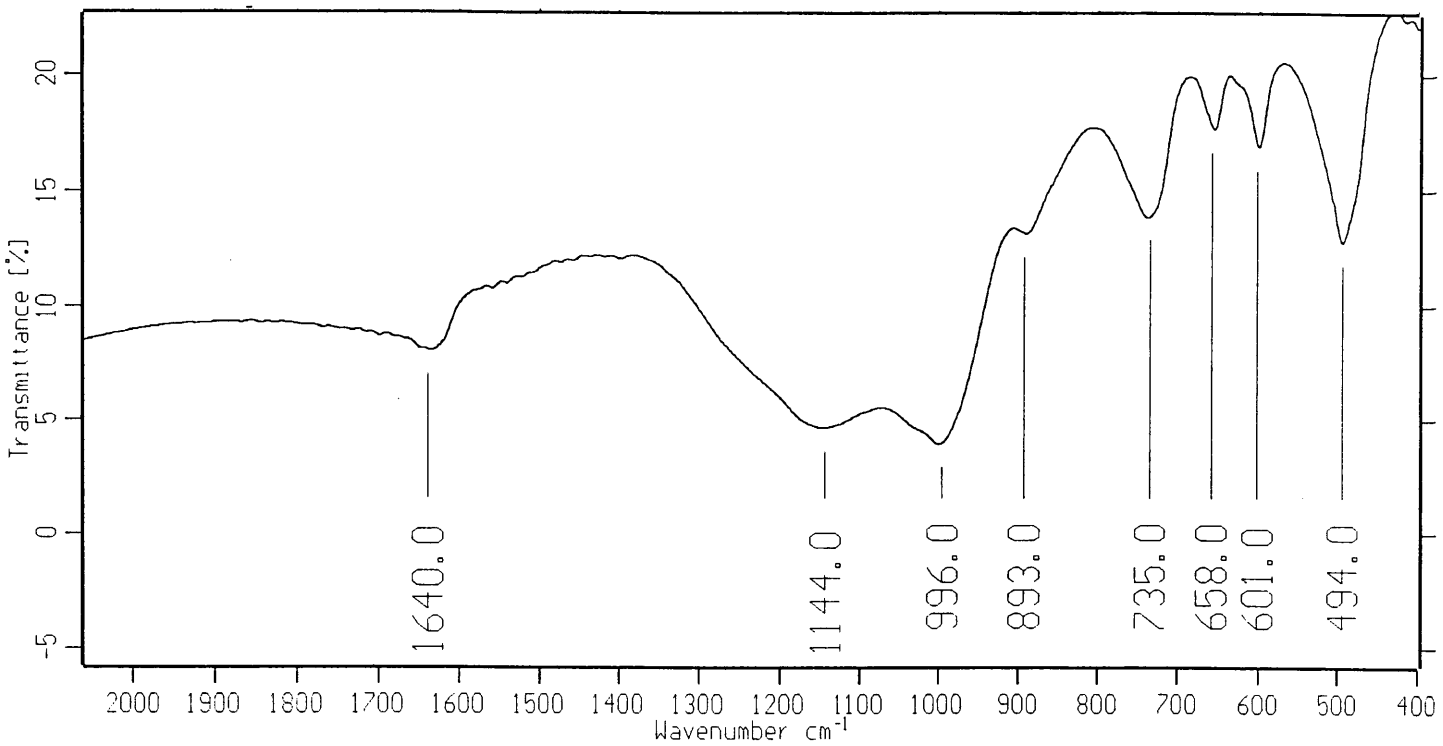

Figure 4.6. Infrared spectrum of sludge Experiment 33.

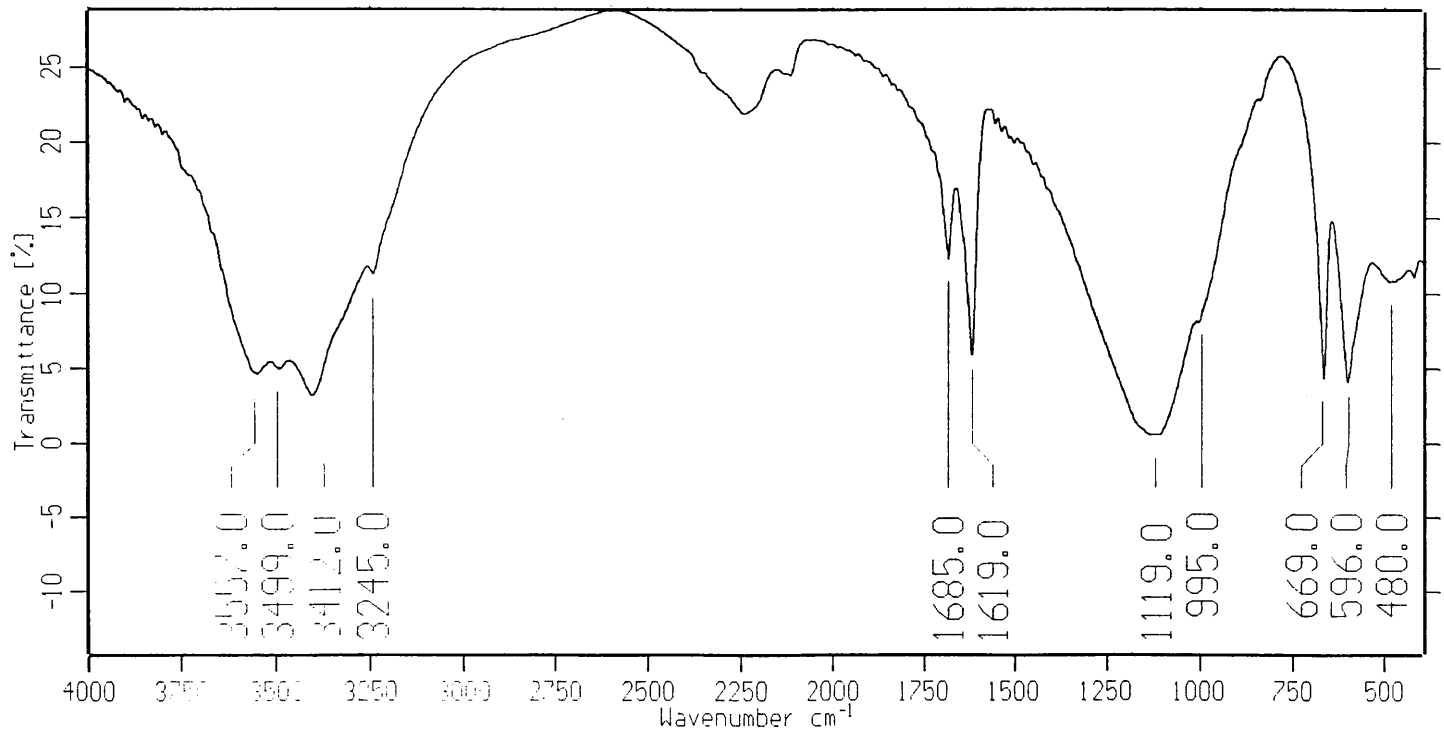

Figure 4.7. Infrared spectrum of gypsum Experiment 35.

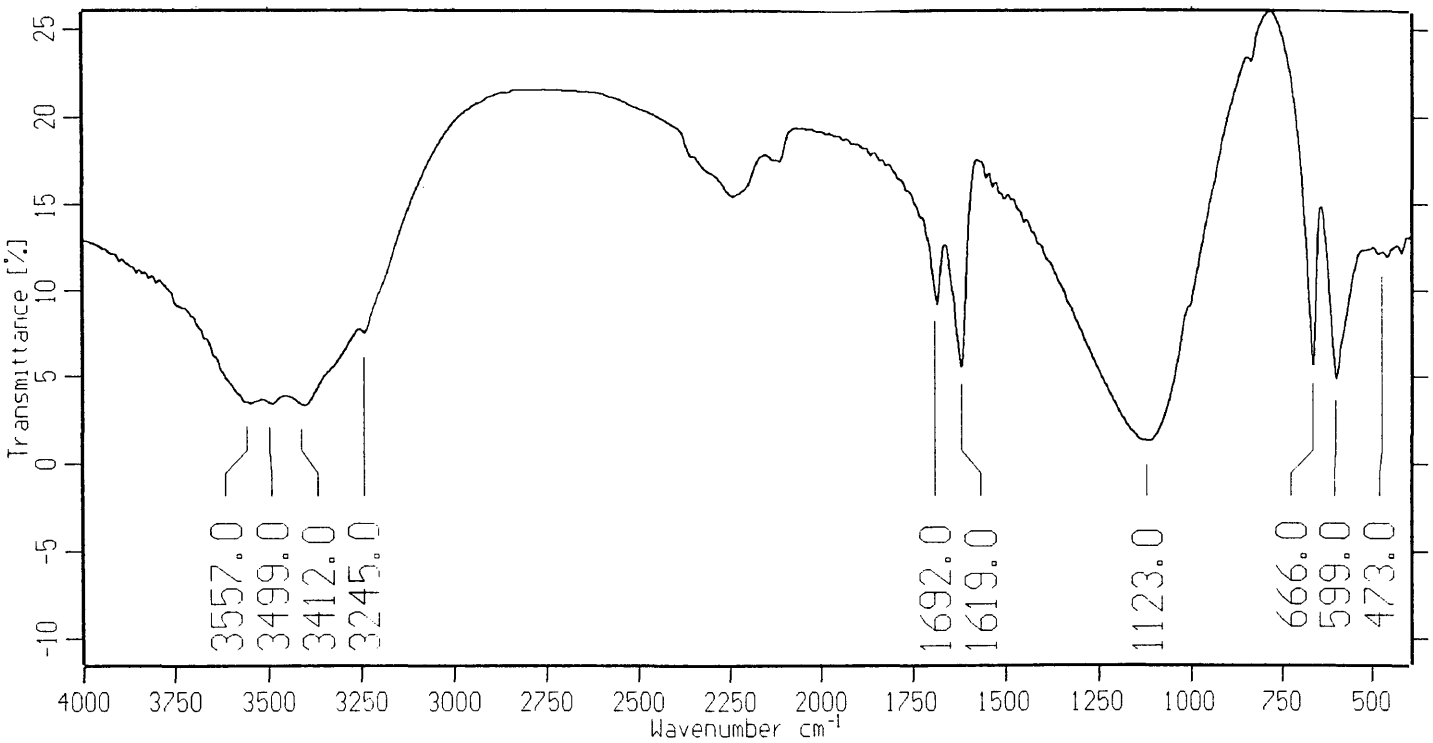

Figure 4.8. Infrared spectrum of postprecipiate Experiment 35.

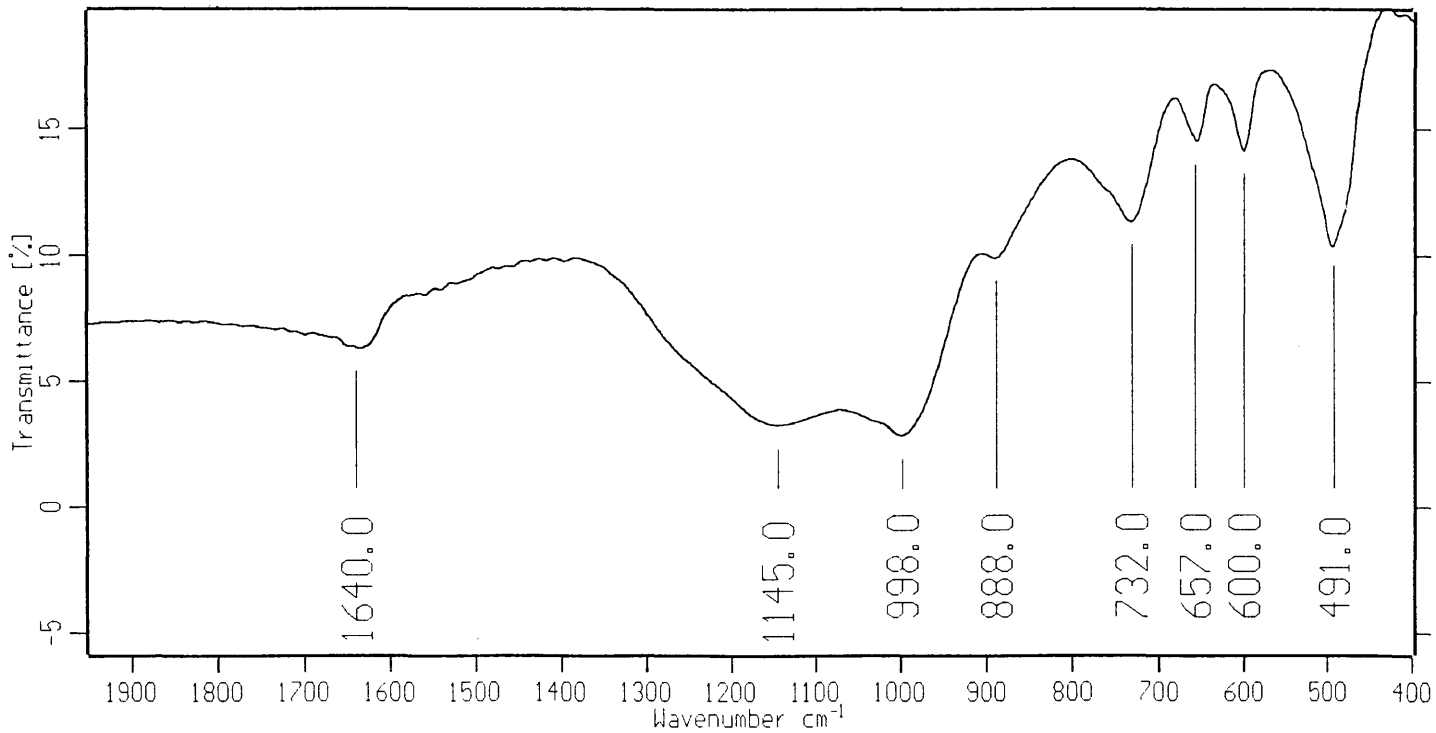

Figure 4.9. Infrared spectrum of sludge Experiment 35.

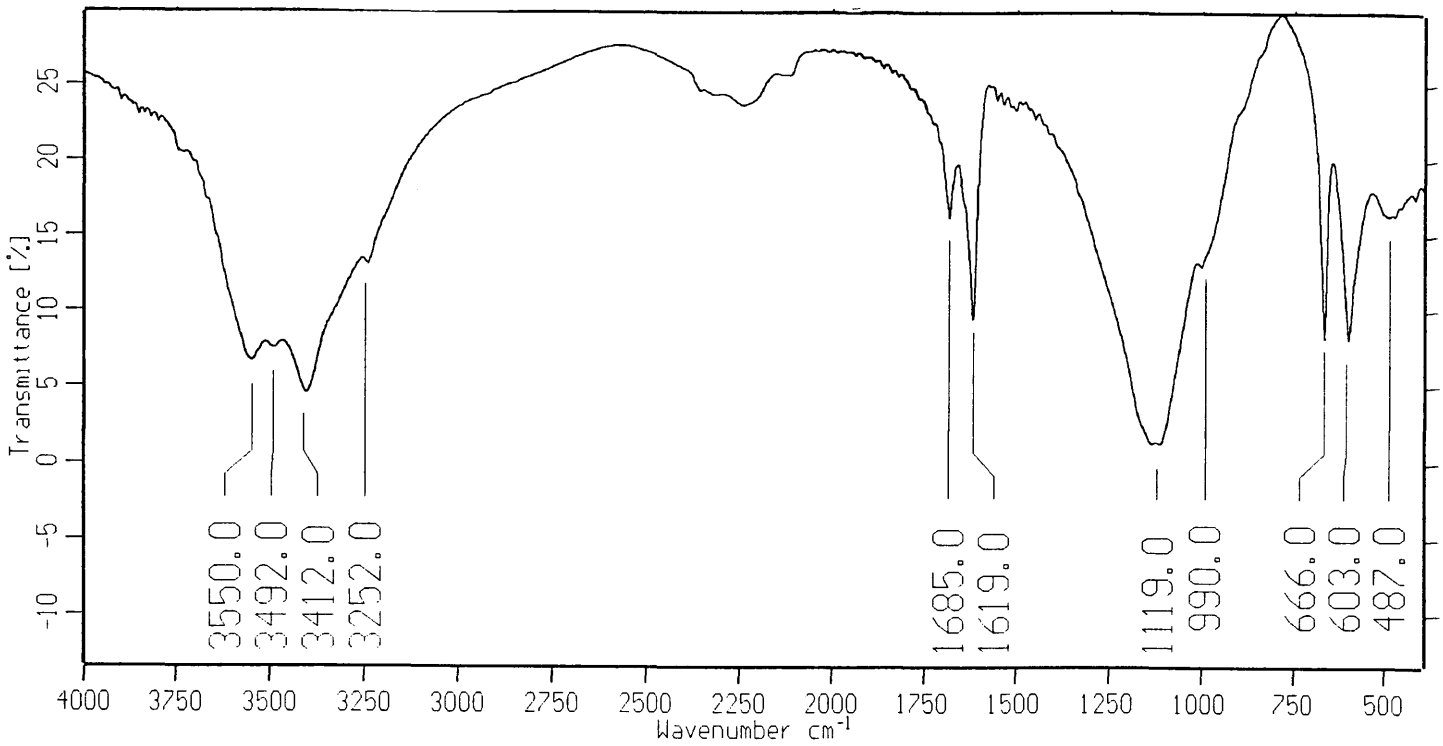

Figure 4.10. Infrared spectrum of gypsum Experiment 37.

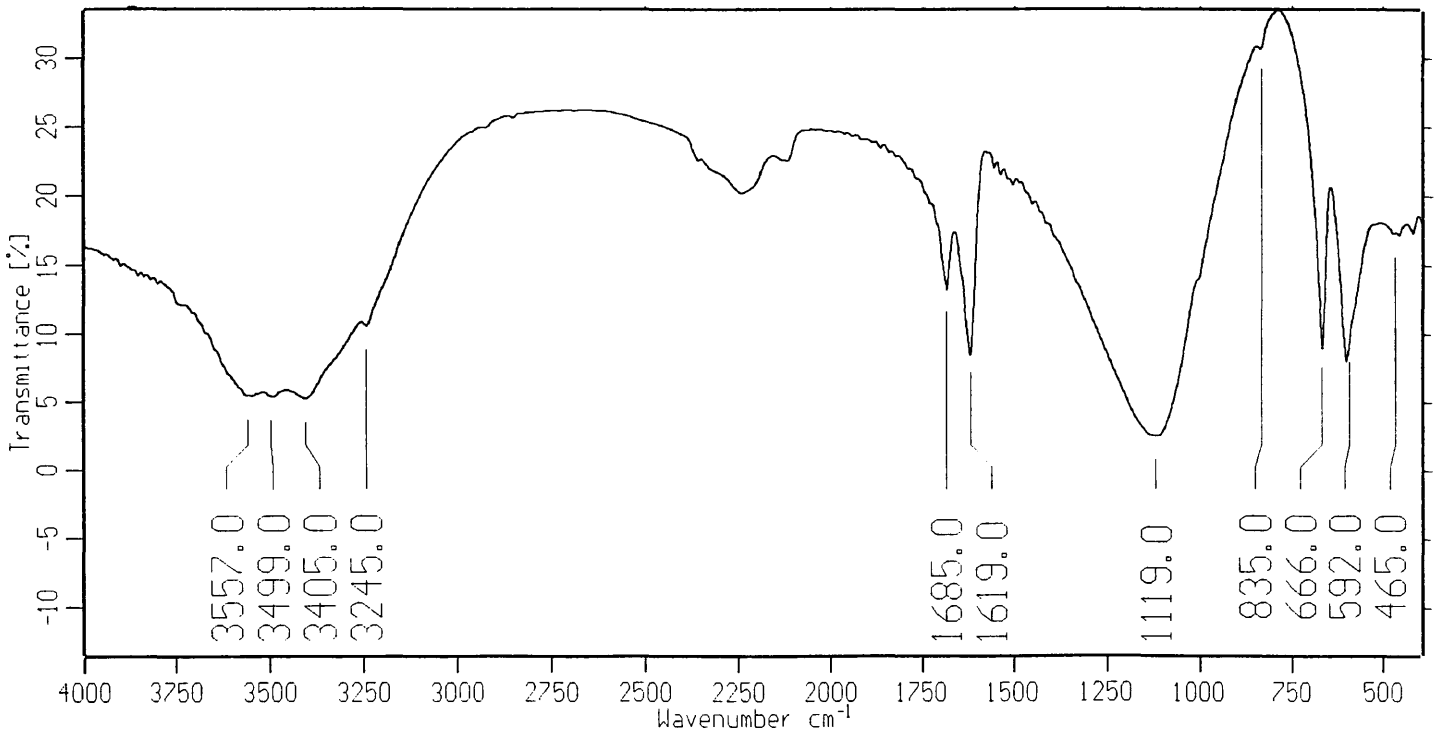

Figure 4.11. Infrared spectrum of postprecipitate Experiment 37.

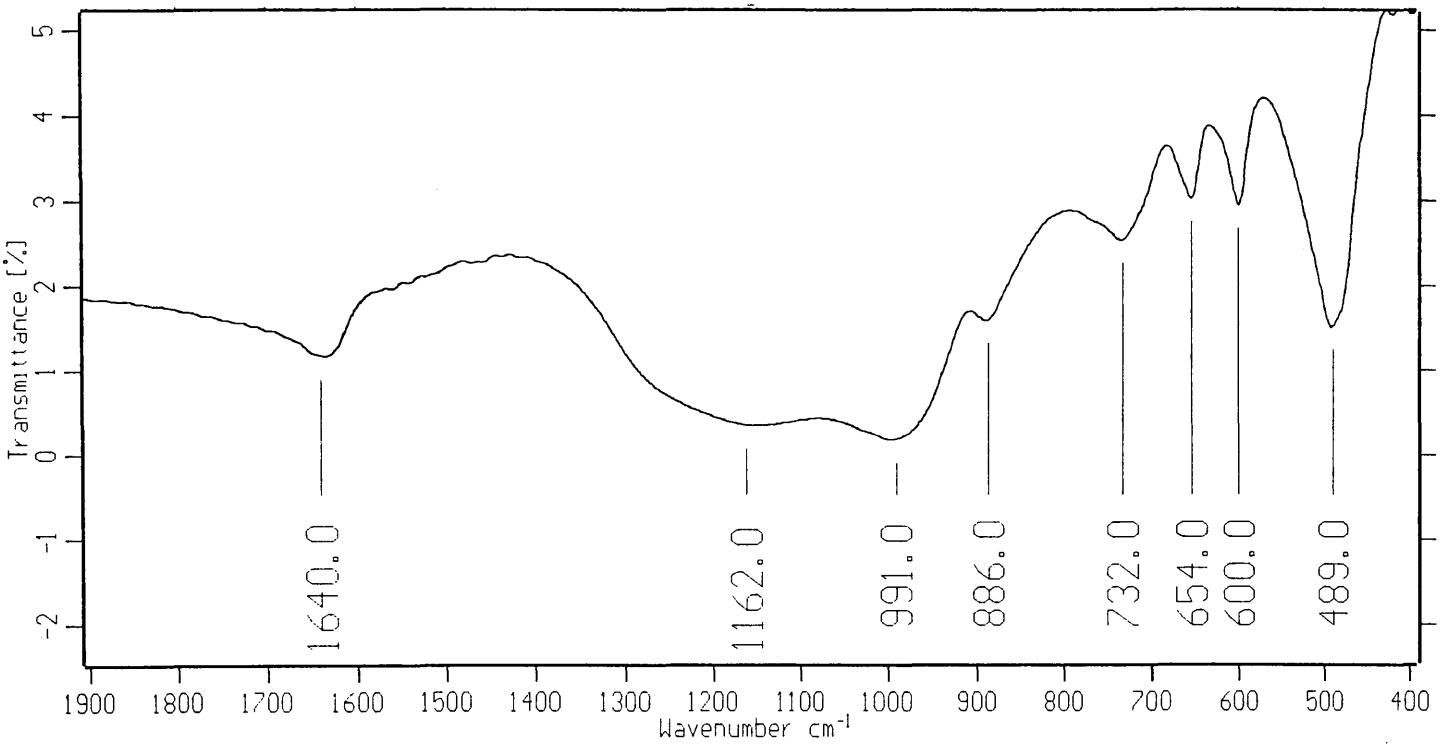

Figure 4.12. Infrared spectrum of sludge Experiment 37.

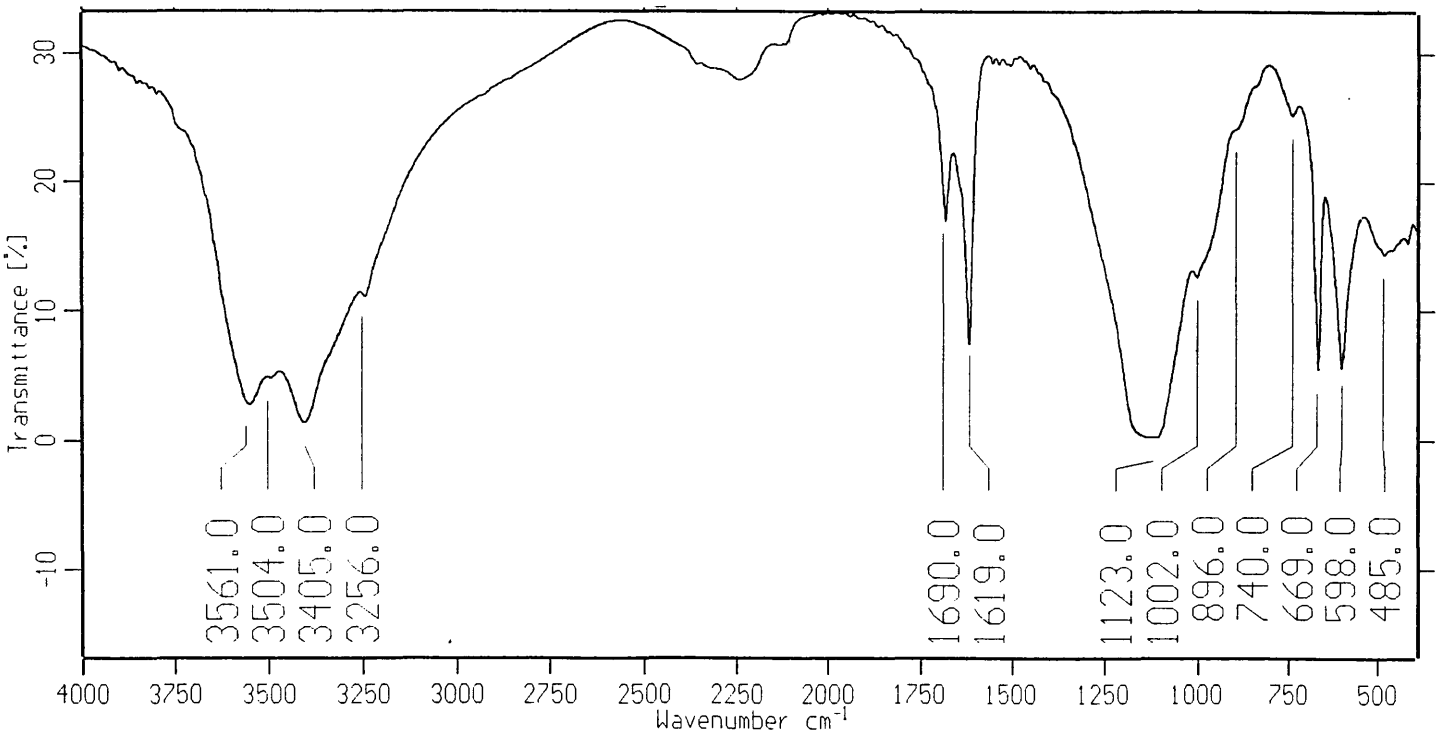

Figure 4.13. Infrared spectrum of gypsum Experiment 39.

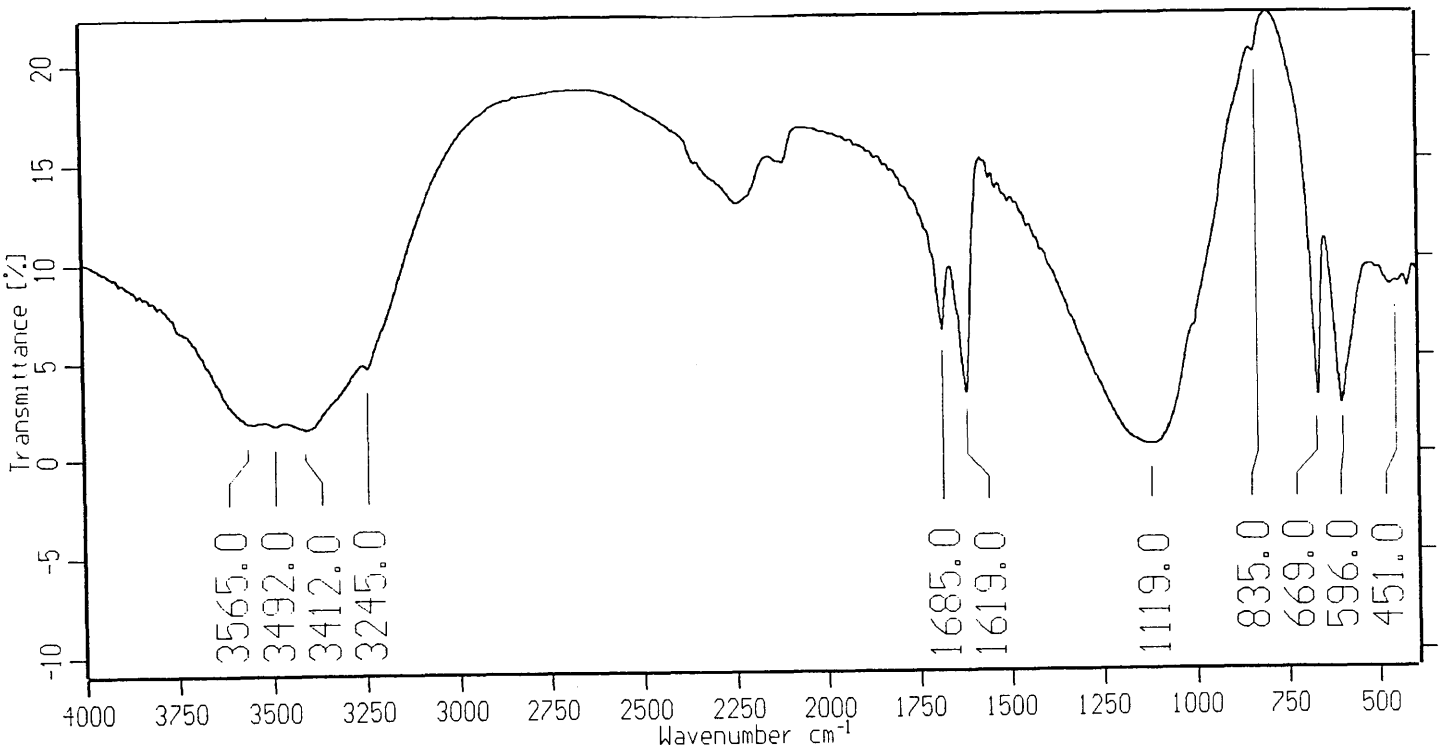

Figure 4.14. Infrared spectrum of postprecipitate Experiment 39.

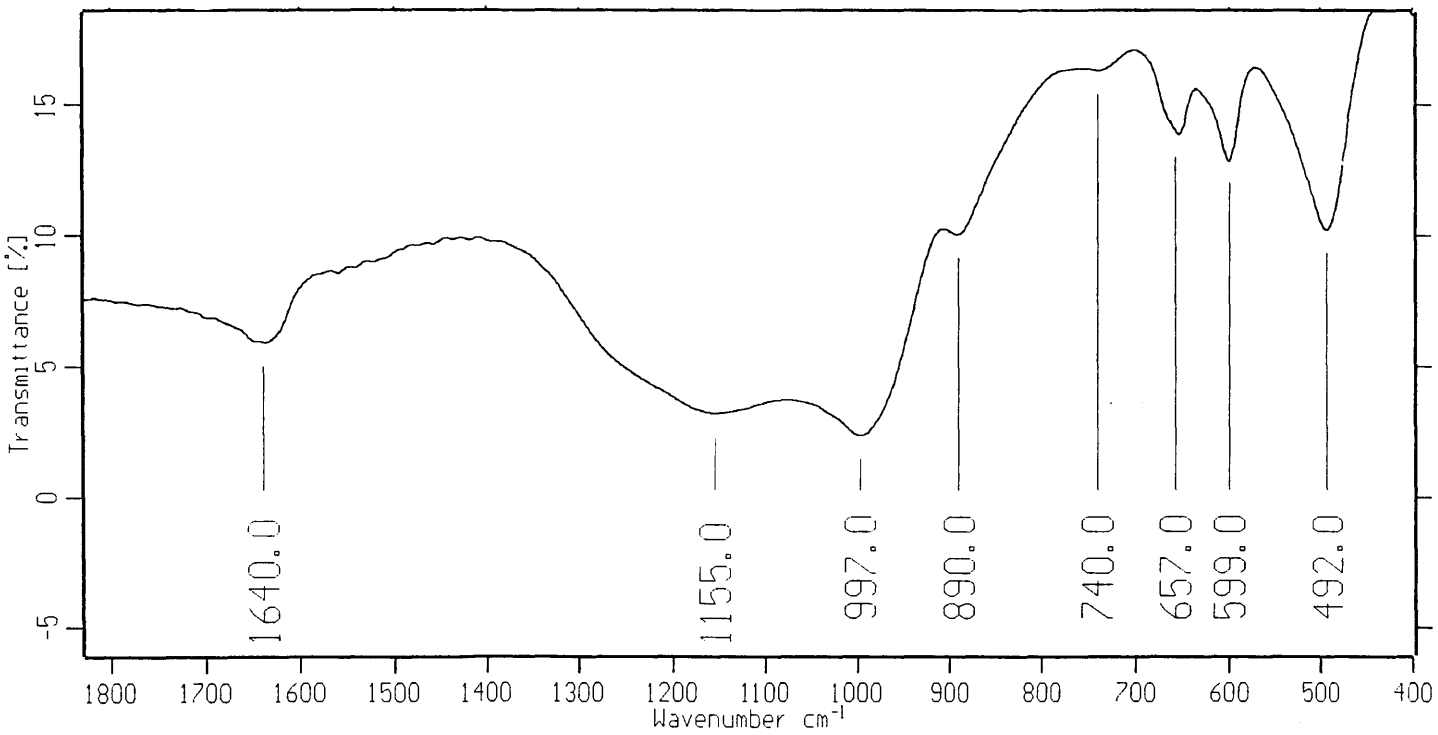

Figure 4.15. Infrared spectrum of sludge Experiment 39.

1.5 INFRARED SPECTRA OF CHAPTER 8:

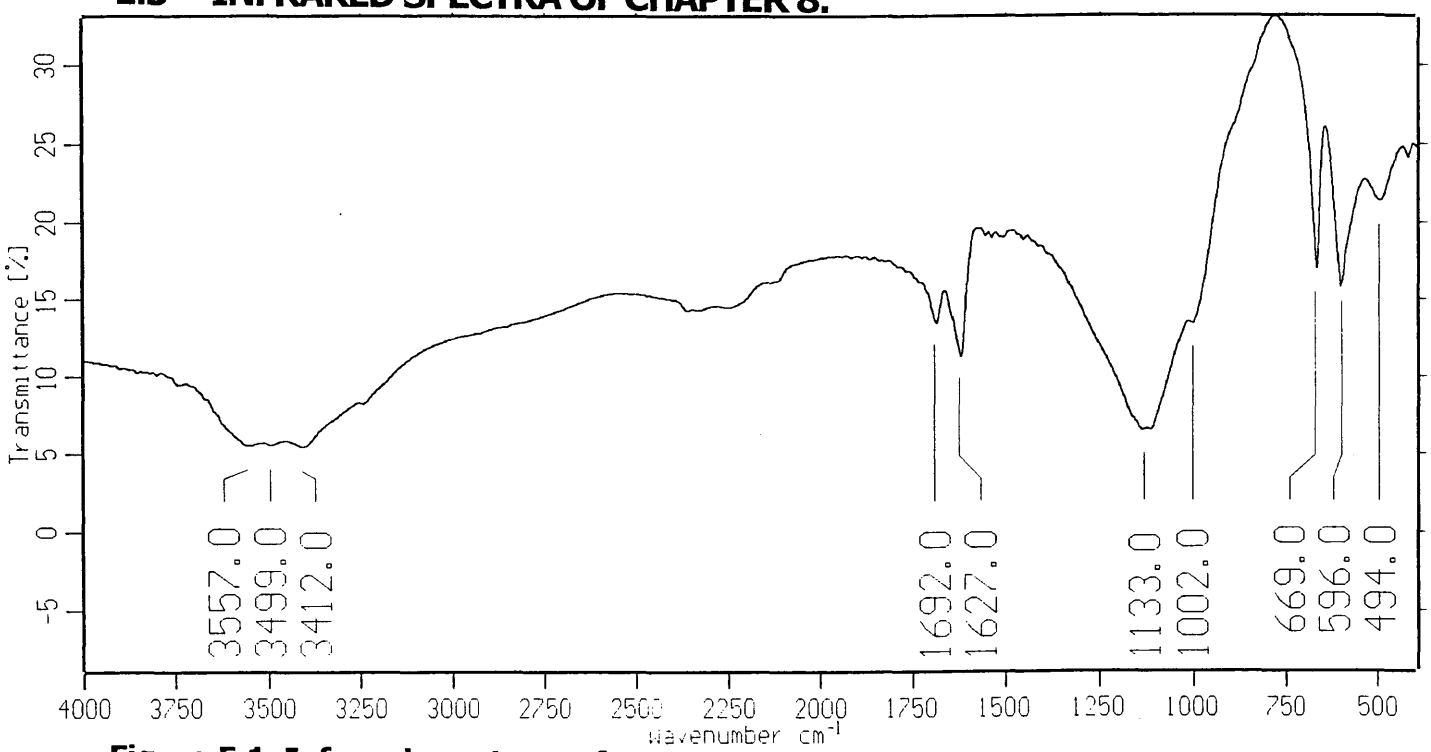

Figure 5.1. Infrared spectrum of gypsum Experiment 41.

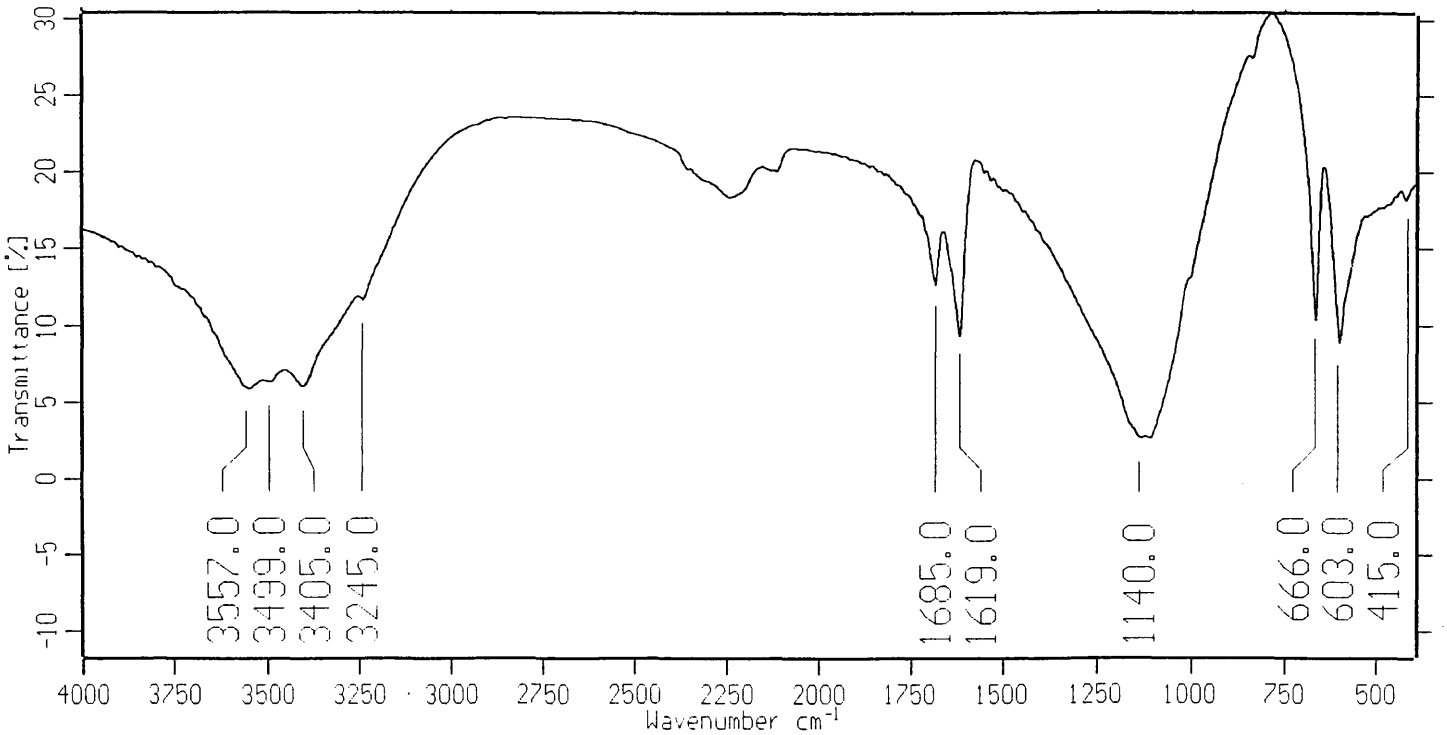

Figure 5.2. Infrared spectrum of postprecipitate Experiment 41.

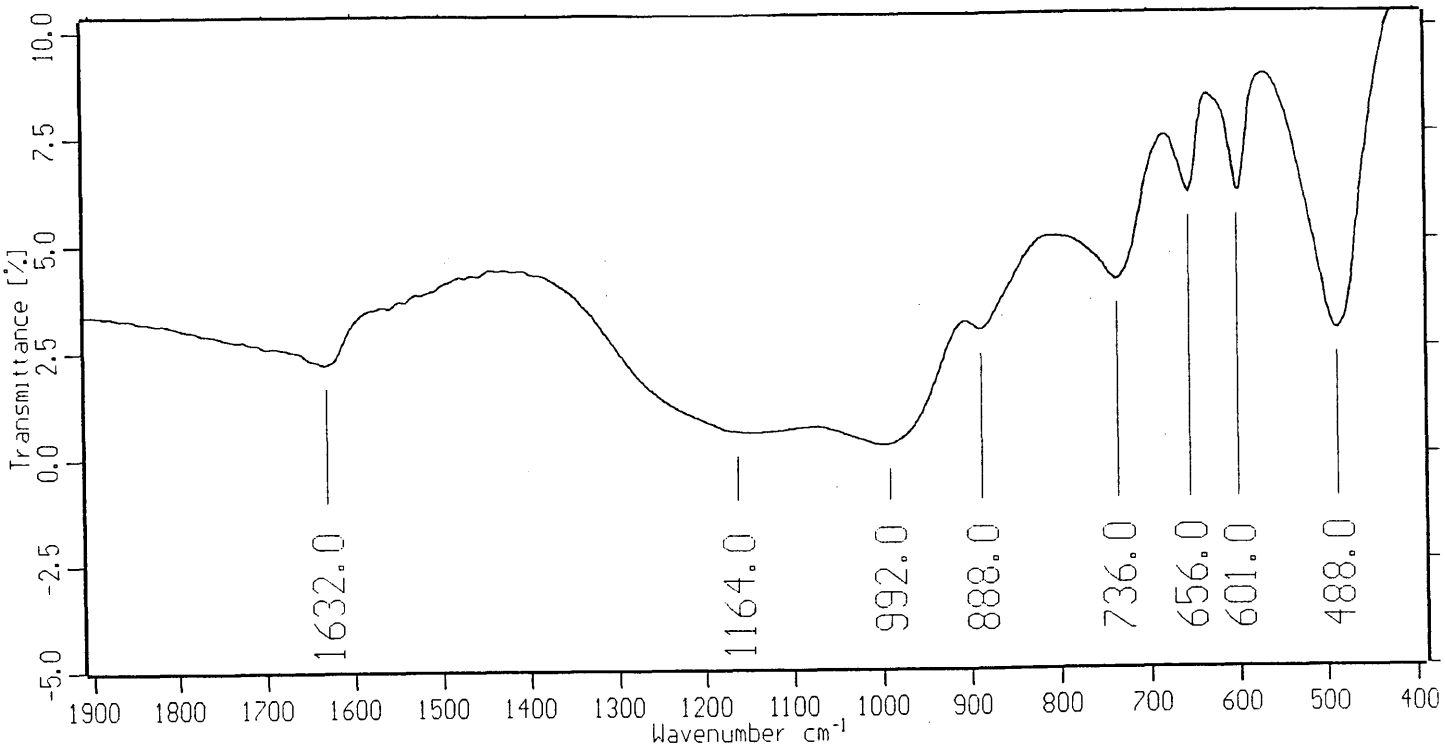

Figure 5.3. Infrared spectrum of sludge Experiment 41.

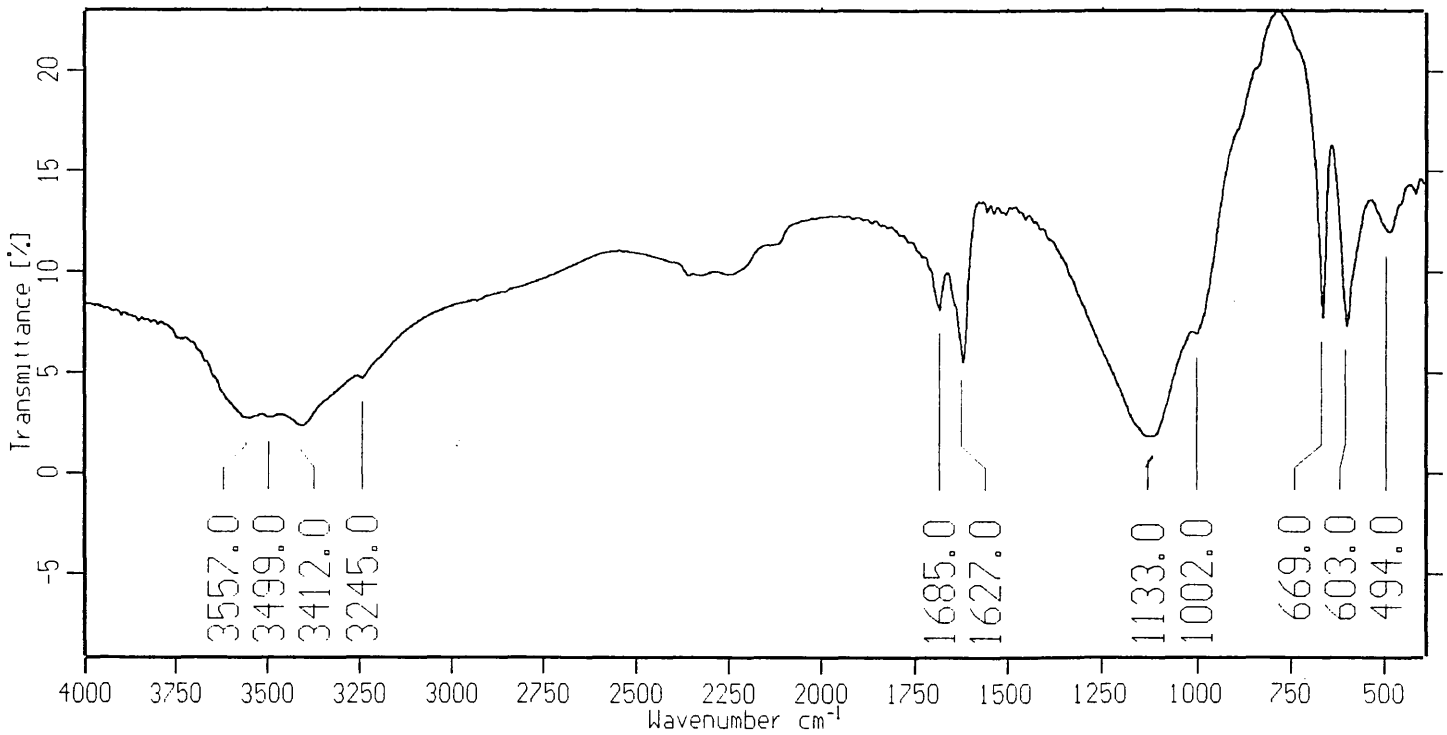

Figure 5.4. Infrared spectrum of gypsum Experiment 43.

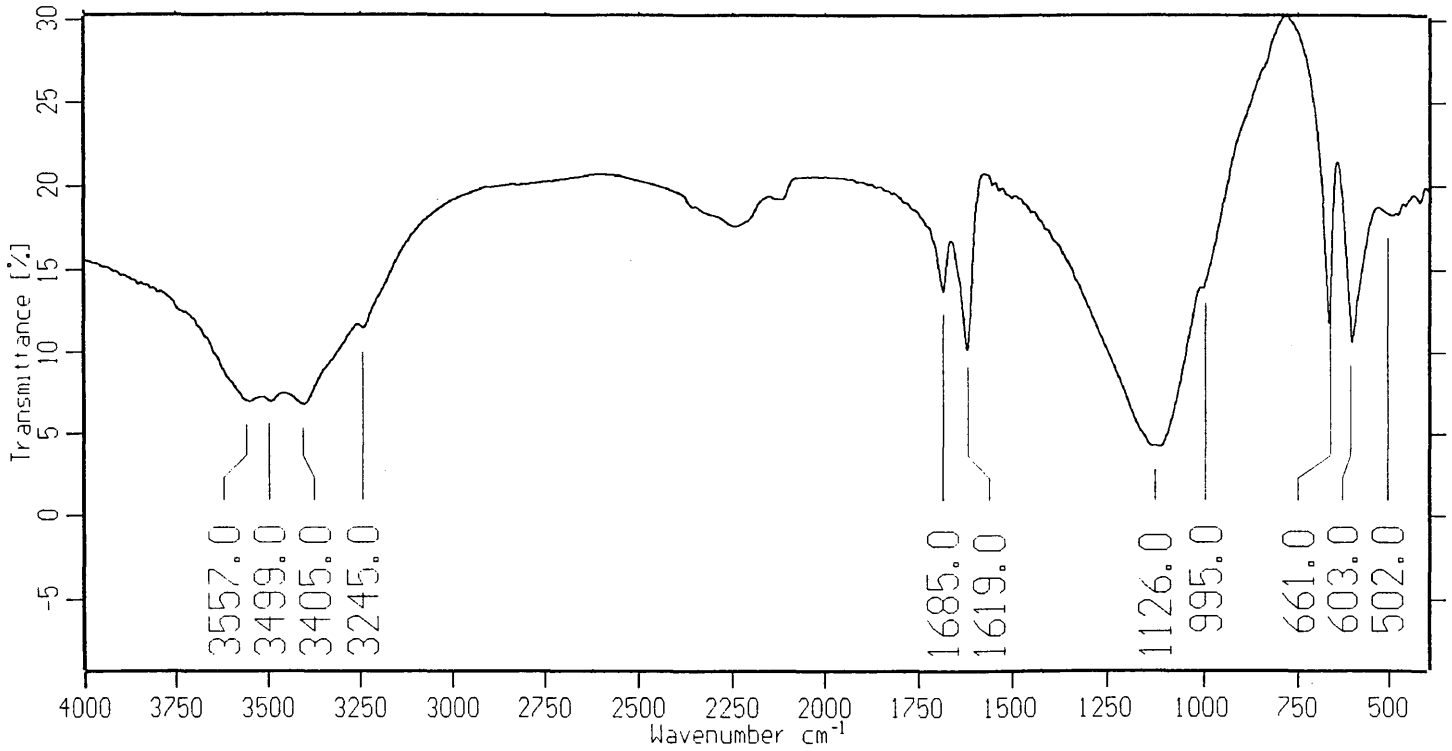

Figure 5.5. Infrared spectrum of postprecipitate Experiment 43.

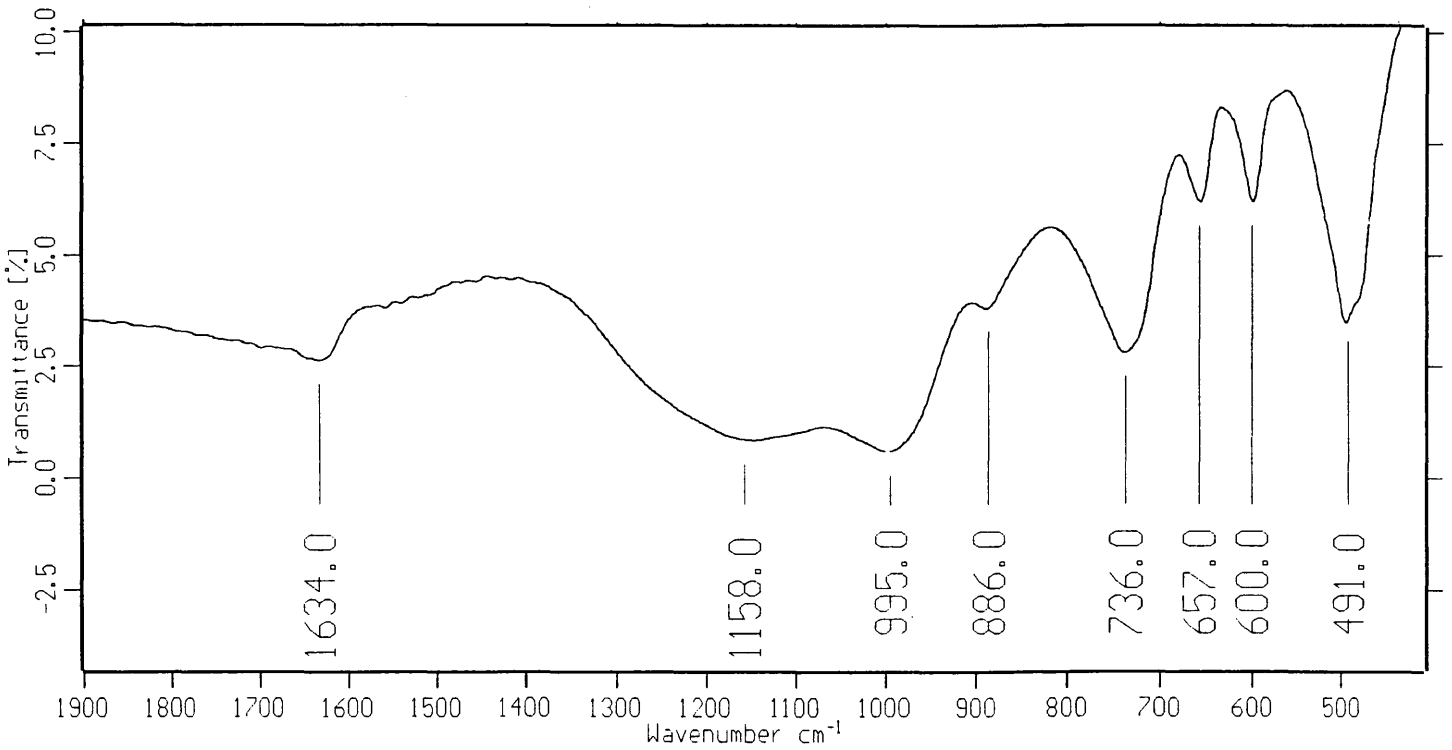

Figure 5.6. Infrared spectrum of sludge Experiment 43.

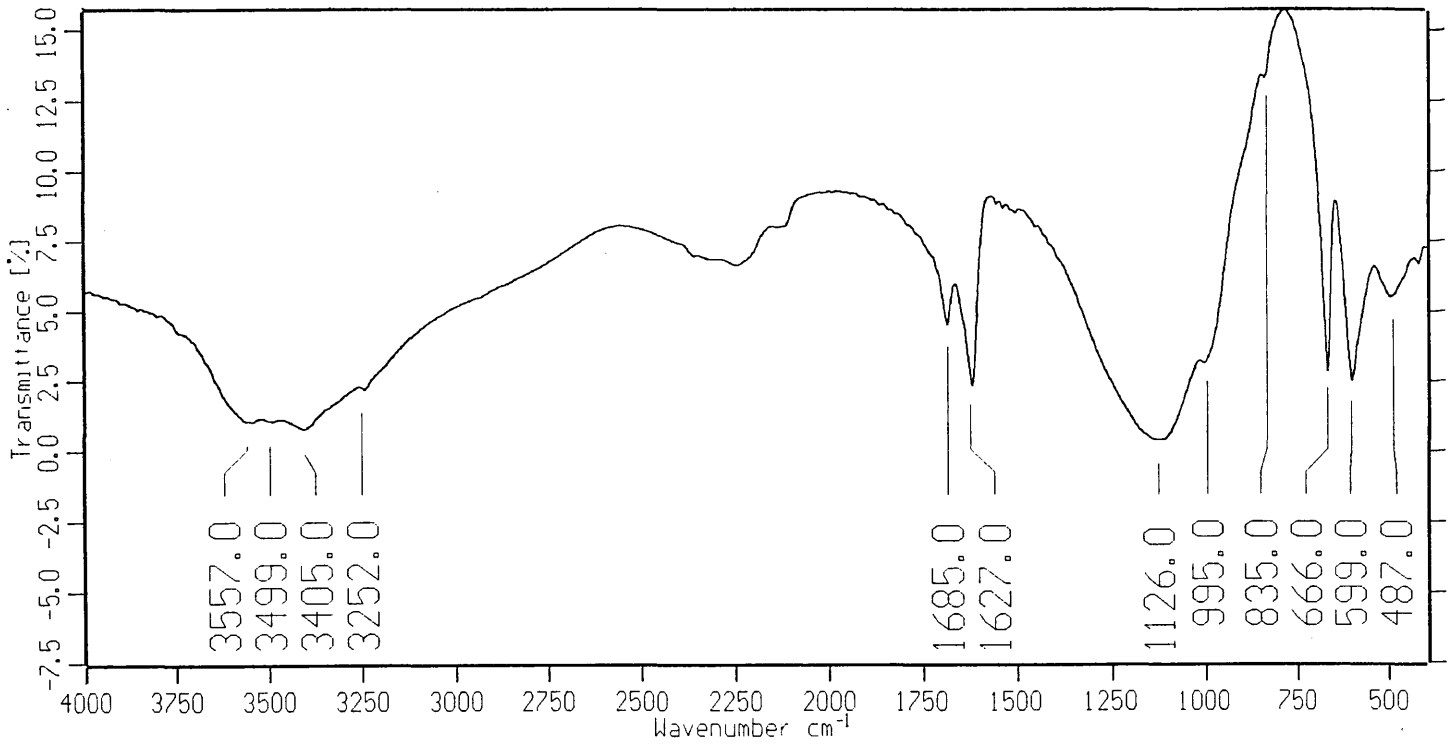

Figure 5.7. Infrared spectrum of gypsum Experiment 45.

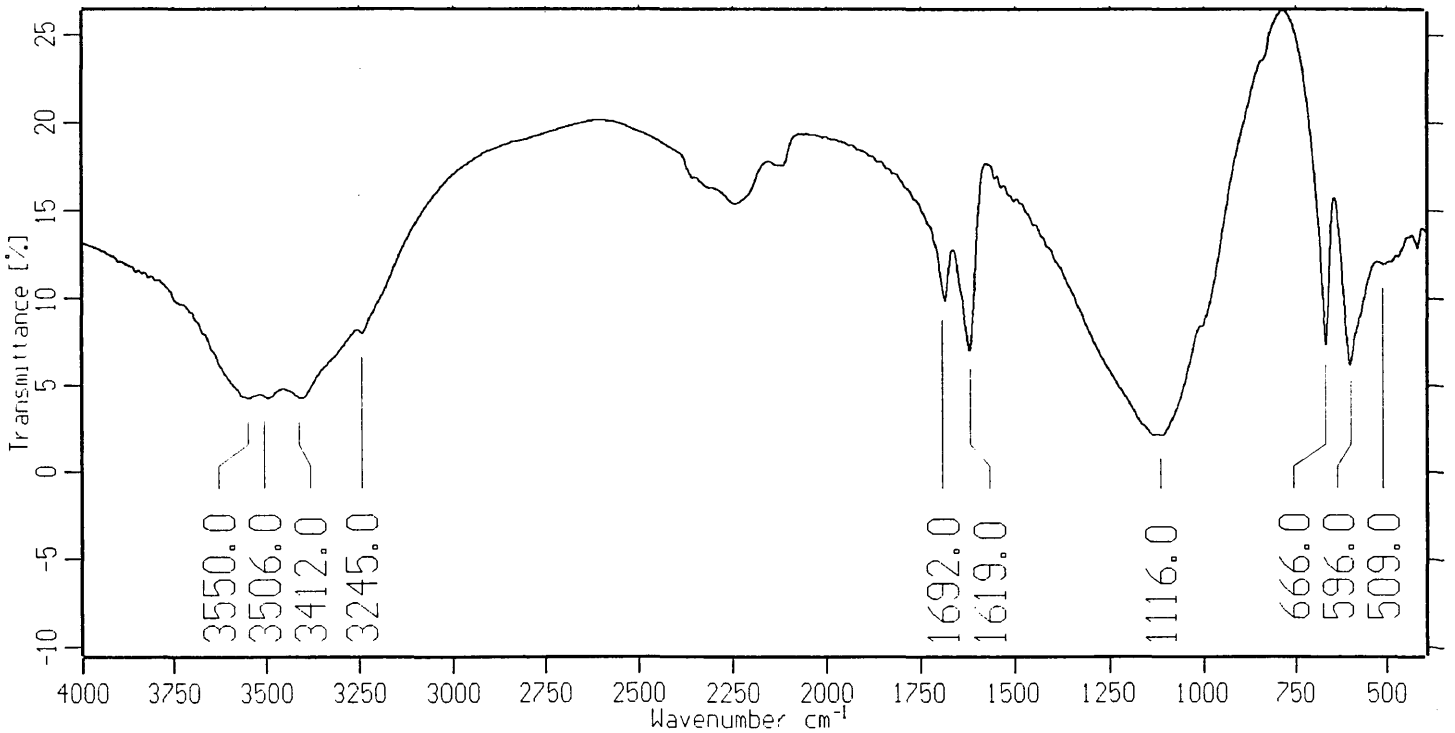

Figure 5.8. Infrared spectrum of postprecipiate Experiment 45.

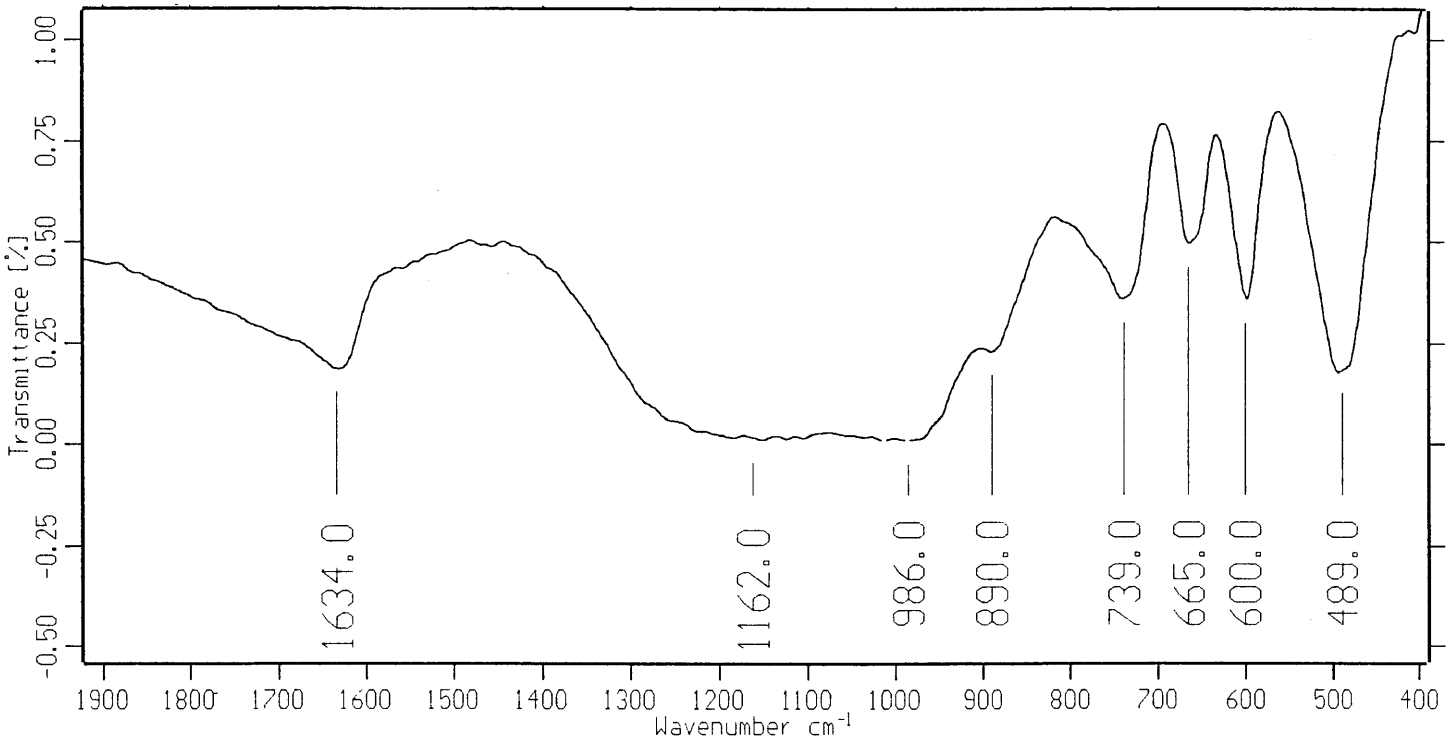

Figure 5.9. Infrared spectrum of sludge Experiment 45.

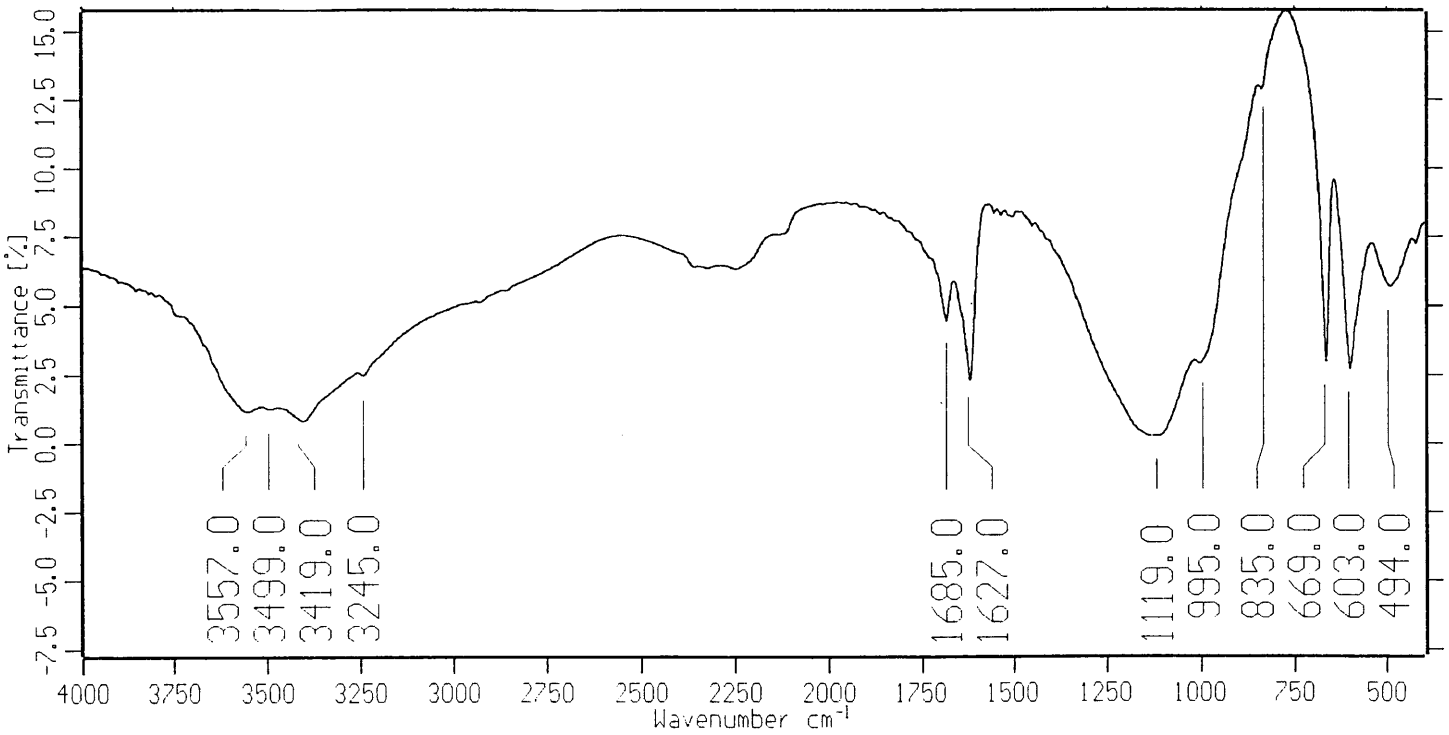

Figure 5.10. Infrared spectrum of gypsum Experiment 49.

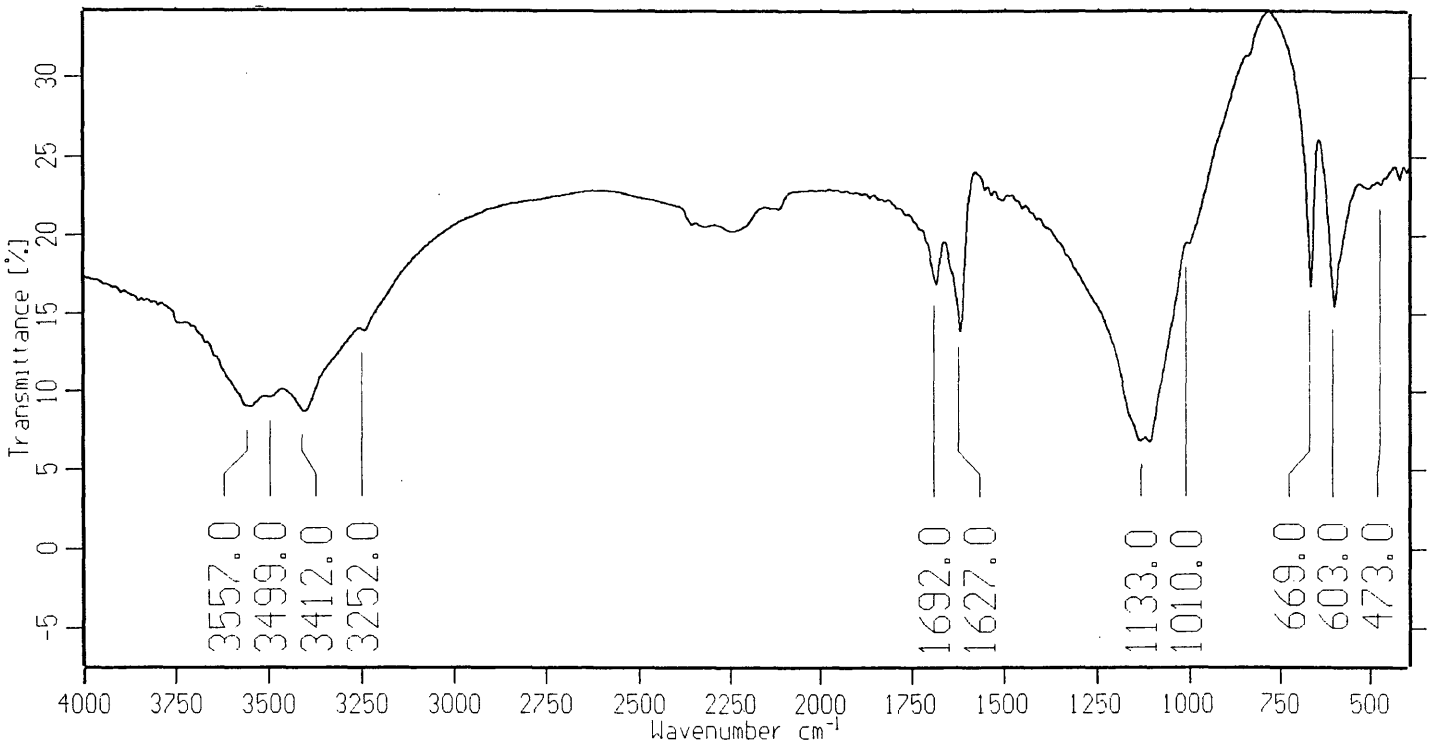

Figure 5.11. Infrared spectrum of postprecipitate Experiment 49.

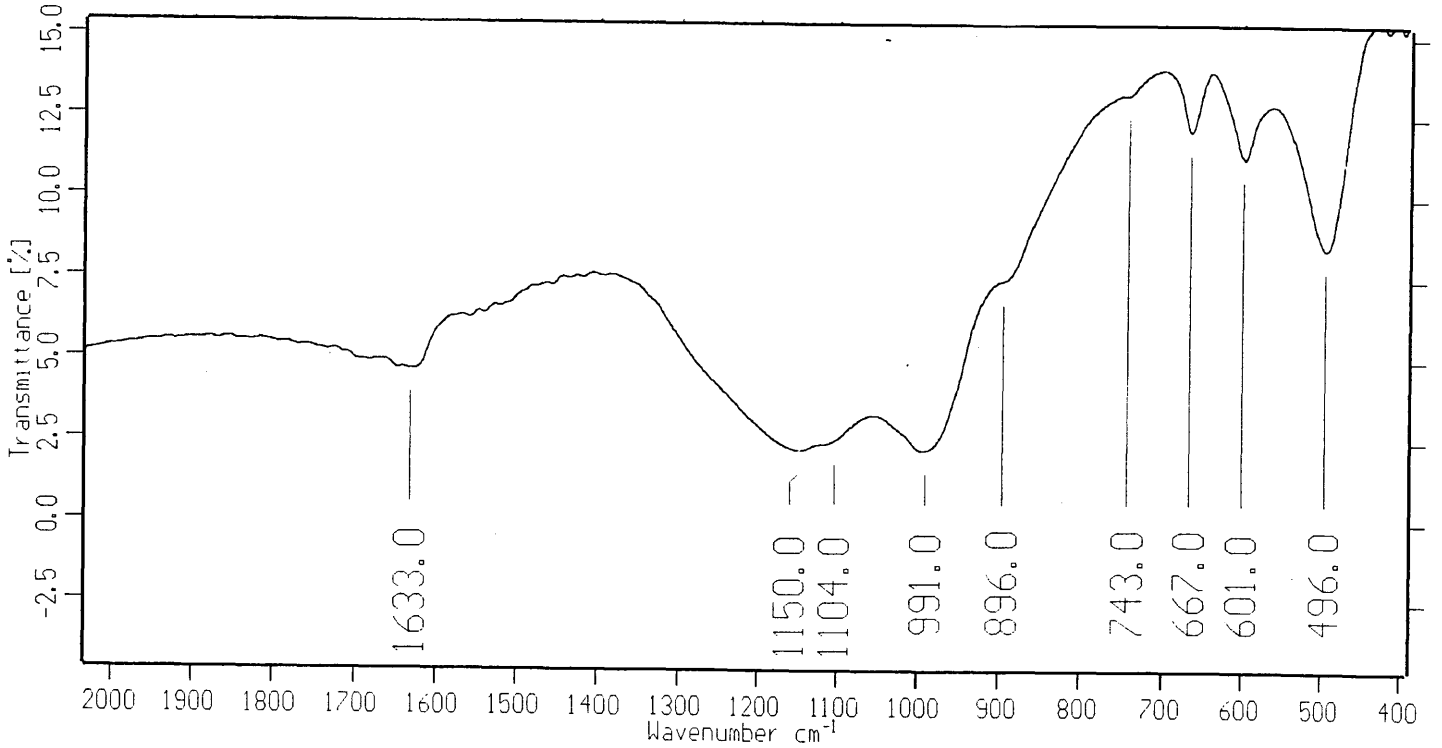

Figure 5.12. Infrared spectrum of sludge Experiment 49.

APPENDIX II

CALCULATION PROCEDURES FOR GROWTH RATE VERSUS RELATIVE SUPERSATURATION GRAPHS

To explain how the growth-rate graphs was determined; the effect of increasing concentrations of sodium impurity is discussed. It must be emphasised that the graphs can not be interpreted as absolute, it is only the relative trends that will be the same under different circumstances.

1.1 RELATIVE SUPERSATURATION:

The relative supersaturation was calculated using:

$\sigma(t) = ((C(t) - C_s)/C_s)$ (1.1)

Where: C(t) = The sulphate concentration (Table 5.2: 1 min. ~1.5 hour and 1 day).

C_s = The sulphate concentration (Table 5.2 at 30 days).

The results for sodium are presented in Table 1.1.

	Cs	C	σ	Time (min.)
0.05%Na	1.9	2.7	0.421	1
		2.4	0.263	107
		2.2	0.157	1440
0.25%Na	2.3	3.4	0.478	1
		3.1	0.347	98
		2.6	0.13	1440
0.5%Na	2.3	3.5	0.521	1
		3.2	0.391	96
		2.5	0.086	1440
0.25%Na	2.7	3.4	0.259	4
		3.2	0.185	114
		2.7	0	1440
3.75%Na	2.12	3.2	0.509	2
		2.6	0.226	120
		2.4	0.132	1440

Table 1.1. Relative supersaturation versus time.

A graphical representation of the results (Table 1.1) is presented in Figure 1.1.

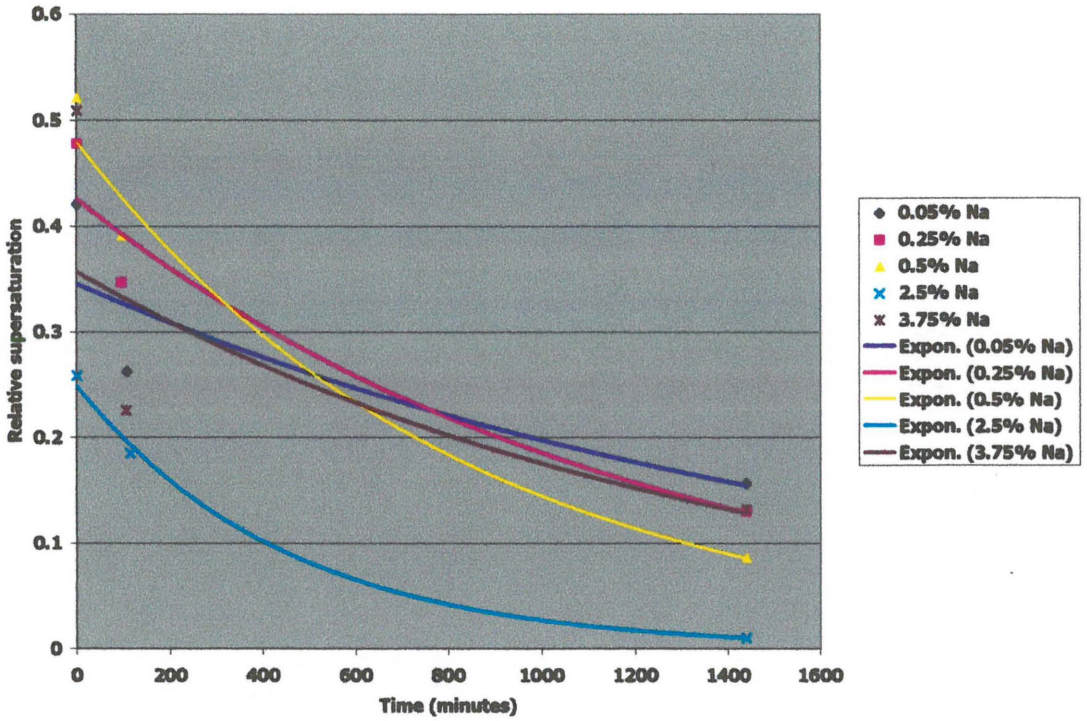

Figure 1.1. Relative supersaturation versus time.

0.05%Na	$\sigma(t)= 0.345e^{-0.0006t}$	$R^2 = 0.8256$
0.25%Na	$\sigma(t)= 0.427e^{-0.0008t}$	$R^2 = 0.9702$
0.5%Na	$\sigma(t)=0.479e^{-0.0012t}$	$R^2 = 0.992$
2.5%Na	$\sigma(t)= 0.249e^{-0.0022t}$	$R^2 = 0.9994$
3.75%K	$\sigma(t)= 0.358e^{-0.0007t}$	$R^2 = 0.7091$

1.2 MEAN LINEAR GROWTH RATE:

The mean linear growth rate was determined as follows:

$R = -d\sigma/dt \times L \times 1/\rho \times 1/S$ cm/min. (4.3)

1. Derivative of relative supersaturation function ($d\sigma/dt$):

0.05%Na : $-d\sigma/dt = -(-0.0002e^{-0.0006t}) = 0.0002e^{-0.0006t}$

0.25%Na : $-d\sigma/dt = -(-0.0003e^{-0.0008t}) = 0.0003e^{-0.0008t}$

0.5%Na : $-d\sigma/dt = -(-0.0005e^{-0.0012t}) = 0.0005e^{-0.0012t}$

2.5%Na : $-d\sigma/dt = -(-0.0005e^{-0.0022t}) = 0.0005e^{-0.0022t}$

3.75%Na: $-d\sigma/dt = -(-0.00025e^{-0.0007t}) = 0.00025e^{-0.0007t}$

2. Solubility at equilibrium for the particular ionic strength in g/cm³ (L):

$[SO_4^{2-}]$ = a %

= a g/100 g acid

Density of acid for example: 1.27 kg/L = 1.27 g/ cm^3

100 g of acid = 78.740 cm^3

$[SO_4^{2-}]$ = a g/78.740 cm^3 = a/78.740 g/cm^3

3. Density in g/cm³ (ρ):

Density of gypsum is 2.14 g/cm^3.

4. Surface of the crystal in cm² per cm³ solution (S):

To estimate the surface area of the crystals, isomorphous growth can be assumed. The surface area is expressed as follows:

$$S = S_o[((\sigma_o - \sigma)L + A_o)/A_0]^{2/3} \quad (4.4)$$

Where: S_o = S at t = 0 and $\sigma_o = \sigma$ at t = 0.

Since it is very difficult to determine the surface area of gypsum precipitated from igneous origins, S_o was taken as S_o = 1. Although the growth rate values can not be interpreted as absolute, the relative influence of different impurity levels would still be evident.

A_o = mass of seed crystals at t = 0 in g per cm^3.

50 g gypsum was added to a volume of 950 cm^3 acid

A_o = 0.052 g/ cm^3.

The results are summarised in Table 1.2, and the growth rate versus relative saturation graph presented in Figure 1.2.

Na	CONC. (% m/m)	TIME (min.)	-dσ/dt	REL SAT (σ)	L (g/cm³)	DENSITY (g/cm³)	A (t=0)	Surface (cm²/cm³)	R (cm/min.)
0.05%	2.7	1	0.000199	0.421	0.024	2.32	0.052	1	2.1E-06
	2.4	107	0.00018	0.263	0.024	2.32	0.052	1.047	1.8E-06
	2.2	1440	0.00008	0.157	0.024	2.32	0.052	1.079	7.7E-07
0.25%	3.4	1	0.000341	0.478	0.028	2.32	0.052	1	4.1E-06
	3.1	105	0.00031	0.347	0.028	2.32	0.052	1.046	3.6E-06
	2.6	1440	0.0001	0.13	0.028	2.32	0.052	1.12	1.1E-06
0.50%	3.5	1	0.00057	0.521	0.028	2.32	0.052	1	6.9E-06
	3.2	96	0.00051	0.391	0.028	2.32	0.052	1.04	5.9E-06
	2.5	1440	0.0001	0.086	0.028	2.32	0.052	1.15	1E-06
2.50%	3.4	4	0.00054	0.259	0.035	2.32	0.052	1	8.1E-06
	3.2	114	0.00042	0.185	0.035	2.32	0.052	1.03	6.2E-06
	2.7	1440	0.000023	0	0.035	2.32	0.052	1.11	3.1E-07
3.75%	3.2	2	0.00024	0.509	0.027	2.32	0.052	1	2.8E-06
	2.6	120	0.00022	0.226	0.027	2.32	0.052	1.09	2.3E-06
	2.4	1440	0.00009	0.132	0.027	2.32	0.052	1.12	9.4E-07

Table 1.2. Growth rate versus relative saturation.

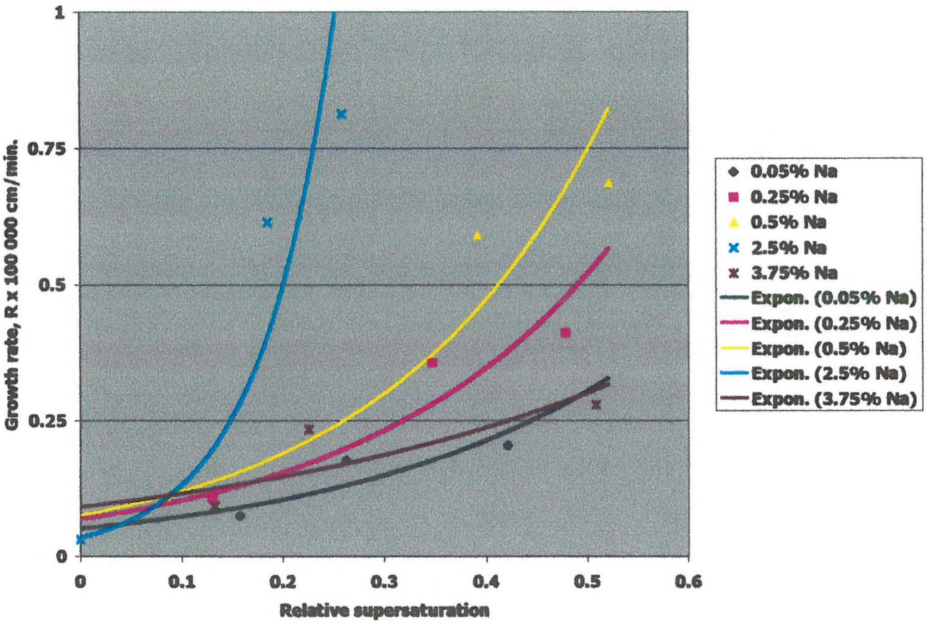

Figure 1.2. The influence of elevated levels of sodium impurity on the growth rate of calcium sulphate dihydrate.

0.05%Na : $R(\sigma) = 0.052e^{3.539\sigma}$ $R^2 = 0.7707$[1]

0.25%Na : $R(\sigma) = 0.069e^{4.036\sigma}$ $R^2 = 0.9201$

0.5%Na : $R(\sigma) = 0.076e^{4.560\sigma}$ $R^2 = 0.9510$

2.5%Na : $R(\sigma) = 0.035e^{13.27\sigma}$ $R^2 = 0.9592$

3.75% Na: $R(\sigma) = 0.091e^{2.383\sigma}$ $R^2 = 0.6282$[1]

1.3 OTHER IMPURITIES:

The other graphs were calculated using exactly the same procedure as described above. The equations and R^2-values of the relevant graphs are reported.

[1] The graphs of 0.05% Na and 3.75% Na were omitted in Figure5.1 (Chapter5 p.83) because the R^2 values are so poor. Other data, eg. analyses and photographs, do not support the fact that the growth rate decrease with the addition of 3.75% Na.

Potassium:

1. Relative supersaturation versus time:

0.01% K : $\sigma(t) = 0.765e^{-0.0018t}$ $R^2 = 0.9959$

0.05% K : $\sigma(t) = 0.474e^{-0.0026t}$ $R^2 = 0.9906$

0.10% K : $\sigma(t) = 0.442e^{-0.002t}$ $R^2 = 0.8651$

0.50% K : $\sigma(t) = 0.380e^{-0.0013t}$ $R^2 = 0.9398$

0.75% K : $\sigma(t) = 0.495e^{-0.0016t}$ $R^2 = 0.9851$

2. Growth rate versus relative supersaturation:

0.01% K : $R(\sigma) = 0.028e^{3.722\sigma}$ $R^2 = 0.9174$

0.05% K : $R(\sigma) = 0.032e^{7.318\sigma}$ $R^2 = 0.8801$

0.10% K : $R(\sigma) = 0.032e^{7.618\sigma}$ $R^2 = 0.9276$

0.75% K : $R(\sigma) = 0.053e^{5.286\sigma}$ $R^2 = 0.9269$

Magnesium:

1. Relative supersaturation versus time:

0.01% Mg : $\sigma(t) = -0.0535\ln(t) + 0.533$ $R^2 = 0.9115$

0.1% Mg : $\sigma(t) = -0.0356\ln(t) + 0.3976$ $R^2 = 0.8804$

0.75% Mg : $\sigma(t) = -0.0436\ln(t) + 0.5056$ $R^2 = 0.8261$

2. Growth rate versus relative supersaturation:

0.01% Mg : $R(\sigma) = 0.0043e^{16.996\sigma}$ $R^2 = 0.963$

0.1% Mg : $R(\sigma) = 0.0031e^{19.34\sigma}$ $R^2 = 0.8687$

0.75% Mg : $R(\sigma) = 0.002e^{21.508\sigma}$ $R^2 = 0.960$

Aluminium/Fluoride:

1. Relative supersaturation versus time:

0.0% Al : $\sigma(t) = -0.0515\ln(t) + 0.4481$ $R^2 = 0.8583$

0.25% Al : $\sigma(t) = -0.0266\ln(t) + 0.2507$ $R^2 = 0.8396$

0.5% Al : $\sigma(t) = -0.0115\ln(t) + 0.0906$ $R^2 = 0.7537$

0.75% Al : $\sigma(t) = -0.0256\ln(t) + 0.2165$ $R^2 = 0.9699$

1.0% Al : $\sigma(t) = -0.0386\ln(t) + 0.3389$ $R^2 = 0.8803$

2. Growth rate versus relative supersaturation:

0.0% Al : $R(\sigma) = 0.0027e^{11.135\sigma}$ $R^2 = 0.8593$

0.25% Al : $R(\sigma) = 0.0011e^{27.763\sigma}$ $R^2 = 0.8333$

0.5% Al : $R(\sigma) = 0.0016e^{69.722\sigma}$ $R^2 = 0.7489$

0.75% Al : $R(\sigma) = 0.0021e^{23.91\sigma}$ $R^2 = 0.9712$

1.0% Al : $R(\sigma) = 0.001e^{23.147\sigma}$ $R^2 = 0.8836$

APPENDIX III

ANALYSES OF ACID AND PHOSPHOGYPSUM FROM FOSKOR'S PILOT PLANT

TOTAL P_2O_5	COPR. P_2O_5	FIXED P_2O_5	FREE MOISTURE	MgO	Al_2O_3	Fe_2O_3	SiO_2	F
18.1%	2.91%	5.4%	31.769%	0.069%	0.0275	0.061%	1.536%	0.42%

Table 1.1. Analyses of gypsum from Foskor's pilot plant.

SiO_2	Al_2O_3	Cu	K_2O	MgO	CaO
0.914%	0.023%	0.15%	0.030%	0.35%	0.100%

Table 1.2. Analyses of phosphoric acid from Foskor's pilot plant.

Element	88S	88P	86S
P_2O_5%	40.2	40.3	40.2
CaO%	53.0	53.9	53.9
MgO%	0.54	0.44	0.65
Al_2O_3%	0.06	0.12	0.05
Fe_2O_3%	0.19	0.14	0.21
F%	2.48	2.38	2.41
Cl ppm	670	240	670
SiO_2%	0.37	0.82	0.41
La_2O_3%	0.11	0.14	0.09
CeO_2%	0.24	0.30	0.21
ThO_2 ppm	150	132	<100
TiO_2 ppm	130	128	130
SrO%	0.45	0.47	0.55
Y_2O_3 ppm	214	240	214
Na_2O%	0.13	0.13	0.13
K_2O%	0.03	0.07	0.03

Table 1.3. Typical analyses of phosphate rock.

APPENDIX IV

INSTRUMENTATION

1.1 INFRARED SPECTRA:

Infrared spectra were recorded on a Bruker IFS 113V spectrophotometer in the form of pressed KBr pellets.

1.2 ELECTRON MICROSCOPE PHOTOGRAPHS:

Electron micrograph studies were carried out with a JEOL JSM-840 scanning electron microscope.

1.3 ICP ANALYSES:

Analyses of solid samples, that is gypsum, postprecipitate and sludge, were done by Foskor's analytical laboratory, while analyses of acid samples were done by Avmin Research Laboratory.

1.4 UV-MEASUREMENTS:

UV measurements, for total P_2O_5 analyses, were done on a Genesys 5 spectrophotometer at 490 cm^{-1}.

APPENDIX V

PUBLICATIONS

1. Kruger A. and Fowles R.G., **"The Effect of Extraneous Soluble Ions in Igneous Rock Phosphate on Crystallography of Gypsum Dihydrate and Thus Phosphoric Acid Production"**, To be published, IFA proceedings, September (1998).

2. Kruger A., Heyns A.M. and Folwes R.G., **"The Growth of Calcium Sulphate Dihydrate"**, To be published.

3. Kruger A., Heyns A.M. and Fowles R.G., **"The Effect of Extraneous Soluble Ions in Igneous Rock Phosphate on Crystallography of Gypsum Dihydrate and Thus Phosphoric Acid Production. Part 1: Sodium and Potassium"**, To be published.

4. Kruger A., Heyns A.M. and Fowles R.G., **"The Effect of Extraneous Soluble Ions in Igneous Rock Phosphate on Crystallography of Gypsum Dihydrate and Thus Phosphoric Acid Production. Part 2: Magnesium, Aluminium and Fluorine"**, To be published.